# Theoretical study of nonlocal electron transport in plasmas relevant to inertial confinement fusion

Antoine Chrisment

**Thesis**

Submitted in partial fulfillment of the requirements

for the degree of

**Doctor of Philosophy in Physics**

Université de Bordeaux

École doctorale des sciences physiques et de l'ingénieur

Section: Astrophysique, Plasmas, Nucléaire

# Étude théorique du transport électronique non local dans les plasmas de fusion par confinement inertiel

Theoretical Study of Nonlocal Electron Transport in Plasmas Relevant to Inertial Confinement Fusion

*by* Antoine Chrisment

*under the supervision of* Pascal Loiseau *and* Philippe Nicolaï

Defended on July 3, 2024 in Talence, France, in front of the jury composed of:

| | | | |
|---|---|---|---|
| N. Crouseilles | Research Associate | INRIA/ENS Rennes (IRMaR) | Reviewer |
| M.-C. Firpo | Director of Research | CNRS/Ecole Polytechnique (LPP) | Examiner |
| J. Mathiaud | Professor | Rennes University (IRMaR) | Examiner |
| P. Mora | Director of Research Emeritus | CNRS/Ecole Polytechnique (CPhT) | Examiner |
| Ph. Nicolaï | Research Associate | CEA/Bordeaux University (CeLIA) | Director |
| C. Ridgers | Professor | York University (YPI) | Reviewer |
| V. Tikhonchuk | Professor Emeritus | ELI/Bordeaux University (CeLIA) | President |
| P. Loiseau | Research Associate | Paris-Saclay University/CEA (LPPL) | Invited |

This page is unintentionally left not blank.

This page is unintentionally left not blank.

This page is unintentionally left not blank.

# Remerciements

Cette thèse s'est déroulée sous l'égide de la Direction des Applications Militaires du CEA. Je suis gré à sa hiérarchie de la confiance qu'elle m'a accordé, et en particulier à la cheffe de service du Département de Conception et Simulation des Armes, ainsi qu'à mon directeur de laboratoire, pour leur impartialité, soutien et écoute à plusieurs moments clefs.

Je suis reconnaissant envers mes directeurs de thèse, Pascal Loiseau et Philippe Nicolaï; le premier, pour m'avoir permis de démarrer ce projet, et le second, pour s'être assuré de son aboutissement avec professionalisme. J'ai eu le privilège de soutenir devant un jury prestigieux, que j'aimerais remercier pour l'attention qu'il a porté à mon travail. À mes rapporteurs, Nicolas Crouseilles et Christopher Ridgers, j'exprime toute ma gratitude pour avoir décortiqué mon manuscrit dans leur comptes rendus remplis de précieuses remarques. Ce fut un honneur d'avoir eu les commentaires de Patrick Mora, dont la lecture approfondie m'a permis de corriger plusieurs coquilles typographiques. Je n'aurais peut-être pas choisi ce thème de recherche sans l'excellente initiation que m'en a faite Marie-Christine Firpo à l'X; j'ai été ravi qu'elle accepte le rôle d'examinatrice. À Julien Mathiaud, je voudrais signifier combien nos interactions quotidiennes m'ont épaulé. Cette aide fut plus que déterminante dans l'achèvement de ma thèse. Mes travaux ont été suivis de près par Vladimir Tikhonchuk, dont les critiques en ont continuellement amélioré la qualité. J'ai admiré la justesse de son jugement, ainsi que sa ténacité pour maintenir un niveau d'exigence élevé. Je suis flatté qu'il ait présidé ma soutenance.

Ma thèse a bénéficié de collaborations avec Arnaud Debayle, Bruno Dubroca, Jean-Luc Feugeas et Paul-Édouard Masson-Laborde. Je leur suis redevable pour leurs contributions, qu'ils ont su apporter avec une réactivité sans faille. J'ai eu le plaisir d'échanger avec une multitude d'autres chercheurs sur une ribambelle de sujets, allant du refroidissement d'un verre de whisky aux problèmes ouverts en électrodynamique quantique non perturbative, en passant par la dynamique des interactions dans l'écosystème de la recherche. Pour ces à-côtés qui furent de réelles bouffées d'oxygène, je voudrais notamment remercier Xavier Ribeyre, Didier Rafestin, Olivier Larroche, Sébastien Guisset, Émeric Falize, Jean-Marie Clarisse et Michel Casanova. De ce dernier j'ai bénéficié d'un appui solide lorsque mon désarroi était à son paroxysme. Je m'en souviendrai toujours. J'ai partagé d'inoubliables moments avec tant de camarades stagiaires, doctorants et post-doctorants à Paris et Bordeaux que l'idée de les évoquer tous me donne le vertige. Plutôt que d'en gâcher la mémoire par des énumérations trop creuses, je voudrais leur écrire que ce manuscrit n'existerait sans doute pas sans eux. Nos discussions, rires et sorties sont gravés dans mon esprit. J'accorderai toutefois une mention spéciale aux trois d'entre eux qui ont particulièrement excellé dans l'art de me détourner de mes préoccupations quotidiennes : Victor Tranchant, pour m'avoir partagé son enthousiasme à l'égard de l'Univers examiné sous le prisme des algèbres de Lie; Charles Colavolpe, pour m'avoir poussé dans mes derniers retranchements par son insatiable curiosité pour le chaos déterministe et la physique statistique hors équilibre; Thomas Vigier, pour m'avoir embarqué avec ardeur dans de périlleux débats philosophiques sur la terminologie, l'amour et la nature des mathématiques. Quel plaisir d'avoir eu d'aussi riches échanges :-)

Mon équilibre dut énormément à mon chaleureux entourage en dehors du laboratoire. Pour sa générosité à mon égard, je remercie Magali Garcia. Mon confort à Bordeaux, surtout au milieu des intempéries, ainsi que l'éducation de mes papilles au Sainte-Croix-du-Mont lui durent beaucoup. À Paris, je salue les prouesses de mes tortionnaires réguliers, Sarah Ditsriporn et Valentin Leroy, grâce auxquelles l'exquise douleur des courbatures fut régulièrement réveillée; que serais-je devenu sans elle ? Ces entraînements furent d'inestimables bulles de bien-être, merci ! À ces réjouissances s'ajoutèrent chacuns des instants passés en compagnie de mes collègues professeures et professeurs, techniciennes et techniciens de laboratoire. À eux, qui ne

manquèrent pas d'encourager mon penchant pour les calembours douteux, je dus une allégresse résistante aux *calembredaines* des élèves. Ils m'ont promu au rang d'icône du groupe de disscussion, une faveur dont je me délecte encore ;-) Cette jovialité fut largement alimentée par mes colocataires dans la dernière ligne... sinueuse plutôt que droite. Ainsi je paie de retour Matteo De Franscesco, pour son indulgence face à mes choix fantaisistes de garnitures des pâtes; Aristide Ganci, pour sa prévenance inspirante et son petit accent, que tout le monde savoure et que je lui prierai de bien vouloir continuer à cultiver; Mathieu Louaib-Pannetier, pour son initiation aux tacos et aux sonnets de Shakespeare, un cocktail insolite de graisse et de grâce auquel j'ai succombé. Toutes ces années je fus nourri par mon intarissable amitié avec Eva et Nicolas Moutal, qui ne cessèrent de m'encourager. Ils suivirent tous les méandres de mes épopées doctorantes avec une assiduité, patience et bienveillance inouïes. Quelle chance j'ai eu ! À lui, au contact duquel j'ai tant appris, je dus un certain renouement avec ma passion première, les sciences dures, à une époque où, peut-être un peu lassé, je m'engageais dans l'agrégation en regardant la philosophie du coin de l'oeil. Aurais-je frôlé la catastrophe ? Notre belle entente intellectuelle fut une aubaine, et chacune de nos inombrables disccusions depuis, un régal.

À toi, mon adorée, que pourrais-je écrire encore ? Dans le tumulte des derniers efforts, ton amour m'a empli d'une force exaltante. Chaque fois que, loin l'un de l'autre, le mien restait suspendu à mes lèvres, j'entamais comme un pèlerinage dans l'aridité de ton absence — vers l'oasis de notre complicité. Que la pénombre de ces mots en préserve ici l'éclat.

*À mes parents,*
*pour leurs conseils souvent décisifs*

This page is unintentionally left not blank.

# Contents

# List of Figures

# List of Tables

This page is unintentionally left not blank.

# Chapter 1

# Introduction

Current primary sources of energy are combustion of oil (30.9 %), coal (26.9 %), and natural gas (24.4 %), together with nuclear fission (4.3 %), and renewable conversions (13.5 %, among which 6.8 % comes from hydraulic dams). These proportions are those of the year 2021 [1]. Such a high dependency to fossil fuels is a worrying problem, not just because of declining world reserves.

The accumulation, within the atmosphere, seas and oceans, of the greenhouse gases released by their usage is responsible for the climate drift. Besides global warming, it manifests through increasingly intense and frequent droughts, floods and storms. This process is enhanced by the huge amount of carbon dioxide released during the permafrost melting, which, in addition, is expected to spread bacteria, viruses and microbes [2]. This will expose living beings to unknown diseases. Such a degradation of living conditions on earth is accentuated by the population growth, making humanity even more sensitive to deprivation of food, potable water or health care.

As tensions between people will intensify, triggering conflicts more and more often, we will thus have fewer and fewer material means to manage them. Dealing with this situation requires to design a carefully thought strategy, which must encompass structural changes at all scales, from individual lifestyles to global societal organization. Among the urgent changes is the severe reduction of fossil fuels consumption, which is only possible by adopting more sober ways of life while developing alternative methods of energy conversion. One of the most promising of them is controlled fusion.

## 1.1 Current status of nuclear energy

As is well known, the mass, $m$, of a given nucleus is smaller than the sum of the masses of its nucleons, $Zm_p + Nm_n$, with $m_p$ and $m_n$ the masses of the proton and the neutron, respectively. This defect of mass is explained by the attractive interaction between the constituents of the nucleus. By definition, it is equal to $B/c^2$, where $B$ is called the binding energy,

$$B/c^2 = Zm_p + Nm_n - m,$$

with $c$ the velocity of light in vacuum. A nuclear reaction is exothermic if the sum of nuclear binding energies of products is higher than the sum of nuclear binding energies of reactants. As visible in Fig. 1.1, it both concerns fission of heavy atoms ($A > 56$) in lighter fragments, and fusion of light atoms ($A < 56$) in heavier ones. Although fusion reactions are the main source of energy in the Universe, current nuclear plants deliver electricity through fission reactions. On its side, controlled fusion for sustainable energy production has been an active area of research for about seventy years now. To understand why requires to briefly recall the physical mechanisms on which these two kinds of reactions rely on.

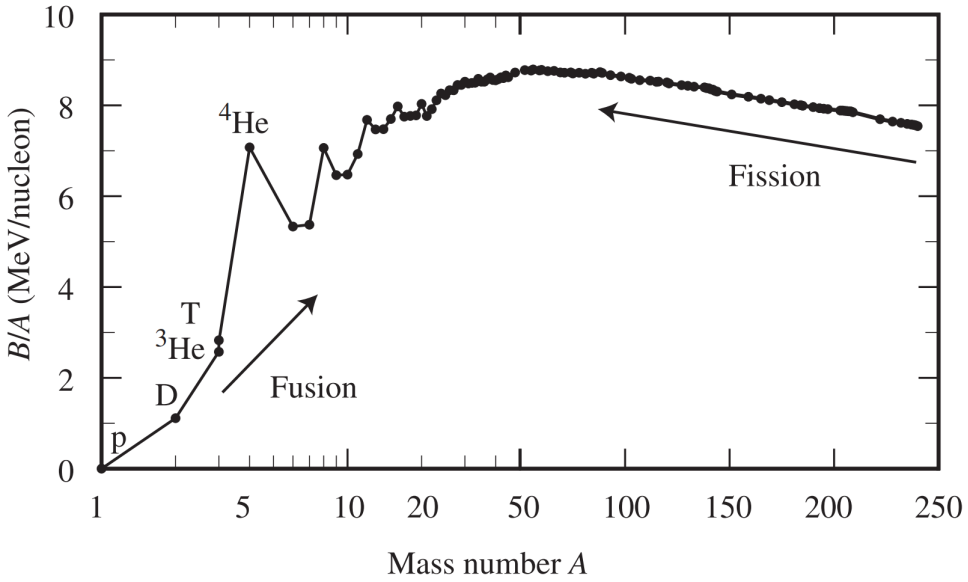


Figure 1.1: Nuclear binding energy per nucleon $B/A$ as a function of $A$. Abscissa axis is in logarithmic scale for $A < 50$, and in linear scale for $A > 50$. Extracted from Ref. [3].

### 1.1.1 Prospects for the fission industry

The fission sector owes its success to neutron-induced chain reactions. The absorption of a neutron $^{1}$n by a fissionable nucleus like $^{235}$U leads to an unstable exited state, $^{236}$U$^{*}$, which in turn fragments into lighter edifices including several neutrons [4]:

$$^{1}\mathrm{n} + {}^{235}\mathrm{U} \rightarrow \mathrm{FF} + k\ {}^{1}\mathrm{n}, \tag{1.1}$$

with $k \geq 1$. The fission fragments, FF, are almost always two, with mass numbers distributed around 95 and 138. On average, the life span of $^{236}$U$^{*}$ is about 10 ps and the number of neutrons is $k = 2.47$. These produced neutrons then trigger new fission reactions in cascade provided that they are slowed down by passing through a moderator media. Indeed, the absorption in Eq. (1.1) is optimal for incident neutrons with energies around 1/40 eV, whereas those released have energies around 1.9 MeV. The chain reactions is sustained if a sufficient amount of neutrons encounter nuclei per unit time without, however, exceeding a certain threshold which would lead to a uncontrollable, runaway reaction. The first condition requires the use of a nuclear fuel containing at least 3% of $^{235}$U, and therefore

the enrichment of natural uranium in that isotope. The rest of the uranium nucleus within the resulting fuel, which consists of solid uranium oxide (UOX), are almost exclusively $^{238}$U. The second condition is ensured through an appropriate usage of control rods absorbing neutrons. The goal is to maintain the reactor in a stationary regime corresponding to an effective multiplication factor of neutrons around unity.

It can be seen in Fig. 1.1 that the binding energies per nucleon of the fission fragments are about 8.4 MeV, whereas that of $^{235}$U is 7.5 MeV. Hence, the energy released during the reaction described by Eq. (1.1) is about 0.9 MeV per nucleon, *i.e* just over 200 MeV per uranium atom in total. In parallel to the reaction (1.1), there appears the fission of some isotopes of the plutonium, especially $^{239}$Pu. These nuclei are produced *in situ* by transmutation through the captures of energetic neutrons by $^{238}$U, followed by two successive minus beta decays with $^{239}$Np as intermediate products. Like for $^{235}$U, the absorption $^{1}\mathrm{n} + {}^{239}\mathrm{Pu} \rightarrow \mathrm{FF} + k\ {}^{1}\mathrm{n}$ is optimal for thermal neutrons. The average number of neutrons produced is $k = 2.91$, and the atomic numbers of the fission fragments are almost distributed like in Eq. (1.1). Nevertheless, the renewal rate of fissionable atoms does not compensate their consumption. After a typical duration of one year, the fuel roughly contains depleted uranium (1 % of $^{235}$U and 94 % of $^{238}$U), together with 1 % of $^{235}$Pu and 4 % of ultimate wastes. Such densities of $^{235}$U and $^{239}$Pu are insufficient to maintain the chain reactions. The fuel must be replaced.

One of the problems facing the current nuclear industry is the supply of uranium, which is far from being unlimited. If it continues to be consumed as UOX within conventional reactors, it will be depleted in a century. Such an estimate concerns uranium with cost less than three times the present spot prices [5]. For that reason the fuel cycle must be optimized. A solution already in place is to recycle spent UOX in the form of reprocessed uranium (RepU) and mixed oxide (MOX) fuel. Depending on its content in $^{235}$U, the RepU is not necessarily used as fresh fuel, but can be blend to produce MOX. The latter mainly serves to exploit the plutonium. It is a mixture of about 9 % of $^{239}$Pu with depleted uranium derived from UOX. Nowadays, the MOX represents only 5 % of the nuclear fresh fuel worldwide, and 10 % in France. It is always used in conjunction with UOX, except within the latest reactors of the third generation, such as the Evolutionary Power Reactor (EPR), or the Advanced Passive 1000 (AP1000) one, which can operate with MOX exclusively as fuel if required. In addition to the MOX, a more advanced recycled fuel, the regenerated mixture (REMIX), is manufactured without separating the fissile uranium and plutonium nuclei in the spent UOX. However, it is not yet on the market. Although the development of these recycled fuels is an important issue, the ultimate step toward long-term viability of the fission sector is the broad deployment of the fourth generation of reactors [6]. Unlike their predecessors, these fast neutron reactors (FNR) [7] operate without moderator by consuming a fuel constituted by a mixture of either $^{238}\mathrm{U}/^{239}\mathrm{Pu}$ or $^{232}\mathrm{Th}/^{233}\mathrm{U}$. Here, the cross sections associated to the absorption of neutrons, with energies around 2 MeV, are two orders of magnitude lower than for thermal neutrons and, although the resulting fission probability is higher, the fraction of fissile nuclei within the fuel must reach approximately 20 % to ensure the chain reaction. Nevertheless, the absence of any medium to slow down the neutrons has several advantages. Besides

simpler reactor designs, the transmutation rate of fertile nuclei into fissile ones is significantly increased. It can even exceed the rate at which fissile nuclei are consumed. Such breeder reactors also allow to burn some of the ultimate wastes produced by the conventional sector. These are long-lived, activated actinides which failed to fission because of the too low energy of the absorbed, thermal neutrons.

Used alongside the current fleet of reactors, FNRs would make it possible to significantly optimise the use of the uranium available on earth, postponing its disappearance at a reasonable price by a thousand years. They would make the nuclear industry cleaner and safer. In spite of these facts, the fission sector is in difficulty for several decades, destabilized by short-term political decisions. The situation, however, is currently being reversed. Facing the alarms of the Intergovernmental Panel on Climate Change (IPCC), the public debate on the potentialities of nuclear energy intensifies, leading to a re-examination of the benefices/risks balance.

### 1.1.2 Requirements for controlled fusion

Fusion reactions are much more demanding to exploit for the following reasons. By not carrying a charge, a neutron does not have to overcome electrostatic repulsion to cross the electron cloud and reach a nucleus. As described in Ref. [4], the probability for fission is thus determined by the energy of the exited state compared to the fission barrier. The latter is defined as the energy of the most unstable state on the path toward the complete separation of the fragments. After the absorption of a thermal neutron, the state $^{236}\mathrm{U}^*$ has an energy of about 6.5 MeV, whereas the fission barrier is 6.2 MeV. Fission is therefore the most probable way for the nucleus to decay. Unfortunately, for fusion a neutron-induced chain of exothermic reactions does not exist. It is obviously not possible, due to nucleons conservation, to simultaneously form a product with an higher number of mass while releasing more than one neutron. A naïve bombardment of *e.g.* hydrogen nuclei with neutrons is either endothermic or leads to neutron multiplication: $^1\mathrm{n} + {}^2\mathrm{D} \rightarrow {}^1\mathrm{H} + 2\ {}^1\mathrm{n}$ is endothermic and $^1\mathrm{n} + {}^1\mathrm{H} \rightarrow {}^2\mathrm{D}$ does not produce any neutrons. Thus, a self-sustained chain of fusion reactions necessarily involves edifices with charges.

The fusion of two nuclei occurs when they are sufficiently close for the strong interaction to act. This means a separation of only few femtometers. At a distance $r$, however, the electrostatic energy between two nuclei of charges $Ze$ and $Z'e$ is about $1.44ZZ'(1\text{ fm}/r)$ MeV , whereas the thermal energy is $k_BT \simeq 0.87(T/10^7\text{ K})$ keV. Even at the center of the sun, whose temperature is roughly $1.5 \times 10^7$ K, the thermal energy remains three orders of magnitude below the electrostatic barrier. Therefore, most of the encounters that lead to fusion occur through the tunnel effect. Their cross section is by a factor $\exp(-\sqrt{\epsilon_G/\epsilon})$ weaker than that one of elastic collisions, where [8]:

$$\epsilon_G = 2\pi^2\alpha^2(ZZ')^2\mu c^2,$$

is the Gamow's energy, $\epsilon$ is the kinetic energy of the center-of-mass, $\alpha \simeq 1/137$ is the fine-structure constant, and $\mu$ is the reduced mass of reactants. In order to sustain a fusion chain reactions, energy losses must be at least compensated and the kinetic energies of the products together with the number of fusion reaction

per unit time must be simultaneously maximized. The Gamow's energy, $\epsilon_G$, is the lowest for small atomic numbers, and $B/A$ admits a pronounced local maximum for $A = 4$, meaning that fusion reactions leading to ${}^4_2\mathrm{He}$ are particularly exothermic. As a result of these constraints, the most promising fusion reaction for energy production is:

$$ {}^2\mathrm{D} + {}^3\mathrm{T} \rightarrow {}^4\mathrm{He} + {}^1\mathrm{n}. \tag{1.2} $$

It releases $\epsilon_{DT} = 17.6$ MeV of energy, among which $(4/5)\epsilon_{DT} = 14.1$ MeV is carried by the neutron. As shown in Fig. 1.2a, this reaction has indeed the highest cross-section, $\sigma_{DT}$. It is an increasing function of $\epsilon$ up to, approximately, 60 keV. Even at this energy the corresponding Gamow's factor is only about 1%. This implies that thermodynamic equilibrium, whose realization is ensured by elastic collisions, is necessarily reached in the duration required for a sufficient amount of fusion reactions to occur. Hence, the trigger of self-burning imposes a sufficient *confinement* of the energy within the fuel.

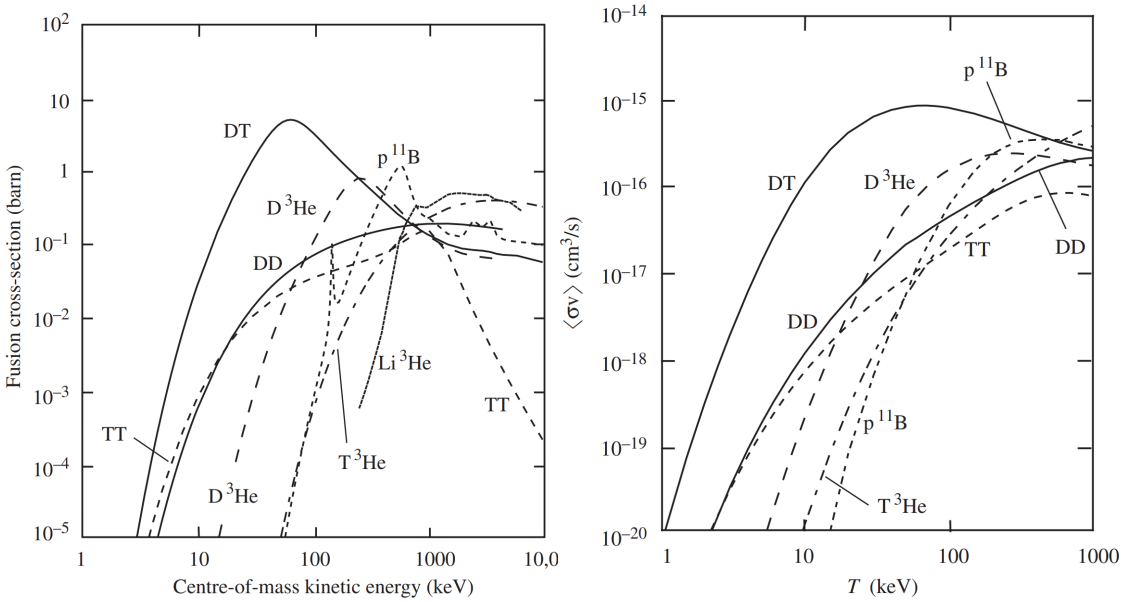


Figure 1.2: (a) Fusion cross-section in function of the center-of-mass kinetic energy $\epsilon$. (b) Reaction rate at thermal equilibrium, for one particle of each reactants in a $\mathrm{cm}^3$, in function of the temperature $T = T_i = T_e$. Extracted from Ref. [3].

The cross section $\sigma_{DT}$ can be defined as follows. The bombardment of a uniform distribution of tritium nuclei at rest, with density $n_T$, by a flux $n_D v$ of a mono-kinetic beam of deuterium nuclei, leads to a rate of fusion reaction per unit volume equal to $n_D n_T \sigma_{DT} v$. This expression must be averaged by the distribution function of relative velocity $v = (2\epsilon/\mu)^{1/2}$ between reactants within the plasma. The result, the average reaction rate per unit volume, can be expressed as $n_D n_T \langle \sigma_{DT} v \rangle$, where $\langle \sigma_{DT} v \rangle$ is plotted in Fig. 1.2b. It grows faster than $T_i^2$ within the energy range $3 - 20$ keV. Because they have no charge, the neutrons produced in reaction (1.2) escape from the plasma without losing energy. An optically thick plasma for neutrons would have too large dimensions, greater than those of the sun. Therefore, the fraction of the fusion power per unit volume redeposited in the plasma is only

due to alpha particles energy losses. It is equals to $P_\alpha = n_D n_T \langle \sigma_{DT} v \rangle \epsilon_{DT}/5$, by supposing that all alpha particles stay confined in the plasma. Under the constraint $n_D + n_T = n_i$, the product $n_D n_T$ reaches a maximum for $n_D = n_T = n_i/2$, corresponding to a stoichiometric mixture of deuterium and tritium. By making this choice, $P_\alpha$ therefore grows at least as $n_i^2 T_i^2$. Sustaining a fusion chain reaction implies to keep the temperature at least constant in spite of power losses. Without any external source of power, the minimum requirement is

$$P_\alpha \geq P_B,$$

where $P_B$ is the power loss per unit volume due to bremsstrahlung radiations. They are the electromagnetic waves mainly emitted during momentum exchanges of collisions. Alpha particles with energies comprised between $\epsilon_{DT}/5 = 3.52$ MeV to few hundreds of keV mainly transfer their energy to electrons. Momentum and energy exchanges with the ions only becomes significant for lower energies, for which alpha particles have already lost about 90% of $\epsilon_{DT}/5$ [9]. Therefore, the energy transfer from electrons to ions is the determinant mechanism to sustain self-burning. This implies a strong thermal coupling between these two populations: $T_e = T_i = T$. As electrons are lighter than ions, they experience a greater acceleration and bring the major contribution to radiation losses during electron-ion encounters. These emissions occur in the X-rays domain, for which a thermonuclear plasma of accessible size on earth is optically thin. Therefore, the radiative equilibrium is never reached, and the emitted power does not follow the Stefan-Boltzmann's law, as being not proportional to $T^4$. This makes ignition possible. Indeed, even if the elastic collisions are much more frequent than the fusion reactions, $P_B$ grows slower than $P_\alpha$ with respect to the temperature, as being proportional to $Z^2 n_i n_e T^{1/2}$. Moreover, since $n_e = Z n_i$ to high accuracy, $P_\alpha$ and $P_B$ have the same dependence on ion density. Consequently, the condition $P_\alpha \geq P_B$ is fulfilled for sufficiently high temperatures. The threshold value is the Post's temperature,

$$k_B T_P = 4.4 \text{ keV}.$$

This condition therefore imposes a sufficient level of *heating* of the fuel, at least initially, by an external source of power per unit volume, $P_e$. In fact, the critical temperature is even higher. Because the plasma obviously has a finite volume, there exists lost power due to heat transport and mechanical work. The sum of all the power losses per unit volume can be noted $U/\tau_\mathcal{E}$, where $U$ is the internal energy of the burning plasma, and $\tau_\mathcal{E}$ is the characteristic duration of energy confinement. Hence, the equation of energy conservation has the form

$$\partial_t U = \left(1 + \frac{5}{Q}\right) P_\alpha - \frac{U}{\tau_\mathcal{E}},$$

where $Q = 5P_\alpha/P_e$ is the gain factor. In the absence of the heating terms, $P_\alpha = P_e = 0$, the internal energy decreases exponentially on the characteristic duration $\tau_\mathcal{E}$. The desired thermal instability of burn is triggered if $(1 + 5/Q)\, P_\alpha > U/\tau_\mathcal{E}$. For a DT plasma, the internal energy is $U = (3k_B/2)(n_e T_e + n_i T_i) = 3nk_B T$ because $Z = 1$ and so $n_e = n_i = n$. Likewise, $P_\alpha = (n^2/20)\langle \sigma_{DT} v \rangle \epsilon_{DT}$. Hence, the aforementioned inequality can be expressed as

$$n\tau_\mathcal{E} > \frac{60 k_B T}{\langle \sigma_{DT} v \rangle \epsilon_{DT}\,(1 + 5/Q)}.$$

This condition, together with its equivalent formulations, is referred to as the Lawson's criterion [10]. It is the more restrictive in the ideal situation where $Q = +\infty$, defining the *ignition* threshold. In that case, the right hand side reaches its minimum at $k_B T = 26$ keV, whose value is $1.5 \times 10^{20}$ s/m$^3$. However, the burning plasma already behaves as a power amplifier for a gain factor superior to unity. The corresponding threshold, $Q = 1$, is called the *breakeven*.

In order to approach ignition, two main technological paths have been followed. They are materialized by either inertial or magnetic confinement devices. The latter aim at confining a low density plasma ($n \sim 10^{20}$ m$^{-3}$) for a long time ($\tau_\mathcal{E} \sim 1$ s), by using an elaborated magnetic field topology. On the opposite, in facilities dedicated to inertial confinement fusion, the burning plasma has an high density ($n \sim 10^{31}$ m$^{-3}$), but is confined for a very short duration ($\tau_\mathcal{E} \sim 10$ ps). Thanks to this second strategy, further explained in the next section, breakeven was achieved for the first time in history on 8 August 2021 at the National Ignition Facility (NIF) [11]. It has been reproduced at the same place on 5 December 2022 [12].

### 1.1.3 Challenges common to all methods

In spite of these breakthroughs, the path toward commercial fusion is strewn with pitfalls. By examining Eq. (1.2), two of them can be already identified. One concerns the management of the highly energetic neutrons, and the other one, the production of tritium.

Deuterium is abundant: one cubic meter of ocean water contains approximately 33 g of $^2$D. Since the volume of oceans is of the order of $10^{18}$ m$^3$, the potential reserve of deuterium amounts to $10^{19}$ g. With today's energy consumption, this represents hundreds of billions years [9]. Indeed, although the energy released by the fission reaction (1.1) is roughly 12 times more than the fusion reaction (1.2), it also involves a reactant with 47 times more nucleons. Hence, even by accounting for the difference of binding energies, the resulting energy density per unit mass of fuel is lower. More precisely, 1 g of DT releases roughly 337 GJ, which is obtained with 674 g of natural uranium, or with 7.5 tons of petroleum [13]. The extraction process of deuterium, an isotopic separation, already exists at an industrial stage since heavy water is used to moderate neutrons in fission nuclear plants. Tritium, however, does not exist on earth as being radioactive with an half-life of $12,3$ years. The considered solution, in the design of the future fusion nuclear plants, is to produce $^3$T inside the reactor chamber by covering its walls with a lithium blanket. The neutron streams released by the fusion reactions may cross it and produce tritium according to

$$^1\mathrm{n} + {}^6\mathrm{Li} \rightarrow {}^3\mathrm{T} + {}^4\mathrm{He}.$$

Lithium is abundant on earth. However, this reaction has a significant cross section for thermal neutrons only. Unfortunately, the cross section of the reaction with $^7$Li, the most abundant isotope, is about four orders of magnitude lower. Therefore, neutrons must be slowed down by a moderator media. As in fission nuclear plants, the deposited energy may be used to heat a calorific fluid in order to extract power. However, these neutrons, created through reaction (1.2), are seven times more

energetic than those coming from the fission of $^{235}$U. They knock atoms out of their usual lattice positions, causing swelling and fracturing of the blanket structure. They activate material, producing radioactive wastes. It is worth mentioning, however, that their half-lives are much lower than those resulting from fission. In any case, such problems are still subjected to intense research [14].

It clearly appears that a fusion reaction with no neutrons produced would be desirable. For this purpose, the most promising reactions are $^{1}\mathrm{p}+^{11}\mathrm{B} \rightarrow 3\ ^{4}\mathrm{He}$ and $^{2}\mathrm{D} + ^{3}\mathrm{He} \rightarrow ^{1}\mathrm{p} + ^{4}\mathrm{He}$. Since they release charged edifices, a non-thermal energy conversion is even conceivable, avoiding the limitation imposed by the Carnot's efficiency. The main problem of both these reactions is that their cross sections, plotted in Fig. 1.2, only become appreciable for temperature above 100 keV$/k_B$ and 50 keV$/k_B$ respectively. In addition, the usage of the DHe fuel would have two drawbacks. It would be responsible for a small production of neutrons through satellite reactions, and $^{3}$He is rare on earth. Exploiting the reserves on the moon is possible, but the financial viability of this option can raise some doubts. On the contrary, $^{11}$B is abundant, and the difficulty for a nuclear plant based on proton-boron fusion lies elsewhere. For a given ion thermal energy, $k_B T_i$, the fraction of borons with an energy higher than $\epsilon_5 = 0.3$ keV, the ionization energy associated to the fifth electrons of $^{11}$B, is

$$\frac{2}{\pi^{1/2}} \int_{\epsilon_5}^{\infty} e^{-\epsilon/(k_B T_i)} \frac{\epsilon^{1/2} d\epsilon}{(k_B T_i)^{3/2}}.$$

This integral is equal to 98.7% for $k_B T_i = 4.4$ keV, the Post's temperature in case of a deuterium-tritium plasma. For higher temperatures, necessarily required, it is therefore reasonable to consider that all borons within the plasma have lost all their five electrons. In that case the bremsstrahlung power emitted from a proton-boron plasma is $5^2 = 25$ times greater than in the case of a deuterium-tritium plasma with the same electron density and temperature. Concerning the reaction rate per unit volume of the former, it is five order of magnitude weaker than the latter. These two reasons make the ignition of a pB fuel at thermal equilibrium extremely unlikely.

Faced with such a severe conclusion, a quite natural idea is to explore the effect of sustaining the burning plasma in an out-of-equilibrium state, the nature of which is suggested by the will to maximize $P_\alpha/P_B$. As already mentioned, the energy carried by the alpha particles is mainly transferred to the electrons, which are responsible for the bremsstrahlung emissions, before being in turn released to the ions, responsible for the fusion reactions. This two steps clearly make the self-heating less effective. As a result, the exploitation of any mechanism of energy transfer avoiding to heat the electrons would be welcome. This would mean maintaining the plasma in a state where $T_e \ll T_i$. Going further, an exponential distribution of ion energies does not seem optimal. There, most of the energy is carried by thermal ions not giving rise to many fusion reactions, instead of being concentrated around those with energies close to the value at which the maximum of the reaction rate occurs. Regardless of the practical ways by which these kinds of disequilibrium might be sustained, they corresponds to certain re-arrangements in the phase space. These are opposing the spontaneous trend toward equilibrium, and therefore represent a certain cost. It can be estimated, as done by Rider

[15]. His conclusion is harsh: the power required to maintain any of these out-of-equilibrium states will always be much larger than the power released by the fusion reactions themselves. Obviously, this assessment is not definitive as being based on assumptions which can be discussed, as Rider himself admits. Because of its enormous attractiveness to ensure viable electricity production, research into proton-boron fusion has never stopped. It has even intensified in recent years. The renewed interest is partly due to a novel estimate of the reaction cross section [16], which turns out to be larger than previously thought. Nevertheless, the review of the latest results in this area would lead us too far.

Nowadays, the fusion sector is extremely active. Motivated by the constant progresses made by the most advanced facilities, many private companies are created [17, 18]. The underlying machines they wish to build do not have a unique design, but reflect the wide range of technologies through which the Lawson's criterion can be fulfilled. These investments also involve academic researchers, whose expertise is needed to help engineers handling the scientific issues inherent to controlled fusion [19]. Such a craze strengthens the community which, as a consequence, is expected to grow massively in the near future. This will make feasible the huge and coordinated effort required to push the development of a fusion nuclear plant at an industrial stage.

## 1.2 Inertial fusion by lasers

### 1.2.1 Overview

Aside from military applications, inertial confinement fusion (ICF) [3, 20, 21] aims at providing energy through a pulsed regime of successive explosions. Each of them is the thermonuclear burn of a spherical pellet of fuel. In order to not put too much strain on the reactor vessel, the energy released per explosion is chosen to not exceed a few hundred megajoules. This implies to operate with pellets of no more than few milligrams in case of a DT mixture as fuel. Consequently, around one gigawatt might be expected from the underlying facility if it achieves roughly ten burns per second. Unlike in magnetic machines, there is no device here to contain the fuel: it burns as long as its inertia allows it to remain assembled despite its own pressure. The burned fraction per explosion is roughly

$$\Phi_B = \frac{\rho R}{\rho R + H_B},$$

where $\rho$ is the average mass density of the fuel, $R$ the radius of the spherical pellet and $H_B = 8mc_s/\langle\sigma_{DT}v\rangle$ is a function of the temperature with $m = \rho/n$ the average ion mass and $c_s = (\gamma k_B T/m)^{1/2}$ the sound speed within the fuel, with $\gamma$ the corresponding heat capacity ratio. For temperature ranging from 20 to 80 keV/$k_B$, $H_B$ is approximately constant, equals to 6 g/cm$^2$. Given the expected efficiency of the whole chain of energy conversion, $\Phi_B \geq 1/3$ is required to obtain a sufficiently high gain factor of few hundreds. This corresponds to

$$\rho R \geq 3 \text{ g/cm}^2.$$

Since $\rho R = [3/(4\pi)]^{1/3} M^{1/3} \rho^{2/3}$, any attempt to exceed such a threshold for a given mass, $M$, of few milligrams necessitates to compress the fuel at a mass

density exceeding a thousand times that of solid DT at 300 K. This can be driven by a short pulse of radiation illuminating the spherical pellet. The outer part of it, the ablator, absorbs the incident energy, heats up intensely until it evaporates in the form of an expanding plasma. The reactive impulse associated to it creates a pressure up to few hundreds gigabars on the inner part of the pellet causing its implosion at a radial velocity of several hundreds kilometers per second.

Without any precautions, however, the strong compression would result in the generation of an high amplitude shock wave propagating inside the reacting medium. It would cause the irreversible heating of the fuel, preventing its further compression due to the associated increase of the internal pressure. Thus, the implosion must be nearly isentropic. Only after its achievement, the rise of the fuel temperature required to satisfy the Lawson's criterion should be triggered. Such an endeavour requires to carefully design the structure of the spherical pellet, together with the temporal shape of the illuminating pulse. For that purpose the conventional method in ICF is the *hot-spot ignition* scheme [22].

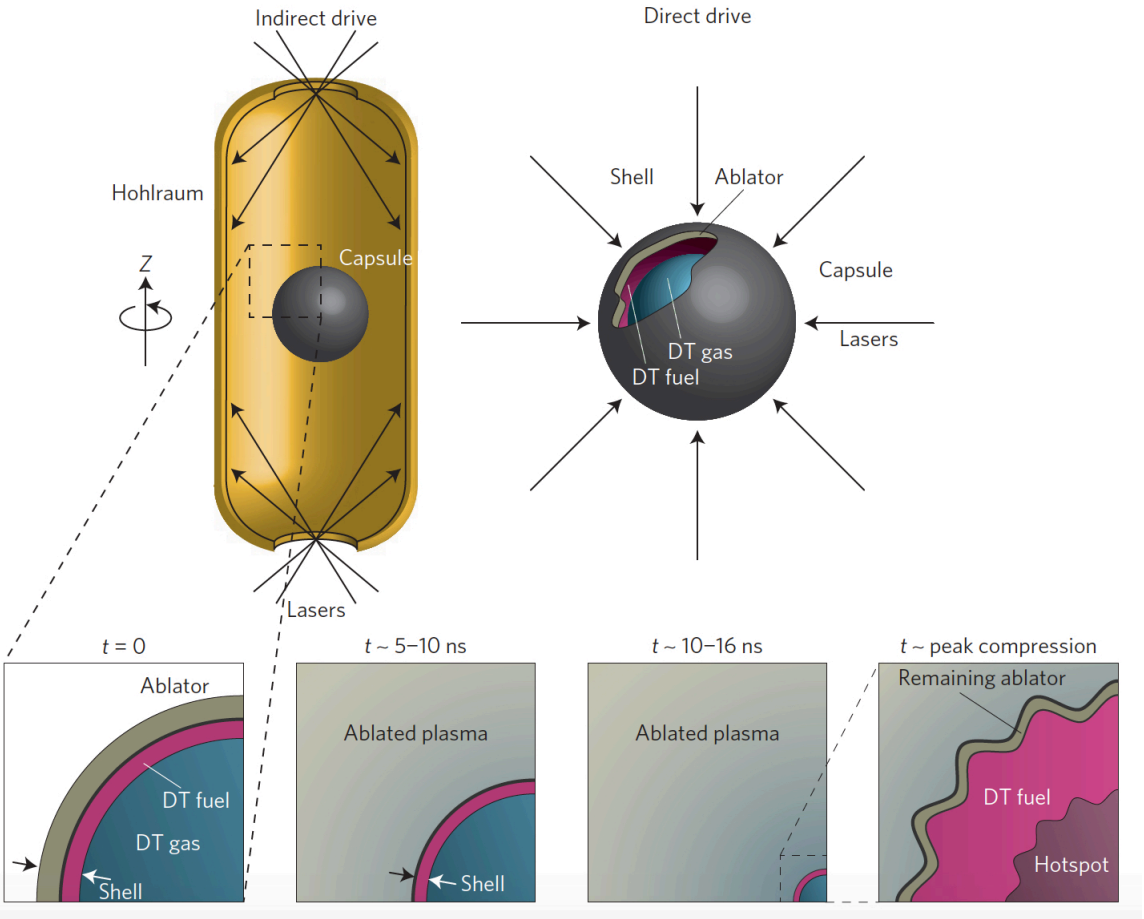


Figure 1.3: Indirect (left) and direct (right) drive configurations of the laser beams used to implode the capsule of fuel. After about ten nanoseconds, the compression phase ends, triggering the hot spot formation (below). Extracted from [21].

The architecture of the fuel target is visible in Fig. 1.3. It is constituted by a thin layer of cryogenic DT, surrounding a spherical cavity with a radius of about 1 mm filled with 10 $\mu$g of DT gas at a concentration just below 5 $\mu$g/mm$^3$. Given the heat

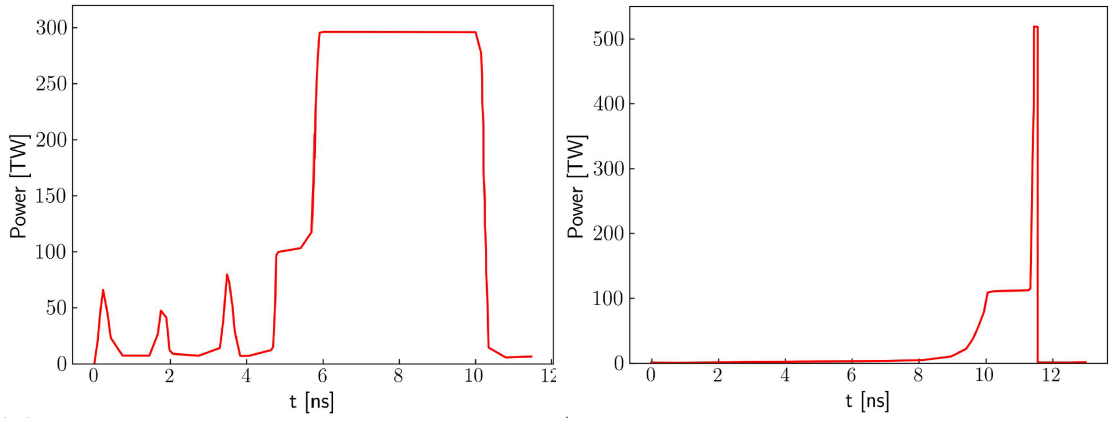


(a) (b)

Figure 1.4: Profiles of the lasers pulse in the (a) hot-spot and (b) shock ignition schemes, as they are described in Refs. [23] and [24] respectively. To be comprehensive, they must be considered together with the specific designs chosen for the capsules. For that purpose the reader is referred to the aforementioned articles. Extracted from [25].

capacity of the hydrogen gas, the energy required to raise these few micrograms at an ignition temperature of, say, 10 keV/$k_B$ is roughly 16 kJ. Then, the resulting hot spot radially extends itself in the form of a burn wave propagating within the surrounding cold fuel, through the energy deposition of the alpha particles released by the fusion reactions. The supply of energy to ensure its initial formation is provided by the imploding shell. While the majority of its kinetic energy serves as mechanical work required to perform the implosion, the remaining 20 % is converted into internal energy, almost entirely at the end of the compression phase. The invested energy from the shell is therefore around 80 kJ. Since its mass is about 1 mg, this corresponds to an implosion velocity of 400 km/s. By accounting for the efficiency of the radiation absorption together with that of the generation of the ablation pressure, only a maximum of 8 % of the driving energy is converted into kinetic energy. Hence, it must deliver at least 1 MJ to accelerate the shell. At a mean velocity of, say, 100 km/s, it takes around 10 ns to reduce the radius of the capsule by the desired factor, greater than 10. Given the aforementioned minimum energy of the incident radiation flux, the underlying driver therefore generates an average power of more than 100 TW. This corresponds to an irradiance exceeding 10 TW/mm$^2$ distributed on the entire surface of the pellet. Such high values are accessible to lasers.

Currently, these are mostly neodymium glass lasers delivering ultraviolet pulses at a wavelength of 351 nm with an energy slightly below 10 kJ. Thus, a few hundreds of beams are needed to deliver the required driving energy. They can either be used in the direct or indirect drive configurations, both illustrated in Fig. 1.3. In the latter, the laser beams irradiate the inner walls of a gold enclosure called the *hohlraum*. The created high-Z plasma, with a temperature of few hundreds of eV/$k_B$, emits X-rays illuminating the target, with a spectrum of emission following the Stefan-Boltzmann's law. Compared to the direct drive approach, a part of the laser's driving energy is lost, but the resulting irradiance is more uniform. This,

in particular, minimizes the growth of the hydrodynamic instabilities associated to the surface defects of the capsule. These might be responsible for the severe degradation of the compression by breaking the implosion symmetry. Unfortunately, they are also more likely to develop for an high implosion velocity, which turns out to be necessary here to reach ignition since the major source of the hot spot's internal energy is the mechanical one carried by the shell. In fact, such an issue can be overcome by using the *shock ignition* scheme [26, 24].

As it is visible by comparing Figs. 1.4a and 1.4b, this approach differs from hot spot ignition by the temporal shape of the underlying lasers pulse. In both schemes, the first few nanoseconds consist of a low intensity pre-pulse, either constant or constituted by a succession of pickets, intended to accelerate the capsule without increasing too much the entropy of the fuel. In case of no power modulation, during this phase the laser launches a primary shock wave within the ablator which propagates through the ice by compressing it, until the inner surface of the shell where it breaks. There, the rear target interface abruptly starts to move forward, generating a concentric shock in the gas while leaving within the ice a rarefaction wave moving outward. When the latter reaches the ablation front, it is reflected inward as a shock wave with smaller amplitude, further accelerating the shell. This scenario repeats itself several times. The interest of power modulation like that visible in Fig. 1.4a is to make the fuel compression as close as possible to an ideal isentropic process. Here, the laser pickets are carefully timed to launch shock waves coalescing near the ice/gas interface forming a single discontinuity front [23]. Just before the primary compression front breaks out into the gas, the laser power rises suddenly up to a plateau value, generating a stronger secondary shock front that merges with the previous one. By doing so, the shell closely follows the shock front propagating within the vapour.

In the hot spot ignition scheme, the reached power is maintained constant until the laser is turned off. This marks the end of the acceleration phase of the shell, which then travels at constant velocity before being decelerated. This latter phase starts when the concentric shock bounces back at the center of the capsule, heads towards the incoming shell until reaching its inner part. Then, the shock experiences a series of reflections and bounces, decaying its amplitude while impulsively braking the shell. Before its complete stopping, the latter acts like a spherical piston on the vapour within which the pressure is almost uniform. The hot spot gradually forms, seeing its temperature and density increased by the mechanical work it undergoes. This leads to ignition, followed by the burning wave through the compressed ice fuel. In the shock ignition approach, the pre-pulse intensity is one to two orders of magnitude weaker, and the plateau value, about a third of that used in the hot spot ignition scheme. As a result, the velocity of the shell there is only about 200 to 300 km/s. Its implosion is more stable, but its kinetic energy is insufficient to trigger the thermonuclear burn. In fact, this is achieved thanks to an high intensity spike at the very end of the pulse. It launches a strong shock aimed at colliding with the outward bouncing shock that started the shell's deceleration. The collision takes place in the dense ice near the interface with the gas. The inward moving shock generated by it leads to a further compression of the hot spot and to a peaked pressure distribution at its center. This non isobaric configuration lowers the ignition threshold while requiring less input laser energy to be created.

In combination with the direct drive configuration, the shock ignition scenario appears to be one of the most promising choices for a potential thermonuclear plant [27].

After the recent milestones achieved by the NIF, inertial fusion by lasers is entering a new era. The second largest facilities, the Laser Mégajoule (LMJ), is now for sure commissioned to deliver more than 1 MJ by 2030 [28]. However, the experiments performed in these infrastructures are mostly dedicated to military applications and, as a consequence, have designs that do not allow to fully investigate the issues related to commercial fusion. For that purpose, the scientific community needs the construction of a megajoule-scale facility dedicated to it. In Europe the underlying research program is already mature [29] but is waiting for an audacious political decision to fully take place.

### 1.2.2 Focus on heat transport within the ablative flow

Whatever the nature of the driving configuration, the ablative flow has, under several assumptions precised later, the structure illustrated in Fig. 1.5 [30, 31]. The irradiation flux propagates from the left to the right within the interaction region until the critical surface at the vicinity of which it deposits its energy. Mostly carried by electrons for not too high values of $Z$, the former then crosses the conduction region to reach the ablation layer, the region where the plasma is created. The recoil associated to its expansion is responsible for the compression region which extends to the shock front.

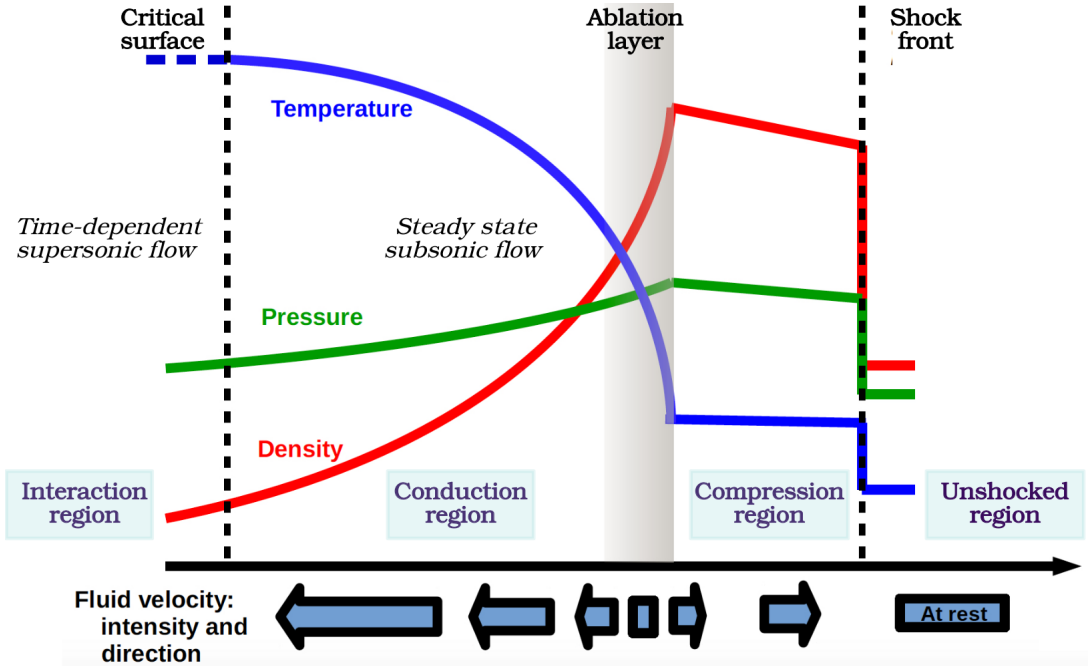


Figure 1.5: Schematic structure of the ablative flow. Adapted from [32].

The critical surface, where the electron density reaches the threshold value beyond which the light cannot propagate, turns out to be a sonic point separating two regimes of flow connected by the Chapman-Jouguet's condition. The underdense side consists of an almost isothermal rarefaction wave. Within such a time-dependent supersonic flow, the propagation of the incident light is almost devoid of

non localized absorption by inverse bremsstrahlung. On the contrary, the transfer of energy to electrons is supposed to occur at the entrance of the dense region. One quarter is converted into outward heat flux which prevents the corona to cool down in spite of its expansion. The remaining three quarters constitutes the inward heat travelling within the conduction zone. It serves to ablate the cold material whose subsonic flow carries an outward flux of kinetic energy and enthalpy. For negligible preheating of the ablation layer, these opposite fluxes compensate so that the conduction region is in a steady state.

This picture relies on many approximations. As it is well known, a weakly-out-equilibrium plasma is characterized by local distribution functions of electrons and ions close to that of Maxwell-Boltzmann. Because the latter is completely specified by its first three velocity moments, the deviation from global equilibrium is described satisfactorily, for any species $s$ of charge $q_s$, by the set of equations governing the evolution of these moments, which are the density $n_s$, the mean velocity $\mathbf{u}_s$ and the temperature $T_s$. Written in a Galilean frame of reference, such macroscopic equations are [33], without external source terms:

$$\partial_t n_s + \boldsymbol{\nabla} \cdot n_s \mathbf{u}_s = \mathbf{0},$$

$$\partial_t n_s m_s \mathbf{u}_s + \boldsymbol{\nabla} \cdot \mathsf{P}_s = q_s n_s (\mathbf{E} + \mathbf{u}_s \times \mathbf{B}) + \sum \mathbf{R}_{ss'},$$

and

$$\partial_t \left( \frac{3}{2} p_s + \frac{1}{2} n_s m_s u_s^2 \right) + \boldsymbol{\nabla} \cdot \left[ \mathbf{q}_s + \left( \frac{5}{2} p_s + \frac{1}{2} n_s m_s u_s^2 \right) \mathbf{u}_s + \mathsf{\Pi}_s \cdot \mathbf{u}_s \right] = q_s n_s \mathbf{E} \cdot \mathbf{u}_s + \sum \mathbf{W}_{ss'},$$

where $\mathsf{P}_s = n_s m_s \mathbf{u}_s \otimes \mathbf{u}_s + p_s \mathsf{I} + \mathsf{\Pi}_s$ is the pressure tensor in which there appears the scalar pressure $p_s = n_s k_B T_s$ and the stress viscosity tensor

$$\mathsf{\Pi}_s = \int f_s m_s \left( \mathbf{w} \otimes \mathbf{w} - \frac{w^2}{3} \mathsf{I} \right) \, d^3\mathbf{w},$$

with $\mathbf{w} = \mathbf{v} - \mathbf{u}_s$, $\mathbf{v}$ being the velocity variable for the population $s$ and $f_s$ its distribution function. $\mathbf{E}$ and $\mathbf{B}$ are the self-consistent Vlasov's mean fields,

$$\mathbf{q}_s = \int \frac{m_s w^2}{2} f_s \mathbf{w} \, d^3\mathbf{w}$$

is the heat flux density. Finally, $\mathbf{R}_{ss'}$ and $\mathbf{W}_{ss'}$ are the friction force per unit volume undergoes by the population $s$ and the algebraic energy per unit volume it gained due to collisions with species $s'$. They are respectively proportional to the difference in mean velocities and temperatures between the populations $s$ and $s'$. Hence, for each species $s$ the set of equations is closed if the components of $\mathsf{\Pi}_s$ and $\mathbf{q}_s$ are functions of only the first three velocity moments $n_s$, $\mathbf{u}_s$ and $T_s$. This is considered to be the case for a plasma in a weakly out-of-equilibrium state, as it is assumed within the framework leading to the structure illustrated in Fig. 1.5. The underlying approach goes even further by neglecting the magnetic field effect together with the disparity between the dynamics of electrons and ions. They

are supposed to behave at unison forming a neutral fluid whose movement is governed by macroscopic equations [30, 31] having almost the same structure as those written above. Within them in particular, the inertial terms associated with the non-Galilean character of the implosion capsule's frame of reference are neglected. It is well justified since these are first order corrections in the small parameter equals to the ratio of the mass of the corona to the mass of the shell.

Nevertheless, the interplay between the mean fields' behaviours and the flow is not accounted for. The latter is assumed to be planar, although effects associated to the curvature of the capsule must be expected [34]. Last but not least, the Fourier's law is used for modelling heat flux density, mostly carried by electrons. Unfortunately, it is not accurate as there are several sources of disequilibrium inducing a significant deviation of the local electron distribution function from that of Maxwell-Boltzmann [35]. The distortion is caused by two kinds of mechanisms. The first one regroups processes associated to the nonlinear interaction of the incident light with the plasma. These are parametric instabilities, resonant absorption and Langdon's effect [3]. Their descriptions are beyond the scope of this manuscript. The second kind of mechanism results from the steepness of the temperature gradient. It induces the leakage by diffusion of electrons from hot regions towards colder ones within which they are weakly coupled to plasma. These phenomena modify the macroscopic behaviour of the plasma and, as a consequence, the overall structure of the ablative flow is altered. In principle, they would require a kinetic description. This, as it is well known, is computationally too demanding on the scales associated to the implosion process [36]. The development of alternative paradigms is necessary.

The nonlocal hydrodynamic approach reviewed by Brantov and Bychenkov [37, 38] provides a closure to hydrodynamic equations - through mean fields, heat flux density and stress viscosity tensor [33] - while being precise enough in order to account for the effects of kinetic processes at a macroscopic level. It is, however, limited to weakly inhomogeneous plasmas. This means that the variations of hydrodynamic profiles are supposed to be small compared to their mean values over space, without, however, any restriction on the steepness of their gradients with respect to the electron mean free path [39]. This situation is encountered in the under-dense region where laser speckles produce localized small-amplitude perturbations of density and temperature in the plasma [40]. Their evolution is fast at the temporal scale defined by collision frequencies, resulting in pulsation-dependent transport coefficients expressed in Fourier's space. However, the approach of Refs. [37, 38] fails in the conduction zone or within the burning fuel. In these regions the existence of large variations of hydrodynamic profiles necessitates a kinetic treatment of electron transport. To accommodate the detail of the kinetic processes over macroscopic scales in a practical way, a *reduced* kinetic model may be constructed. It is aimed at being coupled to macroscopic equations by providing an approximate microscopic state associated to the macroscopic constraints of density, mean velocity and temperature. The utility of such an approach must strike a balance between numerical implementation efficiency and the requirements that both the electron distribution function and the self-consistent mean fields be accurately represented.

In this thesis, we only explore a part of such a vast problem. Our main concern is the proper description of the electron heat flux density induced by a steep temperature gradient within a one-dimensional, unmagnetized plasma. Although the effects of the magnetic field are determinant in the transport mechanism, its account would add considerable technical difficulties to those we will already face. Our undertaking will be accompanied by an analysis of the underlying distribution functions, the necessity of which must be attributed to the need for estimating the potential of an approach to satisfy the ambitious program described above. Throughout the manuscript, numerical comparisons will be made in the case of a temperature profile close to that existing in the conduction region of Fig. 1.5. Along the $z$-axis, it will be initially of the form [41]

$$T_e(z) = T_H - \frac{(T_H - T_C)}{2}\Big(1 + \tanh[s(z - z_0)]\Big), \tag{1.3}$$

with $T_H > T_C$. Hence the profile is such that $T_e(z_0) = (T_H + T_C)/2$. For $z \ll z_0$, $T_e(z) = T_H$, whereas for $z \gg z_0$, $T_e(z) = T_C$. Depending on the steepness of the gradient, the temperature may have changed by the time the codes are compared. This subtlety will be further precised in due course.

## 1.3 Outline of the manuscript

The manuscript contains three main chapters. Two of them are accompanied with two appendices. These should not be considered optional; they are set aside because they contain long developments which would have weighed down the text too much and, consequently, obscured the guideline. Some complementary notes can be found at the end of the manuscript, after the bibliography. They intend to satisfy the curious reader about some points mentioned in the body text.

The Chap. 2 constitutes a state-of-the-art. It presents the problem of describing heat transfer in a plasma whose temperature evolution is slow compared to the establishment of the electron flux density. Under this quasi-static approximation the starting point for studying the question is the stationary Vlasov-Landau's kinetic equation, whose theoretical foundations are discussed in the App. 2.A. Depending on the steepness of the electron temperature profile, two transport regimes are distinguished. The local one, for which the Fourier's law provides a satisfying modeling, and the nonlocal one, for which this is not the case. Although the transition from one regime to another occurs continuously as the gradient increases, the mathematical treatment of nonlocal transport is only possible by abandoning the local thermodynamic equilibrium hypothesis. The kinetics of the electrons responsible for the disequilibium can be described by an operator, reviewed in the App. 2.B, whose more or less simplified forms serve as a basis for most of the approaches to nonlocal electron heat transport. These are exposed with the aim of bringing out a guiding thread justifying the transition from one to the other.

The model of interest in this thesis is examined from a physical point of view in Chap. 3. It provides a reduced kinetic description through a set of two partial differential equations whose unknowns are components of the electron distribution function on a certain basis. This strategy reflects a will opposed to that animating

the formulation reviewed in the Complementary Note 6.1, which aims at integrating the kinetic equation as accurately as possible. Unlike what may have been the case for decades, here the approach does not consist of obtaining an explicit formula of the heat flux density by approximately solving the coupled equations. Their solutions are obtained by a direct numerical integration. The system draws its specificity from a particular choice of the operator modeling collisions among electrons. The hypothesis leading to it are highlighted with an original examination of their effects on the distribution function. By doing so an important improvement of the collision operator is proposed. New behaviors of the resulting model are found based on analytical calculations and numerical observations. Some qualitative interpretations are echoing a mathematical study reviewed and deepened in the Complementary Note 6.2. Almost all the results of this chapter are published in our article [42].

The issues related to the numerical implementation of the model are addressed in Chap. 4. The scheme exploits the hyperbolic nature of the system of partial differential equations, which is derived in the App. 4.A in a refreshing manner. A new analysis of its characteristics provides a qualitative understanding of the limitations of schemes previously proposed in the literature, as well as a quantitative criterion giving their range of applicability. The latter is restricted by the steepness of the electron temperature profile. Our method, whose framework is presented in the App. 4.B, extends these works to an arbitrary degree of disequilibrium. Its success relies on a time marching strategy to estimate the stationary solutions, the efficiency of which comes from the use of a non-uniform and non-stationary time step. Although there is no formal proof of convergence of the resulting algorithm, it is shown that the error with respect to the numbers of cells behaves as expected. The performances, as well as a potential coupling to a hydrodynamic code are discussed at the end of the chapter, where an original analysis of the conservation properties of the model is made. Our article [43] brings together all these results.

This page is unintentionally left not blank.

# Chapter 2

# State-of-the-art on quasi-static nonlocal electron heat flux

All along this manuscript, we consider a weakly coupled, fully ionized and unmagnetized plasma with a ionization number $Z$. The used reference frame - supposed Galilean - is the one moving at the mean velocity of ions, the inhomogeneities of which are supposed small compared to its mean value over space. In this reference frame, the electron mean velocity is $\mathbf{u}_e = \mathbf{0}$ as their macroscopic flow is supposed to be adiabatically attached to ions due to the ambipolar field. The electron temperature, $T_e$, is monotonically decreasing from a hot region with temperature $T_H$ to a cold one with temperature $T_C$. The problem is treated in the quasi-static approximation, relevant within the conduction region [44, 45]. This means that we are examining the stationary kinetic state reached in the presence of fixed hydrodynamic constraints. The delayed response of electrons to changing macroscopic conditions is a third order correction in the Chapman-Enskog's expansion, the principle of which will be recalled later. This statement is shown by Brodrick *et al* in the reference mentioned above. The electron distribution function $f_e(\mathbf{r}, v, \mathbf{\Omega})$ thus obeys the stationary kinetic equation:

$$\begin{aligned} v\,\mathbf{\Omega}\cdot\boldsymbol{\nabla} f_e - e\mathbf{E}/m_e\cdot[\mathbf{\Omega}\,\partial_v f_e + (\mathsf{I}-\mathbf{\Omega}\otimes\mathbf{\Omega})/v\cdot\partial_{\mathbf{\Omega}} f_e] \\ = \mathcal{C}_{ei}[f_e, f_i] + \mathcal{C}_{ee}[f_e, f_e], \end{aligned} \tag{2.1}$$

where the electron-ion, $\mathcal{C}_{ei}$, and electron-electron, $\mathcal{C}_{ee}$, collision operators are Landau's integrals [46], $v$ is the absolute value of the electron velocity, $\mathbf{\Omega} = (\Omega_x, \Omega_y, \Omega_z)$ is the unit vector in the velocity direction, $-e$ and $m_e$ are the electron charge and mass, and $\mathbf{E}$ is the self-consistent electric field. This equation, reviewed in the App. 2.A, here describes the distribution function associated to the diffusion of electrons driven by a temperature gradient. For the purpose of determining the heat flux density on the macroscopic domain of the temperature variation, it must be solved in an approximate manner.

This chapter presents the main approaches to handle this endeavour. In Sec. 2.1, the phenomenology of the heat transfer in a zero-current-carrying plasma is recalled, with emphasis on the interplay between the heat flux density and the electric field. For a smooth enough temperature gradient, the Fourier's law is verified, with a thermal conductivity which depends on $Z$ in a non-trivial way.

This results from the competition between electron-electron and electron-ion collisions during the diffusion process, as it is described in Sec. 2.2. The situation in which the Fourier's law fails is considered in Sec. 2.3. It corresponds to a temperature gradient whose high steepness induces the existence of a strongly out-of-equilibrium population of electrons. Their dynamics can be described by an approximate operator discussed in App. 2.B. With or without additional simplifications, it constitutes one of the starting points of many attempts to extend the Fourier's formula. These approaches roughly are of three kinds, which are successively considered on the basis of key papers while citing some of the most recent improvements.

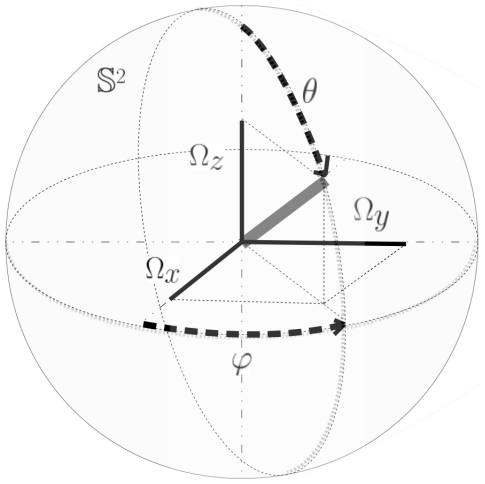


Figure 2.1: Scheme of the unit sphere $\mathbb{S}^2$. The Cartesian variables $(\Omega_x, \Omega_y, \Omega_z)$ are linked to the spherical coordinates $(\theta, \varphi)$ by: $\Omega_x = \sin\theta\cos\varphi$, $\Omega_y = \sin\theta\sin\varphi$ and $\Omega_z = \cos\theta$.

## 2.1 Thermoelectric effect: coupling of the heat flux density to the electric field

The electron mean free path in the hot region is by a factor $(T_H/T_C)^2$ greater than in the cold one. This produces a forward electron current in the direction opposite to the temperature gradient, $-\boldsymbol{\nabla} T_e$. As electrons are charged, such a diffusion is responsible for a space charge creating an electric field $\mathbf{E}$. This electric field both slows down forward-moving electrons and drives a return current of slow electrons in the direction of $+\boldsymbol{\nabla} T_e$. As $\mathbf{u}_e = \mathbf{0}$ everywhere in the plasma, these fluxes of electrons are locally opposed and $\mathbf{E}$ takes a value such that the electric current density

$$\mathbf{j}_e = -en_e\mathbf{u}_e = -\frac{4\pi}{3}\int_0^\infty ev\mathbf{f}_1 v^2 dv, \tag{2.2}$$

vanishes, where $\mathbf{f}_1$ is the integral of $3/(4\pi)\boldsymbol{\Omega} f$ over the unit sphere $\mathbb{S}^2$. Because the mean free path $\lambda_{ei}$ is a monotonically increasing function of the velocity, $\mathbf{f}_1$ has only one zero - say, at $v = v_1$ - and the forward current at any point of the plasma is composed by the fastest electrons with velocities greater than $v_1$. To ensure $\mathbf{j}_e = \mathbf{0}$, the sum of $v^3\mathbf{f}_1$ over velocities of the return current of electrons

- from 0 to $v_1$ - is thus the opposed to that of the forward current of electrons. Consequently, more electrons contribute to the return current. Being slower, the macroscopic gap to neutrality - over a distance larger than the Debye's length - persists consistently with the existence of the mean electric field $\mathbf{E}$.

However, this algebraic excess of electrons per unit of volume is negligible compared to the electron density $n_e$, which stays approximately equal to $Zn_i$ to high accuracy, where $n_i$ is the ion density. At equilibrium, the mean electric potential is constant: the polarization clouds within the whole plasma are statistically identical. As the Debye's length depends on electron density and temperature, in an out-of-equilibrium state these clouds have inhomogeneous sizes. They experience a velocity-dependent distortion associated to the opposite, macroscopic displacements of electrons belonging to forward and return currents. The combination of these two effects determines the spatial profile of $\mathbf{E}$ [47]. This aspect will be discussed later.

As the integrals of $v^3\mathbf{f}_1$ over the velocities of forward and return electron currents compensate each other, it cannot be the case for integrals of $v^5\mathbf{f}_1$. This results in a nonzero heat flux density

$$\mathbf{q}_e = \frac{4\pi}{3}\int_0^\infty \frac{m_e v^2}{2} v\mathbf{f}_1 v^2 dv, \tag{2.3}$$

directed from the hot to the cold region. This phenomenological description emphasizes the importance of simultaneous evaluation of $\mathbf{q}_e$ and $\mathbf{E}$.

## 2.2 Local regime

For smooth temperature gradients, the electron distribution function is weakly perturbed: its isotropic part $f_0$, defined as the integral of $f_e/(4\pi)$ over the unit sphere $\mathbb{S}^2$, is close to the local Maxwellian distribution function [48],

$$f_M = \frac{n_e}{(2\pi)^{3/2} v_T^3} e^{-v^2/2v_T^2}, \tag{2.4}$$

where the electrostatic potential is accounted for implicitly in $n_e$, given by the Boltzmann's law. Although the isotropic part is specified, it remains to analyse the anisotropic part of the distribution function. Its behaviour depends in particular on the ionization number $Z$, which sets the relative importance of collisions between electrons and ions compared to those among electrons. In Sec. 2.2.1, the operator describing the former is presented, before discussing in Sec. 2.2.2 the possible families of its eigenfunctions over which the electron distribution can be expanded. As it will be justified, not all the terms are of interest, and the mathematical procedure to limit the study on the first few of them is exposed. The formulae for $\mathbf{q}_e$ and $\mathbf{E}$ are finally written in Sec. 2.2.3 for an arbitrary value of $Z$. They are accompanied by a physical interpretation which describes, among other points, how the influence of electron-electron collisions have been handled.

### 2.2.1 High-$Z$ limit: dominance of electron-ion collisions

The anisotropic part of the electron distribution function mainly depends on collisions with momentum exchanges. For this reason the problem of determining

both the heat current density $\mathbf{q}_e$ and the electric field $\mathbf{E}$ can be solved analytically to high accuracy in the high-$Z$ limit, because electron-ion collisions dominate. Indeed, the electron-ion Landau's integral is by a factor $n_i Z^2 \ln\Lambda_{ei}/[n_e \ln\Lambda_{ei}] \simeq Z$ greater than the electron-electron Landau's integral, where $\ln\Lambda_{ei}$ and $\ln\Lambda_{ee}$ are the Coulomb's logarithms related to electron-ion and electron-electron collisions, respectively. With Einstein summation convention over the repeated index $k$ and $l$, the former is:

$$\begin{aligned}\mathcal{C}_{ei}[f_e, f_i] &= -\frac{Y_{ei}}{m_e}\frac{\partial}{\partial v_k}\int U_{kl}(\mathbf{v}-\mathbf{v}')\left(\frac{f_e}{m_i}\frac{\partial f_i}{\partial v'_l} - \frac{f_i}{m_e}\frac{\partial f_e}{\partial v_l}\right) d^3\mathbf{v}' \\ &= \frac{Y_{ei}}{m_e^2}\frac{\partial}{\partial v_k}\left[\left(\int U_{kl}(\mathbf{v}-\mathbf{v}')f_i d^3\mathbf{v}'\right)\frac{\partial f_e}{\partial v_l} - \frac{m_e}{m_i}f_e\left(\int U_{kl}(\mathbf{v}-\mathbf{v}')\frac{\partial f_i}{\partial v'_l}d^3\mathbf{v}'\right)\right],\end{aligned} \tag{2.5}$$

where the integration is done over the whole velocity space. $U_{kl}(\mathbf{v}-\mathbf{v}')$ is the $kl$-component of the Landau's kernel tensor:

$$U_{kl}(\mathbf{w}) = \frac{1}{w}\left(\delta_{kl} - \frac{w_k w_l}{w^2}\right), \tag{2.6}$$

evaluated at $\mathbf{v}-\mathbf{v}'$. Within Eq. (2.1), the $(v, \mathbf{\Omega})$-variables are used. Hence, the differential operator $\partial/\partial\mathbf{v}$ in Eq. (2.5) must be understood as $\mathbf{\Omega}\partial_v + (\mathsf{I} - \mathbf{\Omega}\otimes\mathbf{\Omega})/v \cdot \partial_{\mathbf{\Omega}}$, and the measure $d^3\mathbf{v}' = dv'_x dv'_y dv'_z$ should be read as $v'^2 dv' d^2\Omega'$, where $d^2\Omega'$ is the usual volume form induced by the Riemannian metric of $\mathbb{S}^2$. The author would be grateful if the reader forgives him these kind of abuses concerning notations. They avoid to write long expressions unnecessarily weighing down the formulae. Finally, $Y_{ei} = Z^2 e^4 \ln\Lambda_{ei}/(8\pi\epsilon_0^2)$, where $\epsilon_0$ is the dielectric permittivity of the vacuum.

Due to the small ratio of masses between electron and ion, $\mathcal{C}_{ei}[f_e, f_i]$ can be approximated by a convenient form. For sufficiently regular distribution functions, the term proportional to $m_e/m_i$ in Eq. (2.5) can be neglected, such that:

$$\mathcal{C}_{ei}[f_e, f_i] \simeq \frac{Y_{ei}}{m_e^2}\frac{\partial}{\partial v_k}\left(\int U_{kl}(\mathbf{v}-\mathbf{v}')f_i \; d^3\mathbf{v}'\right)\frac{\partial f_e}{\partial v_l}.$$

The electron thermal velocity is by a factor $[m_i T_e/(m_e T_i)]^{1/2}$ greater than the ion thermal velocity. For ion temperatures, $T_i$, that do not exceed 18 $T_e$, this ratio stays greater than 10, and is equal to 43 for equal temperatures. Therefore, the extension of $f_i$ along the velocity axis is much smaller than that of $f_e$. It will be neglected by supposing $f_i \simeq n_i\delta$, such that:

$$\int U_{kl}(\mathbf{v}-\mathbf{v}')f_i \; d^3\mathbf{v}' \simeq n_i U_{kl}(\mathbf{v}).$$

Hence, the electron-ion collision operator is equal to $n_i Y_{ei}/m_e^2$ multiplied by:

$$\begin{aligned}\frac{\partial}{\partial v_k}U_{kl}\frac{\partial f_e}{\partial v_l} &= \frac{\partial}{\partial v_k}\frac{1}{v^3}(v^2\delta_{kl} - v_k v_l)\frac{\partial f_e}{\partial v_l} \\ &= \frac{1}{v^3}\frac{\partial}{\partial v_k}(v^2\delta_{kl} - v_k v_l)\frac{\partial f_e}{\partial v_l} - \frac{3v_k}{v^5}(v^2\delta_{kl} - v_k v_l)\frac{\partial f_e}{\partial v_l}.\end{aligned}$$

The second term is zero because

$$v_k(v^2\delta_{kl} - v_k v_l) = 0,$$

and the first one is $1/v^3$ multiplied by:

$$\begin{aligned}\frac{\partial}{\partial v_k}v_m v_m\frac{\partial f_e}{\partial v_k} - \frac{\partial}{\partial v_k}v_k v_l\frac{\partial f_e}{\partial v_l} &= \delta_{km}v_m\frac{\partial f_e}{\partial v_k} + v_m\frac{\partial}{\partial v_k}v_m\frac{\partial f_e}{\partial v_k} - \delta_{kl}v_k\frac{\partial f_e}{\partial v_l} - v_l\frac{\partial}{\partial v_k}v_k\frac{\partial f_e}{\partial v_l}\\ &= (\delta_{mk}\delta_{nl} - \delta_{ml}\delta_{kn})v_m\frac{\partial}{\partial v_n}v_k\frac{\partial f_e}{\partial v_l}\\ &= \epsilon_{pmn}v_m\frac{\partial}{\partial v_n}\epsilon_{pkl}v_k\frac{\partial f_e}{\partial v_l} = -\mathsf{L}^2 f_e,\end{aligned}$$

where $-\mathsf{L}^2$ is the negative of the square of the quantum angular momentum operator in velocity space. It is equal to the angular part of the Laplacian. As shown at the end of the App. 2.B, it takes the following form in the $(v, \mathbf{\Omega})$ variables:

$$-\mathsf{L}^2 = (\delta_{ij} - \Omega_i\Omega_j)\frac{\partial}{\partial\Omega_j}(\delta_{ik} - \Omega_i\Omega_k)\frac{\partial}{\partial\Omega_k}. \tag{2.7}$$

As a result of all the approximations made, the electron-ion Landau's integral is reduced to the Lorentz's operator, which describes, by looking to Eq. (2.7), elastic angular deflections without energy exchange:

$$\mathcal{C}_{ei}(f_e) = \frac{\nu_{ei}}{2}(-\mathsf{L}^2)f_e, \tag{2.8}$$

where $\nu_{ei} = 2n_i Y_{ei}/(m_e^2 v^3) = Z^2 e^4 \ln\Lambda_{ei}/(4\pi\epsilon_0^2 m_e^2 v^3)$ is the velocity-dependent electron-ion collision frequency. The energy exchange between electrons and ions can, obviously, only be modelled by considering a finite ratio $m_e/m_i$. This means accounting for higher orders terms in the expansion of the Landau's integral with small parameter $m_e/m_i$. They can be obtained easily in the case of an equilibrium distribution of ions, $f_i = f_{Mi}$, by slightly adapting the result obtained in the App. 2.B. By doing so the lowest order term is found to be

$$\frac{1}{2}\frac{m_e}{m_i}\nu_{ei}v\partial_v\left(f_e + \frac{T_i}{T_e}\frac{v_T^2}{v}\partial_v f_e\right). \tag{2.9}$$

As it will be seen in Chap. 3, this term is $Zm_e/m_i$ times smaller than the electron-electron collision operator of the model considered in this manuscript. Therefore, this negligible correction will not be further considered.

## 2.2.2 P1 closure

### 2.2.2.1 A mathematical digression. Maxwell's multipoles

For any $\mathbf{r}$ and $v$, the partial application $\mathbf{\Omega} \mapsto f_e(\mathbf{r}, v, \mathbf{\Omega})$ can be developed on any generating family of $L^2(\mathbb{S}^2)$, the functional space of square integrable functions over $\mathbb{S}^2$. The latter is a real Hilbert's space when associated to the inner product of squared integrable functions defined by the integral of their product over $\mathbb{S}^2$.

In the case of an axial symmetry in the velocity space, the velocity direction $\mathbf{\Omega}$ can be identified by one cosine direction only. By choosing, without lost of generality,

the symmetry axis as being the $z$-axis, this cosine direction is $\Omega_z$. The spherical Laplacian is reduced to

$$\frac{\partial}{\partial\Omega_z}(1-\Omega_z^2)\frac{\partial}{\partial\Omega_z},$$

whose Legendre polynomials of the variable $\Omega_z$ are an orthogonal basis of eigenfunctions. As it has been done by Rosenbluth *et al.* [49], a solution of the kinetic equation can be expressed in the form of an expansion on that basis up to an arbitrarily high number of terms.

In the absence of any axial symmetry, the specification of $\mathbf{\Omega}$ requires two independent variables. The natural extension of Legendre's polynomials are spherical harmonics, which are the restriction to $\mathbb{S}^2$ of harmonic homogeneous polynomials of $\mathbb{R}^3$ [50]. This point deserves a mathematical digression. A polynomial of $\mathbb{R}^3$, $Q(v_x, v_y, v_z)$, is *homogeneous* with degree $k$ if, and only if, for any real $r$, $Q(rv_x, rv_y, rv_z) = r^k Q(v_x, v_y, v_z)$. It is *harmonic* if, and only if, it belongs to the kernel of the Laplacian on $\mathbb{R}^3$. Its *restriction* to $\mathbb{S}^2$, noted $Q|_{\mathbb{S}^2}$, is the application defined on $\mathbb{S}^2$ which coincides with $Q$ on $\mathbb{S}^2$: for any triplet $(\Omega_x, \Omega_y, \Omega_z)$ that belongs to $\mathbb{S}^2$, $Q|_{\mathbb{S}^2}(\Omega_x, \Omega_y, \Omega_z) = Q(\Omega_x, \Omega_y, \Omega_z)$. The cardinal of $\ell$-degree spherical harmonics is $2\ell+1$. It is instructive to recover this result here. The $\ell$-degree homogeneous monomials of $\mathbb{R}^3$ are of the form

$$v_x^{\ell_x} v_y^{\ell_y} v_z^{\ell_z} = v_x ... v_x \times v_y ... v_y \times v_z ... v_z,$$

with $\ell_x + \ell_y + \ell_z = \ell$. The two written multiplicative signs, $\times$, are delimiting the borders between products of two different variables. The number of possible monomials is thus obtained by counting the possible positions of those two signs in the following list of symbols, $v_x, ..., v_x, \times, v_y, ...v_y, \times, v_z, ..., v_z$, containing $\ell+2$ elements. The result is the dimension of the space of homogeneous polynomial of degree $\ell$ on $\mathbb{R}^3$, *i.e* the $\ell$-symmetric power of $\mathbb{R}^3$:

$$\dim S^\ell\mathbb{R}^3 = \binom{\ell+2}{2} = \frac{(\ell+2)(\ell+1)}{2}.$$

where $S^\ell\mathbb{R}^3 = \mathbb{R}^3 \times ... \times \mathbb{R}^3/S(\ell)$, with $S(\ell)$ the symmetric group of permutations of $\ell$ factors. As the Laplacian, $\Delta$, is linear and surjectively maps $S^\ell\mathbb{R}^3$ onto $S^{\ell-2}\mathbb{R}^3$, we have:

$$\dim S^\ell\mathbb{R}^3 = \dim\ker\Delta|_{S^\ell\mathbb{R}^3} + \dim S^{\ell-2}\mathbb{R}^3.$$

By definition, spherical harmonics of degree $\ell$ form a base of $\ker\Delta|_{S^\ell\mathbb{R}^3}$. Therefore their cardinal is $\dim\ker\Delta|_{S^\ell\mathbb{R}^3} = (\ell+2)(\ell+1)/2 - \ell(\ell-1)/2 = 2\ell+1$, as previously affirmed. The zero, first and second order real spherical harmonics are: $Y_{00} = 1/\sqrt{4\pi}$,

$$Y_{1,-1} = \sqrt{\frac{3}{4\pi}}\Omega_y, \quad Y_{1,0} = \sqrt{\frac{3}{4\pi}}\Omega_z, \quad Y_{1,+1} = \sqrt{\frac{3}{4\pi}}\Omega_x,$$

and

$$Y_{2,-1} = \sqrt{\frac{15}{4\pi}}\Omega_y\Omega_z, \quad Y_{2,0} = \sqrt{\frac{15}{16\pi}}\Big(2\Omega_z^2 - \Omega_x^2 - \Omega_y^2\Big), \quad Y_{2,+1} = \sqrt{\frac{15}{4\pi}}\Omega_x\Omega_z,$$

$$Y_{2,-2} = \sqrt{\frac{15}{4\pi}}\Omega_x\Omega_y, \quad Y_{2,+2} = \sqrt{\frac{15}{4\pi}}\Big(\Omega_x^2 - \Omega_y^2\Big).$$

An $\ell$-degree homogeneous polynomial of $\mathbb{R}^3$ is a combination of homogeneous monomials $v_x^{\ell_x} v_y^{\ell_y} v_z^{\ell_z} = v^\ell\ \Omega_x^{\ell_x}\Omega_y^{\ell_y}\Omega_z^{\ell_z}$. Thus, it is a product of $v^\ell$ by a function of $\Omega_x$, $\Omega_y$ and $\Omega_z$. Such a function is, by construction, the restriction to $\mathbb{S}^2$ of the polynomial. Therefore, if this homogeneous polynomial is harmonic, then this function is, by definition, a certain spherical harmonic $Y_{\ell m}$. Consequently, all homogeneous harmonic polynomials of $\mathbb{R}^3$ are of the form $v^\ell Y_{\ell m}$. This implies that spherical harmonics are eigenfunctions of the spherical Laplacian. Indeed, on the one hand,

$$\Delta\ v^\ell Y_{\ell m} = 0,$$

and, on the other hand,

$$\begin{aligned}\Delta\ v^\ell Y_{\ell m} &= \left[v^{-2}\partial_v v^2 \partial_v + v^{-2}(-\mathsf{L}^2)\right] v^\ell Y_{\ell m} \\ &= v^{\ell-2}\left[\ell(\ell+1)Y_{\ell m} + (-\mathsf{L}^2)Y_{\ell m}\right].\end{aligned}$$

Hence, $Y_{\ell m}$ are eigenfunctions of $-\mathsf{L}^2$ with eigenvalues $-\ell(\ell+1)$. As a consequence, spherical harmonics of different degrees are orthogonal. Indeed, it can be shown that $-\mathsf{L}^2$ is self-adjoint, for instance, by using the expression of $-\mathsf{L}^2$ in $(\theta,\varphi)$-variables and performing two successive by parts integration over each of these two angles. In particular,

$$\begin{aligned}-\ell(\ell+1)\int_{\mathbb{S}^2} Y_{\ell m}Y_{\ell' m'}d^2\Omega &= \int_{\mathbb{S}^2}\Big[(-\mathsf{L}^2)Y_{\ell m}\Big]Y_{\ell' m'}d^2\Omega \\ &= \int_{\mathbb{S}^2} Y_{\ell m}\Big[(-\mathsf{L}^2)Y_{\ell' m'}\Big]d^2\Omega = -\ell'(\ell'+1)\int_{\mathbb{S}^2} Y_{\ell m}Y_{\ell' m'}d^2\Omega.\end{aligned}$$

So, $\int_{\mathbb{S}^2} Y_{\ell m}Y_{\ell' m'}d^2\Omega \propto \delta_{\ell\ell'}$, as announced. However, as described by Johnston in Ref. [51], some difficulties appear when trying to obtain equations for the components of the distribution function on spherical harmonics with orders higher than one. Johnston found more convenient to use Cartesian coordinates on $\mathbb{S}^2$ with an expansion on homogeneous $\ell$-degree monomials $\Omega_{i_1}\Omega_{i_2}...\Omega_{i_\ell}$. Yet these monomials are neither all mutually orthogonal nor eigenfunctions of the spherical Laplacian. This makes tedious the calculation of the projections of the kinetic equation for orders higher than two. For these reasons, it seems judicious, instead, to decompose $f_e$ on the generating family of Maxwell's multipoles [50, 52],

$$f_e = f_{\ell,i_1\ldots i_\ell}P_{\ell,i_1\ldots i_\ell}, \tag{2.10}$$

with Einstein's summation convention over the repeated indices $i_1\ldots i_\ell$. The components $f_{\ell,i_1\ldots i_\ell}$ are normalized to the squared norms $||P_{\ell,i_1\ldots i_\ell}||^2$ of the corresponding Maxwell's multipole. The zero, first and second order of such polynomials are:

$$P_0 = 1; \quad P_{1,i} = \Omega_i; \quad P_{2,ij} = \Omega_i\Omega_j - \frac{\delta_{ij}}{3}.$$

All these polynomials can be obtained by restricting to $\mathbb{S}^2$ the results of successive differentiation of $1/v$ along $v_{i_1}, ....v_{i_l}$. This non-trivial result is referred to as

Maxwell's theorem by Arnold [50]. Hence, such polynomial are eigenfunctions of $-\mathsf{L}^2$, as being restriction of harmonic functions of $\mathbb{R}^3$. This implies that all $\ell$-order Maxwell's multipoles belong to the subspace of $\ell$-order spherical harmonics, $\ker\Delta|_{S^\ell\mathbb{R}^3}$. Since all these eigenspaces provide a direct sum decomposition of the square integrable function of the two-dimensional sphere,

$$L^2(\mathbb{S}^2) = \bigoplus_{\ell=0}^{\infty} \ker\Delta|_{S^\ell\mathbb{R}^3},$$

any two of such Maxwell's multipoles with different degrees are orthogonal,

$$\int_{\mathbb{S}^2} P_{\ell,i_1\dots i_\ell} P_{\ell',j_1\dots j'_\ell}\, d^2\Omega \propto \delta_{\ell\ell'}. \tag{2.11}$$

Hence, Maxwell's multipoles can also be built step by step through the Gram-Schmidt's algorithm, applied on the degree only, from the monomials $\Omega_{i_1}\Omega_{i_2}\dots\Omega_{i_\ell}$. It can be seen that, apart from the prefactors, the Maxwell's multipoles of zero and first order coincide with the spherical harmonics of these degrees. This is no longer the case for $\ell \geq 2$. Indeed, the cardinal of Maxwell's multipoles of order $\ell$ is $(\ell+2)(\ell+1)/2$, that of homogeneous polynomial of degree $\ell$. For instance, there are 5 different second-order spherical harmonics but 6 different Maxwell's multipoles of that degree; the latter are

$$\Omega_x^2 - 1/3; \quad \Omega_x\Omega_y; \quad \Omega_x\Omega_z; \quad \Omega_y^2 - 1/3; \quad \Omega_y\Omega_z; \quad \Omega_z^2 - 1/3.$$

It therefore appears that the set of Maxwell's multipoles is not a free family of $L^2(\mathbb{S}^2)$, despite being a generating one. From this point of view, the expansion (2.10) cannot be *equivalent* to that on spherical harmonics. To write the opposite, as Decoster does in Ref. [53], therefore requires some clarifications precising what is meant by this. Instead of viewing $P_{\ell,i_1\dots i_\ell}$ as a function of $L(\mathbb{S}^2)$ labelled by the integers $\ell, i_1 \dots i_\ell$, it can be viewed as the component of a $\ell$-rank tensor. Such a tensor, $P_\ell$, is fully symmetric under permutations of indices and trace-free,

$$\delta_{i_1 i_2} P_{\ell,i_1\dots i_\ell} = 0. \tag{2.12}$$

As a consequence, it has only $2\ell+1$ independent components. Indeed, each index among $i_1 \dots i_\ell$ can only be $x, y$ or $z$. Since their arrangement is unimportant, this brings us back to the enumeration problem already encountered in determining $\dim S^\ell\mathbb{R}^3$. Thus, just by being fully symmetric, $P_\ell$ has at most $(\ell+2)(\ell+1)/2$ independent components. Then, the Eq. (2.12) expresses independent conditions. Their number is equal to the number of values that the indices $i_3 \dots i_\ell$ can take, that is, $\ell(\ell-1)/2$. Hence, $P_\ell$ has well $(\ell+2)(\ell+1)/2 - \ell(\ell-1)/2 = 2\ell+1$ independent components, the cardinal of $\ell$-order spherical harmonics. Therefore, the set of all symmetric trace-free tensor of rank $\ell$, noted here STFT-$\ell$, is isomorphic to that of $\ell$-order spherical harmonics,

$$\text{STFT-}\ell \approx \ker\Delta|_{S^\ell\mathbb{R}^3}$$

This is not a coincidence. STFT-$\ell$ forms a $2\ell+1$-dimensional irreducible representation of $SO(3)$, the group of rotations in $\mathbb{R}^3$. $SO(3)$ is a compact Lie's group,

so each representation of it is a direct sum of irreducible representations of finite dimensions [54]. Here, these representations are the infinite number of spaces STFT-$\ell$. In virtue of the Schur's lemma, on each of these representations labelled by $\ell$, the spherical Laplacian is proportional to identity because it is commuting with all the generators of the group, $\mathsf{L}_x$, $\mathsf{L}_y$ and $\mathsf{L}_z$. In other words, all of these tensors $P_\ell$, viewed as functions of $\Omega_x, \Omega_y, \Omega_z$, are eigenfunctions of the spherical Laplacian. A lot of details on multipole expansion are reviewed by Thorne in Ref. [55]. A stratospheric discussion around the topological content of the Maxwell's theorem, in relation with some aspects mentioned above, is led by Arnold in Ref. [56].

#### 2.2.2.2 Closed system

For the purpose of determining the heat flux density and electric field, the minimum set of required terms in the expansion (2.10) is composed by the first four. They corresponds to the components of the electron distribution function on zero and one orders on Maxwell's multipoles or, equivalently for these degrees, spherical harmonics. The procedure which consists of restricting the study to these components is the *P1 closure* [42, 53].

As already mentioned, energy exchange between electrons affects the isotropic part $f_0$ of the distribution function, whereas the anisotropic part is constrained by momentum exchanges. This simplified picture must be completed by the coupling between the isotropic and anisotropic parts. As visible from Eq. (2.10), the latter is, *a priori*, composed by the sum of an arbitrarily large number of terms. However, the fact that the electric current (2.2) and heat flux (2.3) densities only depend on $\mathbf{f}_1$ suggests that the problem may be reduced to the study of a coupled system with unknown functions $f_0$ and $\mathbf{f}_1$. Such a system is obtained by projecting the kinetic equation (2.1) on $P_0 = 1$ and $\mathbf{P}_1 = \mathbf{\Omega}$. These projections form a closed system on $f_0$ and $\mathbf{f}_1$ upon expressing the integral $\int_{\mathbb{S}^2} \mathbf{\Omega} \otimes \mathbf{\Omega} f_e \; d^2\Omega$ in terms of $f_0$ and $\mathbf{f}_1$ only. For that purpose it is sufficient to impose $\mathsf{f}_2 = 0$:

$$\int_{\mathbb{S}^2} (\mathbf{\Omega} \otimes \mathbf{\Omega} - \mathsf{I}/3) \, f_e \; d^2\Omega = 0. \tag{2.13}$$

It yields the following system of coupled equations:

$$\frac{v}{3} \boldsymbol{\nabla} \cdot \mathbf{f}_1 - \frac{e}{3 m_e v^2} \mathbf{E} \cdot \partial_v v^2 \mathbf{f}_1 = \mathcal{C}^0_{ee} + \mathcal{C}^0_{ei}, \tag{2.14}$$

$$v \boldsymbol{\nabla} f_0 - \frac{e}{m_e} \mathbf{E} \, \partial_v f_0 = \boldsymbol{\mathcal{C}}^1_{ee} + \boldsymbol{\mathcal{C}}^1_{ei}, \tag{2.15}$$

where $\mathcal{C}^0_{ee}$, $\mathcal{C}^0_{ei}$ and $\boldsymbol{\mathcal{C}}^1_{ee}$, $\boldsymbol{\mathcal{C}}^1_{ei}$ are the projections of the electron-electron and electron-ion collision operators on $P_0$ and $\mathbf{P}_1$, respectively. By using the expression (2.8) and expansion (2.10), we obtain:

$$\mathcal{C}^0_{ei} = 0; \quad \boldsymbol{\mathcal{C}}^1_{ei} = -\nu_{ei} \mathbf{f}_1. \tag{2.16}$$

The expressions of $\mathcal{C}^0_{ee}$ and $\boldsymbol{\mathcal{C}}^1_{ee}$ in the case of the electron-electron Landau's integral are of little interest here. They can be found, for instance, in Ref. [53]. The relation (2.13) sets the electron stress viscosity tensor to zero. Higher order terms $\ell \geq 3$ in

expansion (2.10) are maintained to their initial values by the P1 closure. Those values are zeros in the diffusion problem we address, because the hydrodynamic constraints are entirely encoded in the initialisation $f_0 = f_M$. In that context, the P1 closure is thus equivalent to seeking a solution of the form $f_0 + \mathbf{\Omega} \cdot \mathbf{f}_1$ [42]. For an homogeneous plasma without mean fields the non-stationary kinetic equation is reduced to $\partial_t f_e = \mathcal{C}_{ei}(f_e)$ (2.8) if energy exchanges are neglected. In that case all the modes $P_{\ell,i_1\ldots i_\ell}$ relax as

$$\exp\left(-\frac{\ell(\ell+1)}{2}\nu_{ei}t\right),$$

and on a time of order $\nu_{ei}^{-1}$, the modes $\ell \geq 2$ have already decreased at least ten times more than the mode $\ell = 1$. The plasma inhomogeneities and energy exchange may prolong or reduce the lifespans of those modes but it is supposed, by making the P1 closure, that the aforementioned hierarchy between their relaxation remains valid. As it will be shown in Chap. 3, the error created by omitting high order terms $\ell \geq 2$ can be compensated by an appropriate renormalization of the electron-electron collision frequency. The electric field entering in Eqs. (2.14) and (2.15) is determined by the condition $\mathbf{j}_e = \mathbf{0}$. The Poisson's equation cannot be used for this purpose because charge neutrality is imposed through $n_e = Zn_i$. By multiplying (2.15) by $v^6$ and using the zero electric current condition, we obtain:

$$\mathbf{E} = -\frac{m_e}{e}\left[\int_0^\infty v^6 \boldsymbol{\mathcal{C}}_{ee}^1 \, dv - \int_0^\infty v^7 \boldsymbol{\nabla} f_0 \, dv\right] \Bigg/ \int_0^\infty v^6 \partial_v f_0 \, dv. \tag{2.17}$$

Being proportional to $v^{-3}\mathbf{f}_1$, the contribution of $\boldsymbol{\mathcal{C}}_{ei}^1$ vanishes. The set of expressions (2.3), (2.13), and (2.17) provides a complete kinetic closure to electron hydrodynamic equations.

It must be mentioned that, while solving the P1 system of equations, it is not necessary to rebuild the distribution function $f_e$ by performing the sum $f_0 + \mathbf{\Omega} \cdot \mathbf{f}_1$. As soon as the values of $f_0$ and $\mathbf{f}_1$ are accurate enough, the same is for the heat flux density and electric field. However, this situation does not guarantee that $f_0 + \mathbf{\Omega} \cdot \mathbf{f}_1$ is positive since higher orders terms are absent. This can be awkward for calculating quantities which are functions of $f_e$, without, however, being explicitly expressed in terms of $f_0$, $\mathbf{f}_1$ and $\mathbf{f}_2$ only. For this reason, the distribution function can be searched as the exponential of a P1 expansion. This procedure, called the *M1 closure*, is discussed in App. 6.2 in the form of a digression. The resulting system of equations on $f_0$ and $\mathbf{f}_1$ is only slightly modified. Its numerical predictions have been compared to that of the P1 closure by Del Sorbo *et al* [57]. As no significant differences where observed in the cases of interest here, it will not be further discussed.

### 2.2.3 Finite $Z$: importance of electron-electron collisions

As $Z$ decreases, the electron-electron collisions, which are solely responsible for energy exchange given the reduced form (2.8) of the electron-ion collision operator used above, play an increasingly important role. Nevertheless, energy exchanges are, *a priori*, not decisive in the case of a smooth temperature gradient because

the departure of $f_0$ from $f_M$ is negligible. Concerning momentum exchanges, the electron-electron contribution is $Z$ times smaller than electron-ion collisions.

Spitzer and Härm [58] performed numerical simulations for calculating $\mathbf{E}$ and $\mathbf{q}_e$, by solving the kinetic equation in the P1 approximation with the electron-electron Landau's integral. From their results they shown that electron-electron collisions can be implicitly accounted for by introducing $Z$-dependent coefficients $\xi$ and $\zeta$ in formulas obtained in the Lorentz's approximation ($Z \gg 1$):

$$\mathbf{E}_{\mathrm{SH}} = -\frac{m_e v_T^2}{e}\left(\frac{\boldsymbol{\nabla} n_e}{n_e} + \xi(Z)\frac{\boldsymbol{\nabla} T_e}{T_e}\right) \tag{2.18}$$

and

$$\mathbf{q}_{\mathrm{SH}} = -\kappa_{\mathrm{SH}}\boldsymbol{\nabla} T_e, \quad \kappa_{\mathrm{SH}} = \frac{128 k_B n_e v_T^2}{3\pi\zeta(Z)\nu_{ei}^T}, \tag{2.19}$$

where $\nu_{ei}^T = \nu_{ei}(v_T)/[3(\pi/2)^{1/2}]$ is the average electron-ion collision frequency. The derivation of Eq. (2.18) in the high-$Z$ limit is immediate by substituting $f_0 = f_M$ (2.4) in the formula (2.17). The obtention of Eq. (2.19) in the same limit will be reviewed in the next chapter, at a better time. Being only dependent on the *local* values and shape of electron density and temperature, the transport regime these formulae describe is said to be *local*. Although it is clear from Eqs. (2.3)-(2.17) that the heat flux density and electric field at a point in space depend only on the electron distribution function at that point, there is no reason, *a priori*, why they should depend solely on the local values of its first three hydrodynamical moments, $n_e$, $\mathbf{u}_e$ (which is null here), and $T_e$. Remember that this property exists when the mean free path of electrons, $\lambda_{ei}^T = v_T/\nu_{ei}^T$, is small compared to the gradient length $L_T = T_e/|\boldsymbol{\nabla} T_e|$,

$$\mathrm{Kn} = \lambda_{ei}^T/L_T \ll 1,$$

where Kn is called the Knudsen's number. In average, an electron travels over a distance of order $\lambda_{ei}^T$ without having its momentum changed by collisions with ions. On the way, the temperature may have changed by an amount $\delta T_e \sim \lambda_{ei}^T|\boldsymbol{\nabla} T_e|$. Hence, the electrons are carrying an heat flux density equal to $n_e v_T \delta(k_B T_e) \sim n_e v_T k_B \lambda_{ei}^T|\boldsymbol{\nabla} T_e|$. By comparing to $-\kappa_e|\boldsymbol{\nabla} T_e|$, we thus find $\kappa_e \sim n_e v_T^2 k_B/\nu_{ei}^T$, in agreement with Eq. (2.19). For lower and lower values of $Z$, the trend toward local equilibrium, ensured by electron-electron collisions, is more and more efficient. It becomes harder for a group of electrons with some high velocities to subsist over several mean free paths. This results in an inhibition of the heat flux density, which explain the division of $\kappa_e$ by a factor $\zeta(Z) > 1$. It is interesting to note that $\kappa_e$ does not depend on the electron density because $\nu_{ei}^T \propto n_e$. This characteristic of weakly coupled plasmas is shared by dilute neutral gases. The reason is that increasing the density simultaneously increases the number of particles which carry energy but decreases the average distance, $\lambda_{ei}^T \propto 1/n_e$, a particle can travel before transferring its energy to another one.

On the contrary, the thermoelectric field (2.18) explicitly depends on $n_e$. In the quasi-static approximation it only has a capacitive component, *i.e* it derives from a potential, $\mathbf{E}_{\mathrm{SH}} = -\boldsymbol{\nabla}\langle\varphi\rangle$. By linearity of the Maxwell's equations, $\mathbf{E}_{\mathrm{SH}}$ can be seen

as the superposition of two electric fields, associated to the gradient of electron density and temperature, respectively. In particular, their physical origins can be discussed separately. For $\boldsymbol{\nabla} T_e = \mathbf{0}$, the Eq. (2.18) leads to the electrostatic potential $e\langle\varphi\rangle/(k_B T_e) = \ln(n_e/n_{e0})$, where $n_{e0}$ is the electron density for $\langle\varphi\rangle = 0$. This is the Boltzmann's law. Here, $n_e$ is considered to be a given macroscopic constraints. Hence, this component of the electric field is equal to the exterior field within which the plasma would have been placed to have such inhomogeneous electron density. Now, for $\boldsymbol{\nabla} n_e = \mathbf{0}$, the electrostatic potential is $e\langle\varphi\rangle/(k_B T_e) = \xi(Z)$. Such a macroscopic electric field results from the difference in the size and structure of the dynamical screening clouds within the plasma. This is confirmed by a calculation performed by Krainov *et al* [59]. The potential created at a point $\mathbf{r}$ by a moving test charge $q_s$ located at $\mathbf{r}' = \mathbf{R} + \mathbf{v}t$ is

$$\varphi_s = \int \frac{q_s e^{i\mathbf{k}\cdot(\mathbf{r}-\mathbf{r}')}}{\epsilon_0 k^2 \epsilon(\mathbf{k}\cdot\mathbf{v}, \mathbf{k})} \frac{d^3\mathbf{k}}{(2\pi)^3},$$

where $\mathbf{v}$ is the velocity of the test charge in the frame of the ions mean flow. The above formula is nothing else than the inverse Fourier's transform of $q_s/[\epsilon_0 k^2 \epsilon(\mathbf{k}\cdot\mathbf{v}, \mathbf{k})]$, the Fourier's transform of the Coulomb's potential, $q_s/(\epsilon_0 k^2)$, screened through the division by the dielectric function (2.50) evaluated at the pulsation $\omega = \mathbf{k}\cdot\mathbf{v}$. For Maxwellian distribution functions of electrons and ions, it is

$$\epsilon(\omega, \mathbf{k}) = 1 + \sum_s k^{-2}\lambda_{D_s}^{-2}\left[1 + \frac{\omega}{k v_{T_s}\sqrt{2}} \mathcal{Z}\left(\frac{\omega}{k v_{T_s}\sqrt{2}}\right)\right],$$

with summation over each charged species $s$, electrons and ions. $\mathcal{Z}$ is the plasma dispersion function, which has here, for any real number $x$, the expression $\mathcal{Z}(x) = \pi^{-1/2}\,\mathsf{P}\int_{-\infty}^{+\infty} e^{-y^2}/(y-x)\,dy + i\pi^{1/2}e^{-x^2}$ where $\mathsf{P}$ stands for the Cauchy's principal value of the integral. This expression is the result of the Landau's analytical continuation of $\omega \mapsto \epsilon(\omega, \mathbf{k})$. It is discussed in the App. 2.A. Then, Krainov *et al.* computed the average of these single charge potentials over the Maxwellian distribution functions, $f_{Ms}$,

$$\sum_s \int \varphi_s f_{Ms}\; d^3\mathbf{R} d^3\mathbf{v}.$$

They found this sum, after having integrated over a certain duration probably of the order of a collision time, to be proportional to $T_e$. The underlying coefficient only depends on $ZT_e/T_i$. This suggests to identify the result as being $\langle\varphi\rangle$. Unfortunately, they gave absolutely no details about their calculations and we ignore the expression of such a function. We have not attempted yet to fill this gap and will content ourselves with the qualitative conclusion of their calculation mentioned above. The coefficients $\xi$ and $\zeta$ have been obtained by interpolation by Spitzer and Härm. In their notation, $\xi = 1 + 3/2\gamma_T/\gamma_E$ and $\zeta = (5/2\epsilon\delta_T)^{-1}$. Popular approximations are [60]:

$$\xi(Z) = 1 + \frac{3}{2}\frac{Z + 0.48}{Z + 2.2}, \qquad \zeta(Z) = \frac{Z + 4.2}{Z + 0.24} \tag{2.20}$$

In fact, these expressions, or more precise ones, can be found by developing $\mathbf{f}_1$ over Sonine-Laguerre's polynomials. This has even been done by Braginskii [33]

for magnetised plasma. The P1 system of Eqs. (3.13)-(3.14), with $f_0 = f_M$, is projected on that basis and the corresponding set of matrix equations are solved to find the coefficients of the expansion. The (3/2)-order Sonine-Laguerre's polynomials, $L_p^{(3/2)}$, seemed appropriate to Braginskii because of the occurrence of the following integral weighting factor, or measure,

$$\left(\frac{v}{v_T\sqrt{2}}\right)^2 \frac{e^{-v^2/(2v_T^2)}}{(2\pi)^{3/2}v_T^3}\ v^2dv = \ \frac{x^{3/2}e^{-x}}{2\pi^{3/2}}\ dx,$$

which emerges from $f_M$. Indeed, with respect to that measure, Sonine-Laguerre's polynomials verify the following orthogonality relation,

$$\int_0^{+\infty} L_p^{(3/2)}(x)L_q^{(3/2)}(x)\ x^{3/2}e^{-x}\ dx = \frac{\Gamma(p+5/2)}{\Gamma(p+1)}\delta_{pq}.$$

An alternative basis, the set of Hermite's polynomials, have been chosen by Balescu in his book [61]. For them an orthogonality relation is verified with the Gaussian measure $e^{-w^2}dw$, the variable being then $w = v/[v_T\sqrt{2}]$. His approach differs not only in this respect, but also by the fact he directly expanded the electron distribution function on the set of irreducible Hermite's tensors. They roughly are the product of some Maxwell's multipoles by some Hermite's polynomials. In spite of this different formalism, Balescu's results agree within an error of 1% with those of Braginskii. The same applies to other approaches, on which we will not dwell on. It is worth mentioning, however, the recent work of Krommes [62, 63]. He proposed a compact formalism to recover Braginskii's results by deepening their physical content.

For increasing values of Kn, the electric field and heat flux density deviate more and more from the values given by the formulae (2.18)-(2.19). The difference can become so great that it qualitatively changes the dynamics of heat transport, signing the failure of all the aforementioned approaches. Indeed, the local thermodynamic equilibrium hypothesis is no longer valid and there is a significant departure of $f_0$ from $f_M$. Let us precise this point before moving on to the next section.

The derivative of the electron temperature (1.3) is $dT_e/dz(z) = (T_H - T_C)s\big(1 - \tanh^2[s(z-z_0)]\big)/2$. As a result we can express the Knudsen's number at any point. We will be satisfied with its value at $z = z_0$, which will still be noted Kn. Since $\lambda_{ei}^T = 3(\pi/2)^{1/2}k_B^2T_e^2/(2Zn_eY_{ee})$, we obtain,

$$\mathrm{Kn} = \frac{3(\pi/2)^{1/2}k_B^2}{2Zn_eY_{ee}}\ \frac{T_H+T_C}{2}\ \frac{T_H-T_C}{2}\ s.$$

Obviously, if the electron density increases, so is the number of collision partners per unit volume. Hence the mean free path decreases, leading to a smaller value of the Knudsen's number. Let us focus on the three other factors considering a constant electron density. The product of the steepness, $s$, by the half jump, $(T_H - T_C)/2$, controls the spatial rate at which the electron distribution's tail is changing. Therefore, the higher is such a rate the higher the displacements of electrons will provoke local deformation of the tail. The mean electron temperature, $(T_H + T_C)/2$, determines the number of electrons having a mean free path above a certain value. So, if $(T_H + T_C)/2$ increases, which corresponds to an upward translation of the temperature profile, the deformation of distribution's tails induced by the displacements of electrons will be more visible.

## 2.3 Nonlocal regime

The direct consequence of this last statement is the necessity of considering now $f_0$ as a mathematical unknown. Throughout the literature, there appears several systems of equations coupling this isotropic component to the anisotropic ones. They mainly differ from each other by the operator chosen to describe electron-electron collisions. Beyond the slight variations, more important are the methods employed to solve these systems, which all share the aim of obtaining a practical estimate of the heat flux density. By examining the different forms the latter takes, it seems relevant to us to distinguish three main types of strategy.

The first one, presented in Sec. 2.3.1, leads to a correction of the Spitzer-Härm's formula (2.19) as a sum of terms proportional to the successive derivatives of the electron temperature. Its derivation relies on a somewhat arbitrary truncation of a divergent expansion with the Knudsen's number as a small parameter. As it will be detailed, one source of dissatisfaction lies in identifying the radius of convergence, or, equivalently, a certain critical velocity separating the energy axis in two domains. This problem is present in several articles, including recent ones. In fact, there exists a proper resummation of the complete series resulting in an integral formula for $\mathbf{q}_e$. Such a kind of expressions is considered in Sec. 2.3.2, where essentially two paths to get it are identified which together constitute the second class of the aforementioned strategies. Although many formulae can be found in the literature, most of them turns out to give close results. Nevertheless, by providing the heat flux density as an integral over space, latter approach suffers from a lack of computational efficiency while making difficult any extension to dimensions two or three. These flaws are overcame with the strategy exposed in Sec. 2.3.3. Here, a judicious and physically justified three-dimensional integral representation serves only as a starting point for finding a differential equation on $\mathbf{q}_e$, the design of which is suited for a robust numerical resolution. The resulting heat flux density is the Spitzer-Härm's one plus the integral over energies of a differential form.

### 2.3.1 Approaches involving a critical velocity

The Spitzer-Härm's formula for the heat flux density appears to be the first term of a development in the successive powers of the Knudsen's number,

$$|\mathbf{q}_{\mathrm{SH}}| \propto \mathrm{Kn}\; n_e v_T k_B T_e.$$

Hence, for increasing values of Kn, a quite natural attempt to account for deviation from Eqs. (2.18)-(2.19) consists of retaining higher order terms in this Chapman-Enskog's expansion. Such a procedure has been studied in detail by Kishimoto and Mima in Refs. [64, 65]. The authors combined an expansion on Maxwell's multipoles together with a perturbation expansion with small parameter $\eta = \mathrm{Kn}/[3(\pi/2)^{1/2}]$:

$$f_0 = \sum_{r=0}^{\infty} \eta^{2r} f_{0r}; \quad \mathbf{f}_1 = \eta \sum_{r=0}^{\infty} \eta^{2r} \mathbf{f}_{1r}; \quad \mathsf{f}_2 = \eta^2 \sum_{r=0}^{\infty} \eta^{2r} \mathsf{f}_{2r}; \quad \mathbf{E} = \sum_{r=1}^{\infty} \eta^r \mathbf{E}_r \quad (2.21)$$

They considered the kinetic equation (2.1) with the Lorentz's operator (2.8) to describe electron-ion collisions, together with the following operator,

$$\mathcal{C}_{ee}[f_e, f_M] = \frac{\nu_{ee}}{2}\mathcal{H}\left(\frac{v}{v_T\sqrt{2}}\right)(-\mathsf{L}^2)f_e + \nu_{ee}v\partial_v\left[\left(\frac{v}{v_T}\right)^2\mathcal{G}\left(\frac{v}{v_T\sqrt{2}}\right)\left(f_e + \frac{v_T^2}{v}\partial_v f_e\right)\right],$$

to describe electron-electron collisions. Its derivation, together with its physical content, are exposed in App. 2.B. The factors $\mathcal{H}\left(v/[v_T\sqrt{2}]\right)$ and $\mathcal{G}\left(v/[v_T\sqrt{2}]\right)$ are the functions (2.76)-(2.75) given in the aforementioned Appendix, evaluated at $w = v/[v_T\sqrt{2}]$. Kishimoto and Mima approximated them as

$$\mathcal{H}(w) \simeq 1; \quad \mathcal{G}(w) \simeq \frac{2}{3\sqrt{\pi}}\frac{w}{1+\frac{4}{3\sqrt{\pi}}w^3}. \tag{2.22}$$

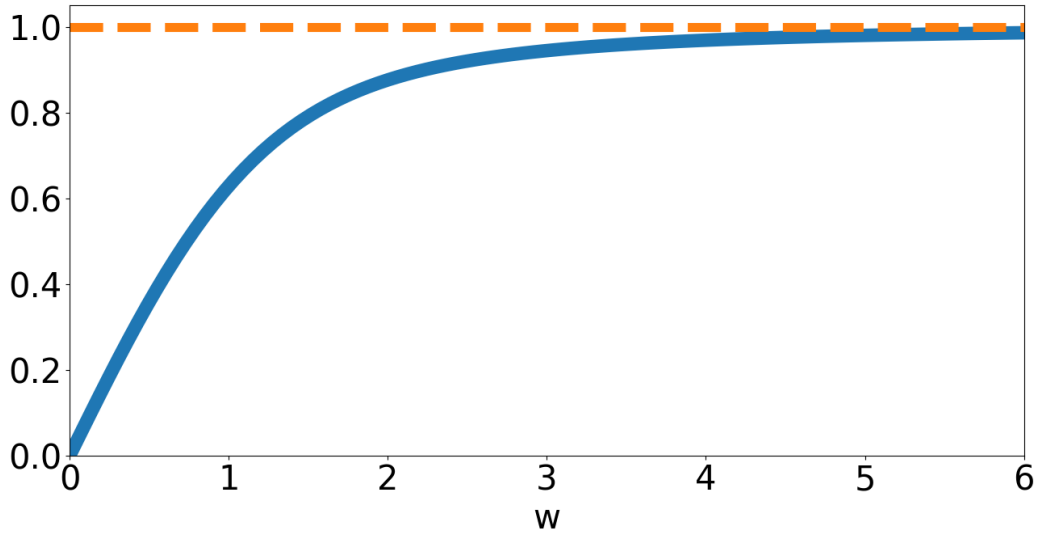


Figure 2.2: Graphs of the function $\mathcal{H}$ (2.76) (solid, blue) together with the approximate form (2.22) (dashed, orange) chosen by Kishimoto and Mima.

This approximate form of $\mathcal{G}$ corresponds to an interpolation of its expressions in the limits $w \ll 1$ and $w \gg 1$. The function $\mathcal{H}$ is approximated by its expression in the high velocity limit, $w \gg 1$. All these functions are plotted in Figs. 2.2-2.3. Kishimoto and Mima restricted themselves to the situation of a one dimensional plasma along the $z$-axis with an high, but finite, ionization number $Z$. They neglected energy exchanges in the projections of the kinetic equation on first and second order Maxwell's multipoles. By restricting their calculations to the first four terms of expansions (2.21), they obtained the heat flux density as a sum. The first term is the Spitzer-Harm's value (2.19) with $\zeta(\infty) = 1$. The three other terms are corrections proportional to $(dT_e/dz)^3$, $(dT_e/dz)(d^2T_e/dz^2)$ and $(d^3T_e/dz^3)$, respectively. The coefficients in front of these terms are so high that they become comparable to the Spitzer-Harm's value for $\mathrm{Kn} \lesssim 10^{-3}$.

Hence, a significant deviation from the Spitzer-Härm's law arise for smaller Knudsen's number than for neutral gas. This is a consequence of the long range Coulombian interactions between charged particles. The velocity-dependent electron mean

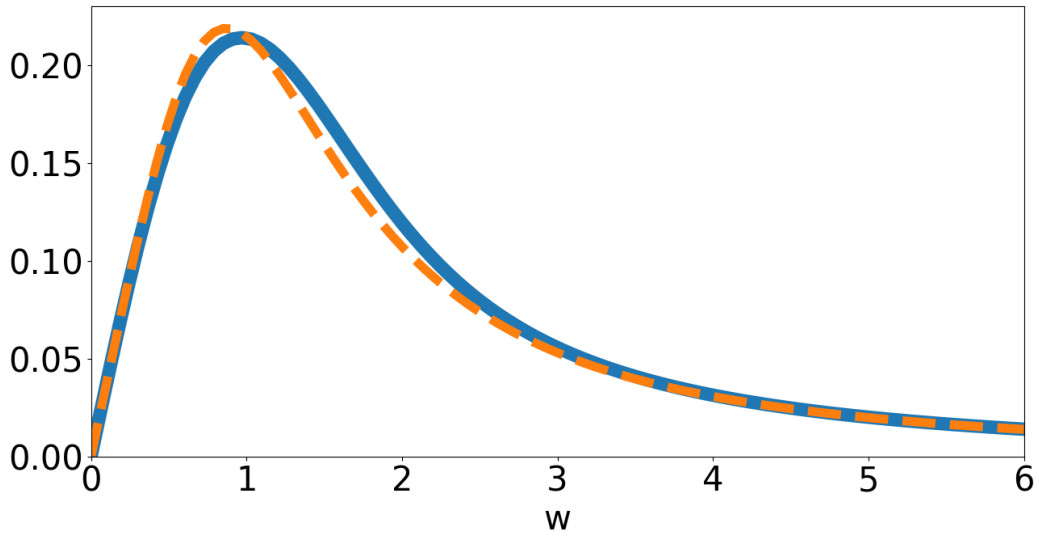


Figure 2.3: Graphs of the function $\mathcal{G}$ (2.75) (solid, blue) together with the approximate form (2.22) (dashed, orange) chosen by Kishimoto and Mima.

free path, $\lambda_{ei} = v/\nu_{ei}$, grows as the power fourth of the velocity, whereas it grows linearly in a neutral gas. Therefore, the number of electrons with a mean free path comparable to the gradient length becomes significant even for small Knudsen's number. This means that expansions (2.21), whose radii of convergence depend on the velocity, become divergent even for low Knudsen's numbers for velocities greater than a certain critical value $v_c$. Kishimoto and Mima estimated it as

$$v_c = \frac{v_T\sqrt{2}}{\eta^\mu}, \tag{2.23}$$

with $\mu \simeq 1/6$ to $1/4$. In order to avoid the divergence, they separated the resolution for velocities under and beyond this limit. Following the terminology of Gurevich and Istomin [66], the corresponding solutions will be respectively designated as the *diffusive* and *convective* parts. While keeping the same method for $v \leq v_c$, Kishimoto and Mima used expansions in the parameter $\eta^{-1}$ for $v \geq v_c$. They retained the following zeroth order solution: $f_C = f_M$ for $0 \leq \Omega_z \leq 1$ and $f_C = \sigma f_M$ for $-1 \leq \Omega_z \leq 0$. The free parameter $\sigma$ depends upon the back-scattering rate of the electrons. As a consequence of the axial symmetry along the $z$-axis, the zeroth and first order components of this solution are:

$$f_{C\ 0} = \frac{1}{2}\int_{-1}^{+1} f_C\, d\Omega_z = \frac{1+\sigma}{2} f_M, \quad f_{C\ 1z} = \frac{1}{2}\int_{-1}^{+1} \Omega_z f_C\, d\Omega_z = \frac{3}{4}(1-\sigma) f_M.$$

The electric field is computed up to order three from the zero electric current density condition, as $E_z = \eta E_{1z} + \eta^2 E_{2z} + \eta^3 E_{3z}$. By assuming the contribution of the convective part, $\int_{v_c}^{\infty} v^3 f_{C\ 1z}\, dv$, to be small by an order $\eta$ compared to the diffusive one, Kishimoto and Mima found:

$$\eta e E_{1z} = -\left[\frac{\gamma\big(5; v_c^2/[2v_T^2]\big)}{\gamma\big(4; v_c^2/[2v_T^2]\big)} - \frac{3}{2}\right] \frac{dk_B T_e}{dz}, \tag{2.24}$$

and

$$\eta^2 e E_{2z} = \frac{9(1-\sigma)}{4}\left(\frac{\pi}{2}\right)^{1/2}\frac{\Gamma\left(2; v_c^2/[2v_T^2]\right)}{\gamma\left(4; v_c^2/[2v_T^2]\right)}\frac{k_B T_e}{\lambda_{ei}^T}. \tag{2.25}$$

These terms are plotted in Figs. 2.4-2.5. The third order one, $\eta^3 E_{3z}$, depends upon $E_{1z}$ and is not explicitly written. We introduced the lower, $\gamma$, and upper, $\Gamma$, incomplete gamma functions to express their results. They are defined as [67]:

$$\gamma(s;w) = \int_0^w x^{s-1}e^{-x}dx; \quad \Gamma(s;w) = \int_w^\infty x^{s-1}e^{-x}dx.$$

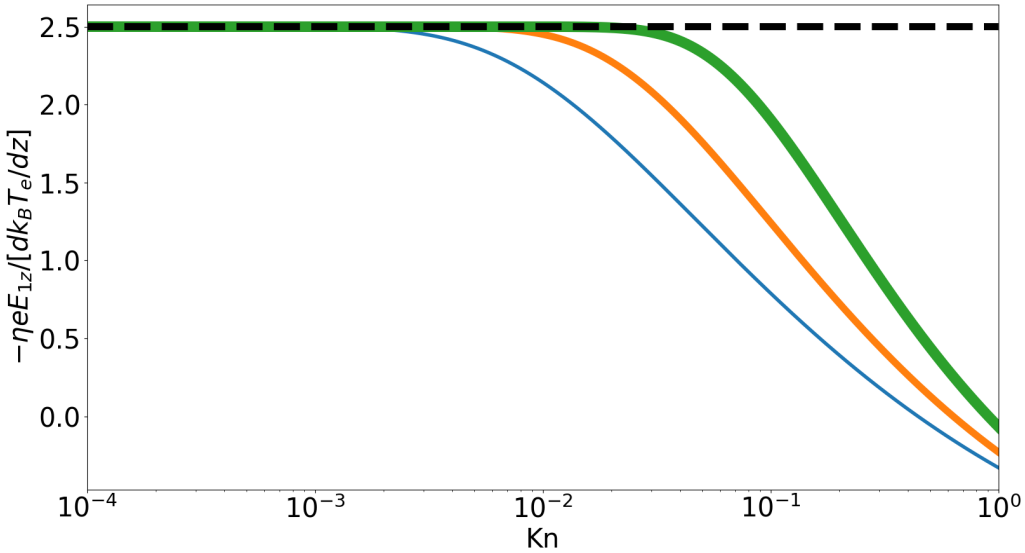


Figure 2.4: Graph of $-\eta E_{1z}/[dk_B T_e/dz]$ as function of Kn, for critical velocity parameter $\mu = 1/6$ (thin solid, blue), $1/5$ (solid, orange), $1/4$ (thick solid, green). The horizontal black dashed line represents the values, $5/2$, corresponding to the Spitzer-Härm's coefficient, $\xi(Z)$ (2.20), in the high-$Z$ limit.

For increasingly small Knudsen's numbers, $\eta E_{1z}$ approaches the Spitzer-Härm's value (2.18). The higher the $\mu$, the faster the trend. This is because, for a fixed value of Kn, $v_c$ (2.23) is an increasing function of $\mu$, and so is the number of electrons with small mean free paths compared to the gradient length. However, the reached value is $\xi(\infty) = 5/2$ (2.20), which is independent from $Z$. This may seem surprising since Kishimoto and Mima have taken into account electron-electron collisions, which are responsible for the $Z$-dependent corrective term, $\xi(Z)$. In fact, their account is partial, as being restricted to one equation: the projection of the kinetic equation on the zeroth order Maxwell's multipole. Although it is obvious by examining Eq. (2.17) that for $\boldsymbol{\mathcal{C}}_{ee}^1 = \mathbf{0}$, no correction for finite $Z$ can appear, it will be further discussed in the next chapter.

As visible in Fig. 2.5, the second order term, $\eta^2 E_{2z}$, is at most ten times smaller than $\eta E_{1z}$ for Kn $\lesssim 10^{-2}$, but becomes comparable to it for Kn $\simeq 10^{-1}$ in the extreme case $\mu = 1/6$. It is clear that, at least for the electric field, this marks the

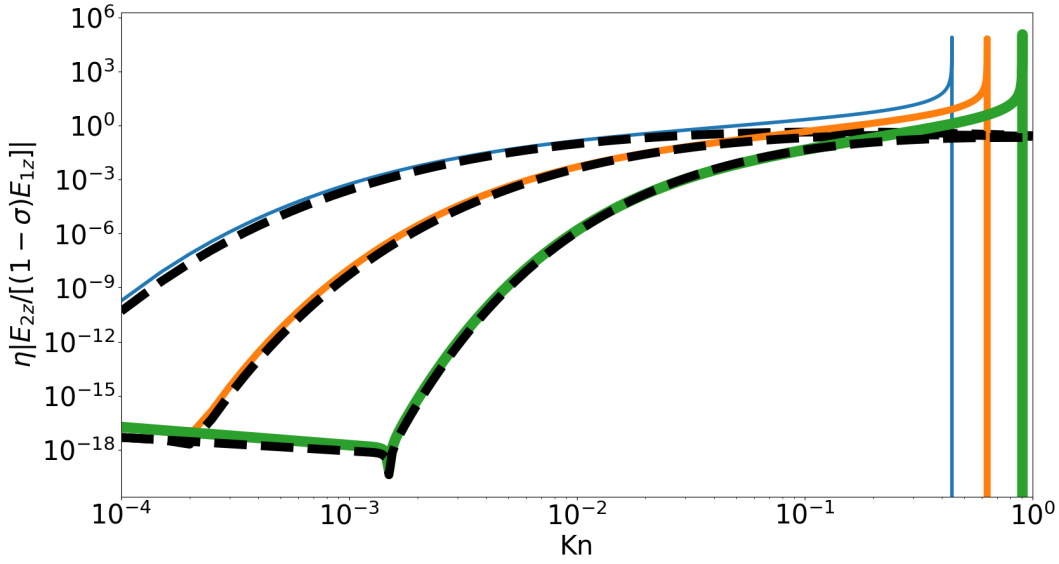


Figure 2.5: Graph of the ratio $\eta|E_{2z}/[(1-\sigma)E_{1z}]|$ as function of Kn, for critical velocity parameter $\mu = 1/6$ (thin solid, blue), $1/5$ (solid, orange), $1/4$ (thick solid, green). The black dashed lines represents the empirical approximation, $|\Gamma(2;\eta^{-2\mu})|/[2\mathrm{Kn}^{3/4}]$, for the corresponding values of $\mu$. The divergences occur at $\mathrm{Kn} \simeq 3(\pi/2)^{1/2}/1.43^{1/\mu}$, the value for which $E_{1z}$ vanishes.

end of validity of the Chapman-Enskog's expansion. Below that extreme value of the Knudsen's number, the ratio of these terms is roughly

$$\left|\frac{\eta E_{2z}}{(1-\sigma)E_{1z}}\right| \simeq \frac{|\Gamma(2;\eta^{-2\mu})|}{2\ \mathrm{Kn}^{3/4}}.$$

We found the above formula empirically. The heat flux density can be expressed as $q_{ez} = q_{eD\ z} + q_{eC\ z}$, where the diffusive term, $q_{eD\ z}$, is equal to $q_{SH\ z}$ multiplied by

$$R + \left(\frac{\lambda_{ei}^{T}}{3(\pi/2)^{1/2}}\right)^{2}\left(\delta_1\left[T_e^{-1}\frac{dT_e}{dz}\right]^{2} + \delta_2 T_e^{-1}\frac{d^2T_e}{dz^2} + \delta_3\left[\frac{dT_e}{dz}\right]^{-1}\frac{d^3T_e}{dz^3}\right), \qquad (2.26)$$

with $R, \delta_1, \delta_2$ and $\delta_3$ functions of $v_c/(v_T\sqrt{2}) = 1/\eta^{\mu} = [3(\pi/2)^{1/2}]^{\mu}/\mathrm{Kn}^{\mu}$. They are plotted in Fig. 2.6 for $Z = 1$ and $\mu = 1/5$. The function $R$, whose expression is

$$R\left(\frac{v_c}{v_T\sqrt{2}}\right) = \frac{1}{24}\left[\gamma\big(6; v_c^2/[2v_T^2]\big) - \frac{\gamma\big(5; v_c^2/[2v_T^2]\big)}{\gamma\big(4; v_c^2/[2v_T^2]\big)}\right], \qquad (2.27)$$

together with the term in which $\delta_1$ appears, only depend on the first order spatial derivative of $T_e$. Their sum must be interpreted as the reduction factor observed within regions of linear variation of the temperature profile. As visible from Fig. 2.6b, however, the second term, proportional to $\delta_1\mathrm{Kn}^2$, is negligible compared to $R$. The third term in Eq. (2.26), containing $\delta_2$, is positive where the electron temperature profile is convex, *i.e* above its tangents. Having in mind the structure

of the ablative flow, this term enhances the heat flux density at the foot of the temperature gradient. For a given value of $d^2T_e/dz^2 > 0$, the lower the temperature in the cold region, $T_C$, the greater the increase of such a preheating because of the factor $T_e^{-1}$. In the hot region at the entrance to the gradient, on the contrary, the temperature profile is concave. As a result, the considered term reduces the heat flux density. For the same magnitude of curvature in both regions, cold and hot, the effect of the considered term is by a factor $T_C/T_H$ weaker in the later one compared to the former one. The fourth term in Eq. (2.26), in which $\delta_3$ appears, also has effect at the edges of the region of almost linear variation of temperature. Geometrically, it is related to the *aberrancy* [68] of the temperature profile, *i.e* the tangent of the angle the axis of the osculating parabola makes with the normal line at a given point. In a word, it quantifies the local degree of asymmetry of the curve with respect to the normal line. Looking at Fig. 2.6b, it is unlikely that this term is of the same order of magnitude as the others except, maybe, within the under-dense region.

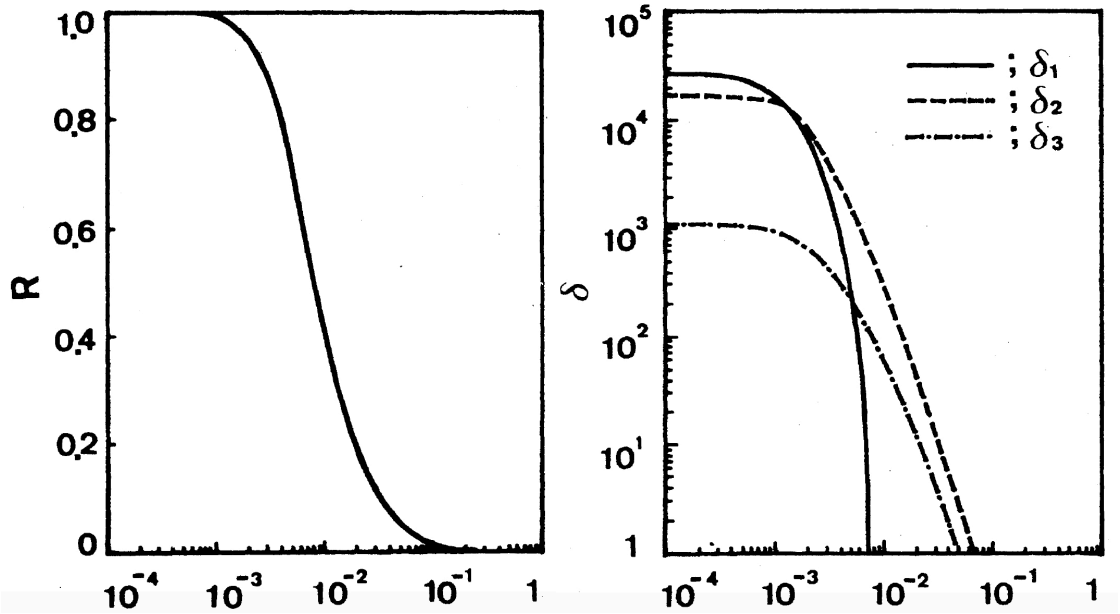


(a) (b)

Figure 2.6: Graphs of (a) $R$ and (b) $\delta_1$, $\delta_1$, $\delta_3$, as functions of Kn, for the critical velocity parameter $\mu = 1/5$. Extracted from Ref. [64].

The convective part of the heat flux density, plotted in Fig. 2.7, has the following expression:

$$q_{eC\ z} = (1-\sigma)\left[\Gamma\left(3; v_c^2/[2v_T^2]\right) - \frac{\gamma\left(5; v_c^2/[2v_T^2]\right)}{\gamma\left(4; v_c^2/[2v_T^2]\right)}\Gamma\left(2; v_c^2/[2v_T^2]\right)\right]\frac{n_e k_B T_e v_T}{(2\pi)^{1/2}}. \tag{2.28}$$

There appears the free-streaming flux, $n_e k_B T_e v_T/(2\pi)^{1/2}$. It is equal to $k_B T_e$ multiplied by the electron flux, $n_e(8k_B T_e/[\pi m_e])^{1/2}/4$, where

$$\left(\frac{8k_B T_e}{\pi m_e}\right)^{1/2} = \int_0^\infty v f_M\ 4\pi v^2 dv,$$

is the average norm of electron velocities in the case of a Maxwellian electron distribution function. The free-streaming flux also corresponds to the heat flux density associated to a distribution function with first order component on Maxwell's multipole equal to $3f_M/8$. The division by $(2\pi)^{1/2}$ is often omitted in the literature.

For a given value of Kn, $q_{eC\ z}$ is a decreasing function of $\mu$, and so of the critical velocity $v_c$, as expected. We found empirically the following estimation,

$$\frac{q_{eC\ z}}{(1-\sigma)n_e k_B T_e v_T/(2\pi)^{1/2}} \simeq 2\exp\left(-\frac{1}{2\eta^{9\mu/4}}\right),$$

which highlights a threshold value: $q_{eC\ z}$ cannot exceed $2(1-\sigma)$ times the free-streaming flux. The ratio between the diffusive and the convective parts, $q_{eC\ z}/[(1-\sigma)q_{eD\ z}]$, is plotted in Fig. 2.8. Their magnitudes become comparable for Knudsen's numbers of about ten percents in the limit case $\mu = 1/6$.

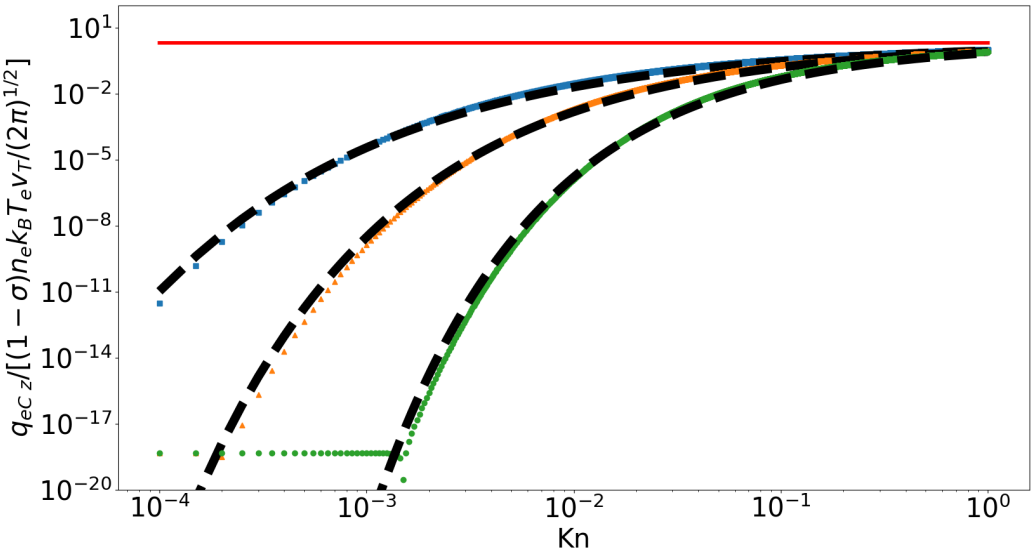


Figure 2.7: Graph of $q_{eC\ z}/[(1-\sigma)n_e k_B T_e v_T/(2\pi)^{1/2}]$ as function of Kn, for critical velocity parameter $\mu = 1/6$ (squares, blue), $1/5$ (triangles, orange), $1/4$ (circles, green). The black dashed lines represent the empirical approximation, $2\exp(-1/[2\eta^{9\mu/4}])$, for the corresponding values of $\mu$. The thin solid red line is the limit, 2, reached at infinity.

Kishimoto and Mima applied their formulae to the problem of temperature relaxation considered by Bell *et al* [69]. Their numerical results seem in qualitative agreement with the complete kinetic simulation performed by latter authors. In particular, Bell *et al.* observed that the heat flux density behaves as a multivaluated function of the Knudsen's number. A linear dependence (2.19) cannot account for this fact, justifying the account for a sum of higher order polynomial terms of Kn. Nevertheless, the approach of Kishimoto and Mima is not entirely satisfactory. In addition to $\sigma$, it contains the free parameter $\mu$ which determines the critical velocity (2.23). This uncertainty about such a threshold persists in most of the studies, as a consequence of its empirical introduction within the models.

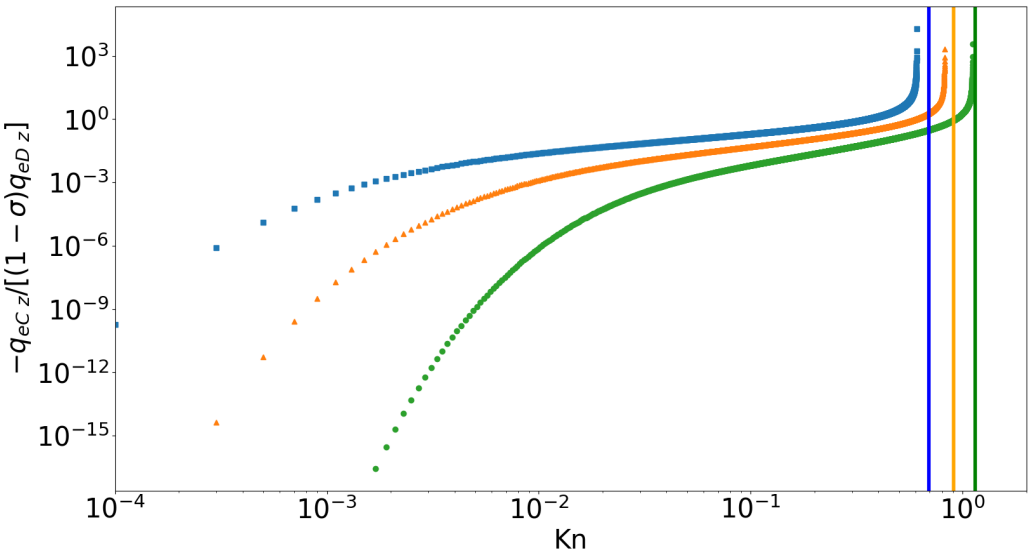


Figure 2.8: Case of a linear temperature profile. Graph of $-q_{eC\ z}/[(1-\sigma)q_{eD\ z}]$ as function of Kn, for critical velocity parameter $\mu = 1/6$ (squares, blue), $1/5$ (triangles, orange), $1/4$ (circles, green). The divergences occur at Kn $\simeq 3(\pi/2)^{1/2}/1.35^{1/\mu}$, the value for which $R$ vanishes.

Among them we want to mention the work of Ljepojevic and MacNeice [70], together with that of Manheimer *et al* [71]. Describing their work here would be too much of a detour for our concerns. An exception is the treatment of Gurevich and Istomin. There, the separation in two groups of electrons naturally emerges from the discontinuous character of the solution to their equations. Here, Kishimoto and Mima justified the expression of $v_c$ by determining the radius of convergence of their expansion. Hence, the indeterminacy of $\mu$ simply reveals the difficulty of this estimation.

In fact, the Chapman-Enskog's development is known to be asymptotic in the case of neutral gas [72]. An even more extreme behavior can be expected for plasmas. The series of partial sums might diverge as a monotonic, increasing function of the number of terms without going through any minimum. This issue has been studied by Luciani and Mora [44]. Although they did not analyse the expansion by itself in details, they demonstrated the possibility of its resummation. By extracting sub-sums converging toward finite terms they obtained a converging expansion with, however, nonlocal coefficients. Their procedure no longer leads to an expression of the heat flux density as an infinite sum of terms proportional to local derivatives, but to an integral expression involving a delocalization kernel. This kind of representation is the subject of the next section.

## 2.3.2 Integral formulae with delocalization kernels

### 2.3.2.1 Idea

Although the electron mean free path increases as the fourth power of the velocity, the number of electrons, however, decreases approximately as a Maxwellian. As

a result, the dominant contribution to the integrand of the heat flux density, proportional to $v^5\mathbf{f}_1$ (2.3), comes from electrons with velocities around 3.5 $v_T$. In average, they travel over distances $3.5^4 \simeq 160$ times greater than thermal electrons before experiencing a collision. It therefore seems reasonable to describe this group of electrons by an advection equation with a source term. We will momentarily assume that, in fact, all the electrons behave in this way. Let us consider as a source term the most rudimentary operator, that of Bhatnagar *et al* [73]: $v\mathbf{\Omega}\cdot\boldsymbol{\nabla} f_e = -\nu_d(f_e - f_M)$. This equation can obviously be seen as a reduced form of the kinetic equation (2.1); the right hand side accounting for both the electric field term and the nonlinear collision operators. The projections of this advection equation on the zeroth and first order Maxwell's multipoles are $(v/3)\boldsymbol{\nabla}\cdot\mathbf{f}_1 = -\nu_d(f_0 - f_M)$ and $v\boldsymbol{\nabla} f_0 = -\nu_d\mathbf{f}_1$. Substituting the second equation in the first one leads to a diffusion equation on $f_0$. Without lost of generality, we restrict ourselves to the case of a one-dimensional plasma along the $z$-axis. Hence, the equation is

$$\partial_z\left[\nu_d\lambda_d^2\partial_z f_0\right] - \nu_d f_0 = -\nu_d f_M \tag{2.29}$$

where we introduced $\lambda_d = v/(\nu_d\sqrt{3})$ for convenience. So far, no assumptions have been made about $\nu_d$, except the fact we have, implicitly, considered it independent of $\mathbf{\Omega}$.

If $\nu_d$ is independent of $z$, the Eq. (2.29) can be solved in an elementary way. The solutions to the associated homogeneous equation are of the form $C_- e^{-z/\lambda_d} + C_+ e^{+z/\lambda_d}$. A particular solution is researched in that form, with $C_\mp$ functions of $z$. Their derivatives must verify the following system,

$$C_-' e^{-z/\lambda_d} + C_+' e^{+z/\lambda_d} = 0; \quad -\frac{C_-'}{\lambda_d}e^{-z/\lambda_d} + \frac{C_+'}{\lambda_d}e^{+z/\lambda_d} = -\frac{f_M}{\lambda_d^2},$$

whose solution is $C_\mp' = \pm f_M e^{\pm z/\lambda_d}/\lambda_d$. Supposing that $C_\mp$ vanishes at $\mp\infty$, we obtain $C_\mp = \mp\int_z^{\mp\infty} f_M e^{\pm z'/\lambda_d}\, dz'/2\lambda_d$. Then, the solution of Eq. (2.29) is the sum of the homogeneous and particular solutions. Since $f_0(z = \pm\infty) = 0$, the homogeneous part actually vanishes. The sum of the two remaining terms is

$$f_0 = \frac{1}{2\lambda_d}\int_{-\infty}^{+\infty} f_M e^{-|z'-z|/\lambda_d}\, dz', \tag{2.30}$$

from which we deduce

$$\begin{aligned} f_{1z} &= -\lambda_d\sqrt{3}\partial_z f_0 \\ &= \frac{\sqrt{3}}{2\lambda_d}\left[e^{-z/\lambda_d}\int_{-\infty}^{z} f_M e^{z'/\lambda_d}\, dz' - e^{+z/\lambda_d}\int_z^{+\infty} f_M e^{-z'/\lambda_d}\, dz'\right] \\ &= \frac{\sqrt{3}}{2}\int_{-\infty}^{+\infty} f_M\left[\frac{d}{dz'}e^{-|z'-z|/\lambda_d}\right] dz' = -\frac{\sqrt{3}}{2}\int_{-\infty}^{+\infty} e^{-|z'-z|/\lambda_d}\partial_{z'} f_M\, dz'. \end{aligned} \tag{2.31}$$

In the last step, we integrated by parts. This expression can also be obtained by integration from Eq. (2.29) which yields $\partial_z f_{1z} = \sqrt{3}(f_M - f_0)/\lambda_d$. A third option, which does not require the integral formula (2.30) of $f_0$, is to solve the diffusion equation verified by $f_{1z}$,

$$\partial_z^2 f_{1z} - \frac{f_{1z}}{\lambda_d^2} = \frac{\sqrt{3}}{\lambda_d}\partial_z f_M - \frac{3(f_0 - f_M)}{v}\partial_z\nu_d,$$

in the considered case $\partial_z \nu_d = 0$. It is possible, in the expression (2.31) of $f_{1z}$, to write explicitly the derivative of $f_M$. When determining the heat flux density, we found that it leads to heavier calculations than the following way. It is based on symbol inversions, the possibility of which is justified by the correctness of the final result. Let us assume that $\lambda_d$ is independent of $v$, implying that $\nu_d$ is a linear function of it. Starting from Eq. (2.3),

$$q_{ez} = -\frac{\pi m_e}{\sqrt{3}} \int_{-\infty}^{+\infty} e^{-|z'-z|/\lambda_d} \frac{d}{dz'} \left( \int_0^{+\infty} v^5 f_M \, dv \right) \, dz' \tag{2.32}$$

There appears the free streaming flux through

$$\frac{2\pi m_e}{3} \int_0^{+\infty} v^5 \left( \frac{3}{8} f_M \right) \, dv = \frac{n_e k_B T_e v_T}{(2\pi)^{1/2}}.$$

Since

$$\frac{d}{dz'}(n_e k_B T_e v_T) = m_e v_T^3 \left( \frac{dn_e}{dz'} + \frac{3n_e}{2T_e} \frac{dT_e}{dz'} \right),$$

the heat flux density (2.32) is the sum of two terms. One of them involves the gradient of electron temperature, for which we find the following expression

$$\int_{-\infty}^{+\infty} \mathcal{W} \, q_{\mathrm{SH}\ z} \, dz', \tag{2.33}$$

with $\mathcal{W}(z, z'; \lambda_d)$ equal to $3(6\pi)^{1/2}\zeta(Z)/[128\lambda_{ei}^T] \; e^{-|z'-z|/\lambda_d}$. The other term, containing the gradient in electron density, has a similar expression. In the limit of small Knudsen's number, the expression (2.32) must tend toward that of Spitzer and Härm (2.19). Thus, the inconsistency of the approach here is twofold. The term containing $dn_e/dz'$ is an anomaly as it does not disappear in that limit. In fact, the reason of its appearance is the neglect of the electric field term in the reduced kinetic equation from which we started. This will become clearer in the next chapter. Even by restricting the analysis to an homogeneous plasma, the kernel $\mathcal{W}(z, z'; \lambda_d)$ still has to converge toward $\delta(z' - z)$. Since the representation involved here of this Dirac's distribution is the continuous sequence of functions $e^{-|z'-z|/\lambda_d}/(2\lambda_d)$, this would impose to define $\lambda_d$ as $64\lambda_{ei}^T/[3(6\pi)^{1/2}\zeta(Z)]$. Such a choice is impossible given the assumed constancy of the delocalization length.

We might hope to solve these problems in part by repeating the above resolution without this later assumption. The difficulty is that the spatial dependence of $\lambda_d$ brings the resolution of Eq. (2.29) back to a non trivial Sturm-Liouville's problem [74] with boundaries conditions $f_0(z = \pm\infty) = \partial_z f_0(z = \pm\infty) = 0$. Like before, $v$ will be omitted as being considered as a parameter. Let us write the Eq. (2.29) as

$$\mathsf{O}[f_0] = -\nu_d f_M; \quad \mathsf{O}[f_0] = \partial_z \left[ \nu_d \lambda_d^2 \partial_z f_0 \right] - \nu_d f_0, \tag{2.34}$$

and denote $\mathcal{W}_0(z, z')$ the Green's function of the linear operator $\mathsf{O}$,

$$\mathsf{O}[\mathcal{W}_0] = \delta(z' - z). \tag{2.35}$$

Then, we compute the following integral, $\int_{-\infty}^{+\infty} \Big( \mathcal{W}_0 \mathsf{O}[f_0] - f_0 \mathsf{O}[\mathcal{W}_0] \Big)\, dz'$, in two ways. Firstly, it is equal to $\int_{-\infty}^{+\infty} \mathcal{W}_0 \mathsf{O}[f_0]\, dz' - f_0$ by using Eq. (2.35). Secondly, from Eq. (2.34), it may be expressed as

$$\int_{-\infty}^{+\infty} \Big( \mathcal{W}_0 \partial_{z'} \left[ \nu_d \lambda_d^2 \partial_{z'} f_0 \right] - f_0 \partial_{z'} \left[ \nu_d \lambda_d^2 \partial_{z'} \mathcal{W}_0 \right] \Big)\, dz' = 0,$$

after two successive by parts integrations of either the first or the second term. Hence, by using Eq. (2.34),

$$f_0 = \int_{-\infty}^{+\infty} \mathcal{W}_0 \, \left[ -\nu_d f_M \right] \, dz', \tag{2.36}$$

as expected. By comparing this expression to Eq. (2.30), it may be deduced that $\mathcal{W}_0$ is equal to $-e^{|z'-z|/\lambda_d}/(2\lambda_d \nu_d)$ in the case of a constant delocalization length. As already visible from this formula, the Green's function is continuous with respect to both variables but has a discontinuous derivative. To determine the value of the jump, we integrate Eq. (2.35) on $[z-\eta; z+\eta]$ with respect to $z'$, where $\eta > 0$. This leads to

$$1 = \Big[ \nu_d \lambda_d^2 \partial_z \mathcal{W}_0 \Big]_{z'=z-\eta}^{z'=z+\eta} - \int_{z-\eta}^{z+\eta} \nu_d \mathcal{W}_0 \, dz'.$$

In the limit of increasingly small values of $\eta$, the integral of the right hand side vanishes by continuity of the integrand, and

$$\partial_z \mathcal{W}_0(z, z^+) - \partial_z \mathcal{W}_0(z, z^-) = \frac{1}{[\nu_d \lambda_d^2](z)} = \frac{3\nu_d(z)}{v}.$$

This relation can be directly verified in the case of a constant delocalization length, for which $\partial_z \mathcal{W}_0(z, z^\pm) = \pm 1/(2\nu_d \lambda_d^2)$. Finally, the Green's function is symmetrical in both its arguments. This property, that it is essential to preserve during a discretization, is obvious in the case of constant $\lambda_d$. Although it can be shown in general, it will be admitted here: $\mathcal{W}_0(z, z') = \mathcal{W}_0(z', z)$.

In order to express $f_{1z}$ and then $q_{ez}$, we need to compute the derivative of $f_0$ (2.36), which is a parameter-dependent integral. The inversion of $\partial_z$ with the integral with respect to $z'$ cannot be done because of the discontinuous derivative of $\mathcal{W}_0$. This leads to the impossibility of expressing the delocalized kernel for the heat flux density, $\mathcal{W}$, in term of $\mathcal{W}_0$. There exists some diffusion equations, different from Eq. (2.29)-(2.34), for which this procedure is feasible, at least in an approximate way. In this respect, many authors have proposed expressions for $\mathcal{W}$ based on more or less complex equations on $f_0$ and $f_{1z}$. Often these equations do not correspond to the projections of a kinetic equation on the corresponding Maxwell's multipoles, but result from different approximations on the behaviours of $f_0$ and $f_{1z}$. Some of such approaches are briefly reviewed in the next section. An alternative strategy to determine an appropriate expression of $\mathcal{W}$ relies on its Fourier's transform. In purpose of illustration, let us consider the kernel we could have wished for in case of constant delocalization length $\lambda_d$:

$$\mathcal{W}(z, z'; \lambda_d) = \frac{1}{2\lambda_d} e^{-|z'-z|/\lambda_d}. \tag{2.37}$$

The exponential can be expressed as an inverse Fourier's transform,

$$e^{-|z'-z|/\lambda_d} = \frac{1}{2\pi}\int_{-\infty}^{+\infty} \frac{2\lambda_d}{1+(k'_z\lambda_d)^2}\cos[k'_z(z'-z)]\ dk'_z.$$

There should appear $e^{ik'_z(z'-z)} = \cos[k'_z(z'-z)] + i\sin[k'_z(z'-z)]$ within the integrand, but the integral with the sine is zero by invariance of the exponential under the exchange of variables $z'$ and $z$. Let us consider an electron temperature with a single Fourier's component, $T_e = \langle T_e\rangle + \delta T_e\ \sin(k_z z)$, where $\langle T_e\rangle$ and $\delta T_e$ are constants such that $\delta T_e < \langle T_e\rangle$. On the one hand,

$$q_{\mathrm{SH}\ z} = -\kappa_{\mathrm{SH}}\delta T_e k_z\cos(k_z z).$$

On the other hand, the heat flux density of the form given by Eq. (2.33) is

$$q_{ez} = \int_{-\infty}^{+\infty}\mathcal{W}\ q_{\mathrm{SH}\ z}\ dz' = -\frac{\kappa_{\mathrm{SH}}\delta T_e k_z}{2\pi}\int_{\infty}^{+\infty}\int_{\infty}^{+\infty}\frac{\cos[k'_z(z'-z)]\cos(k'_z z')}{1+(k'_z\lambda_d)^2}\ dk'_z dz'.$$

The order of integration with respect to $k'_z$ and $z'$ can be inverted. By doing so, there appears

$$\int_{\infty}^{+\infty}\cos[k'_z(z'-z)]\cos(k_z z')\ dz' = \pi\big[\delta(k'_z-k_z)+\delta(k'_z+k_z)\big]\cos(k'_z z).$$

One way of obtaining this relation is to use the Euler's formula together with the well-known identity: $\int_{\infty}^{+\infty} e^{ik_z z'}\ dz' = 2\pi\delta(k_z)$. As expected given the meaning of the Fourier's transform, we obtain

$$q_{ez} = -\frac{\kappa_{\mathrm{SH}}}{1+(k_z\lambda_d)^2}\delta T_e k_z\cos(k_z z).$$

Of course the Fourier's transform of $\mathcal{W}$ could have been determined from the calculation of the integral of $e^{-|z'-z|/\lambda_d}\cos(k_z z')$ through two successive by parts integrations. It must be mentioned that a Fourier's component of the form $\delta T_z\cos(k_z z)$ does not lead to any heat flux density because $\int_{\infty}^{+\infty}\cos[k'_z(z'-z)]\sin(k_z z')\ dz' = \pi\big[\delta(k'_z-k_z)-\delta(k'_z+k_z)\big]\cos(k'_z z)$. Finally, by comparing the expressions of $q_{\mathrm{SH}\ z}$ and $q_{ez}$, it must be concluded that the heat flux density associated to one Fourier's component of the electron temperature follows the Spiter-Härm's law (2.19) with, however, an effective thermal conductivity equal to $\kappa_{\mathrm{SH}}/[1+(k_z\lambda_d)^2]$. Hence, several authors proposed kernels with Fourier's components of the form

$$\frac{1}{1+[\alpha k_z(Z+1)^{1/2}\lambda_0]^\beta}, \tag{2.38}$$

where $\alpha$ and $\beta$ are parameters and

$$\lambda_0 = \frac{\lambda_{ei}(v_T)\lambda_{ee}(v_T)}{\lambda_{ei}(v_T)+\lambda_{ee}(v_T)}, \tag{2.39}$$

is the harmonic mean of the velocity-dependent electron-electron, $\lambda_{ee}$, and electron-ion, $\lambda_{ei}$, mean free paths evaluated at $v_T$. The origin of this expression is clarified in the next section. Most of the time, $\alpha$ and $\beta$ are determined by numerical fits in order to facilitate the comparison between kernels which often have Fourier's components with heavier expressions.

Thus, two possible strategies have been identified to find an appropriate kernel. One is to build and solve a diffusion equation on the distribution functions $f_0$ and $f_{1z}$, the other is to start from the Fourier's representation of $\mathcal{W}$.

#### 2.3.2.2 A gallery of kernels

Of historical importance is the kernel, $\mathcal{W}_{\text{LMV83}}$, proposed by Luciani *et al.* in Ref. [75]. It has the expression (2.37), with the delocalization length equal to $\lambda_d = 32(Z+1)^{1/2}\lambda_0$, together with

$$\tau(z,z') = \frac{1}{n_e(z')}\left|\int_z^{z'} n_e(z'')\,dz''\right|, \tag{2.40}$$

in place of $|z'-z|$. Latter expression is recovered in the case of a constant electron density. Their delocalization length is the product of three factors. The last one, $\lambda_0$ (2.39), is the thermal mean free path associated with all the scattering collisions experienced by a thermal electron. Their frequency is $\nu_{ee}(v_T)+\nu_{ei}(v_T) = (Z+1)\nu_{ee}(v_T)$. As it will be further detailed in the next chapter, the rate of collisions with energy exchanges between high-velocity electrons and thermal ones is roughly $\nu_{ee}(v_T)$. Therefore, the root mean square displacement of a fast electron between two successive energy exchanges is $(Z+1)^{1/2}$ times the aforementioned scattering length $\lambda_0$, as accounted for by Luciani *et al.* By doing so they implicitly assumed the electron's random walk as being Gaussian. Finally, the factor 32 is obtained by comparison with complete kinetic simulations. One is shown in Fig. 2.9. Although the approach for determining $\mathcal{W}_{\text{LMV83}}$ is mostly empirical, similar kernels have been obtained by the same team from iterative resolutions of several reduced P1 systems. Two of them are, for $\delta = \{0,1\}$:

$$\mathcal{W}_\delta = \frac{1}{2\pi}\int_{-\infty}^{+\infty}\frac{1}{24}\left(I_{6,4+\delta} - \frac{I_{5,3+\delta}I_{5,4+\delta}}{I_{4,3+\delta}}\right)e^{ik_z\tau}\,dk_z,$$

where

$$I_{l,m} = \int_0^{+\infty} y^l e^{-y}\int_0^1 x^m \exp\left[-\frac{30-\delta 26}{45}k_z^2(Z+1)\lambda_0^2\big(1-x^{4+\delta}\big)y^{4+\delta}\right]\,dxdy.$$

Following the notations of Mora and Luciani's review [76], $\mathcal{W}_0 = \mathcal{W}_{\text{LMB85}}$, and $\mathcal{W}_1 = \mathcal{W}_{\text{K'}}$. This last kernel is similar to that obtained by Krasheninnikov in Ref. [77]. It would be both difficult and pointless to enumerate all the existing kernels. Readers are invited to refer to the aforementioned review, together with the recent works of Ji and Held [78], Lu *et al* [79], and Dimits *et al* [80].

None of the aforementioned kernels include the electric field, as being derived from equations in which the underlying terms are neglected. This have been justified by Luciani *et al* in Ref. [81] in case of a small temperature jump and constant density. They mentioned that such an account is unnecessary since the effect is already accounted for in the heat flux density on which the kernel acts. The approach of Albritton *et al* [82] was designed to remedy this shortcoming. Their original expression of the heat flux density is not in the form (2.33), but contains an additional term involving the nonlocal part of the electric field. Its complete expression will not be written here. For small temperature jump, however, Holstein and Decoster [83] shown that the Albritton *et al* 's formula can be approximated by the usual form. The underlying kernel, $\mathcal{W}_{\text{AWBS86}}$, has the approximate Fourier's component (2.38) given in Tab. 2.1. Despite their very different appearances, $\mathcal{W}_{\text{AWBS86}} \simeq \mathcal{W}_{\text{LMB85}}$, as visible in Fig. 2.10.

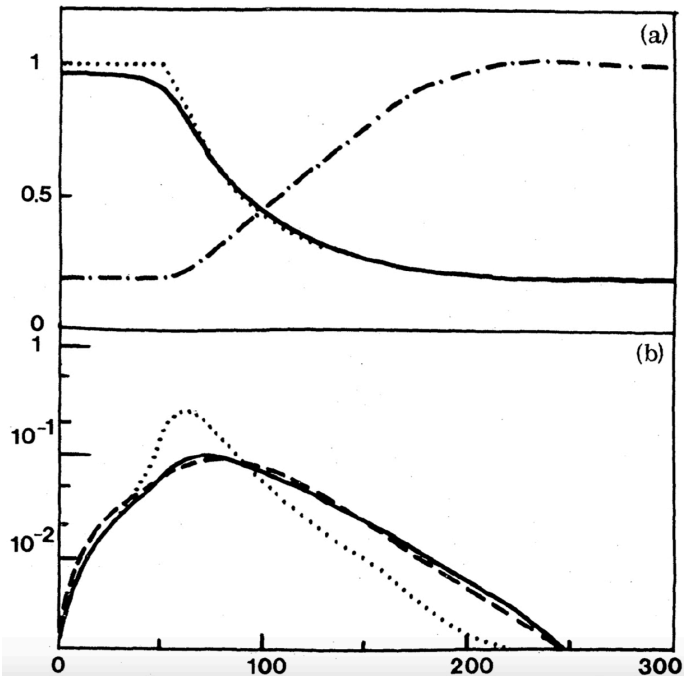


Figure 2.9: Extracted from Ref. [75]. Comparison of heat flux densities in a crossed configuration of electron temperature and density gradients. In the upper part (a) are plotted the initial (dotted line) and final (solid line) temperature profiles, together with the electron density (dash-dotted line). Unfortunately, the authors did not specify the units. Below (b) are plotted the final heat flux densities normalized to $n_e k_B T_e v_T$, given by the kinetic simulation (solid line), the Spitzer-Härm's formula (2.19)(dotted line), and the integral formula with the delocalized kernel $\mathcal{W}_{\text{LMV83}}$ (dashed line). For both figures the abscissa axis is graduated in number of $\lambda_d = 32(Z+1)^{1/2}\lambda_0$ evaluated at the hot temperature.

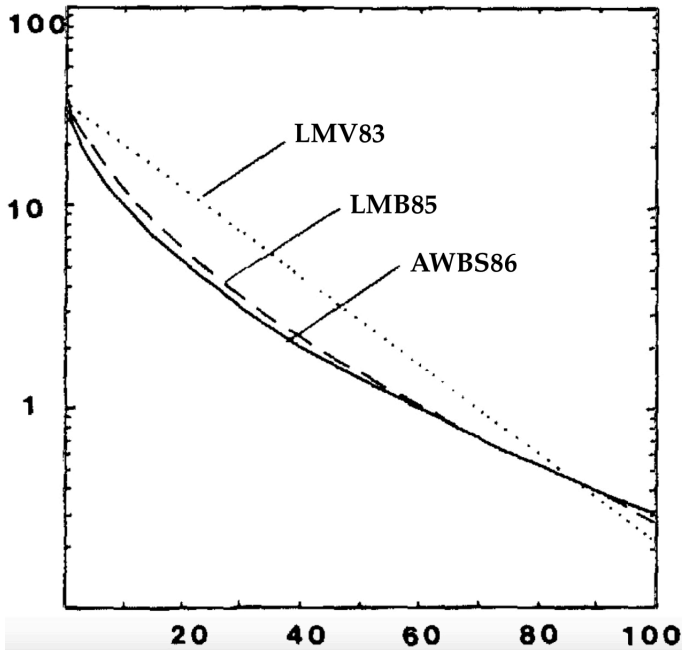


Figure 2.10: Slightly adapted from Ref. [83]. Three kernels as a function of the optical distance $\tau/0.05$ (2.40). Although being homogeneous to the inverse of a length, no unit is specified by the authors for the ordinate axis.

| | LMV83 [75] | AWBS86 [82] | S96 [84] | ES91 [85] | BBDRSCN02 [86] |
|---|---|---|---|---|---|
| $\beta$ | 2 | 3/2 | 10/7 | 1 | 9/10 |
| $\alpha$ | 32.0 | 17.9 | 21.6 | 50 | 37.6 |

Table 2.1: Parameters involved in the formula (2.38) approximating the Fourier's component of some kernels. The value of $\alpha$ for the kernel of Batishchev *et al.* [86] is written in the high-$Z$ limit.

Holstein and Decoster compared the resulting heat flux densities to that of a complete kinetic calculation in the case considered by Albritton in Ref. [87], consisting of a large temperature jump. The results agree within few percent in the conduction region, beyond the critical electron density, if the systematic shift between curves is ignored. Hence, the formulae for $\mathcal{W}_{\text{AWBS86}}$ and $\mathcal{W}_{\text{LMB85}}$ are actually valid outside of the restricted situation in which they have been derived. This indicates the general smallness of the term containing the nonlocal part of the electric field in the heat flux density. In spite of this fact, Bendib *et al* [88] proposed a semi-phenomenological kernel in which the electrostatic potential appears explicitly. The gain seems substantial with regard to some of the criticisms levelled by Prasad and Kershaw [89].

The accuracy of all these models depend on the spatial scale of the electron temperature variations. A convenient way to analyse the problem is to consider the decay of a single Fourier's component of the electron temperature for different wavelengths: $T_e = \langle T_e \rangle + \delta T_e \, \sin(k_z z)$, where $\langle T_e \rangle$ is a constant and $\delta T_e < \langle T_e \rangle$. The electron density is considered constant. The amplitude of the perturbation, $\delta T_e$, evolves according to the energy conservation equation, $(3/2) n_e k_B \partial_t T_e + \partial_z q_{ez} = 0$ which yields $\partial_t \delta T_e + 2\kappa_{\text{SH}} k_z^2 / \left[3 n_e (1 + [\alpha k_z (Z+1)^{1/2} \lambda_0]^\beta)\right] \delta T_e = 0$, given the generic form (2.38) of the Fourier's component of $q_{ez}$. This test, suggested by Epperlein and Short in Ref. [85], allowed to compare a wide variety of kernels. For some of them $\alpha$ and $\beta$ are given in Tab. 2.1. The comparison with the complete kinetic calculation [85, 76] reveals the following tendency. Kernels with $\beta > 1$ can provide accurate heat flux densities for long wavelengths, $k_z \lambda_0 \ll 1$, while resulting in a significant error for $k_z \lambda_0 \lesssim 1$. In the latter limit, the most precise model is that of Batishchev *et al.*, developed within the framework of nonlocal hydrodynamics. Although being written in the high-$Z$ limit, the authors provided its expression for an arbitrary ionization number. This is the case for none of other mentioned kernel. An extension to $\mathcal{W}_{\text{AWBS86}}$ for any value of $Z$ have been proposed [90]. To our knowledge, this work did not lead to comparison yet.

### 2.3.3 Advection equation solved by a multigroup method

For the purpose of determining the heat flux density at a point $\mathbf{r}$, it is not necessary to use the expression

$$\int \mathcal{W}_{ij} \; q_{\text{SH } j} \; d^3\mathbf{r}', \tag{2.41}$$

as previously exposed in the one dimensional case. In principle, the kernel $\mathcal{W}_{ij}$ can be considered as the Green's function of a diffusion equation on $\mathbf{q}_e$, which

may be directly solved numerically. Such an equation is explicitly written in three dimensions at the end of Ref. [76], but has never been implemented due to its intractability. To overcome this difficulty Schurtz *et al* [91] proposed to use

$$\mathcal{W}_{\mathrm{SNB00}\ ij} = \frac{3}{4\pi}\Omega_i\Omega_j\mathcal{W}_{\mathrm{LM86\sharp}}, \tag{2.42}$$

written in spherical coordinates in the space of positions. $\mathcal{W}_{\mathrm{LM86\sharp}}$ is the slightly modified, one dimensional kernel of Luciani and Mora [76] having the following form

$$\mathcal{W}_{\mathrm{LM86\sharp}} = \frac{1}{24}\int_0^{+\infty} y^4 e^{-y}\ \mathcal{W}_{\mathrm{LMV83\sharp}}\ dy. \tag{2.43}$$

$\mathcal{W}_{\mathrm{LMV83\sharp}}$ is the first kernel of Luciani *et al* [75] we presented, with a different delocalization length $\lambda_\sharp$. It is a function of $(s, s')$ with $s = \mathbf{r}\cdot\mathbf{\Omega}$. Within the above integral over $y$, only this length depends on the integration variable in $\mathcal{W}_{\mathrm{LMV83\sharp}}$. Inserted in Eq. (2.41), the kernel (2.42) leads to

$$q_{e\ i} = \frac{3}{4\pi}\int_{\mathbb{S}^2}\Omega_i Q\ d^2\Omega; \quad Q = \int_0^{+\infty}\mathcal{W}_{\mathrm{LM86\sharp}}\ [\Omega_j q_{\mathrm{SH}\ j}]\ ds'. \tag{2.44}$$

The interpretation is rather clear. The heat flux density appears as the projection on the first order Maxwell's multipole of a function $Q$. This function, of the form (2.36), turns out to be the solution of a linear differential equation whose Green's function is $\mathcal{W}_{\mathrm{LM86\sharp}}$, with a source term equal to the scalar product $\Omega_j q_{\mathrm{SH}\ j}$. The appearance of $\Omega_i\Omega_j$ in Eq. (2.42) has nothing to do with the electron's paths. As suggested by the authors themselves, echoing what a Green's function is, their formula is obtained by considering each point $\mathbf{r}'$ of space as a source of heat flux density. Such a source is not isotropic since its contribution in the direction $\mathbf{\Omega}$ is the projection of the Spitzer-Härm's heat flux density on that direction, $\Omega_j q_{\mathrm{SH}\ j}$. As the integral over $\mathbb{S}^2$ of this scalar product is zero, the negative and positive contributions of the source cancel each other. So, no heat flux density is created at that point, as it must be. The contribution, $Q$, of the source to the heat flux density at a certain point $\mathbf{r}$, is the source's magnitude at the point $\mathbf{r}'$, $\Omega_j q_{\mathrm{SH}\ j}$, attenuated along the straight line that links the points by an almost exponential factor $\mathcal{W}_{\mathrm{LM86\sharp}}$. Then, each component $q_{e\ i}$ is the angular average of all these contributions. Readers will have noticed the analogy with the Huyghens-Fresnel's principle in optics.

Unfortunately, it appears difficult to find the differential operator to which $\mathcal{W}_{\mathrm{LM86\sharp}}$ is the Green's function. In the case of $\mathcal{W}_{\mathrm{LMV83\sharp}}$, however, it reads $\lambda_\sharp\ \mathbf{\Omega}\cdot\boldsymbol{\nabla}+\mathsf{I}$, where the modified optical length $\tau(s, s')$ (2.40) must be replaced by $\tau_\sharp = \int_s^{s'}(ds''/\lambda_\sharp)$, the number of delocalization lengths $\lambda_\sharp$ over the segment of size $|\mathbf{r}' - \mathbf{r}|$. By doing so the resulting kernel is symmetrical with respect to the exchange of $\mathbf{r}$ and $\mathbf{r}'$. This leads to a self-adjoint equation convenient for numerical implementation. The authors used a multigroup technique [92]. It consists of solving separately the transport problem for groups of electrons with different velocities. By noting $\beta = v^2/(2v_T^2)$, the real axis is considered as the reunion of the infinite sequence of

segments $[\beta_{g-1};\beta_g]$ for $g=1\dots\infty$ with $\beta_0=0$. Then $Q$ (2.44) is written as

$$\int_0^\infty \left(\sum_{g=1}^{+\infty}\int_{\beta_{g-1}}^{\beta_g}\frac{1}{24}y^4e^{-y}\,\mathcal{W}_{\mathrm{LMV83}\sharp}\,dy\right)[\Omega_j q_{\mathrm{SH}\ j}]\,ds' \simeq \sum_{g=1}^{+\infty}\int_0^\infty \mathcal{W}_{\mathrm{LMV83}\sharp\ g}\,[\Omega_j U_{g\ j}]\,ds',$$

with $\mathcal{W}_{\mathrm{LMV83}\sharp\ g}$ the average value of the kernel over the segment $[\beta_{g-1};\beta_g]$, and $U_{g\ j}=q_{\mathrm{SH}\ j}\int_{\beta_{g-1}}^{\beta_g}y^4e^{-y}/24\,dy$. As a result, $Q$ can be viewed as the infinite sum of functions, $Q_g$, defined as

$$Q_g=\int_0^\infty \mathcal{W}_{\mathrm{LMV83}\sharp\ g}\,[\Omega_j U_{g\ j}]\,ds'.$$

Each of these functions therefore verifies $\lambda_{\sharp\ g}\,\boldsymbol{\Omega}\cdot\boldsymbol{\nabla}Q_g+Q_g=\Omega_jU_{g\ j}$. The source term is now the fraction, $\int_{\beta_{g-1}}^{\beta_g}y^4e^{-y}/24\,dy$, of the Spitzer-Härm's heat flux density associated to the group $g$. The component $q_{e\ i}$ is the infinite sum of $q_{e\ i\ g}=\int_{\mathbb{S}^2}\Omega_iQ_g\,d^2\Omega$. Hence it appears sufficient to solve the advection equation in the P1 approximation. By noting

$$H_g=\frac{1}{4\pi}\int_{\mathbb{S}^2}Q_g\,d^2\Omega,$$

the P1 system is composed by $-(\lambda_{\sharp\ g}/3)\boldsymbol{\nabla}\cdot\mathbf{q}_{e\ g}+H_g=0$ and $\lambda'_{\sharp\ g}\boldsymbol{\nabla}H_g+\boldsymbol{q}_{e\ g}=\mathbf{U}_g$. Hence, $H_g$ verifies the following diffusion equation,

$$-\boldsymbol{\nabla}\cdot\lambda'_{\sharp\ g}\boldsymbol{\nabla}H_g+\frac{3}{\lambda_\sharp}H_g=\boldsymbol{\nabla}\cdot\mathbf{U}_g,$$

and the heat flux density is

$$\mathbf{q}_e=\mathbf{q}_{\mathrm{SH}}-\sum_{g=1}^{+\infty}\lambda'_{\sharp\ g}\boldsymbol{\nabla}H_g.$$

Here, $\lambda'_\sharp$ is the delocalization length modified *a posteriori* by Schurtz *et al* whose expression will be specified below. The above equations are quite similar to those of Sec. 2.3.2.1. Indeed, the starting advection equations verified by $f_e$ and $Q_g$ are almost the same, so are the associated P1 systems. Although the kinetic character of the multigroup formalism is obvious, the link between $H_g$ and the components of $f_e$ on the first two orders Maxwell's multipoles is not immediate. In fact, the method can be interpreted as a first order perturbation resolution [91] of the system (2.14)-(2.15) with the Bhatnaghar *et al*'s collision operator for electron-electron energy exchange,

$$\mathcal{C}^0_{ee}=-r(Z)\nu_{ee}(f_0-f_M),$$

together with the approximation $\boldsymbol{\mathcal{C}}^1_{ei}+\boldsymbol{\mathcal{C}}^1_{ee}=-\zeta(Z)\nu_{ei}\mathbf{f}_1$. The zero-order solutions are given by expressions in the local regime: $f_0=f_M$ (2.4), $\mathbf{f}_1=\mathbf{f}_{1,\mathrm{L}}$ and $\mathbf{E}=\mathbf{E}_{\mathrm{L}}$,

whose formulae are given in the next chapter. The perturbation $\delta f_0 = f_0 - f_M$ obeys the following equation:

$$-\boldsymbol{\nabla}\cdot\frac{v^2}{3\nu_{ei}^E}\boldsymbol{\nabla}\delta f_0 + r(Z)\nu_{ee}\delta f_0 = -v\boldsymbol{\nabla}\cdot\frac{v f_M}{3\zeta(Z)\nu_{ei}}\frac{\boldsymbol{\nabla}T_e}{T_e}, \tag{2.45}$$

and $\delta\mathbf{f}_1 = \mathbf{f}_1 - \mathbf{f}_{1,\mathrm{L}}$ is deduced from the relation $\delta\mathbf{f}_1 = -(v/\nu_{ei}^E)\boldsymbol{\nabla}\delta f_0$. The effective electron-ion collision frequency,

$$\nu_{ei}^E = \zeta(Z)\nu_{ei} + 2e|\mathbf{E}_{\mathrm{SH}}|/(m_e v), \tag{2.46}$$

indirectly accounts for the electric field effect on these perturbations. Hence, the link with the original formulation of the model is provided by the following relations:

$$\lambda_\sharp' = v/\nu_{ei}^E; \quad \lambda_\sharp = v/[r(Z)\nu_{ee}] \tag{2.47}$$

In Ref. [93], Brodrick *et al* showed numerically that a multiplicative factor, $r$, equal to 2 significantly improved the agreement of the Schurtz *et al*'s results with complete kinetic simulations. Sherlock *et al* [94] further confirmed this empirical choice. Their finding will be analytically recovered in the next chapter. Let us now compare the expression of the heat flux density perturbation, $\delta\mathbf{q}_e$ with the multigroup discretization. On the one hand, it is equal to the sum over $g$ of $-\lambda_{\sharp g}'\boldsymbol{\nabla}H_g$. On the other, to the sum of $(2\pi m_e/3)v_g^5\delta\mathbf{f}_{1g}\Delta v_g$, with $\Delta v_g$ the length of the segment of the velocity axis in which the electrons of the group $g$ belong. Hence,

$$\delta\mathbf{f}_1 = \sum_{g=0}^{\infty}\delta\mathbf{f}_{1g}, \quad \delta\mathbf{f}_{1g} = -\frac{3\lambda_{\sharp g}'}{2\pi m_e v_g^5\Delta v_g}\boldsymbol{\nabla}H_g,$$

from which we also deduce:

$$\delta f_0 = \sum_{g=0}^{\infty}\delta f_{0g}, \quad \delta f_{0g} = \frac{H_g}{2\pi m_e v_g^5\Delta v_g}.$$

The multigroup method developed by Schurtz *et al* is probably the most widely used within the community. It is implemented in many codes such as CHIC [95] in Bordeaux, DRACO [96] in Rochester, HYDRA [97] in Livermore, or DUED [98] in Rome. This popularity makes a detailed understanding of the model's limitations especially important.

In one spatial dimension, the aforementioned studies by Brodrick *et al.* [93] and Sherlock *et al.* [94] reported, with only a few exceptional cases, acceptable accuracy of the model compared to full kinetic computations of the heat flux density induced by a steep temperature gradient. In the latter study, however, the authors pointed out unsatisfactory behaviors of the underlying distribution function. Such undesired features will be visible to the reader in the following chapter. These observations make the approach unattractive for improvements taking into account other kinetic mechanisms affecting transport. Apart from being compared to reference codes, the multigroup model of Schurtz *et al.* was used to interpret

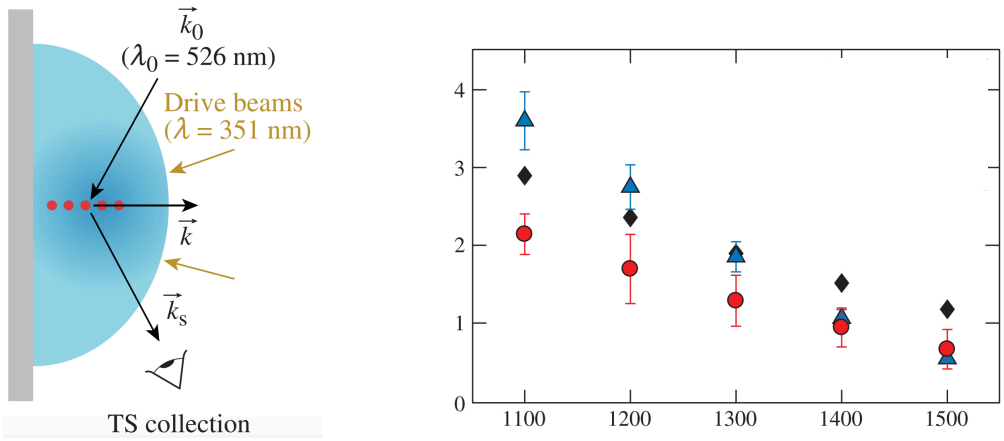


(a) (b)

Figure 2.11: Extracted from Ref. [99].(a) Experimental setup. An incident beam with wave vector $\mathbf{k}_0$ serves to probe an expanding aluminium plasma (blue) at five different positions (red points). The scattered light is collected in the direction $\mathbf{k}_s$ to determine its Thomson's power spectrum per unit angle. (b) Heat flux density, in TW/cm$^2$, estimated by direct calculation (red circles) from the electron distribution function inferred from the Thomson's spectrum, and by the Spitzer-Härm's expression (2.19) (blue triangles) or through the multigroup method (black diamonds) through the electron density and temperature profiles deduced from it. The values are given at five different locations, identified by their distance to the target in $\mu$m.

recent experiments based on collective Thomson's scattering [99, 100]. There, the heat flux density was inferred within an ablative flow by probing the relative spectral amplitudes of electron plasma waves along the normal of a planar target in aluminium.

The experimental setup is shown in Fig. 2.11a. The plasma was created through six drive beams having a wavelength $\lambda = 351$ nm. The Thomson's scattering diagnostic consisted of an incident beam with wavelength $\lambda_0 = 526$ nm in the direction $\mathbf{k}_0$, scattered by a probed volume of about $(50\ \mu\text{m})^3$, and then collected in the direction $\mathbf{k}_s$ by a spectrometer onto a streak camera. These wave vectors were chosen to ensure that $\mathbf{k} = \mathbf{k}_s - \mathbf{k}_0$ belongs to the symmetry axis of the expanding plasma bubble, along which the distortion of the electron distribution function induced by heat transport is expected to be maximal. The scattered light was analysed in five different locations along this axis, identified by their distance in $\mu$m from the target: 1100, 1200, 1300, 1400 and 1500. To each of them, the electron distribution function was indirectly determined by fitting the experimental Thomson's power spectrum per unit angle with an appropriate analytical formula about which we refer to the original paper. As visible in Fig. 2.11b, this allowed to compute the corresponding heat flux density (red circles) at the five points as well as the electron density and temperature. These latter values were used to rebuild the spatial profiles that served to estimate the heat flux density through the Spitzer-Härm's expression (2.19) (blue triangles) and the multigroup method (black diamonds). One can see that the model of Schurtz *et al.* overestimates the values by about 40 % compared to the direct calculation from the inferred

electron distribution function. Such a tendency was further confirmed by the same team in Ref. [100] through an analogous experiment. It is unclear, however, whether the authors used a corrected mean free path (2.47) or not. In any case, these experimental results invite us to remain cautious about the robustness of the approach in one dimensional configurations, even if it undoubtedly represents great progress in nonlocal transport modeling.

Nevertheless, its extension to more than one spatial dimension turned out to be disappointing. Indeed, the model does not treat the electric field self-consistently but through the indirect way proposed by Bendib *et al.* [88] through Eq. (2.46). Hence the expression of the electric stopping length is independent of the velocity direction. As pointed out by Manheimer *et al* [101], this implies that in two or three dimensions the account of the electric field effect is the same for electrons moving in its direction or, for instance, perpendicular to it. The work of Nicolaï *et al* [102] partly remedied these shortcomings by providing a multidimensional reformulation with a self-consistent treatments of the electric and magnetic fields. Unfortunately, the associated computational cost causes the method to lose its initial benefit, preventing it from being widely used in the community. Such verdict motivates the further revisions of the strategies devoted to electron heat transport.

## 2.4 Conclusion

The displacement of electrons triggered by a temperature gradient creates an electric field responsible for a return current from the cold region to the hot one of the plasma. Taking this thermoelectric effect into account is crucial to construct a method aimed at estimating the heat flux density. For that purpose the starting point is the stationary kinetic equation, whose solution is the electron distribution function reflecting the asymptotic response of the plasma to the fixed macroscopic constraints of density and temperature. The resolution is performed through an expansion on eigenfunctions of the spherical Laplacian in velocity space, the Maxwell's multipoles. Although other families are possible, they all coincide with the latter if restricted to components of orders zero and one. Doing so is mathematically sufficient since the heat flux density only depends explicitly on the latter.

The local regime is characterized by an isotropic component nearly equals, everywhere in the plasma, to the the local equilibrium distribution function. The only unknown therefore is the anisotropic part. It can be analytically found in the high-$Z$ limit because electron-electron collisions are negligible. This leads to an heat flux density proportional to the electron temperature gradient. For lower and lower values of $Z$, collisions among electrons become increasingly important. However, their contributions to momentum exchanges remain $Z$ times smaller than those of electron-ion encounters. The intensification of energy exchanges they make possible to describe is not decisive because the isotropic part of the distribution function is already that of Maxwell-Boltzmann with great precision. Hence, electron-electron collisions do not *qualitatively* modify the transport regime. They have, nevertheless, a *quantitative* influence by reducing the overall magnitude of the anisotropic component. The $Z$-dependent corrective coefficients in the Spitzer-Härm formulae are the signatures of this.

The nonlocal regime appears when the isotropic component of the electron distribution undergoes significant distortion. This implies to consider it as a mathematical unknown to properly describe its out-of-equilibrium behaviour. Over the last fifty years, several approaches were developed to solve the system of equations - itself subject to numerous variations - coupling the isotropic and anisotropic components of the electron distribution function on Maxwell's multipoles. Sometimes the underlying resolution is either not explicit nor nonexistent at all because mathematical shortcuts are employed to get the heat flux density directly. In spite of some well identified features in existing works, such a reservoir of models can make it difficult through its diversity to clearly determine the key ingredients necessary to ensure a satisfying description of electron heat transport. This rather unclear picture may prevent to draw with confidence the path towards further extensions of a model to several dimensions including other mechanisms. It is clear that the existing strategies do not introduce gratuitous simplifications, but are designed to avoid excessive numerical computations associated to the direct resolutions of the coupled partial differential equations. Our ambition in this thesis will be to keep the flexible framework they provide by demonstrating how it is possible to reconcile kinetic precision and numerical efficiency.

This page is unintentionally left not blank.

This page is unintentionally left not blank.

# Appendix

## 2.A Kinetic equation for a classical, weakly coupled and stable plasma

This appendix briefly reviews the kinetic theory applicable for a stable thermonuclear plasma. While writing it, we have preferred to leave aside the calculations and concentrate on the assumptions leading to the adopted kinetic description. In Sec. 2.A.1 a short, qualitative overview of the physical background is presented before entering into the mathematical formalism in Sec. 2.A.2. There, the problem of closing the Bogoliubov–Born–Green–Kirkwood–Yvon's chain of coupled equations on correlation functions is exposed. The equation verified by the electron distribution function, $f_e$, is written explicitly. It contains a source term, representing collisions, in which there appears the velocity gradient of the pair correlation functions, $g_{es}$. At leading order in a certain coupling parameter, it can be neglected. By doing so the resulting relation verified by $f_e$ is the Vlasov's equation, whose solutions are discussed with emphasis on Landau's damping. This last phenomenon makes the effect of binary correlations increasingly significant over time. Their account as a collision operator is then discussed, insisting on the passage from the expression of Balescu, Guernsey and Lenard to that of Landau.

### 2.A.1 Overview. The dressed quasi-particles principle.

The system under consideration is a fully ionized plasma, that is, a gas constituted by electrons and ions without any atoms. For convenience we assume that there exists only one kind of ions, and denotes $Z$ the corresponding ionization number. Due to the ratio of masses between theses two charged particles, the heat flux density is mainly due to electrons, on which we will focus. Their thermal velocity, $v_T$, is supposed sufficiently small compared to the velocity of light in vacuum, $c$, to neglect relativistic corrections. The same is for quantum ones, by supposing the thermal de Broglie's wavelength of electrons, $h/[(2\pi)^{1/2} m_e v_T]$, small compared to the average distance between them, which is proportional to $n_e^{-1/3}$. This means that, for a given temperature, the electron gas is considered sufficiently diluted. Such a picture is not valid inside, or at the edges of the solid fuel, where the electron degeneracy pressure becomes dominant during implosion. We will leave aside this point.

Let us focus on a single charge within the plasma. It will be regarded as a moving test particle within a background of field particles [103]. Paraphrasing Ichimaru [104], such a charge is carrying a screening cloud with it as a manifestation of the

local polarization of the medium it induces. The establishment of this cloud occurs in a time of order $\omega_p^{-1}$, and its spatial extension is about $\lambda_D$. During its motion, the test charge experience abrupt variation of momentum and/or energy, resulting in a deformation of the surrounding Debye's structure. Each of these events is a collision with field particles, after which the polarization cloud must adjust itself. If the mean free time, of order $\nu^{-1}$, between two successive collisions is large compared to $\omega_p^{-1}$, the test charge can be considered as having a well-established screening cloud between encounters. For a stable, weakly coupled plasma this is well verified.

Although being established, the screening cloud is not spherically symmetrical because of the motion of the charge. Such an asymmetry is responsible for a drag force exerted on it. This results in a wake consisting of the emission of plasma waves, which are, in turns, absorbed by charges in resonance with the underlying mean electric field. Hence, there appears a balance, on average, between emission and absorption. From the fluctuations around this balance emerges a certain level of noise, whose manifestation precisely is what was called collisions. As first rigorously shown by Rostoker [105], and further discussed *e.g* by Krommes [106], everything happens as if the plasma consists of an assembly of uncorrelated charges dressed by Debye's clouds. Each charge simultaneously serves as the nucleus of a cloud and is a member of another particle's cloud. However, despite their overlap, these clouds can be considered mathematically independent. This is the dressed quasi-particles principle. It provides the physical picture associated to the mathematical kinetic description of a plasma.

## 2.A.2 The Vlasov-Landau's equation

### 2.A.2.1 Chain of equations

The electrons interact with each other and with ions through electromagnetic fields. Therefore, their dynamics is in principle fully determined, provided that their positions and velocities, together with that of the ions, are known at a given moment. The feeling of being faced with a purely technical problem, that of solving these huge number of equations numerically, is illusory. Even if we have access to a computer machine capable of solving them in a reasonable duration, the result would be unintelligible. We would still need an averaging procedure to obtain experimentally accessible macroscopic observables. As it is well-known, such a program is the aim of statistical physics.

Among its founding concepts is that of *ensemble* [48]. The study of the system of interest is replaced by that of a set of copy systems, which are dynamically identical but differ in their initial conditions. Each of these systems is described at any time by a point in the phase space, and its evolution through the motion of this point in that space. The ensemble representing the system of interest in the phase space is therefore a cloud constituted by a continuum of points. Its mathematical description is given by the density, $\mathcal{D}$, of the cloud at each point. We will denote $\mathbf{X}_{s,k} = (\mathbf{r}_{s,k}, \mathbf{v}_{s,k})$ the coordinates in the phase space of the $k$-th charged particle among the $N_s$ of species $s$, either electron $e$ or ion $i$. Then,

$$\mathcal{D}(t, \mathbf{X}_{e,1}, ..., \mathbf{X}_{e,N_e}, \mathbf{X}_{i,1}, ..., \mathbf{X}_{i,N_i})\ d^6\mathbf{X}_{e,1}...d^6\mathbf{X}_{e,N_e}\ d^6\mathbf{X}_{i,1}...d^6\mathbf{X}_{i,N_i}$$

may be interpreted as the probability of finding the system, at the time $t$, within the infinitesimal volume of size $d^6\mathbf{X}_{e,1}...d^6\mathbf{X}_{e,N_e}\ d^6\mathbf{X}_{i,1}...d^6\mathbf{X}_{i,N_i}$ centered at the point $(\mathbf{X}_{e,1},...,\mathbf{X}_{e,N_e},\mathbf{X}_{i,1},...,\mathbf{X}_{i,N_i})$. More precisely, it gives the probability that the electron labelled 1 has a position and velocity within the volume of size $d^6\mathbf{X}_{e,1}$ centered at $\mathbf{X}_{e,1}$, and so on for all remaining $N_e - 1 + N_i$ charged edifices. Since no electron nor ion disappear, neither do their representative points, and so the density $\mathcal{D}$ verifies a continuity equation in the phase space. As soon as the force field is divergence free, from the continuity equation we obtain the well-known Liouville's equation,

$$\frac{\partial \mathcal{D}}{\partial t} + \sum_{k=0}^{N_e} \left( \dot{\mathbf{X}}_{e,k} \cdot \frac{\partial \mathcal{D}}{\partial \mathbf{X}_{e,k}} \right) + \sum_{k=0}^{N_i} \left( \dot{\mathbf{X}}_{i,k} \cdot \frac{\partial \mathcal{D}}{\partial \mathbf{X}_{i,k}} \right) = 0.$$

Hence, the density $\mathcal{D}$ provides a measure for the averaging process of any observable, and later equation gives the behaviour of that measure. However, the amount of information contained in $\mathcal{D}$ is excessive at the spatial and time scales from which the system is examined. It is of little interest to know the probability of finding each of these specific charge edifices in a particular state and it would be more appropriate to know the probability to find *one of them*, no matter its specific identity, in the volume of size $d^6\mathbf{X} = d^3\mathbf{r}d^3\mathbf{v}$ centered at $\mathbf{X} = (\mathbf{r}, \mathbf{v})$. For electrons such a probability,

$$f_e(t, \mathbf{X})\ d^6\mathbf{X},$$

defines the electron distribution function $f_e$. It is equal to $N_e$ multiplied by the integral of $\mathcal{D}$ over the positions and velocities of all the ions and all the electrons except one. Due to their interactions, these $N_e$ electrons and $N_i$ ions do not behave as a set of independent bodies. This implies that the evolution of $f_e$ must depend on the joint probabilities of finding several electrons and ions in some given states. These joint probabilities are given by the set of $(l+m)$-order reduced distribution functions [107],

$$d_{lm}(t, \mathbf{X}_{e,1}...\mathbf{X}_{e,l}, \mathbf{X}_{i,1}...\mathbf{X}_{i,m}) = \frac{N_e!}{(N_e - l)!} \frac{N_i!}{(N_i - m)!} \int \mathcal{D}\ d^6\mathbf{X}_{e,l+1}...d^6\mathbf{X}_{e,N_e} d^6\mathbf{X}_{i,m+1}...d^6\mathbf{X}_{i,N_i}.$$

The indexes in argument of $d_{lm}$ are kept for convenience without referring to any particular electrons nor ions. For that reason these functions are normalised to the product of $N_e!/(N_e - l)!$, the number of possibility to choose $l$ electrons among the $N_e$, by $N_i!/(N_i - m)!$. By doing so $f_e$ coincides with $F_{10}$. Each reduced distribution function, $F_{lm}$, obeys a Liouville-like equation with, however, a source term at the right hand side that represents the influence of the forgotten $(N_e - l)$ electrons and $(N_i - m)$ ions on the $l$ and $m$ considered ones. As expected, later term depends upon $d_{l+1\ m}$ and $d_{l\ m+1}$. The obtained set of equations is the famous Bogoliubov–Born–Green–Kirkwood–Yvon's chain. In the considered case of a non-relativistic plasma the microscopic force is dominated by its electrostatic component, such that the evolution of $f_e$ depends on $d_{20} := f_{ee}$ and $d_{11} := f_{ei}$ according to

$$\partial_t f_e + \langle \dot{\mathbf{X}} \rangle \cdot \frac{\partial f_e}{\partial \mathbf{X}} = -\sum_s \frac{e q_s}{4\pi\epsilon_0 m_e} \int \left( \frac{\partial}{\partial \mathbf{r}} \frac{1}{|\mathbf{r} - \mathbf{r}'|} \right) \cdot \frac{\partial g_{es}}{\partial \mathbf{v}}\ d^6\mathbf{X}', \tag{2.48}$$

as first obtained by Bogoliubov [108]. The summation is performed on each species $s$ of electric charge $q_s$, electrons $e$ and ions $i$. We noted the second order, or pair, correlation functions,

$$g_{es}(t, \mathbf{X}, \mathbf{X}') = f_{es}(t, \mathbf{X}, \mathbf{X}') - f_e(t, \mathbf{X}) f_s(t, \mathbf{X}'), \tag{2.49}$$

together with $\langle \dot{\mathbf{X}} \rangle = \Big( \mathbf{v}, -em_e^{-1}(\mathbf{E} + \mathbf{v} \times \mathbf{B}) \Big)$, where $\mathbf{E}$ is the mean electric field created by all the electrons and ions,

$$-\frac{\partial}{\partial \mathbf{r}} \sum_s \int \frac{q_s}{4\pi\epsilon_0 |\mathbf{r} - \mathbf{r}'|} f_s \; d^6\mathbf{X}'$$

plus an eventual exterior field. Likewise, $\mathbf{B}$ is the exterior magnetic field. Although the microscopic magnetic field is not taken into account in the right hand side of Eq. (2.48), it is common to consider as a component of $\mathbf{B}$ the self-consistent magnetic field produced by the internal electric currents, defined as the integrals over velocities of $q_s \mathbf{v} f_s$. The expression of the electric field, together with the possibility of considering external fields or not comes from the linearity of the Maxwell's equations and the Lorentz's force. Indeed, in plasma relevant to controlled fusion, the electromagnetic field strength is not sufficient to induce local vacuum polarisation, which would lead to quantum radiative corrections of the Coulomb's law. The meaning of the pair correlation function (2.49) is rather clear. The second order reduced distribution function, $f_{es}(t, \mathbf{X}, \mathbf{X}')$, multiplied by $d^6\mathbf{X} d^6\mathbf{X}'$, is the probability to simultaneously find at time $t$ an electron in a state close to $\mathbf{X}$ *and* a body of kind $s$ in a state close to $\mathbf{X}'$. If the dynamics of these charged edifices are completely uncorrelated, later probability is the product of the probabilities of finding each a them in the aforementioned states, $f_e(t, \mathbf{X}) d^6\mathbf{X} \; f_s(t, \mathbf{X}') d^6\mathbf{X}'$. In that case, $g_{es} = 0$ and Eq. (2.48) is called the Vlasov's equation [109].

### 2.A.2.2 Vlasov's mean fields. Landau's damping.

The Vlasov's equation describes the plasma as a set of dynamically independent electrons and ions. Its characteristics are the electron orbits of equation $d\mathbf{X}/dt = \langle \dot{\mathbf{X}} \rangle$, *i.e*

$$\frac{d\mathbf{r}}{dt} = \mathbf{v}, \quad \frac{d\mathbf{v}}{dt} = -em_e^{-1}(\mathbf{E} + \mathbf{v} \times \mathbf{B}),$$

along which the electron distribution function stays constant. Therefore the Vlasov's equation is analogous to the Liouville's one in the phase space of a single electron. This makes its study, in principle, equivalent to that of the above dynamical equations. However, solutions to the Vlasov's equation exhibit richer behaviours because of the self-consistent coupling between charged edifices and fields: the sources of $\mathbf{E}$ and $\mathbf{B}$ are the spatial distributions of charges and currents averaged by $f_e$, and the evolution of $f_e$ is determined by $\mathbf{E}$ and $\mathbf{B}$. The orbit theory is not adapted to account for such an interplay since the feedback loop on the fields leans on the knowledge of $f_e$. Hence the study of the dynamic of a single electron becomes sufficient when an stationary state is reached. In that case the solutions to the Vlasov's equation are directly obtained by studying its characteristics, and are, according to Jean's theorem, functions of the integrals of motion of the dynamical equations. Later remark is the starting point used by Chandrasekhar in

Ref. [110] for the systematic study of the dynamics of a charge in several field configurations. In Ref. [111], Rosenbluth and Rostoker even analyzed the stability of these stationary states through a perturbation approach of electron orbits.

An electron distribution function that satisfies the Vlasov's equation does not fulfill the $H$-theorem: for an isolated plasma initially out-of-equilibrium, the $H$ function,

$$H = -k_B \int f_e \ln\left(\frac{h^3}{e^1 m_e^3} f_e\right) d^6\mathbf{X},$$

stays constant instead of growing in time. The spatial integration is performed on the entire volume $V = \int d^3\mathbf{r}$ of the plasma, $e^1 = \exp(1)$ and $h$ is the Planck's constant. Let us recover this result. We momentarily note $\widetilde{f}_e = h^3 f_e/(e^1 m_e^3)$. To express $dH/dt$, we multiply the Vlasov's equation by $\ln \widetilde{f}_e$ and integrate over the entire phase space. In a first time, it is instructive to perform the integration over velocities only. This leads to

$$\begin{aligned} 0 = \int \ln \widetilde{f}_e \partial_t f_e \; d^3\mathbf{v} + \int \ln \widetilde{f}_e v_k \nabla_k f_e \; d^3\mathbf{v} \\ - e m_e^{-1} \int \ln \widetilde{f}_e \big(E_k + \epsilon_{klm} v_l B_m\big) \frac{\partial f_e}{\partial v_k} \; d^3\mathbf{v}, \end{aligned}$$

with Einstein's summation convention over repeated indices $k, l$ and $m$. $\epsilon_{klm}$ is the Levi-Civita's symbol. The first integral is equal to $\partial_t \int f_e \ln \widetilde{f}_e \; d^3\mathbf{v} - \partial_t n_e$, and the second one to $\nabla_k \int v_k f_e \ln \widetilde{f}_e \; d^3\mathbf{v} - \nabla_k n_e u_{e\;k}$ with $\mathbf{u}_e = n_e^{-1} \int \mathbf{v} f_e \; d^3\mathbf{v}$ the electron mean velocity. Leaving aside the prefactor $-e m_e^{-1}$, the electric field term is

$$E_k \int \ln \widetilde{f}_e \frac{\partial f_e}{\partial v_k} \; d^3\mathbf{v} = -E_k \int \frac{\partial f_e}{\partial v_k} \; d^3\mathbf{v} = 0,$$

after having integrated by parts. In the same way, the magnetic field term is zero,

$$\epsilon_{klm} B_m \int \ln \widetilde{f}_e v_l \frac{\partial f_e}{\partial v_k} \; d^3\mathbf{v} = -\epsilon_{klm} B_m \delta_{kl} \int f_e \big(\ln \widetilde{f}_e - 1\big) \; d^3\mathbf{v} = 0,$$

as a product of symmetric and anti-symmetric tensors. Therefore, by virtue of the electron conservation, $\partial_t n_e + \boldsymbol{\nabla} \cdot n_e \mathbf{u}_e = \mathbf{0}$, the spatial density of $H$, $-k_B \int f_e \ln \widetilde{f}_e \; d^3\mathbf{v}$, also verifies the continuity equation in space. Integrating this equation over the volume $V$ leads to $dH/dt = 0$. Such a result deserves a discussion. With some precautions that are investigated in Sec. 6.2.1.2 in appendix, $H$ can be considered as being the entropy of the plasma. Hence we arrive to the following picture. On the one hand, as the dynamics of a single electron is reversible, so is that of an assembly of totally uncorrelated electrons and the entropy conservation appears quite natural. On the other hand, there are exchanges of energy between fields and charges, which should be accompanied by the production of entropy.

Since the magnetic Lorentz's force cannot produce any work, the transfer of energy occurs through the electric field. For that reason, we will consider that the mean magnetic field is zero $\mathbf{B} = \mathbf{0}$, and will not further discuss how the following

results can be extended to magnetized plasma. The small transfers of energy can be studied through the linearized Vlasov and Maxwell-Gauss' equations. These transfers manifest, for a stable plasma, by the decay of the electric field amplitude, together with a sharper and sharper structure of the distribution function fluctuations in the phase space. Such a phenomenon is called Landau's damping [112]. As shown by Mouhot and Villani [113], most of its characteristics hold in the non-linear case of finite energy transfer. Their results will be not discussed here. In Ref. [112], Landau studied the evolution of a single spatial Fourier component of the electric field and distribution function of fluctuations by mean of the Laplace's transform. Indeed, the asymptotic behaviour of a given function can be determined by studying the order and location, in the complex plane, of the poles of its Laplace's transform. Let us briefly recall these results.

We will define the Laplace-Fourier's transform of a function $(t, \mathbf{r}) \mapsto Y(t, \mathbf{r})$ by

$$\widehat{Y}(\omega, \mathbf{k}) = \int Y(t, \mathbf{r}) e^{+i\omega t - i\mathbf{k}\cdot\mathbf{r}} \, dt d^3\mathbf{r},$$

where the integration over $t$ is performed between 0 and $+\infty$. Here, $\omega$ is complex whereas $\mathbf{k}$ is real. The link with the usual variable, often noted $p$, for the Laplace's transform is $p = -i\omega$. The Laplace's transform of $Y$ is well defined if there exists $\sigma > 0$ such that $|Y| < e^{\sigma t}$ for $t \to +\infty$. This is because

$$\left| \int_0^{+\infty} Y e^{+i\omega t} \, dt \right| \leq \int_0^{+\infty} |Y| e^{-\Im(\omega)t} \, dt \leq \int_0^{+\infty} e^{[\sigma - \Im(\omega)]t} \, dt,$$

which exists for $\Im(\omega) > \sigma$. The minimum value, $\sigma_0$, such that $\omega \mapsto \widehat{Y}(\omega, \mathbf{k})$ is analytic for $\Im(\omega) > \sigma_0$ is called the ordinate of convergence. Obviously, we can proceed to an analytical continuation of $\omega \mapsto \widehat{Y}(\omega, \mathbf{k})$ to the lower half-plane $\Im(\omega) \leq \sigma_0$. The resulting function, regular for $\Im(\omega) > \sigma_0$, necessarily has singularities in the domain $\Im(\omega) \leq \sigma_0$ in virtue of the Liouville's theorem, which affirms that if a bounded function is holomorphic on the entire complex plane, then it is a constant. By definition of $\sigma_0$, there is a singularity just below the line $\Im(\omega) = \sigma_0$. However, the nature - pole, branch point or essential singularity - together with the position of any other singularity cannot be determined by general considerations. In the following all the singularities will be supposed to be poles. The inverse Laplace-Fourier's transform giving $Y$ is

$$Y(t, \mathbf{r}) = (2\pi)^{-4} \int \widehat{Y}(\omega, \mathbf{k}) e^{-i\omega t + i\mathbf{k}\cdot\mathbf{r}} \, d\omega d^3\mathbf{k},$$

where the integration over $\omega$ is performed on the line $]-\infty + i\sigma; +\infty + i\sigma[$. Such an integration, which provides the inverse Laplace transform, corresponds to the Bromwich-Mellin's formula. One of the factor $(2\pi)^{-1}$ comes from it.

The integral of $\omega \mapsto \widehat{Y}(\omega, \mathbf{k})$ is unchanged by substituting the line $]-\infty+i\sigma; +\infty+i\sigma[$ by any path belonging to the same class of homotopy in the complex plane. In particular, as it is shown in Fig. 2.A.1, the line can be translated to the lower half-plane arbitrarily far along the imaginary axis, while being hanged to the poles by passing above them. Since $e^{-i\omega t} = e^{-i\Re(\omega)t + \Im(\omega)t}$, the contributions to the integral

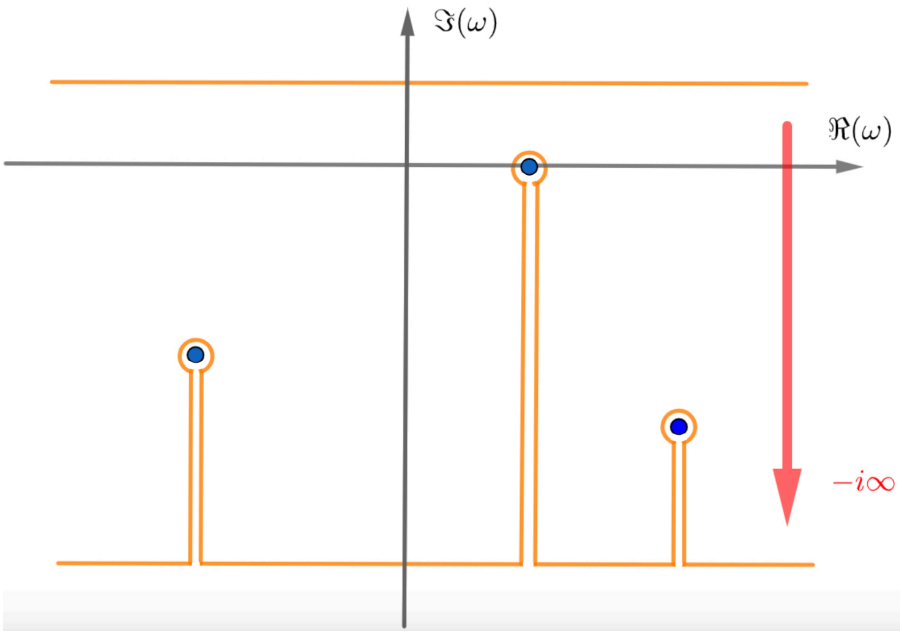


Figure 2.A.1: Deformation of the Bromwich-Mellin's contour (orange) around the poles (circles, blue).

of $\widehat{Y}$ over $\omega$ of the horizontal segments are exponentially small with time, and the characteristic time of the decay, $-1/\Im(\omega)$, becomes arbitrarily small as the line is shifted downward. Therefore they vanish in the limit $\Im(\omega) \to -\infty$. Likewise, the contributions of the segments leading to each poles exactly cancel each other. The remaining terms are the residues of the poles. Let us consider a pole $\omega_\ell$ of order $\ell$. In a neighborhood of $\omega_\ell$, $\omega \mapsto \widehat{Y}(\omega, \mathbf{k})$ has a Laurent's development of the form

$$\sum_{j=1}^{\ell} \frac{y_{-j}}{(\omega - \omega_\ell)^j} + \widehat{\mathcal{Y}},$$

where $\widehat{\mathcal{Y}}$ is the regular part of $\widehat{Y}$ with respect to the $\omega$ variable. By designating $\gamma_\ell$ the small circle enclosing the pole, the residue of $\widehat{Y}$ at that pole is

$$\mathrm{Res}(\widehat{Y}, \omega_\ell) = \frac{1}{2\pi i} \int_{\gamma_\ell} \widehat{Y}\, d\omega = y_{-1} = \lim_{\omega \to \omega_\ell} \frac{1}{(\ell-1)!} \frac{d^{\ell-1}}{dw^{\ell-1}} \left[ (\omega - \omega_\ell)^\ell\, \widehat{Y} \right].$$

However, the function to integrate here is not $\widehat{Y}$ but $\widehat{Y} e^{-i\omega t}$, which has the same poles as $\widehat{Y}$ but different residues. At $\omega = \omega_\ell$ the later is a polynomial of order $\ell - 1$ in the variable $(-it)$, multiplied by $e^{-i\omega_\ell t}/(\ell-1)!$. For instance, $\mathrm{Res}(\widehat{Y} e^{-i\omega t}, \omega_1) = y_{-1} e^{-i\omega_1 t}$, $\mathrm{Res}(\widehat{Y} e^{-i\omega t}, \omega_2) = \Big[(-it) y_{-2} + y_{-1}\Big] e^{-i\omega_2 t}$, $\mathrm{Res}(\widehat{Y} e^{-i\omega t}, \omega_3) = \Big[(-it)^2 y_{-3} + 2(-it) y_{-2} + y_{-1}\Big] e^{-i\omega_3 t}/2$. The general formula can obviously be written through the Leibniz's formula for the $(\ell-1)$-derivative of the product between $(\omega - \omega_\ell)^\ell\, \widehat{Y}$ and $e^{-\omega t}$. Writing it explicitly seems of little interest and we will be satisfied by

$$\mathrm{Res}(\widehat{Y} e^{-i\omega t}, \omega_\ell) = \mathcal{P}_{\ell-1}(it) e^{-i\omega_\ell t},$$

with $\mathcal{P}_{\ell-1}$ a polynomial or order $\ell-1$. Hence we explicitly have

$$\int_{\gamma_\ell} \widehat{Y} e^{-i\omega t}\, d\omega = 2\pi i\ \mathrm{Ind}(\gamma_\ell, \omega_\ell)\ \mathrm{Res}(\widehat{Y} e^{-i\omega t}, \omega_\ell),$$

with $\mathrm{Ind}(\gamma_\ell, \omega_\ell)$, the index of $\gamma_\ell$ with respect to $\omega_\ell$. It represents the algebraic number of rounds done by $\gamma_\ell$ around the pole, here always equal to $-1$. Obviously, the above integral depends on the coefficients of the Laurent's expansion of $\widehat{Y}$ around the pole: $2\pi i\ y_{-j}$ is the integral on $\gamma_\ell$ of $\widehat{Y}/(\omega-\omega_\ell)^{-j+1}$. It therefore depends on $\mathbf{k}$. Finally, up to exponentially small terms,

$$\int_{-\infty+i\sigma}^{+\infty+i\sigma} \widehat{Y} e^{-i\omega t}\, d\omega \sim -2\pi i \sum \mathrm{Res}(\widehat{Y} e^{-i\omega t}, \omega_\ell),$$

where the sum is performed all over the poles. Despite the fact we followed the way Landau presented the calculation, we can think of obtaining the above equality directly from the residue theorem with the closed contour consisting of the line $]-R+i\sigma; +R+i\sigma[$ closed from below by the half-circle, $\Gamma_R$, of radius $R>0$ chosen to enclose all the poles. Then,

$$-2\pi i \sum \mathrm{Res}(\widehat{Y} e^{-i\omega t}, \omega_\ell) = \int_{-R+i\sigma}^{+R+i\sigma} \widehat{Y} e^{-i\omega t}\, d\omega + \int_{\Gamma_R} \widehat{Y} e^{-i\omega t}\, d\omega$$

$\Gamma_R$ can be parameterized as $\omega = i\sigma + Re^{i\theta}$ with $\theta$ varying from 0 to $-\pi$, such that the modulus of the integral over it satisfies,

$$\begin{aligned}\Big|\int_0^{-\pi} \widehat{Y} e^{-(i\sigma+Re^{i\theta})t}\ iRe^{i\theta}\, d\theta\Big| &\le \max_{\Gamma_R}|\widehat{Y}|\ Re^{\sigma t}\int_{-\pi}^{0} e^{R\sin\theta\ t}\, d\theta \\ &\le \max_{\Gamma_R}|\widehat{Y}| e^{\sigma t}\pi t^{-1}\big(1-e^{-Rt}\big).\end{aligned}$$

To obtain the second inequality, we used the fact that sin is convex on $[-\pi, 0]$. Its graph lies below $-2(\theta+\pi)/\pi$ on $[-\pi, -\pi/2]$, and below $2\theta/\pi$ on $[-\pi/2, 0]$. To conclude we must suppose that the maximum of $|\widehat{Y}|$ on $\Gamma_R$ vanishes for an infinite radius. To summarise,

$$Y(t,\mathbf{r}) \sim -i(2\pi)^{-3}\int e^{i\mathbf{k}\cdot\mathbf{r}}\left(\sum \mathcal{P}_{\ell-1}(it)e^{-i\omega_\ell t}\right)\, d^3\mathbf{k},$$

where both $\mathcal{P}_{\ell-1}$ and $\omega_\ell$ depend on $\mathbf{k}$. Thus, we obtained the asymptotic behaviour of each spatial Fourier component as a sum over the poles of its Laplace's transform. In each term of this sum, the *order* of the pole determines the degree of the polynomial, whereas its *location* governs the behaviour of the exponential, which describes steady ($\Im(\omega_\ell)=0$), growing ($\Im(\omega_\ell)>0$) or decaying ($\Im(\omega_\ell)<0$) oscillations at the pulsation $\Re(\omega_\ell)$.

Back to the physical problem, we consider an electron distribution function $f_e = F_e + \delta f_e$ and an ion distribution function $f_i$ such that

$$\int \big(Zf_i - F_e\big)\, d^3\mathbf{v} = 0,$$

where the integration is performed over all velocities. Both $F_e$ and $f_i$ are stationary and verify the Vlasov's equation. The evolution of the electron distribution function of fluctuation, $\delta f_e$, together with the electric field created by the underlying charge density $-e\int \delta f_e \, d^3\mathbf{v}$, are coupled. They respectively verifies the linearised Vlasov and the Maxwell-Gauss' equations. By linearity we can restrict the study to only *one* spatial Fourier's component for both of them, $\widetilde{\delta f_e}(t,\mathbf{k},\mathbf{v})e^{i\mathbf{k}\cdot\mathbf{v}}$ and $\widetilde{\mathbf{E}}(t,\mathbf{k})e^{i\mathbf{k}\cdot\mathbf{v}}$. Then their asymptotic behaviours are studied through Laplace's transform. The wave vector $\mathbf{k}$ being fixed, we can choose the $z$-axis parallel to it. As a result,

$$i(k_z v_z - \omega)\widehat{\delta f_e}(\omega,\mathbf{k},\mathbf{v}) - \frac{e}{m_e}\widehat{E}_z(\omega,\mathbf{k})\frac{\partial F_e}{\partial v_z} = \widetilde{\delta f_e}(t=0,\mathbf{k},\mathbf{v}),$$

and

$$ik_z\widehat{E}_z(\omega,\mathbf{k}) = -\frac{e}{\epsilon_0}\int \widehat{\delta f_e}(\omega,\mathbf{k},\mathbf{v})\; d^3\mathbf{v}.$$

Then,

$$\widehat{\delta f_e}(\omega,\mathbf{k},\mathbf{v}) = \frac{1}{i(k_z v_z-\omega)}\left[\widetilde{\delta f_e}(t=0,\mathbf{k},\mathbf{v}) + \frac{e}{m_e}\widehat{E}_z(\omega,\mathbf{k})\frac{\partial F_e}{\partial v_z}\right],$$

which, substituted in the Maxwell-Gauss' equation leads to

$$\widehat{E}_z(\omega,\mathbf{k}) = \frac{e}{\epsilon_0 k_z^2\epsilon(\omega,\mathbf{k})}\int \frac{\widetilde{\delta f_e}(t=0,\mathbf{k},\mathbf{v})}{v_z-\omega/k_z}\; d^3\mathbf{v}$$

with

$$\epsilon(\omega,\mathbf{k}) = 1 - \frac{\omega_{pe}^2}{n_e k_z^2}\int \frac{\partial F_e/\partial v_z}{v_z-\omega/k_z}\; d^3\mathbf{v} \tag{2.50}$$

In above formulas there appears the real, first order pole $k_z v_z$. Since both $\widetilde{\delta f_e}(t=0,\mathbf{k},\mathbf{v})$ and $\partial F_e/\partial v_z$ are, *a priori*, bounded at that point, the integration along the real $z$-axis of velocities no longer has a meaning for real values of $\omega$. We must consider $v_z$ as a complex variable an perform an analytical continuation of these functions of $\omega$ by precising the path along which their integral is done. There exists two possibilities. The first one is obtained by starting from the function defined for $\Im(\omega) > 0$. In this region of the complex plane the integration is done on the real line. As $\Im(\omega)$ continuously approaches 0 the contour of integration is slightly deformed to avoid from *below* the point $v_z = \omega/k_z$ on the real axis. For $\Im(\omega) < 0$, the contour stays on the same side of $\omega/k_z$ by being deformed as in Fig 2.A.2. In this process the contour always belong to the same class of homotopy, guaranteeing the analytical nature of the continuation. The second possibility of analytical continuation is to start from the function defined for $\Im(\omega) < 0$ and to proceed as in the first case, symmetrically. However $\omega \mapsto \epsilon(\omega,\mathbf{k})$ has no poles in the upper half-plane because of the causality principle [114]. Therefore only the first analytical continuation, often called the Landau's prescription, is physically acceptable.

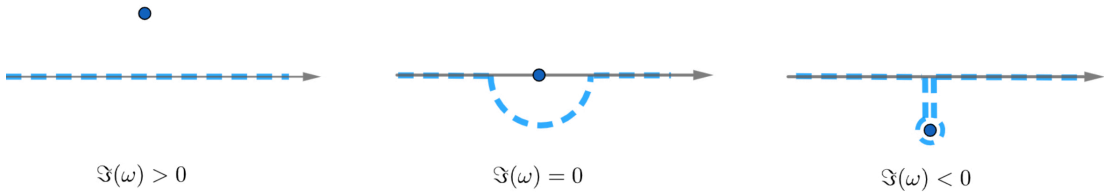


Figure 2.A.2: Landau's contour of integration (dashed, cyan) depending on the sign of the imaginary part of the pole $v_z = \omega/k_z$ (circle, blue).

As a result, the only poles, $\omega_\ell$, of $\widehat{E}_z(\omega, \mathbf{k})$ are the zeros of the dielectric function,

$$\epsilon(\omega_\ell, \mathbf{k}) = 0.$$

The wave vector $\mathbf{k}$ being fixed, the set of poles defined by the above equation is fully determined by the shape of $F_e$ in velocities along $\mathbf{k}$. The link between this shape and the locations of the poles in the complex plane is analogous to the problem treated by Nyquist in Ref. [115]. An extensive report of such an analysis applied to the problem we consider here is done by several authors, among which Balescu in Ref. [107]. The Nyquist's criterion consists of the following sufficient condition: if the function $v_z \mapsto F_{e||}(\mathbf{r}, v_z) = \int F_e \; dv_x dv_y$ has a single maximum, then all the poles have negative imaginary parts, $\Im(\omega_\ell) \leq 0$, *i.e* the electric field is damped. The existence of several maximums does not necessarily lead to growing oscillations. The conclusion depends on the degree of separation of these maxima. In Ref. [116], Penrose derived a quantitative criterion: there exist poles with strictly positive imaginary parts if, and only if, the function $v_z \mapsto F_{e||}(\mathbf{r}, v_z)$ admits a minimum at $v_z = \xi$ for which

$$\frac{n_e k_z^2}{\omega_{pe}^2} < \mathsf{P} \int_{-\infty}^{+\infty} \frac{F_{e||}(\mathbf{r}, v_z) - F_{e||}(\mathbf{r}, \xi)}{(v_z - \xi)^2} \; dv_z,$$

with $\mathsf{P}$ the Cauchy's principal value of the integral. Such poles, with strictly positive imaginary parts, are then eigenmodes of the system constituted by the linearised Vlasov and Maxwell-Gauss' equations, because they are the zeros of the original, non analytically continued, dielectric function within which the integration is performed on the real line. On the contrary, none of the damped modes is an eigenmode *i.e* has only one temporal Fourier's component. This is why, by using the Laplace's transform to formulate the analysis in the form of an initial value problem, Landau bypassed the divergence pointed out by Vlasov, who used a conventional Fourier's analysis in time. Van Kampen in Ref. [117], together with Backus in Ref. [118], further analysed these questions, but entering into the underlying mathematical details would seem inappropriate here.

Like electron oscillations, ion ones can be exponentially enhanced. At present, however, there is no clear experimental evidence to suggest a coupling between heat transport caused by a steep temperature gradient and the emergence of turbulence in plasma relevant to ICF. For this reason we will consider the plasma as *stable* throughout this manuscript. Despite of this, the electron distribution function of fluctuations does not decay because $\widehat{\delta f_e}(\omega, \mathbf{k}, \mathbf{v})$ possesses the first order kinetic pole $k_z v_z$ in addition to the zeros of the dielectric function. Therefore

the dominant term of the asymptotic behaviour of $\delta f_e$ is proportional to $e^{-ik_z v_z t}$, which describes undamped steady oscillations at the velocity-dependent pulsation $k_z v_z$. As a consequence, $\delta f_e$ acquires a sharper and sharper structure in the phase space,

$$\left| \frac{1}{\delta f_e} \frac{\partial \delta f_e}{\partial v_z} \right| \sim k_z t.$$

This phenomenon is called *phase mixing*. The energy carried by the electric field in a coherent form is dispersed among electrons which increasingly behaves like incoherent sources of the field. Indeed, each spatial Fourier component of the electric fields tends to be proportional to

$$\int_{-\infty}^{+\infty} e^{-ik_z v_z t} \, dv_z,$$

which is equal to zero for $k_z t \neq 0$. Because of the increase of $|\partial \delta f_e / \partial v_z|$, the right hand side of the Eq. (2.48), within which appears $\partial g_{es}/\partial v_z$, is growing in time until being comparable to the Vlasov's mean field terms. This means that collisions can no longer be ignored. Before this happens, however, the energy transfer from the electric field to the electrons is purely reversible. The damping results from the dispersion in velocity of electrons. The energy they accumulate can be returned to the field, as confirmed experimentally by Malmberg *et al.* [119] through the echo phenomenon [120].

### 2.A.2.3 Coupling parameter. Landau's collision operator.

Taking into account the collisions means that the right hand side of Eq. (2.48) is no longer considered to be zero, $g_{es} \neq 0$. For this kinetic equation to continue to form a closed system with Maxwell's equations, the pair correlation functions must be explicitly expressed as a function of $f_e$ only. As already mentioned, the difficulty lies in the fact that the evolution of $g_{es}$ is governed by higher-order reduced distribution functions, which brings us back to the problem of truncating the corresponding chain of equations. Such a truncation at a given order relies on a hierarchy between the values of these reduced distribution functions. The later turn out to be proportional to the successive powers of a certain coupling parameter.

As a measure of the strength of the correlations, such a coupling parameter should account for the competition between collective behaviour of charged edifices, managed by the electromagnetic interaction, and their tendency to move freely, independently from other bodies. This last tendency is measured by the thermal energy, $k_B T_e$. In the considered case of a non-relativistic plasma the microscopic force is dominated by its electrostatic component. The associated potential energy for electrons separated by a distance $n_e^{-1/3}$ is $e^2/(4\pi\epsilon_0 n_e^{-1/3})$. Hence the coupling parameter for electron-electron interaction will be defined as

$$\Gamma_{ee} = \frac{e^2 n_e^{1/3}}{\epsilon_0 k_B T_e} = \left[ \frac{4\pi}{3 N_{De}} \right]^{2/3}, \tag{2.51}$$

with $N_{De} = (4\pi/3) n_e \lambda_{De}^3$ the number of electrons contained in a Debye's ball. The coupling parameter for electron-ion interaction is $\Gamma_{ei} = Z\Gamma_{ee}$. For a thermonuclear

plasma, such coupling parameters are about few percents, $\Gamma_{es} \ll 1$. For this reason they are called *weakly coupled* plasmas, and

$$g_{es}/f_e \sim \Gamma_{es}.$$

This identity can be justified from the explicit expression of the pair correlation function at equilibrium [104]. As a consequence of the huge number of charged edifices within a Debye's ball, the Coulomb's collision mean free path, $\ell_c \sim N_D \lambda_D$, is large compared to the radius of the ball, $\lambda_D$ (we omit here the index which refers to a particular species). Therefore, the collision frequency, $\nu$, is small compared to that of long-term collective oscillations, $\nu/\omega_p = (v_T/\ell_c)(v_T/\lambda_D) = \lambda_D/\ell_c \ll 1$. We didn't mention it before, but the reason why collective modes at the pulsation $\omega_p$ have the longest life is because they have the lowest possible damping rate. Let us precise this point by returning to the previous section. The oscillations which are damped with the smaller rate are those whose pulsation is arbitrarily close to the real axis or, in other words, arbitrarily distant from the imaginary one. Each of these equivalent formulations expresses that the negative imaginary part is negligible compared to the real one. None of them, however, has a physical meaning if no physical pulsation is given to fix the scale. In fact, such a scale is determined through the electron distribution function $F_{e||}$. A measure of the extension of its support in velocity space is its variance, that is, the electron thermal velocity $v_T$. As the damping of the electric field corresponds to a transfer of energy to the electrons, the magnitude of its rate depends directly on the number of electrons in resonance with the oscillations. Therefore, weakly damped ones are associated to ratios $|\omega|/k_z$ that are large compared to $v_T$. Consequently, later ratio is large compared to the velocities of most of the electrons. The Cauchy's principal value of the integral that appears in the expression of the dielectric function,

$$\int \frac{\partial F_e/\partial v_z}{v_z - \omega/k_z}\, d^3\mathbf{v} = \mathsf{P}\int_{-\infty}^{+\infty} \frac{F_{e||}}{(v_z - \omega/k_z)^2}\, dv_z + i\pi \left.\frac{\partial F_{e||}}{\partial v_z}\right|_{v_z=\frac{\omega}{k_z}},$$

can therefore be estimated by developing the integrand in power of the small ratio $v_z k_z/\omega$. By doing so up to order two, we obtain the dominant, real part of the pole $\omega = \omega_{epw} - i\gamma_{epw}$ by solving $\Re(\epsilon) = 0$. This leads to

$$\omega_{epw} = \omega_{pe}\left(1 + \frac{3}{2}k_z^2\lambda_{De}^2\right).$$

Then, the imaginary part is

$$\gamma_{epw} = \frac{\Im[\epsilon(\omega_{epw}, \mathbf{k})]}{\partial_\omega \Re[\epsilon(\omega_{epw}, \mathbf{k})]} = -\frac{\pi e^2 \omega_{epw}}{2\epsilon_0 m_e k_z^2} \left.\frac{\partial F_{e||}}{\partial v_z}\right|_{v_z=\omega_{epw}/k_z},$$

which is equal to

$$\left(\frac{\pi}{8}\right)^{1/2} \frac{\omega_{epw}^2/\omega_{pe}}{k_z^3\lambda_{De}^3} \exp\left(-\frac{\omega_{epw}^2}{2k_z^2 v_T^2}\right),$$

for a Maxwellian distribution function, as obtained by Landau [112]. Such a damping rate stays small compared to $\omega_{pe}$ for wavelengths that exceed at least two Debye's lengths, $k_z\lambda_{De} \simeq 1/2$. Below that, it becomes infinitely greater than $\omega_{pe}$,

rendering obsolete the hypothesis from which its expression was derived. To the lowest order in the limit of long wavelengths, $k_z\lambda_{De} \ll 1$, $\gamma_{epw} = 0$ and $\omega_{epw}$ is equal to $\omega_{pe}$, which is independent of $k_z$. This means that such vibrations no longer propagate energy and the associated disturbance stands still in space. The plasma behaves like an infinitely rigid continuous medium that oscillates coherently as a whole. For still large, but finite, wavelength, there appears a small dispersion associated to the non-linear relation between $\omega_{epw}$ and $k_z$. Its physical origin is the incoherent thermal motions of charges that leads to destructive interference of oscillations, that is, to a damping $\gamma_{epw} \neq 0$. The evolution of $\delta f_e$ due to collisions, momentarily noted $\mathcal{C}(\delta f_e)$, is roughly a diffusion in velocity space with coefficient $\nu v_T^2$,

$$\mathcal{C}(\delta f_e) \sim \nu v_T^2 \, \frac{\partial^2 \delta f_e}{\partial v_z^2} \sim \nu v_T^2 k_z^2 t^2 \delta f_e.$$

Therefore, $\mathcal{C}(\delta f_e)$ becomes comparable to $\partial_t \delta f_e \sim \omega_{pe}\delta f_e$ after a duration equal to

$$\frac{1}{v_T k_z}\left(\frac{\omega_{pe}}{\nu}\right)^{1/2} \sim \frac{N_{De}^{1/2}}{k_z\lambda_{De}}\,\omega_{pe}^{-1}.$$

This time is much larger than $\omega_{pe}^{-1}$ in the long wavelength limit. For wavelength comparable to few Debye's lengths, the collective oscillations makes collisions significant after $N_{De}^{1/2} \simeq \Gamma_{ee}^{-3/2} \gg 1$ periods. Let us discuss the mathematical description of this long-term correction of the Vlasov's kinetic equation. By completely neglecting the third-order reduced distribution functions, the evolution of $g_{es} = g_{es}(t, \mathbf{X}, \mathbf{X}')$ is governed by [108],

$$\begin{aligned}
&\partial_t g_{es} + \langle \dot{\mathbf{X}} \rangle \cdot \frac{\partial g_{es}}{\partial \mathbf{X}} + \langle \dot{\mathbf{X}}' \rangle \cdot \frac{\partial g_{es}}{\partial \mathbf{X}'} \\
&\quad + \frac{e}{4\pi\epsilon_0 m_e}\frac{\partial f_e}{\partial \mathbf{v}} \cdot \int \left(\frac{\partial}{\partial \mathbf{r}}\frac{1}{|\mathbf{r}-\mathbf{r}''|}\right)\Big[-e g_{es}(t,\mathbf{X},\mathbf{X}'') + q_s g_{ss}(t,\mathbf{X}',\mathbf{X}'')\Big]\, d^6\mathbf{X}'' \\
&\quad - \frac{q_s}{4\pi\epsilon_0 m_s}\frac{\partial f_s}{\partial \mathbf{v}'} \cdot \int \left(\frac{\partial}{\partial \mathbf{r}'}\frac{1}{|\mathbf{r}'-\mathbf{r}''|}\right)\Big[-e g_{ee}(t,\mathbf{X},\mathbf{X}'') + q_s g_{es}(t,\mathbf{X},\mathbf{X}'')\Big]\, d^6\mathbf{X}'' \\
&\quad = -\frac{e q_s}{4\pi\epsilon_0}\left(\frac{\partial}{\partial \mathbf{r}}\frac{1}{|\mathbf{r}-\mathbf{r}'|}\right)\cdot\left(\frac{1}{m_e}\frac{\partial}{\partial \mathbf{v}} - \frac{1}{m_s}\frac{\partial}{\partial \mathbf{v}'}\right)\big[f_e f_s + g_{es}\big], \qquad (2.52)
\end{aligned}$$

with $\langle \dot{\mathbf{X}}' \rangle = \Big(\mathbf{v}', -e m_e^{-1}(\mathbf{E}+\mathbf{v}'\times\mathbf{B})\Big)$. The Eqs. (2.48)-(2.52) form a closed system with unknown $f_e$ and $g_{es}$. Bogoliubov first wrote it in the case of an homogeneous plasma. Here, the resolution we are interested in aims to provide a kinetic equation on $f_e$ by closing Eq. (2.48). This has been done in an approximate way, and independently, by Guernsey [121] and Lenard [122]. Their methods roughly are as follows. The integral terms in the left hand side of Eq. (2.52), together with the term in which appear $g_{es}$ within the right hand side, are neglected. As a result, $g_{es}$ verifies the Vlasov's equation with a source term consisting of a differential operator applied fo $f_e f_s$. Then, an approximate, formal solution is given through the Green's function of the linearised Vlasov's equation, that is substituted in Eq. (2.48). Balescu [123] obtained the same result through a rather different strategy that will not be discussed here. Although his approach is heavier, he

has highlighted in Ref. [107] the weaknesses of the underlying assumptions made by Guernsey and Lenard, and explained why, in spite of this fact, they got the same result as him. Moreover, he explained how the solution can be extended to inhomogenous plasmas. Hence, the right hand side of Eq. (2.48) is written as the sum over $s$ of $\mathcal{C}_{es}[f_e, f_s]$ with

$$\mathcal{C}_{es}[f_e, f_s] = -\frac{1}{m_e}\frac{\partial}{\partial v_i}\int Q_{ij}(\mathbf{v}-\mathbf{v}')\left(\frac{1}{m_s}\frac{\partial}{\partial v'_j} - \frac{1}{m_e}\frac{\partial}{\partial v_j}\right) f_e f_s \; d^3\mathbf{v}', \tag{2.53}$$

where

$$Q_{ij}(\mathbf{w}) = \int \left|\frac{(-e)q_s}{\epsilon_0 \epsilon(\mathbf{k}\cdot\mathbf{v}, \mathbf{k})k^2}\right|^2 \pi k_i k_j \delta(\mathbf{k}\cdot\mathbf{w}) \; \frac{d^3\mathbf{k}}{(2\pi)^3}. \tag{2.54}$$

This is the BGL's collision operator. Within the integrand of $Q_{ij}(\mathbf{w})$, there appears the Fourier transform of the Coulomb potential energy, $(-e)q_s/(\epsilon_0 k^2)$, divided by $\epsilon(\mathbf{k}\cdot\mathbf{v}, \mathbf{k})$, the dielectric function (2.50) evaluated at the pulsation $\omega = \mathbf{k}\cdot\mathbf{v}$. Such a resulting effective potential accounts for the dynamical screening. The Debye's cloud surrounding an electron with a small velocity nearly has a spherical shape, but is progressively deformed for increasing velocities, until it induces a wake of electron plasma oscillations. As viewed in the previous section, electrons with high velocities are also those which, in resonance with the electric field, mainly absorb the energy of such oscillations. Hence, the BGL's collision operator (2.53)-(2.54) accounts for the modification of Coulomb collisions due to the absorption and emission of electron plasma waves. This has been first clarified by Rostoker and Rosenbluth in Ref. [124], who directly derived the BGL's operator in the particular case $f_s = f_M$, with $f_M$ the Maxwellian electron distribution function.

By being especially important for velocities large compared to $v_T$, the dynamical nature of the screening can be ignored for most of the electrons. If it is neglected for the entire population, $\epsilon(\mathbf{k}\cdot\mathbf{v}, \mathbf{k}) \simeq 1$, the BGL's operator transforms into that of Landau [46]. Indeed, in that case $Q_{ij}(\mathbf{w})$ is $[(-e)q_s/\epsilon_0)]^2$ multiplied by

$$\int \frac{\pi k_i k_j \delta(\mathbf{k}\cdot\mathbf{w})}{k^4} \; \frac{d^3\mathbf{k}}{(2\pi)^3} = \frac{1}{8\pi^2 w}\int \frac{k_{\perp i}k_{\perp j}}{k_\perp^4} \; d^2\mathbf{k}_\perp.$$

We used $\delta(\mathbf{k}\cdot\mathbf{w}) = \delta(w\mathbf{k}\cdot\mathbf{w}/w) = \delta(\mathbf{k}\cdot\mathbf{w}/w)/w$, and noted $\mathbf{k}_\perp = (\mathsf{I} - \mathbf{w}\otimes\mathbf{w}/w^2)\cdot\mathbf{k}$ the component of $\mathbf{k}$ perpendicular to $\mathbf{w}$. Without lost of generality we can choose the $z$-axis parallel to $\mathbf{w}$. For $i = x$ and $j = y$, or vice versa, the above integral vanishes because the integrand, $k_x k_y/k_\perp^4$ is an odd function of each component. The two integrals for $i = j = x$ and $i = j = y$ are equal, and their sum is $1/(8\pi^2 w)\int dk_x dk_y/k_\perp^2 = 1/(4\pi w)\int dk_\perp/k_\perp$, after having switched into polar coordinates. As expected, a mathematical divergence appears that requires to choose appropriate cutoffs for the bounds of the integral. This has been first done by Landau [46] and defines the Coulomb logarithm,

$$\ln\Lambda_{es} = \int_{k_D}^{k_c} \frac{dk_\perp}{k_\perp},$$

where $k_{De} = 2\pi/\lambda_{De}$ and $k_c = 2\pi/\lambda_c$, with $\lambda_c$ the maximum between the electron de Broglie's length and the classical Coulomb's distance of closest approach. We

will not go into further details on these choices and refer the reader to the recent discussions led by Krommes [125] and Mora [126]. To summarize, all the components of $\mathsf{Q}(\mathbf{w})$ (2.54) are zero except the $xx$ and $yy$ ones, which both are equals to $[(-e)q_s/\epsilon_0)]^2$ multiplied by $\ln\Lambda_{es}/(8\pi w)$. As a result,

$$Q_{ij}(\mathbf{w}) \simeq Y_{es}U_{ij}(\mathbf{w}),$$

with $Y_{es} = (-e)^2 q_s^2/(8\pi\epsilon_0^2)$ and $U_{ij}(\mathbf{w}) = (\delta_{ij} - w_i w_j/w^2)/w$, which are the components of the Landau's kernel tensor. The alternative ways of obtaining the Landau's collision operator are evoked in the App. 2.B.

This page is unintentionally left not blank.

## 2.B Operator describing collisions experienced by test electrons moving in an equilibrium background

This appendix is essentially devoted to the derivation of $\mathcal{C}_{ee}[f_e, f_M]$. It is, in particular, the starting point of our analysis in Chap. 3. This operator is associated to a situation in which all electrons do not have the same role. A part of them, constituted by a small group of mutually non-interacting electrons, evolve inside a bulk of electrons at equilibrium. As a result of the scarcity of the out-of-equilibrium electrons, it is assumed that the equilibrium of the background is not affected by the interactions between these two populations.

This picture was considered by Chandrasekhar in Ref. [103] to describe the motion of *test* stars under the gravitational influence of a background of *fields* stars. He assumed that the distribution of test stars obeys a Fokker-Planck's equation, of which he calculated the transition moments, $\langle \delta \mathbf{v} \rangle$ and $\langle \delta \mathbf{v} \otimes \delta \mathbf{v} \rangle$, by averaging over an equilibrium distribution of target stars the velocity change, $\delta \mathbf{v}$, experienced by a test star during an isolated gravitational two-body encounter. Because of the infinite scope of the interaction, the averaging process raised divergent integrals, whose avoidance required appropriate cut-offs of the bounds. This is the same strategy as adopted by Landau in Ref. [46] for a plasma, except the latter averaged on a general distribution of field charges, and started not from the Fokker-Planck's operator, but from the Boltzmann's one by developing its integrand in the small parameter $\delta \mathbf{v}$.

In Ref. [49], Rosenbluth *et al.* recovered Landau's result by taking over the method of Chandrasekhar in case of a plasma. Among their results, they noticed the possibility of expressing the transition moments as gradient and Hessian of scalar functions, designated as Rosenbluth's potentials, that verify Poisson's equations in the velocity space. Hence the problem of calculating an integro-differential operator is transformed into that of successive resolutions of a set of coupled partial differential equations. Apart from the new physical insight, this paradigm provides an efficient algorithm for numerical estimation. This is the reason why we think appropriate to make a brief review of it in Sec. 2.B.1. On this occasion the dynamical friction force together with the diffusion velocity tensor associated to the Fokker-Planck's form of the Landau integral are identified. Their expressions will be useful in Chap. 3 3. Then, in Sec. 2.B.2 $\mathcal{C}_{ee}[f_e, f_M]$ is derived by explicitly solving the Poisson's equations verified by the Rosenbluth's potentials. This method differs from that of Chandrasekhar but, while not being longer, emphasizes certain aspects of the underlying physical framework. Finally, a alternative way of obtaining the high velocity limit of $\mathcal{C}_{ee}[f_e, f_M]$ is written in Sec. 2.B.3.

### 2.B.1 Preliminary: forms of the Landau's collision integral

As shown in the Complementary Note. 2.A, the Landau's integral that describes collisions between two populations of species $s$ and $s'$ is, with Einstein's summation

convention over the repeated index $i$ and $j$:

$$\mathcal{C}_{ss'}[f_s, f'_s] = -\frac{Y_{ss'}}{m_s}\frac{\partial}{\partial v_{si}}\int U_{ij}(\mathbf{v}_s - \mathbf{v}_{s'})\left(\frac{f_s}{m_{s'}}\frac{\partial f_{s'}}{\partial v_{s'j}} - \frac{f_{s'}}{m_s}\frac{\partial f_s}{\partial v_{sj}}\right) d^3\mathbf{v}_{s'}, \tag{2.55}$$

where the integration is done over the whole velocity space. $U_{ij}(\mathbf{v}_s - \mathbf{v}_{s'})$ is the $ij$-component of the Landau's kernel tensor:

$$U_{ij}(\mathbf{w}) = \frac{1}{w}\left(\delta_{ij} - \frac{w_i w_j}{w^2}\right), \tag{2.56}$$

evaluated at $\mathbf{v}_s - \mathbf{v}_{s'}$. This is the projector on $\mathbf{w}^\perp$ divided by $w$. In the prefactor of expression (2.55), $Y_{ss'} = q_s^2 q_{s'}^2 \ln\Lambda_{ss'}/(8\pi\epsilon_0^2)$, where $q_s$ and $q_{s'}$ are the charges of species $s$ and $s'$ respectively, $\ln\Lambda_{ss'}$ is the Coulomb's logarithm related to their collisions, and $\epsilon_0$ is the dielectric permittivity of the vacuum. The expression (2.55) is the original form in which Landau expressed $\mathcal{C}_{ss'}[f_s, f'_s]$ in Ref. [46]. This operator can be put in a Fokker-Planck's form, about which information can be found in Ref. [127]. Indeed, $\mathcal{C}_{ss'}[f_s, f'_s]$ is equal to $-Y_{ss'}/m_s$ multiplied by the divergence, in velocity space, of

$$\int U_{ij}\left(\frac{f_s}{m_{s'}}\frac{\partial f_{s'}}{\partial v_{s'j}} - \frac{f_{s'}}{m_s}\frac{\partial f_s}{\partial v_{sj}}\right) d^3\mathbf{v}_{s'} = \frac{f_s}{m_{s'}}\int U_{ij}\frac{\partial f_{s'}}{\partial v_{s'j}} d^3 v_{s'} - \frac{1}{m_s}\frac{\partial f_s}{\partial v_{sj}}\left(\int U_{ij} f_{s'} d^3\mathbf{v}_{s'}\right).$$

In the right hand side, the integral of the first term is equal to $-\int f_{s'}\partial U_{ij}/\partial v_{s'j} d^3\mathbf{v}_{s'}$, by integrating by parts. Here, $U_{ij}$ is viewed as a function of the two variables $(\mathbf{v}_s, \mathbf{v}_{s'})$, and, as often, we abusively employ the same notation for its composition with $(\mathbf{v}_s, \mathbf{v}_{s'}) \mapsto \mathbf{v}_s - \mathbf{v}_{s'}$. Noticing that $\partial U_{ij}/\partial v_{s'j} = -\partial U_{ij}/\partial v_{sj}$, we finally have the following identity:

$$\int U_{ij}\frac{\partial f_{s'}}{\partial v_{s'j}} d^3\mathbf{v}_{s'} = \frac{\partial}{\partial v_{sj}}\int U_{ij} f_{s'} d^3\mathbf{v}_{s'}.$$

Then, we define

$$\langle \delta v_{si}\delta v_{sj}\rangle = \frac{2Y_{ss'}}{m_s^2}\int U_{ij} f_{s'}\, d^3\mathbf{v}_{s'}, \tag{2.57}$$

and

$$\langle \delta v_{si}\rangle = \frac{1}{2}\left(1 + \frac{m_s}{m_{s'}}\right)\frac{\partial}{\partial v_{sj}}\langle \delta v_{si}\delta v_{sj}\rangle = \left(1 + \frac{m_s}{m_{s'}}\right)\frac{Y_{ss'}}{m_s^2}\frac{\partial}{\partial v_{sj}}\int U_{ij} f_{s'}\, d^3\mathbf{v}_{s'}, \tag{2.58}$$

such that,

$$\mathcal{C}_{ss'}[f_s, f'_s] = -\frac{\partial}{\partial v_{si}}\left(\langle \delta v_{si}\rangle f_s - \frac{1}{2}\frac{\partial}{\partial v_{sj}}\langle \delta v_{si}\delta v_{sj}\rangle f_s\right) \tag{2.59}$$

To arrive at this form, we used the definition of $\langle \delta v_{si}\delta v_{sj}\rangle$, and then the identity $\langle \delta v_{si}\delta v_{sj}\rangle \partial f_s/\partial v_{sj} = \partial(\langle \delta v_{si}\delta v_{sj}\rangle f_s)/\partial v_{sj} - f_s\partial\langle \delta v_{si}\delta v_{sj}\rangle/\partial v_{sj}$, together with the definition of $\langle \delta v_{si}\rangle$. The latter is the $i$-component of the average change per unit time in velocity experienced by a charge $s$ due to collisions with charges $s'$. $\langle \delta v_{si}\rangle$ and $\langle \delta v_{si}\delta v_{sj}\rangle$ respectively are the first and second moments of the transition rate

appearing in the master equation, and the velocity increment, $\delta\mathbf{v}$, is nothing else than the small parameter of the Kramers-Moyal's expansion.

When $m_s \ll m_{s'}$, the Einstein's relation between these coefficients is full-filled, $\langle \delta v_{si} \rangle = -\partial \langle \delta v_{si} \delta v_{sj} \rangle / \partial v_{sj}/2$, and $\mathcal{C}_{ss'}[f_s, f_{s'}]$ takes a quasi-linear form,

$$\frac{1}{2}\frac{\partial}{\partial v_{si}}\langle \delta v_{si}\delta v_{sj}\rangle \frac{\partial f_s}{\partial v_{sj}},$$

already encountered while deriving the Lorentz's operator (2.8). From a mathematical point of view, this reveals the symmetry of the transition rate, that is, the microscopic reversibility property of the underlying Markovian stochastic process of collisions. In that case the Fokker-Planck's operator is describing a pure diffusion in the velocity space. This is the reason why we prefer to call here dynamical *friction force* the vector defined as

$$\begin{aligned} F_{s'i} = m_s \left( \langle \delta v_{si} \rangle - \frac{1}{2}\frac{\partial}{\partial v_{sj}}\langle \delta v_{si}\delta v_{sj}\rangle \right) &= \frac{m_s^2}{2m_{s'}}\frac{\partial}{\partial v_{sj}}\langle \delta v_{si}\delta v_{sj}\rangle \\ &= \frac{Y_{ss'}}{m_s'}\frac{\partial}{\partial v_{sj}}\int U_{ij} f_{s'} d^3\mathbf{v}_{s'}, \end{aligned} \tag{2.60}$$

despite this term is still proportional to the divergence of the momentum *diffusion tensor* that we choose to define as:

$$D_{s'ij} = \frac{m_s^2}{2}\langle \delta v_{si}\delta v_{sj}\rangle = Y_{ss'}\int U_{ij} f_{s'}\ d^3\mathbf{v}_{s'}. \tag{2.61}$$

It is worth mentioning that $F_{s'i}$ is well homogeneous to a force, while $D_{s'ij}$ is homogeneous to a variation of momentum per unit time multiplied by a momentum, that is, a force multiplied by a momentum. With these conventions, the Fokker-Planck's operator has the form

$$\mathcal{C}_{ss'}[f_s, f_s'] = -\frac{1}{m_s}\frac{\partial}{\partial v_{si}}\left( F_{s'i} f_s - D_{s'ij}\frac{1}{m_s}\frac{\partial f_s}{\partial v_{sj}} \right)$$

After these digressions, we now express both $F_{s'i}$ and $D_{s'ij}$ in different ways, by computing explicitly the divergence of the Landau's kernel tensor:

$$\begin{aligned} \frac{\partial U_{ij}}{\partial v_{sj}} = \left[ \delta_{ij} - \frac{(v_{si}-v_{s'i})}{|\mathbf{v}_s - \mathbf{v}_{s'}|^2} \right] \frac{\partial}{\partial v_{sj}}\frac{1}{|\mathbf{v}_s - \mathbf{v}_{s'}|} - \frac{1}{|\mathbf{v}_s - \mathbf{v}_{s'}|^3}\frac{\partial}{\partial v_{sj}}(v_{si}-v_{s'i})(v_{sj}-v_{s'j}) \\ + \frac{(v_{si}-v_{s'i})(v_{sj}-v_{s'j})}{|\mathbf{v}_s - \mathbf{v}_{s'}|}\frac{\partial}{\partial v_{sj}}\frac{1}{|\mathbf{v}_s - \mathbf{v}_{s'}|^2}. \end{aligned}$$

Since, for any real $r$,

$$\frac{\partial}{\partial v_{sj}}\frac{1}{|\mathbf{v}_s - \mathbf{v}_{s'}|^r} = -\frac{r(v_{sj}-v_{s'j})}{|\mathbf{v}_s - \mathbf{v}_{s'}|^{r+2}},$$

and

$$\begin{aligned} \frac{\partial}{\partial v_{sj}}(v_{si}-v_{s'i})(v_{sj}-v_{s'j}) &= \delta_{ij}(v_{sj}-v_{s'j}) + 3(v_{si}-v_{s'i}) \\ &= 4(v_{si}-v_{s'i}), \end{aligned}$$

we obtain, by direct calculation:

$$\frac{\partial U_{ij}}{\partial v_{sj}} = -\frac{2(v_{si} - v_{s'i})}{|\mathbf{v}_s - \mathbf{v}_{s'}|^3} = \frac{\partial}{\partial v_{si}} \frac{2}{|\mathbf{v}_s - \mathbf{v}_{s'}|}.$$

As a consequence of the last equality, the friction force (2.60) can be expressed as:

$$F_{s'i} = \frac{2Y_{ss'}}{m'_s} \frac{\partial h_{s'}}{\partial v_{si}} \quad \text{with} \quad h_{s'} = \int \frac{f_{s'}}{|\mathbf{v}_s - \mathbf{v}_{s'}|} d^3\mathbf{v}_{s'}, \tag{2.62}$$

where $h_{s'}$ will be referred as the second Rosenbluth's potential [49]. It appears that $2Y_{ss'}h_{s'}/m_{s'}$ is homogeneous to a power. Multiplied by a collision time, it may represent the average potential energy of a charge $s$ in the field created by charges $s'$. Moreover, the relation $\partial^2|\mathbf{v}_s - \mathbf{v}_{s'}|/\partial v_{si}\partial v_{sj} = U_{ij}(\mathbf{v}_s - \mathbf{v}_{s'})$, obtained by direct calculation, allows us to write the diffusion tensor (2.61) as

$$D_{s'ij} = Y_{ss'} \frac{\partial^2 g_{s'}}{\partial v_{si}\partial v_{sj}} \quad \text{with} \quad g_{s'} = \int |\mathbf{v}_s - \mathbf{v}_{s'}| f_{s'}\, d^3\mathbf{v}_{s'}, \tag{2.63}$$

where $g_{s'}$ will be referred as the first Rosenbluth's potential. The operator $\mathcal{C}_{ee}[f_s, f_{s'}]$ may then be expressed with $g_{s'}$ and $h_{s'}$, which would lead to Eq. (21) of Ref. [49] by noting $\Gamma_{ss'} = 2Y_{ss'}/m_s^2$, as done by the authors of the aforementioned reference. The Laplacian of the first Rosenbluth's potential is:

$$\begin{aligned}\Delta g_{s'} = \sum_{i=1}^{3} \frac{\partial^2 g_{s'}}{\partial v_{si}^2} = Y_{ss'}^{-1} \mathrm{tr}\ \mathsf{D}_{s'} &= \int f_{s'} \mathrm{tr}\ \mathsf{U}\ d^3\mathbf{v}_{s'} \\ &= \int \frac{2f_{s'}}{|\mathbf{v}_s - \mathbf{v}_{s'}|}\ d^3\mathbf{v}_{s'} = 2h_{s'}, \end{aligned} \tag{2.64}$$

with tr the trace operator. Likewise, the Laplacian of the second Rosenbluth's potential reads:

$$\Delta h_{s'} = \sum_{i=1}^{3} \frac{\partial^2 h_{s'}}{\partial v_{si}^2} = \left(1 + \frac{m_s}{m_{s'}}\right) \int f_{s'} \sum_{i=1}^{3} \frac{\partial^2}{\partial v_{si}^2} \frac{1}{|\mathbf{v}_s - \mathbf{v}_{s'}|}\ d^3\mathbf{v}_{s'} \tag{2.65}$$

$$= -4\pi \int f_{s'}\ \delta(\mathbf{v}_s - \mathbf{v}_{s'})\ d^3\mathbf{v}_{s'} = -4\pi f_{s'}, \tag{2.66}$$

where $f_{s'}$ is evaluated at $\mathbf{v}_s$. Hence, $h_{s'}$ and $g_{s'}$ both satisfy a Poisson equation, justifying their qualifiers. $h_{s'}$ is the potential created by a density $-4\pi f_{s'}$, whereas $g_{s'}$ is created by the density $2h_{s'}$. Therefore, the symmetry properties of $f_{s'}$ imply those of the Rosenbluth's potentials and, so, those of the friction force and diffusion tensor. If $f_{s'}$ is spherically symmetric, $h_{s'}$ and $g_{s'}$ only depend on $v_s = \sqrt{\mathbf{v}_s^2}$, and their values are determined by $f_{s'}(v_{s'})$ for $v_{s'} \geq v_s$. The dynamical friction force and the velocity diffusion tensor that acts on a group of charges with a certain velocity are only determined by the interactions of these charges with slower ones.

### 2.B.2 Derivation of $\mathcal{C}_{ee}[f_e, f_M]$

We then consider the case in which $f_s = f_e$ and

$$f_{s'} = f_M = \frac{n_e}{(2\pi)^{3/2} v_T^3} e^{-v^2/(2v_T^2)},$$

where $n_e$ is the electron density, and $v_T = (k_B T_e/m_e)^{1/2}$ is the thermal velocity with $m_e = m_s = m_{s'}$. Subscripts for velocities will be omitted everywhere. The Rosenbluth's potential, $h_M$ and $g_M$, are isotropic and so their Laplacian is reduced to the radial part $v^{-2}\partial_v v^2 \partial_v$. The Poisson's equation (2.66) verified by the second potential reads

$$v^{-2}\partial_v v^2 \partial_v h_M = -4\pi \frac{n_e}{(2\pi)^{3/2} v_T^3} e^{-v^2/(2v_T^2)}$$

Multiplying by $v^2$ and integrating over $[0, v]$ leads to

$$v^2 \partial_v h_M = -\frac{4n_e}{\pi^{1/2}} \int_0^v \left(\frac{v'}{v_T\sqrt{2}}\right)^2 e^{-v'^2/(2v_T^2)} \frac{dv'}{v_T\sqrt{2}}.$$

In order to compute the integral, we note $w = v/v_T\sqrt{2}$ and perform a by parts integration:

$$\begin{aligned}\int_0^w w'^2 e^{-w'^2} dw' = \int_0^w (-)\frac{1}{2} w'(-)2w' e^{-w'^2} dw' &= -\frac{1}{2} w e^{-w^2} + \frac{1}{2}\int_0^w e^{-w'^2} dw' \\ &= \frac{\pi^{1/2}}{4}\left[-w\mathrm{erf}'(w) + \mathrm{erf}(w)\right],\end{aligned}$$

where erf is the error function defined by

$$\mathrm{erf}(w) = \frac{2}{\pi^{1/2}} \int_0^w e^{-w'^2} dw'.$$

Therefore,

$$v^2 \partial_v h_M = -n_e \left[-\frac{v}{v_T\sqrt{2}} \mathrm{erf}'\left(\frac{v}{v_T\sqrt{2}}\right) + \mathrm{erf}\left(\frac{v}{v_T\sqrt{2}}\right)\right]$$

From the definition (2.62) we deduce that $h_M$ is vanishing at infinity. Thus, dividing by $v^2$ and integrating over $[v, +\infty[$ on either side of the equal sign, the last equality becomes

$$-h_M = -\frac{n_e}{v_T\sqrt{2}} \int_v^\infty \left(\frac{v_T\sqrt{2}}{v'}\right)^2 \left[-\frac{v}{v_T\sqrt{2}} \mathrm{erf}'\left(\frac{v}{v_T\sqrt{2}}\right) + \mathrm{erf}\left(\frac{v}{v_T\sqrt{2}}\right)\right] \frac{dv'}{v_T\sqrt{2}}.$$

By noting again $w = v/(v_T\sqrt{2})$, the integral is

$$\int_w^\infty w'^{-2} \left[-w'\mathrm{erf}'(w') + \mathrm{erf}(w')\right] dw' = -\int_w^\infty \frac{d}{dw'}\left(\frac{\mathrm{erf}(w')}{w'}\right) dw' = \frac{\mathrm{erf}(w)}{w}.$$

Finally,

$$h_M = \frac{n_e}{v} \mathrm{erf}\left(\frac{v}{v_T\sqrt{2}}\right) \tag{2.67}$$

Having determined $h_M$, we can now determine $g_M$ through the following Poisson's equation (2.64),

$$v^{-2}\partial_v v^2 \partial_v g_M = 2h_M = \frac{2n_e}{v}\mathrm{erf}\left(\frac{v}{v_T\sqrt{2}}\right).$$

Multiplying by $v^2$ and integrating over $[0, v]$ leads to

$$v^2\partial_v g_M = 2n_e \int_0^v v'\mathrm{erf}\left(\frac{v'}{v_T\sqrt{2}}\right) dv' = 2n_e(v_T\sqrt{2})^2\mathcal{I}\left(\frac{v}{v_T\sqrt{2}}\right), \tag{2.68}$$

where

$$\mathcal{I}(w) = \int_0^w w'\mathrm{erf}(w')dw'.$$

This integral is not immediate. We shall compute it through a by parts integration, which requires a primitive of the error function. Up to a constant term,

$$\int^w \mathrm{erf}(w')\ dw' = w\mathrm{erf}(w) - \int^w w'\mathrm{erf}'(w)\ dw' = w\mathrm{erf}(w) + \frac{1}{2}\mathrm{erf}'(w).$$

Indeed, the integrand of the integral in the right hand side is $2w'e^{-w'^2}/\pi^{1/2} = -(1/\pi^{1/2})d(e^{-w'^2})/dw'$, such that $\int^w w'\mathrm{erf}'(w')\ dw' = -\mathrm{erf}'(w)/2$. Then, the researched integral can be expressed as

$$\mathcal{I}(w) = w\left[w\mathrm{erf}(w) + \frac{1}{2}\mathrm{erf}'(w)\right] - \int_0^w \left[w'\mathrm{erf}(w') + \frac{1}{2}\mathrm{erf}'(w)\right] dw'.$$

In the right hand side the term $-\mathcal{I}(w)$ is appearing, such that we finally have

$$\mathcal{I}(w) = \frac{1}{2}w\left[w\mathrm{erf}(w) + \frac{1}{2}\mathrm{erf}'(w)\right] - \frac{1}{4}\mathrm{erf}(w) = \frac{1}{2}\left[\left(w^2 - \frac{1}{2}\right)\mathrm{erf}(w) + \frac{w}{2}\mathrm{erf}'(w)\right].$$

From the examination of Eq. (2.63) that defines $g_M$, it appears that the latter does not vanish at infinity. On the contrary, it is expected to grow linearly with the velocity. It is true that $g_M$ is defined up to an harmonic function by the Poisson equation (2.64), but the Eq. (2.63) imposes this function to be identically zero. Therefore the potential cannot be redefined in a bounded one by any gauge transformation. This simply means that we cannot turn a bound state of the potential into a free state by endowing it with a finite amount of energy. The situation in which the potential would be bounded is that of a distribution of sources limited in the velocity space, *i.e* a distribution which is identically zero beyond a certain velocity such that there do not exist sources at infinity. Here, the source of $g_M$ is $h_M$, which, despite vanishing at infinity, is never identically equal to zero.

This digression explains the reason why, unlike the calculation of $h_M$, we shall integrate Eq. (2.68) over $[0, v]$ instead of $[v, +\infty[$, , after having divided by $v^2$:

$$g_M - g_{M0} = 2n_e(v_T\sqrt{2})^2 \int_0^v v'^{-2}\mathcal{I}\left(\frac{v'}{v_T\sqrt{2}}\right) dv' = n_e(v_T\sqrt{2}) \int_0^w 2w'^{-2}\mathcal{I}(w')dw', \tag{2.69}$$

where $w = v/(v_T\sqrt{2})$ and $g_{M0}$ is the value of $g_M$ at $v = 0$. It can be directly computed from Eq. (2.63) by two successive by parts integrations:

$$\begin{aligned} g_{M0} = \int v' f_M d^3v' &= \frac{n_e}{(2\pi)^{3/2} v_T^3} \int_0^\infty 4\pi v'^3 e^{-v'^2/(2v_T^2)} dv' \\ &= -\frac{2n_e}{(2\pi)^{1/2}} \int_0^\infty v'^2 \partial_{v'} e^{-v'^2/(2v_T^2)} dv' \\ &= -\frac{4n_e v_T}{(2\pi)^{1/2}} \int_0^\infty \partial_{v'} e^{-v'^2/(2v_T^2)} dv' = \frac{2n_e v_T \sqrt{2}}{\pi^{1/2}}. \end{aligned}$$

Then, up to a constant term,

$$\begin{aligned} \int^w 2w'^{-2} \mathcal{I}(w') dw' &= \int^w \left[ \left( 1 - \frac{1}{2w'^2} \right) \mathrm{erf}(w') + \frac{1}{2w'} \mathrm{erf}'(w') \right] dw' \\ &= \left( w + \frac{1}{2w} \right) \mathrm{erf}(w) + \frac{1}{2} \mathrm{erf}'(w). \end{aligned}$$

To obtain this primitive, we integrated by parts the integral whose integrand is $(1 - 1/[2w'^2])\mathrm{erf}(w')$, and used an already found primitive of $w'\mathrm{erf}'(w')$, which is $-\mathrm{erf}'(w')/2$. Although the written expression of $\int^w 2w'^{-2}\mathcal{I}(w')dw'$ is not defined at $w = 0$, it can be extended by continuity at that point because $\mathrm{erf}(w) \sim 2w/\pi^{1/2}$. The value at $w = 0$ of the extended function is $2/\pi^{1/2}$, which, multiplied by $n_e v_T\sqrt{2}$, is exactly $g_{M0}$. Hence, from Eq. (2.69) we finally obtain,

$$g_M = \frac{n_e v_T \sqrt{2}}{2} \left[ \mathrm{erf}' \left( \frac{v}{v_T\sqrt{2}} \right) + \left( 1 + \frac{v^2}{v_T^2} \right) \frac{v_T\sqrt{2}}{v} \mathrm{erf} \left( \frac{v}{v_T\sqrt{2}} \right) \right]. \tag{2.70}$$

Then, we shall compute both the dynamical friction force (2.62) and the velocity diffusion tensor (2.63). From Eq. (2.67) we get

$$F_{Mi} = \frac{2Y_{ee}}{m_e} \frac{v_i}{v} \partial_v h_M = -\frac{2n_e Y_{ee}}{m_e v^2} \frac{v_i}{v} \left[ \mathrm{erf} \left( \frac{v}{v_T\sqrt{2}} \right) - \frac{v}{v_T\sqrt{2}} \mathrm{erf}' \left( \frac{v}{v_T\sqrt{2}} \right) \right], \tag{2.71}$$

where we used $\partial/\partial v_i = (v_i/v)\partial_v$. As $D_{Mij}$ is proportional to the Hessian of $g_M$ (2.70), we start by computing

$$\frac{\partial g_M}{\partial v_j} = \frac{n_e v_T \sqrt{2}}{2v} \frac{v_j}{v} \left[ \mathrm{erf}' \left( \frac{v}{v_T\sqrt{2}} \right) + \frac{v_T\sqrt{2}}{v} \left( \frac{v^2}{v_T^2} - 1 \right) \mathrm{erf} \left( \frac{v}{v_T\sqrt{2}} \right) \right].$$

To obtain the above formula, we used the following identities:

$$\begin{aligned} \frac{d}{dv} \left[ (1 + \frac{v^2}{v_T^2}) \frac{v_T\sqrt{2}}{v} \right] &= \frac{v_T\sqrt{2}}{v^2} \left( \frac{v^2}{v_T^2} - 1 \right), \\ \left( \frac{v_T\sqrt{2}}{v} \right)^{-1} \mathrm{erf}'' \left( \frac{v_T\sqrt{2}}{v} \right) &= -\frac{v}{v_T^2} \mathrm{erf}' \left( \frac{v_T\sqrt{2}}{v} \right), \end{aligned}$$

where the second one is directly obtained from

$$\mathrm{erf}''(w) = \frac{d^2}{dw^2} \frac{2}{\pi^{1/2}} \int_0^w e^{-w'^2} dw' = \frac{d}{dw} \frac{2}{\pi^{1/2}} e^{-w^2} = -2w\ \mathrm{erf}'(w).$$

Up to the factor $n_e v_T\sqrt{2}/2$, $\partial g_M/\partial v_j$ is the product of $v_j/v$ by a function of $v$. Therefore $\partial^2 g_M/\partial v_i \partial v_j$ is $n_e v_T\sqrt{2}/2$ times the sum of two terms. The first one is

$$\frac{\partial}{\partial v_i}\frac{v_j}{v} = \frac{1}{v}\left(\delta_{ij} - \frac{v_i v_j}{v^2}\right) = U_{ij}(\mathbf{v}),$$

multiplied by the aforementioned function of $v$, and the second one is $v_j/v$ multiplied by the derivative, $\partial/\partial v_i = (v_i/v)\partial_v$, of this function of $v$:

$$\begin{aligned}&\frac{v_i}{v}\partial_v\left[\frac{1}{v}\mathrm{erf}'\left(\frac{v}{v_T\sqrt{2}}\right) + \frac{v_T\sqrt{2}}{v^2}\left(\frac{v^2}{v_T^2}-1\right)\mathrm{erf}\left(\frac{v}{v_T\sqrt{2}}\right)\right]\\ &= \frac{v_i}{v}\frac{2}{v^2}\frac{v_T\sqrt{2}}{v}\left[\mathrm{erf}\left(\frac{v}{v_T\sqrt{2}}\right) - \frac{v}{v_T\sqrt{2}}\mathrm{erf}'\left(\frac{v}{v_T\sqrt{2}}\right)\right],\end{aligned}$$

where we used the relation between erf$''$ and erf$'$. It is worth mentioning that the same combination of erf and erf$'$ as in the expression of $F_{Mi}$ is appearing. As a result, the velocity diffusion tensor may be expressed as

$$D_{Mij} = \left(\delta_{ij} - \frac{v_i v_j}{v^2}\right) D_{M\perp} + \frac{v_i v_j}{v^2} D_{M\parallel} \tag{2.72}$$

with

$$D_{M\perp} = \frac{n_e Y_{ee}}{2v}\frac{v_T\sqrt{2}}{v}\left[\mathrm{erf}'\left(\frac{v}{v_T\sqrt{2}}\right) + \frac{v_T\sqrt{2}}{v}\left(\frac{v^2}{v_T^2}-1\right)\mathrm{erf}\left(\frac{v}{v_T\sqrt{2}}\right)\right], \tag{2.73}$$

and

$$D_{M\parallel} = \frac{n_e Y_{ee}}{v}\left(\frac{v_T\sqrt{2}}{v}\right)^2\left[\mathrm{erf}\left(\frac{v}{v_T\sqrt{2}}\right) - \frac{v}{v_T\sqrt{2}}\mathrm{erf}'\left(\frac{v}{v_T\sqrt{2}}\right)\right]. \tag{2.74}$$

Then, following Chandrasekhar in Ref. [103], we introduce the functions:

$$\mathcal{G}(w) = \frac{1}{2w^2}\Big[\mathrm{erf}(w) - w\ \mathrm{erf}'(w)\Big], \tag{2.75}$$

and

$$\mathcal{H}(w) = \frac{1}{2w^2}\Big[w\ \mathrm{erf}'(w) + (2w^2-1)\mathrm{erf}(w)\Big], \tag{2.76}$$

such that both the friction force and the diffusion tensor takes the following compact forms:

$$F_{Mi} = -m_e v_T \nu_{ee}(v_T)\mathcal{G}\left(\frac{v}{v_T\sqrt{2}}\right)\frac{v_i}{v}, \tag{2.77}$$

and

$$D_{M\perp} = \frac{1}{2}(m_e v_T)^2 \nu_{ee}(v_T)\frac{v_T}{v}\mathcal{H}\left(\frac{v}{v_T\sqrt{2}}\right), \tag{2.78}$$

$$D_{M\parallel} = (m_e v_T)^2 \nu_{ee}(v_T)\frac{v_T}{v}\mathcal{G}\left(\frac{v}{v_T\sqrt{2}}\right), \tag{2.79}$$

with $\nu_{ee}(v_T)$ the velocity-dependent electron-electron collision frequency, $\nu_{ee} = 2n_e Y_{ee}/(m_e^2 v^3)$, evaluated at $v = v_T$. Obviously, the friction force may have been deduced from the calculation of the diffusion tensor through $F_{Mi} = m_e^{-1}\partial D_{Mij}/\partial v_j$. Finally, we shall put the established collision operator, $\mathcal{C}_{ee}[f_e, f_M]$, in the expected form. The substitution of Eqs. (2.77)-(2.79) into Eq. (2.59) yields to

$$\begin{aligned} C_{ee}[f_e, f_M] &= -\frac{\partial}{\partial v_i}\left[m_e^{-1}F_{Mi}f_e - m_e^{-2}D_{Mij}\frac{\partial f_e}{\partial v_j}\right] \\ &= \frac{v_T^3\nu_{ee}(v_T)}{2}\frac{\partial}{\partial v_i}U_{ij}(\mathbf{v})\mathcal{H}\left(\frac{v}{v_T\sqrt{2}}\right)\frac{\partial f_e}{\partial v_j} \qquad (2.80) \\ &+ v_T\nu_{ee}(v_T)\frac{\partial}{\partial v_i}\left[\frac{v_i}{v}\mathcal{G}\left(\frac{v}{v_T\sqrt{2}}\right)\left(f_e + \frac{v_T^2}{v}\frac{v_j}{v}\frac{\partial f_e}{\partial v_j}\right)\right]. \qquad (2.81) \end{aligned}$$

In the above operator, the first part (2.80) is equal to $v_T^3\nu_{ee}(v_T)/2$ multiplied by

$$v^{-3}\mathcal{H}\left(\frac{v}{v_T\sqrt{2}}\right)\frac{\partial}{\partial v_i}(v^2\delta_{ij} - v_i v_j)\frac{\partial f_e}{\partial v_j} + \left[\frac{v_i}{v}\partial_v v^{-3}\mathcal{H}\left(\frac{v}{v_T\sqrt{2}}\right)\right](v^2\delta_{ij} - v_i v_j)\frac{\partial f_e}{\partial v_j},$$

where the second term vanishes because $v_i(v^2\delta_{ij} - v_i v_j) = 0$. Then, the second part (2.81) is $v_T\nu_{ee}(v_T)$ multiplied by

$$\frac{v_i}{v^3}\frac{\partial}{\partial v_i}\left[v^2\mathcal{G}\left(\frac{v}{v_T\sqrt{2}}\right)\left(f_e + \frac{v_T^2}{v}\frac{v_j}{v}\frac{\partial f_e}{\partial v_j}\right)\right],$$

because $\mathbf{v}/v^3$ is a conservative flux field:

$$\frac{\partial}{\partial v_i}\frac{v_i}{v^3} = 0.$$

Finally, we change the variable by using $(v, \mathbf{\Omega} = \mathbf{v}/v)$ instead of $\mathbf{v}$. The corresponding distribution function will still be noted $f_e$. The differential operator is transformed according to the chain rule as

$$\frac{\partial}{\partial v_i} = \frac{\partial v}{\partial v_i}\frac{\partial}{\partial v} + \frac{\partial \Omega_j}{\partial v_i}\frac{\partial}{\partial \Omega_j} = \Omega_i\frac{\partial}{\partial v} + v^{-1}(\delta_{ij} - \Omega_i\Omega_j)\frac{\partial}{\partial \Omega_j},$$

such that, besides the already used relation $(v_i/v)\partial/\partial v_i = \partial_v$, we have,

$$\Big(v^2\delta_{ij} - v_i v_j\Big)\frac{\partial}{\partial v_j} = v^2\Big(\delta_{ij} - \Omega_i\Omega_j\Big)v^{-1}\Big(\delta_{jk} - \Omega_j\Omega_k\Big)\frac{\partial}{\partial \Omega_k} = v\Big(\delta_{ik} - \Omega_i\Omega_k\Big)\frac{\partial}{\partial \Omega_k}.$$

This allows to write the spherical Laplacian as

$$-\mathsf{L}^2 = \frac{\partial}{\partial v_i}\Big(v^2\delta_{ij} - v_i v_j\Big)\frac{\partial}{\partial v_j} = \Big(\delta_{ij} - \Omega_i\Omega_j\Big)\frac{\partial}{\partial \Omega_j}\Big(\delta_{ik} - \Omega_i\Omega_k\Big)\frac{\partial}{\partial \Omega_k}.$$

Since $\nu_{ee}(v) = (v_T/v)^3\nu_{ee}(v_T)$, we finally obtain

$$\begin{aligned} C_{ee}[f_e, f_M] &= \frac{\nu_{ee}}{2}\mathcal{H}\left(\frac{v}{v_T\sqrt{2}}\right)(-\mathsf{L}^2)f_e \\ &+ \nu_{ee}v\partial_v\left[\left(\frac{v}{v_T}\right)^2\mathcal{G}\left(\frac{v}{v_T\sqrt{2}}\right)\left(f_e + \frac{v_T^2}{v}\frac{\partial f_e}{\partial v}\right)\right]. \qquad (2.82) \end{aligned}$$

### 2.B.3 High velocity limit

The high velocity limit of $C_{ee}[f_e, f_M]$ can be obtained by expanding the functions $\mathcal{H}$ and $\mathcal{G}$ within the last expression of the previous section. This makes apparent the physical consequences of that limit, which are examined in Chap. 3. For the purpose of obtaining the final, used form of the operator, however, this is not at all necessary. The linearization and expansion of the Landau's operator can be performed simultaneously in an elementary way, directly from its original form. For convenience we write $\mathcal{C}_{ee}[f_e, f_M] = -(Y_{ee}/m_e^2)(\partial \mathcal{J}_i/\partial v_i)$, with

$$\mathcal{J}_i = \int U_{ij}(\mathbf{v}-\mathbf{v}')\left(f_e\frac{\partial f_M}{\partial v'_j} - f_M\frac{\partial f_e}{\partial v_j}\right)\, d^3\mathbf{v}' = -\left(\mathcal{V}_i\frac{f_e}{v_T^2} + \mathcal{M}_{ij}\frac{\partial f_e}{\partial v_j}\right),$$

where we expressed $\partial f_M/\partial v'_j = -v'_j f_M/v_T^2$, and introduced

$$\mathcal{V}_i = \int U_{ij}(\mathbf{v}-\mathbf{v}')v'_j f_M\, d^3\mathbf{v}'; \quad \mathcal{M}_{ij} = \int U_{ij}(\mathbf{v}-\mathbf{v}')f_M\, d^3\mathbf{v}'. \tag{2.83}$$

In order to compute these integrals in the desired limit, we proceed to a Taylor's expansion of the Landau's kernel tensor. Up to second order for any strictly positive integer $p$,

$$\frac{1}{|\mathbf{v}-\mathbf{v}'|^p} = \frac{1}{v^p} - v'_\mu(-)\frac{pv_\mu}{v^{p+2}} + \frac{v'_\nu v'_\lambda}{2}\frac{(-)p}{v^{p+2}}\left(\delta_{\nu\lambda} - \frac{(p+2)v_\nu v_\lambda}{v^2}\right),$$

and so

$$\begin{aligned} U_{ij}(\mathbf{v}-\mathbf{v}') \simeq &\left[\frac{1}{v} + v'_\mu\frac{v_\mu}{v^3} - \frac{v'_\nu v'_\lambda}{2v^3}\left(\delta_{\nu\lambda} - \frac{3v_\nu v_\lambda}{v^2}\right)\right] \\ &\times\left[\delta_{ij} - (v_i - v'_i)(v_j - v'_j)\left(\frac{1}{v^2} + v'_\epsilon\frac{2v'_\epsilon}{v^4} - \frac{v'_\alpha v'_\beta}{v^4}\left[\delta_{\alpha\beta} - \frac{4v_\alpha v_\beta}{v^2}\right]\right)\right]. \end{aligned}$$

The usage of different letters for indices is designed to make reading easier. The terms can be grouped according to the successive powers of $1/v$. This leads to write $U_{ij}$ as the sum, for $\ell = 1, 2, 3$, of $U_{ij}^{(\ell)}$ with:

$$U_{ij}^{(1)} = \frac{1}{v}\left(\delta_{ij} - \frac{v_i v_j}{v^2}\right),$$

$$U_{ij}^{(2)} = \frac{1}{v}\left[-v_i v_j v'_\epsilon\frac{2v'_\epsilon}{v^4} + (v_i v'_j + v'_i v_j)\frac{1}{v^2}\right] + v'_\mu\frac{v_\mu}{v^3}\left(\delta_{ij} - \frac{v_i v_j}{v^2}\right),$$

$$\begin{aligned} U_{ij}^{(3)} =& \frac{1}{v}\left[v_i v_j\frac{v'_\alpha v'_\beta}{v^4}\left(\delta_{\alpha\beta} - \frac{4v_\alpha v_\beta}{v^2}\right) + (v_i v'_j + v'_i v_j)v'_\epsilon\frac{2v'_\epsilon}{v^4} - \frac{v'_i v'_j}{v^2}\right] \\ &+ v'_\mu\frac{v_\mu}{v^3}\left[-v_i v_j v'_\epsilon\frac{2v'_\epsilon}{v^4} + (v_i v'_j + v'_i v_j)\frac{1}{v^2}\right] - \frac{v'_\nu v'_\lambda}{2v^3}\left(\delta_{\nu\lambda} - \frac{3v_\nu v_\lambda}{v^2}\right)\left(\delta_{ij} - \frac{v_i v_j}{v^2}\right). \end{aligned}$$

Then, we calculate the contribution of each of these terms to the integral factors (2.83). These contributions will be noted $\mathcal{V}_i^{(\ell)}$ and $\mathcal{M}_{ij}^{(\ell)}$ for convenience. The

integral of $f_M$ over all velocities $\mathbf{v}'$ is $n_e$, and that one of $f_M v'_j$ vanishes. So, $\mathcal{V}_i^{(1)} = 0$ and

$$\mathcal{M}_{ij}^{(1)} = \int f_M U_{ij}^{(1)} d^3\mathbf{v}' = \frac{n_e}{v}\left(\delta_{ij} - \frac{v_i v_j}{v^2}\right).$$

Then, $\mathcal{M}_{ij}^{(2)} = 0$. Indeed $U_{ij}^{(2)}$ only contains linear terms in the components of $\mathbf{v}'$. Therefore all the terms in $\mathcal{M}_{ij}^{(2)}$ contains integrals of the same form as the one appearing in $\mathcal{V}_i^{(1)}$. In the case of $\mathcal{V}_i^{(2)}$, the quadratic integrals

$$\int f_M v'_a v'_b \; d^3\mathbf{v}' = \delta_{ab} n_e v_T^2, \tag{2.84}$$

are involved:

$$\begin{aligned}\mathcal{V}_i^{(2)} = &-\frac{1}{v} v_i v_j \frac{2v_\epsilon}{v^4}\int f_M v'_\epsilon v'_j \; d^3\mathbf{v}' + \frac{v_i}{v^3}\int f_M v'^2 \; d^3\mathbf{v}' \\ &+ \frac{v_j}{v^3}\int f_M v'_i v'_j d^3\mathbf{v}' + \frac{v_\mu}{v^3}\left(\delta_{ij} - \frac{v_i v_j}{v^2}\right)\int f_M v'_j v'_\mu \; d^3\mathbf{v}'\end{aligned}$$

By using Eq. (2.84), the last term vanishes since it involves $v_\mu(\delta_{ij} - v_i v_j/v^2)\delta_{j\mu}$. So,

$$\mathcal{V}_i^{(2)} = \frac{n_e}{v}\frac{v_i}{v}\frac{v_T^2}{v}(-2+3+1) = \frac{2n_e}{v}\frac{v_i}{v}\frac{v_T^2}{v}$$

Finally, $U_{ij}^{(3)}$ is quadratic in the components of $\mathbf{v}'$. Therefore it does not have any contribution to $\mathcal{V}_i^{(3)}$. Indeed, all terms involve integrals of the following form:

$$\int f_M v'_a v'_b v'_c \; d^3\mathbf{v}' = 0$$

In the case of $\mathcal{M}_{ij}^{(3)}$, however, the same type of quadratic integrals (2.84) appear as for $\mathcal{V}_i^{(2)}$:

$$\begin{aligned}\mathcal{M}_{ij}^{(3)} = &\frac{1}{v} v_i v_j \frac{1}{v^4}\left(\delta_{\alpha\beta} - \frac{4v_\alpha v_\beta}{v^2}\right)\int f_M v'_\alpha v'_\beta \; d^3\mathbf{v}' + \frac{1}{v}\frac{2v_\epsilon}{v^4}\int f_M v'_\epsilon (v_i v'_j + v'_i v_j) \; d^3\mathbf{v}' \\ &- \frac{1}{v}\frac{1}{v^2}\int f_M v'_i v'_j \; d^3\mathbf{v}' - \frac{1}{v}\left(\delta_{ij} - \frac{v_i v_j}{v^2}\right)\left(\delta_{\nu\lambda} - \frac{3v_\nu v_\lambda}{v^2}\right)\int f_M v'_\nu v'_\lambda \; d^3\mathbf{v}' \\ &- \frac{v_\mu}{v^3}\int f_M v'_\mu v_i v_j v'_\epsilon \frac{2v_\epsilon}{v^4} \; d^3\mathbf{v}' + \frac{v_\mu}{v^3}\frac{1}{v^2}\int f_M v'_\mu (v_i v'_j + v_j v'_i) \; d^3\mathbf{v}'\end{aligned}$$

The second term of the second line vanishes because

$$\left(\delta_{\nu\lambda} - \frac{3v_\nu v_\lambda}{v^2}\right)\delta_{\nu\lambda} = 0.$$

Likewise, during the calculation of the first term there appears

$$\left(\delta_{\alpha\beta} - \frac{4v_\alpha v_\beta}{v^2}\right)\delta_{\alpha\beta} = 3 - 4 = -1.$$

Finally,

$$\begin{aligned}\mathcal{M}_{ij}^{(3)} &= \frac{n_e}{v}\frac{v_T^2}{v^2}\frac{v_i v_j}{v^2}(-1+4-2+2) - \frac{n}{v}\frac{v_T^2}{v^2}\delta_{ij} \\ &= -\frac{v_T^2}{v^2}\frac{n_e}{v}\left(\delta_{ij} - \frac{v_i v_j}{v^2}\right) + 2\frac{n_e}{v}\frac{v_T^2}{v^2}\frac{v_i v_j}{v^2}.\end{aligned}$$

Thus, the flux in velocity space is

$$\begin{aligned}\mathcal{J}_i &= \left(\mathcal{M}_{ij}^{(1)} + \mathcal{M}_{ij}^{(3)}\right)\frac{\partial f_e}{\partial v_j} + \mathcal{V}_i^{(2)}\frac{f_e}{v_T^2} \\ &= \left(1 - \frac{v_T^2}{v^2}\right)\frac{n_e}{v}\left(\delta_{ij} - \frac{v_i v_j}{v^2}\right)\frac{\partial f_e}{\partial v_j} + \frac{2n_e}{v}\frac{v_i}{v^2}\left(f_e + \frac{v_T^2}{v}\frac{v_j}{v}\frac{\partial f_e}{\partial v_j}\right),\end{aligned}$$

and so its divergence has the following expression:

$$\begin{aligned}\frac{\partial}{\partial v_i}\mathcal{J}_i = &\left(1 - \frac{v_T^2}{v^2}\right) n_e \frac{\partial}{\partial v_i}\frac{1}{v}\left(\delta_{ij} - \frac{v_i v_j}{v^2}\right)\frac{\partial f_e}{\partial v_j} \\ &+ \frac{n_e}{v}\left(\delta_{ij} - \frac{v_i v_j}{v^2}\right)\frac{\partial f_e}{\partial v_j}\frac{\partial}{\partial v_i}\left(1 - \frac{v_T^2}{v^2}\right) + 2n_e\frac{\partial}{\partial v_i}\frac{1}{v}\frac{v_i}{v^2}\left(f_e + \frac{v_T^2}{v}\frac{v_j}{v}\frac{\partial f_e}{\partial v_j}\right).\end{aligned}$$

Since $\partial(1-v_T^2/v^2)/\partial v_i = 2v_T^2 v_i/v^4$, the second term vanishes. Concerning the third one, we use that the divergence of $\mathbf{v}/v^3$ vanishes in order to express $\mathcal{C}_{ee}[f_e, f_M]$ as

$$\frac{n_e Y_{ee}}{m_e^2}\left[\left(1 - \frac{v_T^2}{v^2}\right)\frac{\partial}{\partial v_i}\frac{1}{v}\left(\delta_{ij} - \frac{v_i v_j}{v^2}\right)\frac{\partial f_e}{\partial v_j} + \frac{2}{v^2}\frac{v_i}{v}\frac{\partial}{\partial v_i}\left(f_e + \frac{v_T^2}{v}\frac{v_j}{v}\frac{\partial f_e}{\partial v_j}\right)\right].$$

We leave aside the few remaining manipulations, a major part of which have already been done in Sec. 2.2.1 to bring out the Lorentz's operator. The final result is

$$\mathcal{C}_{ee}[f_e, f_M] \simeq \left(1 - \frac{v_T^2}{v^2}\right)\frac{\nu_{ee}}{2}(-\mathsf{L}^2)f_e + \nu_{ee} v\partial_v\left(f_e + \frac{v_T^2}{v}\partial_v f_e\right).$$

The factor $(1 - v_T^2/v^2)$ in front of $(\nu_{ee}/2)(-\mathsf{L}^2)$ corresponds to a second order expansion of $\mathcal{H}(v/[v_T\sqrt{2}])$ in the high velocity limit. Although it is consistent with the order retained for $\mathcal{G}(v/[v_T\sqrt{2}])$, it is sufficient to approximate it by 1 for reason detailed in the Chap. 3.

This page is unintentionally left not blank.

This page is unintentionally left not blank.

# Chapter 3

# Physical analysis of a kinetic model

In this thesis, rather than seeking to obtain an explicit formula for the heat flux density by approximately solving a certain system of coupled kinetic equations (2.14)-(2.15), an exact numerical resolution is carried out. The algorithm will be exposed in the next chapter. Here the focus is on studying the physical behaviour of the solutions. Because the electron-ion collision operator is already given by the Lorentz's formula (2.8) to high accuracy, the remaining degree of freedom to define a P1 system is the choice of an electron-electron collision operator. Here, it will be the one proposed by Albritton *et al.* [82]. The Sec. 3.1 presents this operator in a refreshing manner, exposing and dissecting as far as possible the simplifications that lead to it while proposing a decisive improvement. This is done after having recalled the motivation for using an approximate form instead of the electron-electron Landau's collision integral itself.

The resulting P1 system is studied in Sec. 3.2. Almost the same model was first considered by Del Sorbo *et al* [57] and further discussed by Holec *et al* [128]. In the former work, the authors focused on comparing the P1 and M1 closures. The distribution function was used for studying the electron heat flux density and the stability of the plasma in the transport region with respect to excitation of small-scale electron plasma and ion acoustic waves. In latter case, however, the conclusions significantly differ from those drawn up by Rozmus *et al.* [129] based on a full scale kinetic analysis. This suggested the need of extensive comparison of the reduced model to complete kinetic computations. This was the purpose of the article by Holec *et al*, in which several new features of the model have been identified. Our analysis extends the works of Del Sorbo *et al* and Holec *et al* which were not presented in the previous chapter to avoid heavy repetitions. Throughout the text, our contribution is carefully highlighted by recalling the results of these previous studies.

## 3.1 Approximate operator for collisions between electrons

As already mentioned, a complete treatment of electron-electron collisions using the Landau's integral is prohibitively expensive on the temporal and spatial scales of interest for ICF. One of the reason is its nonlinear character, inherent to such an operator. The description of the collision process relies on the probabilities to simultaneously find the collision partners in some states, and therefore to the product of the distribution functions of the populations to which they belong. The development of accurate schemes for the Vlasov-Landau's equation is an active area of research. It is justified by the need for precise simulations free of numerical artefacts. One of the most elaborate of them relies, in addition to the well-known Hamiltonian formulation of the Vlasov-Maxwell's system, on the metric structure of the Landau's integral. Few words on this framework can be found in the Complementary Note 6.1. Obviously, an other, older approach is suggested by the work of Rosenbluth *et al* [49]. The authors showed how the integro-differential operator of Landau can be expressed in a purely differential form,

$$-\frac{Y_{ee}}{m_e^2}\frac{\partial}{\partial v_k}\int U_{kl}(\mathbf{v}-\mathbf{v}')\left(f_e\frac{\partial f_{e'}}{\partial v_l'}-f_{e'}\frac{\partial f_e}{\partial v_l}\right)\,d^3\mathbf{v}' = -\frac{2Y_{ee}}{m_e^2}\frac{\partial}{\partial v_k}\left(2f_e\frac{\partial h_{e'}}{\partial v_k}-\frac{1}{2}\frac{\partial}{\partial v_l}\left[f_e\frac{\partial^2 g_{e'}}{\partial v_k\partial v_l}\right]\right)$$

where $h_{e'}$ and $g_{e'}$, the Rosenbluth's potentials, verify the following set of partial differential equations,

$$\Delta g_{e'} = 2h_{e'}; \quad \Delta h_{e'} = -4\pi f_{e'},$$

with $\Delta = \delta_{kl}\partial^2/\partial v_k\partial v_l$ the Laplacian in velocity space. More details about this equivalence can be found in the App. 2.B. As detailed by Karney in Ref. [130], the computational gain is substantial because the above coupled equations can be solved in an approximate way to high accuracy as we are going to explain below. In case of azimuthal symmetry, any function $X$ can be expanded as

$$X(v,\Omega_z) = \sum_{\ell=0}^{+\infty} X_\ell(v)p_\ell(\Omega_z); \quad X_\ell(v) = \frac{2\ell+1}{2}\int_{-1}^{+1} X(v,\Omega_z)p_\ell(\Omega_z)\,d\Omega_z,$$

where the Legendre's polynomials are determined from one to the next thanks to the following recurrence relation, $(\ell+1)p_{\ell+1}(\Omega_z) = (2\ell+1)\Omega_z p_\ell(\Omega_z) - \ell p_{\ell-1}(\Omega_z)$, with $p_0(\Omega_z)=1$ and $p_1(\Omega_z)=\Omega_z$. The components of the Rosenbluth's potentials (2.62)-(2.63) are linked to those of the distribution function by

$$h_{e'\ell}(v) = \frac{4\pi}{2\ell+1}\left[\int_0^v \frac{w^{\ell+2}}{v^{\ell+1}}f_{e'\ell}(w)\,dw + \int_v^{+\infty}\frac{v^\ell}{w^{\ell-1}}f_{e'\ell}(w)\,dw\right],$$

$$g_{e'\ell}(v) = -\frac{4\pi}{4\ell^2-1}\left[\int_0^v \frac{w^{\ell+2}}{v^{\ell-1}}\left(1-\frac{\ell-1/2}{\ell+3/2}\frac{w^2}{v^2}\right)f_{e'\ell}(w)\,dw + \int_v^{+\infty}\frac{v^\ell}{w^{\ell-3}}\left(1-\frac{\ell-1/2}{\ell+3/2}\frac{v^2}{w^2}\right)f_{e'\ell}(w)\,dw\right],$$

where we omitted the space variable within arguments. Then, let us consider a grid of size $G \times A$ to describe the set of pairs $(v, \Omega_z)$ in velocity space. With the integro-differential formula, at each point $(v, \Omega_z)$ of the grid an integration over all points $(v', \Omega'_z)$ in performed. This requires the $GA$ estimations of $f_{e'}(v', \Omega'_z)$. Therefore the number of operations to obtain the Landau's integral is $\mathcal{O}(G^2A^2)$. Now, consider that the expansion of the distribution function on Legendre's polynomials is limited to $N$ terms. For a given value of $\ell$, the computation of $f_{e'\ell}$ from $f_{e'}$ requires $\mathcal{O}(A)$ operations for each velocity $v'$, so $\mathcal{O}(GA)$ in all. The determination of $h_{e'\ell}$ and $g_{e'\ell}$ from $f_{e'\ell}$ further cost $\mathcal{O}(G)$ for each $\ell$. Thus the total number of operations to get all the $N$ components of the Rosenbluth's potentials is $\mathcal{O}(NGA)$. Obtaining $h_{e'}$ and $g_{e'}$ just adds $\mathcal{O}(N)$ operations. Hence, the final cost for estimating the Rosenbluth's potentials from the electron distribution function is $\mathcal{O}(NGA)$.

In the absence of any axial symmetry, the analysis is modified. If the expansion is performed on spherical harmonics, a two-dimensional grid for angles, $A_1 \times A_2$, must be used. Formally, this just leads to set $A = A_1 \times A_2$ above. However, for each value of $\ell$, the number of terms is now $2\ell + 1$ instead of 1. Hence the total cost for estimating Rosenbluth's potential is now $\mathcal{O}(N^2GA_1A_2)$. The usage of Maxwell's multipoles would lead to an even higher number of operations. Unlike spherical harmonics, the cardinal of $\ell$-order Maxwell's multipoles does not grow linearly with $\ell$, but like $\ell^2$. The same is for homogeneous polynomials $\Omega_{i_1} \dots \Omega_{i_\ell}$. As a consequence, the computational cost here is $\mathcal{O}(N^3GC_1C_2C_3)$, where the Cartesian grid on $\mathbb{S}^2$ has a size $C_1 \times C_2 \times C_3$.

Here we wish to further reduce the computational cost compared to these methods. For that purpose, the approach adopted consists of simplifying the Landau's operator itself by considering collisions that only involve the strongly out-of-equilibrium electrons responsible for nonlocal effects. It corresponds to Chandrasekhar's picture [103], reviewed in the App. 2.B, of *test* electrons interacting with a background of *field* electrons in equilibrium. This approximation leads to the following electron-electron collision operator,

$$C_{ee}[f_e, f_M] = \frac{\nu_{ee}}{2}\mathcal{H}\left(\frac{v}{v_T\sqrt{2}}\right)(-\mathsf{L}^2)f_e + \nu_{ee}v\partial_v\left[\left(\frac{v}{v_T}\right)^2\mathcal{G}\left(\frac{v}{v_T\sqrt{2}}\right)\left(f_e + \frac{v_T^2}{v}\partial_v f_e\right)\right]. \tag{3.1}$$

where $\nu_{ee}$ is the velocity-dependent electron-electron collision frequency. The functions $\mathcal{H}$ and $\mathcal{G}$, first tabulated by Chandrasekhar, are defined from the error function as

$$\mathcal{H}(w) = \frac{1}{2w^2}\left[w\ \mathrm{erf}'(w) + (2w^2 - 1)\,\mathrm{erf}(w)\right], \tag{3.2}$$

$$\mathcal{G}(w) = \frac{1}{2w^2}\left[\mathrm{erf}(w) - w\ \mathrm{erf}'(w)\right]. \tag{3.3}$$

They are plotted in Figs. 2.2-2.3. Finally, the function $\mathcal{K}$ is defined as

$$\mathcal{K} = f_e + (v_T^2/v)\partial_v f_e. \tag{3.4}$$

The starting point for deriving Eq. (3.1) is the nonlinear Landau's integral. As explained at the end of the Complementary Note 2.A, it can be seen as the Balescu-Guernsey-Lenard's collision operator (2.53) in which the dynamical nature of the Debye's screening is completely neglected for the entire electron population. Unfortunately, it turns out to be especially important for high-velocity electrons, precisely those whose kinetic behaviours hold our attention. Always within the framework of Chandrasekhar, the corrections made by the dynamical screening clearly appear in the expressions of the friction force and diffusion tensor. The underlying terms have been first obtained by Rostoker and Rosenbluth [124]. They are associated to absorption and spontaneous/stimulated emissions of electron plasma waves by fast electrons. In high temperature plasmas such as those encountered in ICF, those corrections are smaller than the binary collision contribution, even if they may represent up to the half of the later in the high velocity domain [107]. To our knowledge, they are not implemented in any existing codes yet.

In what follows, they will be omitted. On the contrary, two simplifications will be made in order to further approximate the kinetic description of electron-electron collisions concerning the functions $\mathcal{H}$, $\mathcal{G}$ and $\mathcal{K}$. The first one, exposed in Sec. 3.1.1, consists of considering the high velocity limit of the functions $\mathcal{H}$ and $\mathcal{G}$. The consequences of this procedure are examined in an unprecedented way, with a numerical illustration for the most important of them. Our analysis relies in particular on the formula, recovered in App. 2.B, giving the friction force experienced by electrons. The Sec. 3.1.2 discusses the function $\mathcal{K}$. The effort here consists of formalizing as much as possible the simplification introduced for computational convenience but empirically by Albritton *et al*, before introducing our improvement to the resulting operator in Sec. 3.1.3. The latter is a corrective factor to the electron-electron collision frequency, the necessity of which is justified, for the first time, through a physical argumentation.

### 3.1.1 High velocity limit

Strongly-out-of-equilibrium electrons may be thought of as those with the highest velocities because the electron mean free path is proportional to $v^4$. Thus, we shall consider the high velocity limit of functions $\mathcal{H}$ and $\mathcal{G}$ at the lowest order:

$$\mathcal{H}\left(\frac{v}{v_T\sqrt{2}}\right) \simeq 1, \qquad \mathcal{G}\left(\frac{v}{v_T\sqrt{2}}\right) \simeq \left(\frac{v_T}{v}\right)^2. \tag{3.5}$$

These estimates are obtained from Eqs. (3.2)-(3.3) by considering the asymptotic expansion of the error function,

$$\mathrm{erf}(w) \sim 1 - \frac{e^{-w^2}}{w\sqrt{\pi}} \sum_{k=0}^{+\infty} \frac{(-1)^k (2k-1)!!}{(2w^2)^k},$$

where $(2k-1)!!$ is the product $(2k-1)(2k-3)\ldots 1$. Focusing on collisions between supra-thermal and thermal electrons does not mean that they are predominant. On the contrary, an high-velocity electron preferably interacts with partners having velocities close to its own. Nevertheless, such collisions do not have any impact on energy transport because they are not associated to any gain or loss of electrons within this strongly-out-of-equilibrium population. These exchanges between populations are actually the decisive mechanisms we wish to describe here.

The consequence of considering the high velocity limit of $\mathcal{G}$ in Eq. (3.1) is the underestimation of the return electron current. This is shown in Fig. 3.1.1, where the normalized anisotropic part of electron distribution function, $q_{1z} = (2\pi m_e/3)v^5 f_{1z}$, is plotted by either considering the complete Chandrasekhar's (curve a, red, dot-dashed) functions or their high velocity expressions (curve JASMINE, blue, solid) (3.5). The reason for the difference can be found by analysing the norm of the dynamical friction force acting on a test electron with velocity $v$:

$$|\mathbf{F}_M| = m_e v_T \nu_{ee}(v_T)\mathcal{G}\left(\frac{v}{v_T\sqrt{2}}\right) \tag{3.6}$$

As shown in Fig. 3.1.2, the high velocity approximation overestimates the friction force acting on test electrons by more than 10% for $v/(v_T\sqrt{2}) \lesssim 1.8$. This overestimation leads to a reduction of the return electron current. Such a reduction has been observed in all the cases we considered, in both local and non local regimes. On the contrary, considering the high velocity limit of $\mathcal{H}$ has no significant effect of the return current. Within the Eq. (3.1), this function appears as a factor in front of the Lorentz's operator, and thus modulates the rate of the distribution function's isotropization. Fortunately, as it is confirmed through numerical analysis, the anisotropic part of the distribution function is small at low velocities. Consequently, the error that arises due to taking the high velocity limit, 1, of the function $\mathcal{H}$ is negligible.

While $\mathcal{G}\left(v/[v_T\sqrt{2}]\right)$ behaves as $v^{-2}$ in the high-velocity domain, it grows linearly for low velocities,

$$\mathcal{G}\left(\frac{v}{v_T\sqrt{2}}\right) \simeq \frac{2}{3\sqrt{\pi}}\frac{v}{v_T\sqrt{2}}. \tag{3.7}$$

Such a behaviour is typical from the field created by a ball of constant density in velocity space. Indeed, let us recall the relation between the dynamical friction force and the second Rosenbluth's potential, $F_{Mi} = (2Y_{ee}/m_e)(\partial h_M/\partial v_i)$ (2.62). Having in mind the associated Poisson's equation, $\Delta h_M = -4\pi f_M$, we can write the following Gauss' theorem in velocity space,

$$\oint_{\mathbb{S}^2(v)} F_{Mi}\, d^2S_i = -\frac{8\pi Y_{ee}}{m_e}\int_{\mathcal{B}^3(v)} f_M\, d^3\mathbf{v} \tag{3.8}$$

where $\mathbb{S}^2(v)$ is the 2-sphere of radius $v$, and $\mathcal{B}^3(v)$ the corresponding ball. Then, the asymptotic expressions of the friction force (3.6) are recovered by approximating $f_M$ by a step function $\left[1-\Theta(v-\mu v_T\sqrt{2})\right]f_M(v=0)$, with $\Theta$ the Heaviside's function. The parameter $\mu$ will be determined hereafter. By spherical symmetry, the left hand side of Eq. (3.8) is $4\pi v^2|\mathbf{F}_M|$.

For $v \leq \mu v_T\sqrt{2}$, since the ratio volume/surface for a sphere is growing linearly with the radius, we will find that $|\mathbf{F}_M| \propto v$. Indeed,

$$4\pi v^2|\mathbf{F}_M| = \frac{8\pi Y_{ee}}{m_e}\frac{n_e}{(2\pi)^{3/2}v_T^3}\frac{4\pi}{3}v^3,$$

and so

$$|\mathbf{F}_M| = m_e v_T \nu_{ee}(v_T)\frac{2}{3\sqrt{\pi}}\frac{v}{v_T\sqrt{2}},$$

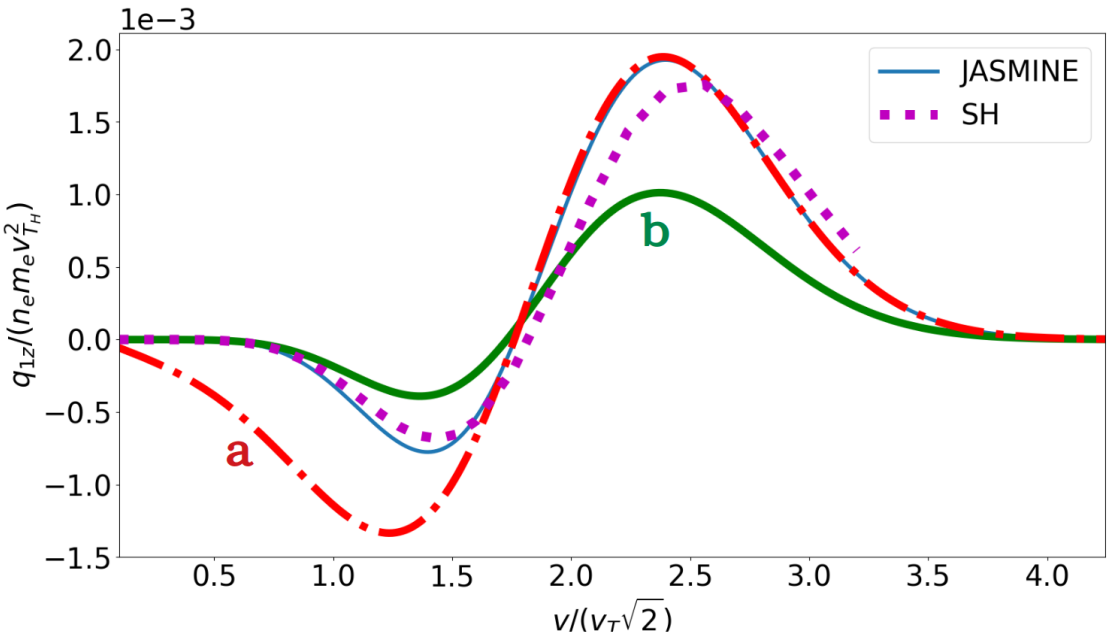


Figure 3.1.1: Effect of approximations (3.5) and (3.11) on the anisotropic part of electron distribution function $q_{1z} = (2\pi m_e/3)v^5 f_{1z}$ in local regime for $Z = 1$ with $\mathrm{Kn} \simeq 10^{-4}$. The Spitzer-Härm (SH) curve is the reference (purple, dotted); JASMINE (blue, solid) accounts for relations (3.5), (3.9) and (3.11). Curves (a, red, dot-dashed) and (b, green, solid) shows the results where approximations (3.5) and (3.11), respectively, were omitted.

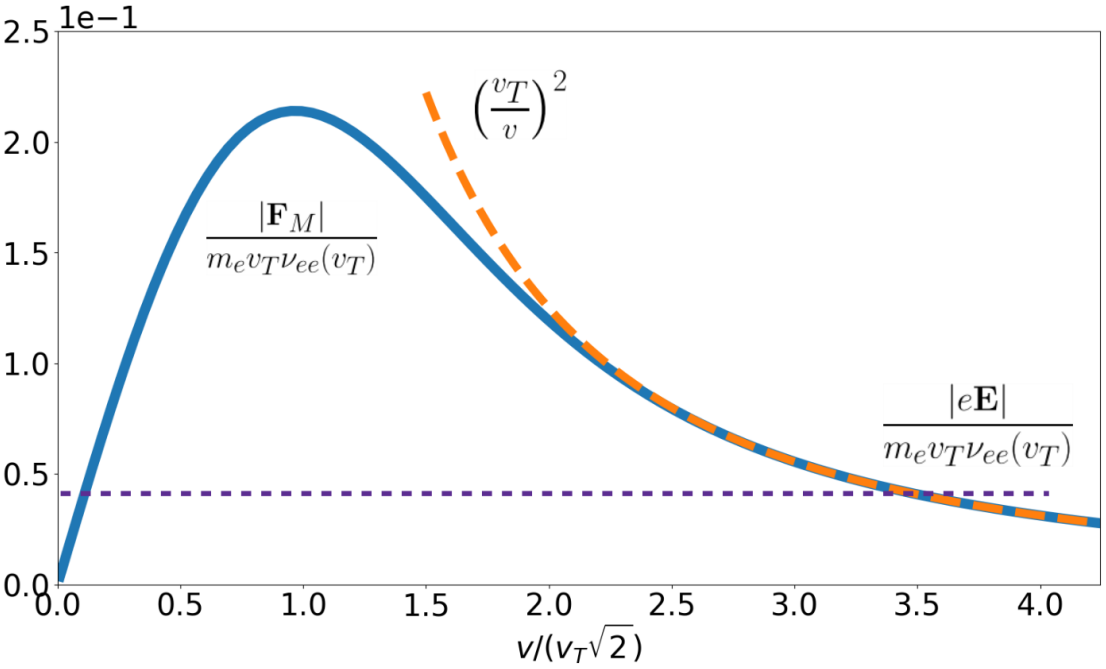


Figure 3.1.2: Graph of the normalized friction force (blue, solid), its high velocity approximation (orange, dashed) and the normalized electric force (violet, fine dashed).

as expected from Eq. (3.7). For $v > \mu v_T\sqrt{2}$, the density is zero. Therefore the right hand side of Eq. (3.8) is a constant proportional to the ball's volume of radius $\mu v_T\sqrt{2}$. As a consequence, $|\mathbf{F}_M| \propto v^{-2}$ outside this ball. Indeed,

$$4\pi v^2|\mathbf{F}_M| = \frac{8\pi Y_{ee}}{m_e}\frac{n_e}{(2\pi)^{3/2}v_T^3}\frac{4\pi}{3}\mu^3(v_T\sqrt{2})^3,$$

such that

$$|\mathbf{F}_M| = m_e v_T \nu_{ee}(v_T)\frac{4\mu^3}{3\pi^{1/2}}\left(\frac{v_T}{v}\right)^2.$$

This formula is in agreement with the high velocity limit of Eq. (3.6) for $\mu = [3\pi^{1/2}/4]^{1/3} \simeq 1.1$. Obviously, this value corresponds to the abscissa, $\mu v_T\sqrt{2}$, at which the two limits of $\mathcal{G}\left(v/[v_T\sqrt{2}]\right)$ meet. Indeed, from Eqs. (3.5)-(3.7), the connection condition yields $2\mu/[3\sqrt{\pi}] = 1/(\mu\sqrt{2})^2$. Such a value of $\mu$ is barely greater than half the value, 1.8, above which the high velocity expression of the friction force agrees with Eq. (3.6) with an error of less than ten percent. For those electrons with a velocity greater than $1.8v_T\sqrt{2}$, the bulk can be approximated by a step function that extends up to that abscissa, with, however, a step height equals to $f_M(v=0)$ multiplied by $3\sqrt{\pi}/[4(1.8)^3] \simeq 0.23$, a value close to the maximum of $\mathcal{G}\left(v/[v_T\sqrt{2}]\right)$.

By using expressions (3.5) in the electron-electron collision operator (3.1), together with the Lorentz's operator for electron-ion collisions (2.8), we obtain

$$\mathcal{C}_{ee}[f_e, f_M] \simeq \frac{\nu_{ee}}{2}(-\mathsf{L}^2)f_e + \nu_{ee}v\partial_v\left(f_e + \frac{v_T^2}{v}\partial_v f_e\right).$$

This is the expression from which, for instance, Gurevich and Istomin [66], or Luciani and Mora [44], started their analysis. As done in the last section of the App. 2.B, it can be obtained directly by simultaneously performing the linearization and high velocity limit expansion of the Landau's integral. Nevertheless, it makes the physical consequences of the high velocity approximation unclear.

Having in mind a direct resolution of the P1 system, we will further approximate $\mathcal{C}_{ee}[f_e, f_M]$ as a first order differential operator. As it will be examined in the Ch. 4, the resulting system, as being hyperbolic, will be suitable for an efficient numerical implementation. The simplification to arrive at our final reduced form of the electron-electron collision operator has been proposed empirically by Albritton *et al.* [82]. It is examined in the next section.

### 3.1.2 Equilibrium velocity diffusion

Within expression (3.4), the second term is of second order in $v_T/v$, and should be neglected in accordance with the expressions (3.5) retained for the Chandrasekhar's functions. However, the function $\mathcal{K}$ will then lose the desirable property to be identically zero when $f_e = f_M$, for which the contribution of friction and diffusion in velocity space cancel each other. The simplification proposed by Albritton *et al.* [82] consists of estimating the diffusion term, $(v_T^2/v)\partial_v f_e$, by its equilibrium value, $-f_M$. This yields

$$\mathcal{K} \simeq f_e - f_M. \tag{3.9}$$

Except the hottest region, each elementary volume of plasma contains an excess of suprathermal electrons. It means that for sufficiently high velocities $|\partial_v f_e| \leq |\partial_v f_M|$, and so expression (3.9) overestimates the diffusion term. The error can be formally estimated by considering Eq. (3.4) as a differential equation on $f_e$. The solutions to the homogeneous equation are of the form $Ce^{-v^2/2v_T^2}$, with $C$ a constant. Using the variation of the constant method, a particular solution is researched as $C(v)e^{-v^2/2v_T^2}$, where the space variable in argument is omitted. Substituted in the differential equation, it leads to $\mathcal{K} = (v_T^2/v)e^{-v^2/2v_T^2}\partial_v C$, a solution of which is $C = \int_0^v \mathcal{K}(w/v_T^2)e^{w^2/2v_T^2}\, dw$. For small velocities, $v/v_T \ll 1$, the electron distribution function is equal to $f_M$. Hence,

$$f_e = f_M + \mathrm{e}^{-v^2/2v_T^2} \int_0^v \mathcal{K}(w) \frac{w}{v_T^2} \mathrm{e}^{w^2/2v_T^2} dw.$$

Although such an equation was first written by Krasheninnikov in the already cited Ref. [77], our interpretation, which spills over into the next sub-section, will be here different. Integrating by parts, we obtain:

$$\mathcal{K} = f_e - f_M + \mathrm{e}^{-v^2/2v_T^2} \int_0^v \mathrm{e}^{w^2/2v_T^2} [\partial_w \mathcal{K}]\, dw, \tag{3.10}$$

where $\partial_w \mathcal{K} = \big[\mathcal{C}_{ee}[f_e, f_M] - (\nu_{ee}/2)(-\mathsf{L}^2) f_e\big]/(w\nu_{ee})$ can be expressed in an other manner from the kinetic equation (2.1). Contrary to appearances, the approach is not completely sterile here. As suggested by the factor $\exp(-v^2/2v_T^2)$, the integral term in (3.10), which is also equal to $(v_T^2/v)\partial_v(f_e - f_M)$, is small in the coldest region and in the high velocity domain. On the contrary, in the hottest region the departure of $f_e$ from $f_M$ due to the loss of the fastest electrons is small compared to the disequilibrium induced by their escape to colder regions. Consequently, expression (3.9) is violated for all velocities. This is numerically confirmed. In spite of this fact, we shall see that approximation (3.9) gives satisfying results. It means that the considered simplification (3.9) partially compensates the omission of collisions between hot electrons, corresponding to a nonlinear term in the electron-electron collision integral.

### 3.1.3 Corrected collision frequency

By taking into account the simplifications expressed by Eqs. (3.5)-(3.9) we obtain the green curve (b) in Fig. 3.1.1. Both forward and return currents are approximately homothetic to those of the solution provided by Spitzer and Härm in Tables I and II of Ref. [58]. Having fixed the contribution of the radial diffusion, their amplitudes can be only modified through the friction force (3.6), which turns out to be proportional to $\nu_{ee}$. Thus, we shall enhance forward and return current amplitudes by using a reduced electron-electron collision frequency $\nu_{ee}^*$:

$$\nu_{ee}^* = \phi(Z)\nu_{ee}. \tag{3.11}$$

The correction factor $\phi(Z)$ is precisely determined in Sec. 3.2.2.1. Based on theoretical considerations developed in Ref. [131], Krasheninnikov proposed to estimate $\mathcal{K}$ as in Eq. (3.9) for $v > v_K$, and as

$$6\left(\frac{v_T}{v}\right)^2 (f_e - f_M)$$

for $v < v_K$, where $v_K = v_T\sqrt{2}(Z/\mathrm{Kn}^2)^{1/8}$. His analysis is restricted to high values of $Z$. As he recognized himself, even for $Z = 10$ the cutoff velocity $v_K$ is so high that, in practice, the second approximation is used for almost the entire velocity axis. The factor $6(v_T/v)^2$ is inferior to one for $v/(v_T\sqrt{2}) \geq \sqrt{3} \simeq 1.7$. Therefore, the Krasheninnikov's prescription well enhances the forward current of electrons, but reduce the return one. In spite of this contradiction with our analysis, he obtained satisfying results on the problem consisting of the relaxation of a single Fourier's component of the temperature. Our interpretation is that there must be approximations in his approach to compensate for the effect of the aforementioned factor on the return current.

## 3.2 Study of the resulting P1 system

As a result of all the approximations discussed in the previous section, the electron-electron collision operator (3.1) is:

$$\mathcal{C}_{ee}[f_e, f_M] \simeq \frac{\nu^*_{ee}}{2}(-\mathsf{L}^2)f_e + \nu^*_{ee} v \partial_v (f_e - f_M). \tag{3.12}$$

Together with the Lorentz's operator (2.8) for electron-ion collisions, it leads to the following system of coupled equations:

$$\frac{v}{3}\boldsymbol{\nabla}\cdot\mathbf{f}_1 - \frac{e}{3m_e v^2}\mathbf{E}\cdot\partial_v v^2 \mathbf{f}_1 = \mathcal{C}^0_{ee}, \tag{3.13}$$

$$v\boldsymbol{\nabla} f_0 - \frac{e}{m_e}\mathbf{E}\,\partial_v f_0 = \boldsymbol{\mathcal{C}}^1_{ee} + \boldsymbol{\mathcal{C}}^1_{ei} \tag{3.14}$$

where the components of the electron-electron and electron-ion collision operators are given by:

$$\mathcal{C}^0_{ee} = v\nu^*_{ee}\partial_v(f_0 - f_M), \tag{3.15}$$

$$\boldsymbol{\mathcal{C}}^1_{ee} = v\nu^*_{ee}\partial_v \mathbf{f}_1 - \nu^*_{ee}\mathbf{f}_1, \tag{3.16}$$

$$\boldsymbol{\mathcal{C}}^1_{ei} = -\nu_{ei}\mathbf{f}_1. \tag{3.17}$$

As mentioned in the introduction of this chapter, almost the same system of equations was first considered by Del Sorbo *et al.* [132] and latter by Holec *et al.* [128].

In the first of these studies, however, the electron-electron collision is not multiplied by any factor. Motivated by other objectives, the authors of Ref. [132] did not compare their results with other kinetic codes, nor did they seek to provide a theoretical analysis of the model, preventing them from guessing the existence of the correction $\phi(Z)$. The latter was in fact introduced by the same team in an empirical way within Ref. [128], and approximated by means of numerical fits. There, the authors paid more attention to the model itself, many of whose properties have been observed numerically. The Secs. 3.2.2-3.2.3 are continuing their work by providing theoretical foundations while exhibiting and discussing new behaviors of the solutions to Eqs. (3.13)-(3.14). Before that, the most general expressions of $\mathbf{f}_1$, $\mathbf{q}_e$ and $\mathbf{j}_e$ are derived in Sec. 3.2.1.

### 3.2.1 Expressions of $\mathbf{f}_1$, $\mathbf{q}_e$ and $\mathbf{j}_e$ valid in any regime

The current densities (2.2) and (2.3) are driven by the competition between the advective and electric force terms acting on $f_0$. Indeed, let us write (3.14) as

$$\partial_v \mathbf{f}_1 + \frac{\alpha}{v}\mathbf{f}_1 = \frac{1}{v\nu_{ee}^*}\left[v\boldsymbol{\nabla} f_0 - \frac{e}{m_e}\mathbf{E}\partial_v f_0\right]$$

where

$$\alpha(Z) = -[1 + Z/\phi(Z)]. \tag{3.18}$$

The left hand side is $v^{-\alpha}\partial_v v^\alpha \mathbf{f}_1$. Integrating between $v$ and $+\infty$ thus leads to:

$$\mathbf{f}_1 = -\int_v^\infty \left(\frac{w}{v}\right)^\alpha \left[\frac{\boldsymbol{\nabla} f_0}{\nu_{ee}^*} - \frac{e\mathbf{E}}{m_e w\nu_{ee}^*}\partial_w f_0\right] dw \tag{3.19}$$

It follows from this expression that spatial inhomogeneities define the value of the electric field. As shown in Fig. 3.1.2, for steep temperature gradients the Lorentz electric force may overcome the friction force induced by collisions over a significant range of velocities. This is at the origin of numerical difficulties because the characteristics of the hyperbolic system of equations (3.13)-(3.14) do not have slopes with constant signs. Consequently, the integration on velocity cannot be performed from high to low values as done in Refs. [132, 128]. This aspect is deepened and resolved in Ref. [43], presented in the final chapter of the thesis.

Instead of using expression (3.19), the heat flux density can be expressed by isolating $\mathbf{f}_1$ in Eq. (3.14): $\mathbf{f}_1 = [v\boldsymbol{\nabla} f_0 - (e/m_e)\mathbf{E}\partial_v f_0]/(\alpha\nu_{ee}^*) - (v/\alpha)\partial_v \mathbf{f}_1$. By multiplying each member of the equation by $2\pi m_e v^5/3$ and integrating over all the positive part of the real axis, we obtain

$$\mathbf{q}_e = -\frac{2\pi m_e}{3\alpha}\int_0^\infty v^6 \partial_v \mathbf{f}_1 dv \\ - \frac{2(2\pi)^{1/2} Z m_e}{9(\phi + Z)v_T^3 \nu_{ei}^T}\int_0^\infty v^8 \left[v\boldsymbol{\nabla} f_0 - \frac{e}{m_e}\mathbf{E}\,\partial_v f_0\right] dv$$

where we used $\nu_{ee}^* = 3(\pi/2)^{1/2}\phi/Z(v_T/v)^3\nu_{ei}^T$. Integrating by parts, the first term in the right hand side of this expression is equal to $6/\alpha\mathbf{q}_e$, such that

$$\mathbf{q}_e = -\frac{2(2\pi)^{1/2} Z m_e}{9(Z + 7\phi)v_T^3 \nu_{ei}^T}\int_0^\infty v^8 \left[v\boldsymbol{\nabla} f_0 - \frac{e}{m_e}\mathbf{E}\,\partial_v f_0\right] dv. \tag{3.20}$$

In the same way, we obtain the following expression for the electric current density:

$$\mathbf{j}_e = \frac{4(2\pi)^{1/2} Z e}{9(Z + 5\phi)v_T^3 \nu_{ei}^T}\int_0^\infty v^6 \left[v\boldsymbol{\nabla} f_0 - \frac{e}{m_e}\mathbf{E}\,\partial_v f_0\right] dv. \tag{3.21}$$

The formulae (3.19)-(3.20)-(3.21) are written for the first time. In particular, the latter allows us to make an important remark now. Since $\mathbf{j}_e = 0$, the correction $\phi(Z)$ to the electron-electron collision frequency has no influence on the value of $\mathbf{E}$. This is a weak point of the model. We examine it in the next section.

### 3.2.2 Local regime

#### 3.2.2.1 Conditions to recover the Spitzer-Härm's electric field and heat flux density

The expression (2.17) for the electric field emphasizes the role of the first moment of the electron-electron operator. Let us deepen this point. As it is well known, the local regime is characterized by a disequilibrium induced by the electron transport which remains small enough to ensure that $f_0$ is equal to $f_M$ to high accuracy. Substituting $f_0$ by $f_M$ in (2.17) yields:

$$\mathbf{E} = -\frac{m_e v_T^2}{e}\left[\frac{\boldsymbol{\nabla} n_e}{n_e} + \frac{5}{2}\frac{\boldsymbol{\nabla} T_e}{T_e} - \frac{(2\pi)^{3/2}}{48 n_e v_T^5}\int_0^\infty v^6 \boldsymbol{\mathcal{C}}_{ee}^1 dv\right].$$

To obtain this result, we used $\partial_v f_M = -(v/v_T^2) f_M$, together with

$$\frac{\boldsymbol{\nabla} f_M}{f_M} = \frac{\boldsymbol{\nabla} n_e}{n_e} + \left(\frac{v^2}{2v_T^2} - \frac{3}{2}\right)\frac{\boldsymbol{\nabla} T_e}{T_e},$$

which we get by deriving the logarithm of Eq. (2.4). From there we used the relation $\int_0^\infty v^{2p+1} e^{v^2/(2v_T^2)}\, dv = p!(v_T\sqrt{2})^{p+1}/2$ with the values $p = 3$ and 4. Comparing the result to Eq. (2.18), we deduce that the Spitzer-Härm's electric field is recovered if, and only if

$$\int_0^\infty v^6 \boldsymbol{\mathcal{C}}_{ee}^1 dv = \frac{48 n_e v_T^5}{(2\pi)^{3/2}}\left[\frac{5}{2} - \xi(Z)\right]\frac{\boldsymbol{\nabla} T_e}{T_e}. \tag{3.22}$$

However, in case of the operator given by Eq. (3.16), the left hand side of this relation is equal to zero. Indeed, the Lorentz's part, $-\nu_{ee}^* \mathbf{f}_1$, gives no contribution because of the condition $\mathbf{j}_e = \mathbf{0}$, and, integrating the other contribution by parts, we find:

$$\int_0^\infty v^6 v \nu_{ee}^* \partial_v \mathbf{f}_1 dv = -\frac{6(2\pi)^{1/2}\phi(Z) v_T^3 \nu_{ei}^T}{Z}\int_0^\infty v^3 \mathbf{f}_1 dv = \mathbf{0}.$$

Thus, the present model only allows the recovery of the Lorentz's electric field $\mathbf{E}_\mathrm{L}$, corresponding to the expression (2.18) in the high-$Z$ limit, in which $\xi = 5/2$. This point is not mentioned by Del Sorbo *et al* [57], but was already noticed numerically by Holec *et al.* [128]. Here, their empirical observation is analytically confirmed by our calculations.

Accounting then for the Lorentz's electric field, the heat flux density (3.20) reads:

$$\mathbf{q}_e = -\frac{128 k_B n_e v_T^2 Z}{3\pi(Z + 7\phi)\nu_{ei}^T}\boldsymbol{\nabla} T_e$$

Here again, we used the aforementioned integral relation with $p = 4$ and 5. The above expression of $\mathbf{q}_e$ has to agree with the Spitzer-Härm's formula (2.19), which implies that $7\phi/Z + 1 = \zeta(Z)$. This condition provides the expression of the electron-electron correction factor:

$$\phi(Z) = \frac{Z}{7}[\zeta(Z) - 1] = \frac{3.96 Z}{7(Z + 0.24)}. \tag{3.23}$$

As shown in Fig. 3.2.1, our formula is consistent with the numerical fit proposed by Holec *et al*:

$$\frac{1}{2} + \frac{0.59Z - 1.11}{8.37Z + 5.15}.$$

The authors suggested to neglect the $Z$-dependent term of their fit in numerical calculations, but it corresponds to a systematic error of about 12%. Without the correction (3.23), the electron heat flux density would be underestimated by 48% for $Z = 1$, by 5% for $Z = 50$ and by 4% for $Z = 79$.

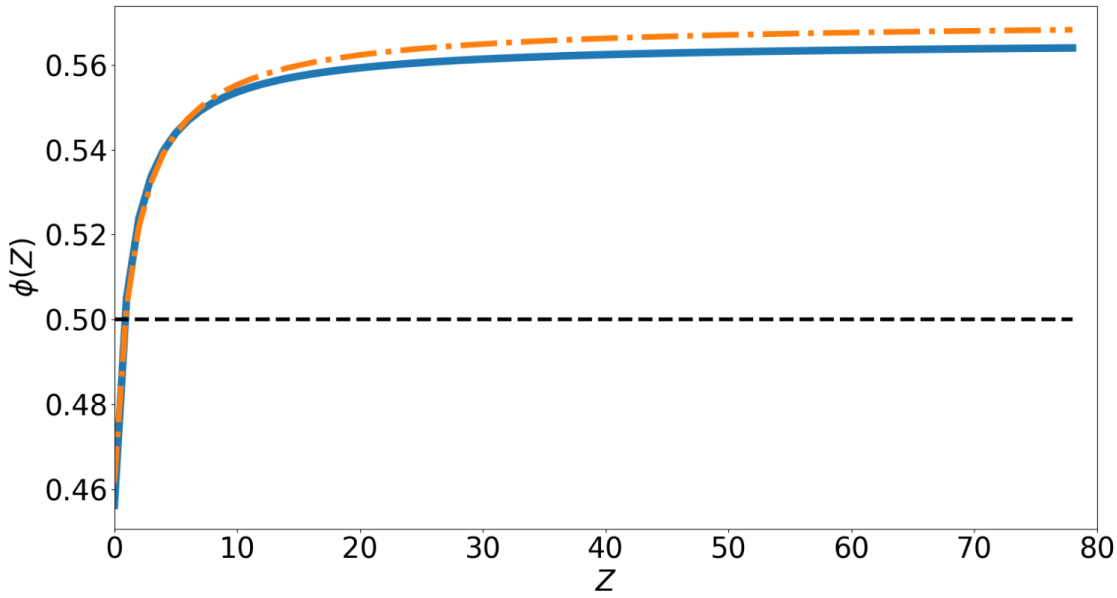


Figure 3.2.1: Correction factor $\phi$ for the electron-electron collision frequency given by the expression (3.23) (blue, solid) and by the fit of Holec *et al.* (orange, dashed-dot). The black dashed line is the value later authors choose to use in Ref. [128] for numerical calculations.

#### 3.2.2.2 Effect of electron-electron collisions on $\mathbf{f}_1$

Substituting $f_0$ by the Maxwellian distribution function $f_M$ (2.4), together with the electric field by the Lorentz's expression in Eq. (3.19), there appears

$$\boldsymbol{\nabla} f_M - \frac{e\mathbf{E}}{m_e w}\partial_w f_M = f_M \left(\frac{w^2}{2v_T^4} - 4\right)\frac{\boldsymbol{\nabla} T_e}{T_e}$$

multiplied by $(w/v)^\alpha/\nu_{ee}^*$ as integrand. Since $\nu_{ee}^* = 3(\pi/2)^{1/2}\phi/Z(v_T/w)^3\nu_{ei}^T$ and $Z/\phi = -(1+\alpha)$, $\mathbf{f}_1$ (3.19) is equal to

$$-\frac{n_e}{3\pi^2 v_T^2 \nu_{ei}^T}\frac{1+\alpha}{(v/v_T\sqrt{2})^\alpha}\int_v^\infty \left(\frac{w^2}{2v_T^2}\right)^{(\alpha+3)/2}\left[4 - \frac{w^2}{2v_T^2}\right] e^{-w^2/2v_T^2}\frac{v_T\sqrt{2}}{w}\, d\left[\frac{w^2}{2v_T^2}\right].$$

Hence, the result wan be expressed as

$$\mathbf{f}_{1,\mathrm{A}} = -\frac{n_e}{3\pi^2 v_T^2 \nu_{ei}^T}\mathcal{F}_{1,\mathrm{A}}\left(\frac{v}{v_T\sqrt{2}}\right)\frac{\boldsymbol{\nabla} T_e}{T_e}, \tag{3.24}$$

where the function $\mathcal{F}_{1,\mathrm{A}}$ is defined as:

$$\mathcal{F}_{1,\mathrm{A}}(w) = \frac{1+\alpha}{w^\alpha}\left[4\Gamma\left(2+\frac{\alpha}{2};w^2\right) - \Gamma\left(3+\frac{\alpha}{2};w^2\right)\right], \tag{3.25}$$

with $\Gamma$ the upper incomplete gamma function [67]: $\Gamma(s;w) = \int_w^\infty x^{s-1}e^{-x}dx$. It is worth mentioning that $\mathcal{F}_{1,\mathrm{A}}$ is not defined at $w = 0$ because the first arguments, $s = \{2,3\} + \alpha/2$, in $\Gamma$ functions are negatives for values of $Z$ greater than $\{1,2\}$. This results in a divergence of $\Gamma(s;w^2)$ as $-w^s/s$ in the vicinity of zero. In order to avoid the latter in the numerical implementation of $\mathcal{F}_{1,\mathrm{A}}$, the lowest velocity of the mesh must be chosen not too low. An expression close to Eq. (3.25) was written by Holec *et al.*, but the authors did not substitute the value of the electric field, that of Lorentz, making it possible to obtain the final form written here.

As shown in Fig. 3.2.3, in the high $Z$ limit $\mathbf{f}_{1,\mathrm{A}}$ tends toward the corrected Lorentz's distribution function $\mathbf{f}_{1,\mathrm{L}}$, defined by Eq. (3.24) in substituting $\mathcal{F}_{1,\mathrm{A}}$ for $\mathcal{F}_{1,\mathrm{L}}$ defined as:

$$\mathcal{F}_{1,\mathrm{L}}(w) = \frac{2w^4}{\zeta}(w^2-4)e^{-w^2}. \tag{3.26}$$

The above expression (3.26) is found by solving the Eq. (3.14) without $\boldsymbol{\mathcal{C}}^1_{ee}$ and by correcting the electron-ion collision frequency by a factor $\zeta(Z)$:

$$\boldsymbol{\mathcal{C}}^1_{ei} + \boldsymbol{\mathcal{C}}^1_{ee} = -\nu_{ei}\mathbf{f}_1 + \boldsymbol{\mathcal{C}}^1_{ee} \simeq -\zeta(Z)\nu_{ei}\mathbf{f}_1 \tag{3.27}$$

Such an approximation for the collision term is used in many publications, *e.g* in Refs. [91, 133], as it simplifies the numerical implementation. It is used in the code ALADIN [134] where, however, a complete nonlinear expression is used for $\mathcal{C}^0_{ee}$ [53]. The simplification (3.27) has two consequences. The first one is the impossibility of recovering the Spitzer-Härm's electric field, as already pointed out in the previous section. The second one is a systematic error that appears in the position of $\mathbf{f}_1$ on the velocity axis for small values of $Z$. This fact is illustrated for $Z = 1$ in Fig. 3.2.2. It corresponds to the case of a plasma with constant density $n_e = 5\times10^{20}$ cm$^{-3}$ and with temperature (1.3) where $k_BT_H = 120$ eV, $k_BT_C = 80$ eV, $z_0 = 425\,\mu$m and $s = 9\times10^{-3}\,\mu$m$^{-1}$. The Knudsen's number at the maximum of the absolute value of the gradient is $\mathrm{Kn} = 7.3\times10^{-4}$.

As shown in Fig. 3.2.3, it follows from Eq. (3.26) that $\mathbf{f}_{1,\mathrm{L}}$ remains homothetic to itself for any variation of $Z$. This is not the case of $\mathbf{f}_{1,\mathrm{A}}$, where the correction $\alpha(Z)$ does not enter as a simple multiplicative factor. This is responsible for a deformation corresponding to a shift toward low velocities compared to $\mathbf{f}_{1,\mathrm{L}}$. For $Z = 1$, this shift is slightly overestimated compared to the solution tabulated by Spitzer and Härm [58], $\mathbf{f}_{1,\mathrm{SH}}$, defined by Eq. (3.19) in substituting $\mathcal{F}_{1,\mathrm{A}}$ for $\mathcal{F}_{1,\mathrm{SH}}$ defined as:

$$\mathcal{F}_{1,\mathrm{SH}}(w) = -\left(4\frac{ZD_T(w)}{B} + 3\frac{\gamma_T}{\gamma_E}\frac{ZD_E(w)}{A}\right)e^{-w^2}, \tag{3.28}$$

where we used the notations introduced in Ref. [58].

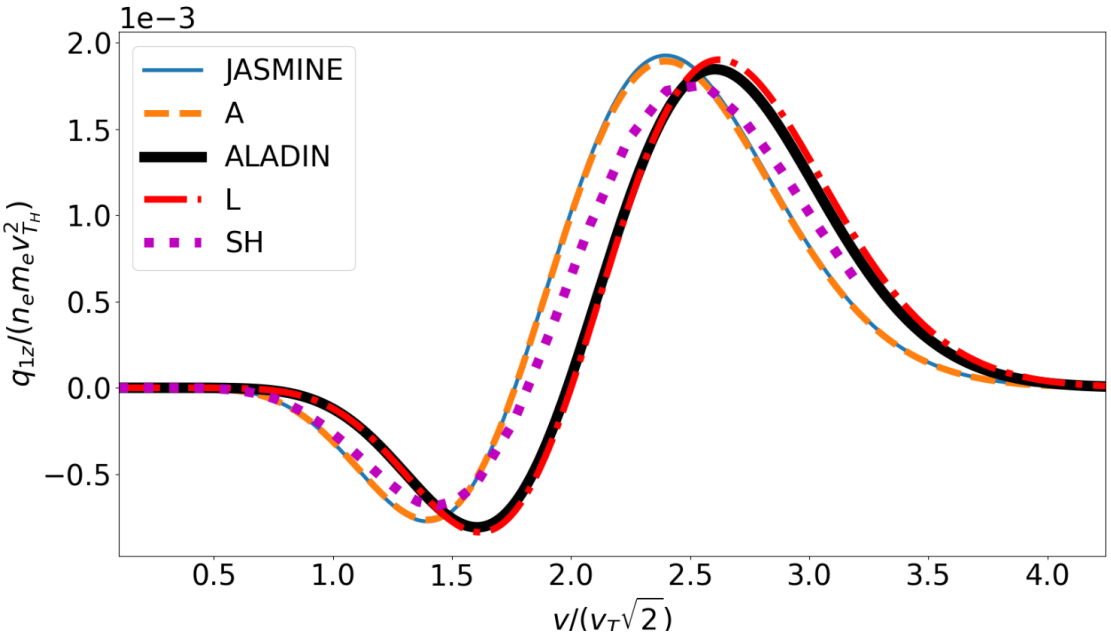


Figure 3.2.2: Local regime, $Z = 1$. Effect of electron-electron collisions on the anisotropic part of electron distribution function $q_{1z} = (2\pi m_e/3)v^5\mathbf{f}_{1z}$ calculated with JASMINE code (blue, solid), ALADIN code (black, solid), Spitzer-Härm's tables (purple, dotted) and analytic solutions (3.24) (orange, dashed) and (3.26) (red, dashed-dot).

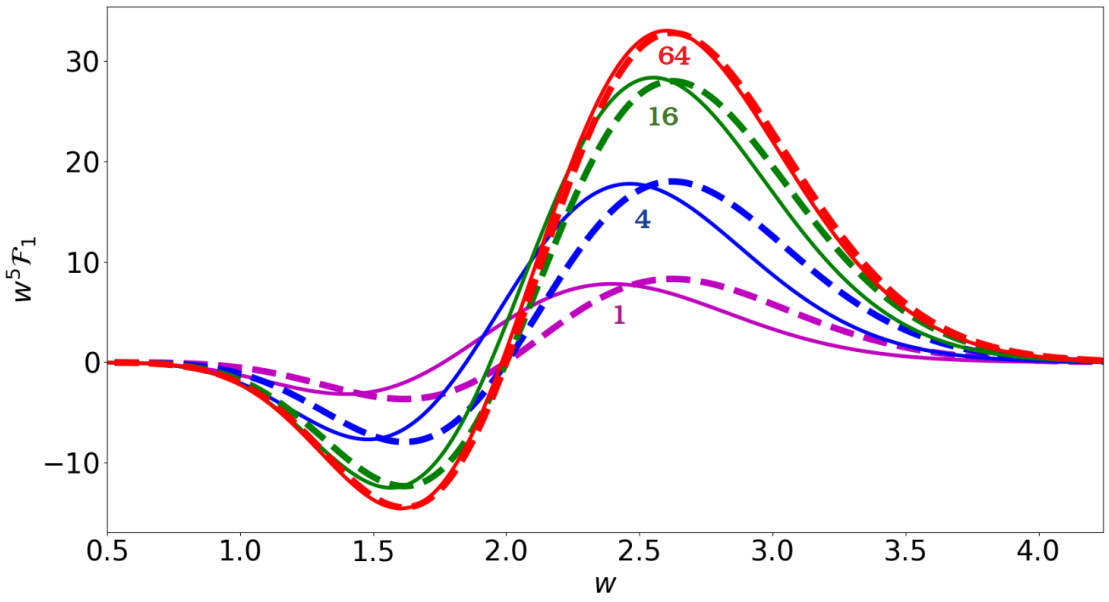


Figure 3.2.3: Graph of $w^5\mathcal{F}_1$ with the function $\mathcal{F}_1$ given by expressions (3.25) (solid) and (3.26) (dashed), for different values of the ionization number: $Z = 1$ (violet), 4 (blue), 16 (green) and 64 (red).

The key feature to obtain the aforementioned effect is the differential nature of the operator describing energy exchange in $\boldsymbol{\mathcal{C}}_{ee}^{1}$. Using for the latter the algebraic Bhatnagar *et al*'s operator, $-\nu_{ee}^{*}(f_e - f_M)$, would not lead to any shift, but only to a modification of the $Z$-correction involved in the electron-electron collision frequency: $\nu_{ee}^{*} = r(Z)\nu_{ee}$ where

$$r(Z) = \frac{Z}{2}\big[\zeta(Z) - 1\big] = \frac{7}{2}\phi(Z). \tag{3.29}$$

The few algebra required to obtain this expression (3.29) will not be written, as being quite similar to that for determining $\phi$ (3.23). As announced in Sec. 2.3.3 of the previous chapter, the Eq. (3.29) is in qualitative agreement with the numerical observations made by Brodrick *et al* [93] and Sherlock *et al* [94]. In the nonlocal regime, discussed in the next section, the low-$Z$ shift persists and is already visible in the numerical results obtained by Holec *et al.* [128].

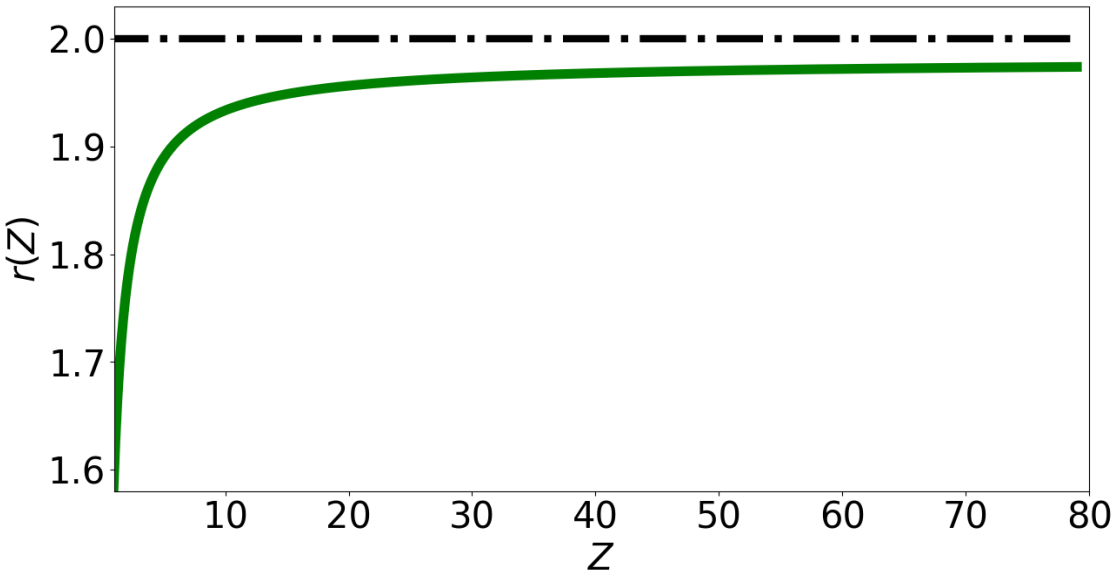


Figure 3.2.4: Correction factor $r$ for the electron-electron collision frequency given by the expression (3.29) (green, solid) and by the value first proposed empirically by of Brodrick *et al.* [93] and Sherlock *et al.* [94] (black, dashed-dot).

### 3.2.3 Nonlocal regime

The results obtained with the reduced model described before, and implemented in our code JASMINE, are compared to the numerical simulations performed with ALADIN, the full kinetic code OSHUN [135, 136] and with the Schurtz *et al*'s model - referred as SNB hereafter - implemented in CHIC.

OSHUN solves the non-stationary kinetic equation with electron-electron and electron-ion Landau's integrals, by expanding the distribution function on spherical harmonics. The number of terms in the expansion is increased until reaching convergence. The P1 system solved in ALADIN was mentioned in Sec. 3.2.2.2, and the SNB's model was exposed at the end of the previous chapter in Sec. 2.3.3.

A situation of nonlocal regime with constant electron density will be studied in the next chapter devoted to numerical issues. Here, the considered case is more representative of the conditions appearing in the conduction region during a laser-driven implosion process. Initially, the electron temperature is given by the expression (1.3) with $k_B T_H = 1.8$ keV, $T_C = 0.2 T_H$, $z_0 = 1200\,\mu$m and $s = 2.6 \times 10^{-2}\,\mu\text{m}^{-1}$. The electron density profile is chosen such as the electron pressure, $n_e k_B T_e$, is constant over the entire computational box and $n_e$ is equal to $n_H = 1 \times 10^{21}$ cm$^{-3}$ in the hot region. In kinetic simulations, the initial heat flux density is zero. After a transient growth it is established in several collision times - a few picoseconds - and then follows, together with the temperature, a quasi-static evolution at the collision timescale according to $(3/2)\partial_t n_e k_B T_e + \partial_z q_{ez} = 0$. At a given time of this evolution, the temperature profile is extracted from OSHUN and used in JASMINE and CHIC. The density, which evolves on the nanosecond timescale, can be considered unchanged. The effective ionization number is $Z = 1$ and for the temperature profile at the considered time the Knudsen number at the maximum of the gradient is $\text{Kn} = \lambda_{ei}^T / L_T = 2.4 \times 10^{-2}$.

#### 3.2.3.1 Comparison of heat flux densities and electric fields

Heat flux densities are compared in Fig. 3.2.5. JASMINE and SNB's calculations agree with the kinetic results within a maximum difference of 10%. In the steepest region, kinetic estimations of JASMINE, SNB, ALADIN and OSHUN are approximately 50% smaller than the Spitzer-Härm's one (2.19), abbreviated SH in the following. This inhibition, together with the preheat at the foot of the temperature gradient due to electrons coming from the hot region, are signatures of the nonlocal regime. The choice of an approximation for the electron-electron collision operator is important. If the term $\boldsymbol{\mathcal{C}}_{ee}^1$ is neglected, a more significant error is obtained in JASMINE's calculation (green dashed line b) in Fig. 3.2.5). However, at the time of comparison, the temperature profiles in OSHUN and ALADIN are slightly different. By using the latter, the results provided by JASMINE are about 5% larger, at the maximum of the heat flux density, than those presented in Fig. 3.2.5. This quantifies the precision below which errors between codes cannot be compared.

Electric fields are compared in Fig. 3.2.6. The OSHUN's result is very close to the SH's electric field (2.18). ALADIN and JASMINE's electric fields are larger and close to the Lorentz's one. This means that electric field is much less affected by the steepness of the temperature gradient and remains close to its value predicted by the local regime expression. It explains the success of the SNB's model [91] because the SH's expression (2.18) of the electric field is used in $\nu_{ei}^E$ for estimating

$$\mathbf{q} - \mathbf{q}_{\text{SH}} = \delta\mathbf{q} = -\frac{2\pi m_e}{3} \int_0^\infty \frac{v^6}{\nu_{ei}^E} \boldsymbol{\nabla} \delta f_0 dv,$$

instead of the Lorentz's expression corresponding to the zero-order solution of the kinetic system considered by the SNB's model. Keeping this observation in mind, we investigate the consequences of using the SH's electric field (2.18) while solving the system of equations (3.13) and (3.14). As it does not ensure the condition $\mathbf{j}_e = \mathbf{0}$, it is responsible for a nonzero electron flux in the direction of $\boldsymbol{\nabla} T_e$ everywhere in the plasma. However, the corresponding velocity $\mathbf{u}_e = -\mathbf{j}_e / e n_e$

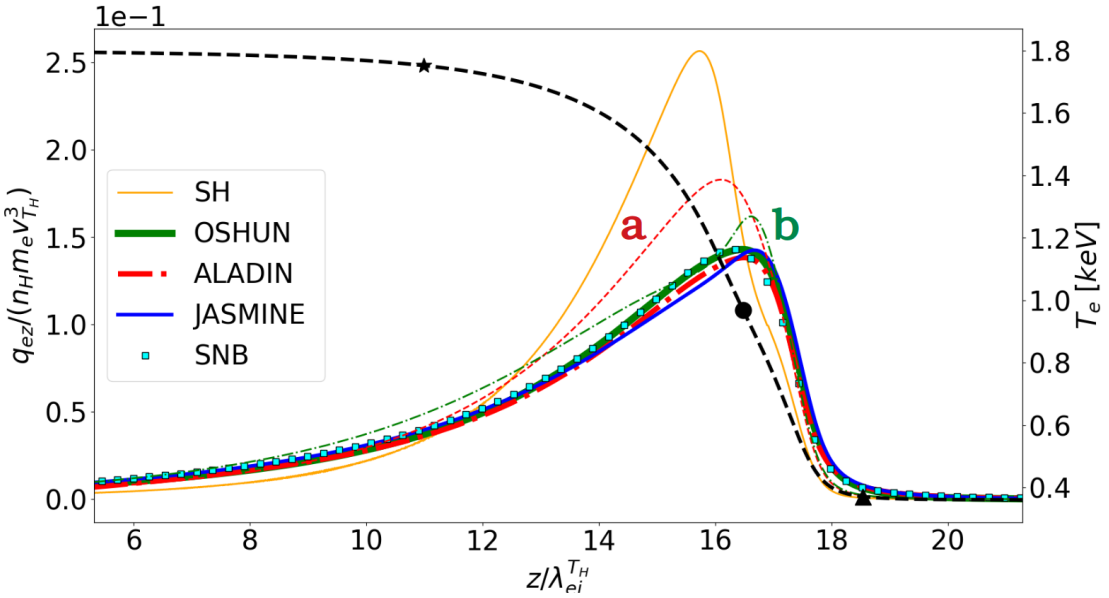


Figure 3.2.5: Heat flux $q_{ez}$ (left axis) and temperature $T_e$ (right axis) distribution in the simulations with JASMINE (blue, solid), ALADIN (red, dashed-dot), OSHUN (green, solid) and SNB (cyan, square). The orange solid line shows the tabulated Spitzer-Härm (SH) heat flux density, fine color lines show JASMINE's calculations (a) with the SH's electric field in red dashed and (b) with approximation (3.27) in green dashed-dot. The heat flux density is normalized by the free streaming flux $n_H m_e v_{T_H}^3$ in the hot region. Star, circle and triangle on the temperature profile mark the positions where distribution functions are shown. The plasma size is $2000\,\mu$m, $T_H = 1.8$ keV, $T_C = 0.2T_H$, $Z = 1$, and $\lambda_{ei}^{T_H} = 73\,\mu$m. The time of comparison is 22 ps.

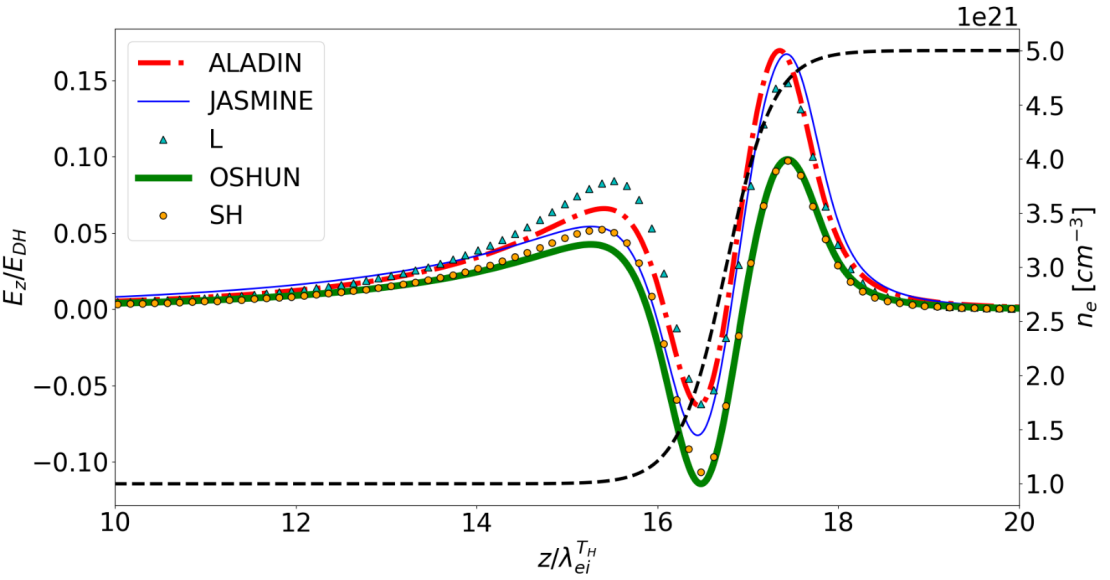


Figure 3.2.6: Electric field $E_z$ (left axis) and density $n_e$ (right axis). Cyan triangles show the analytic Lorentz's (L) electric field. The electric field is normalized by the Dreicer's field $E_{DH} = m_e v_T \nu_{ee}(v_T)/e$ in the hot region. In the SNB's model the electric field is not self-consistently calculated. Other parameters and notations are the same as in Fig. 3.2.5.

related to this flux is negligible compared to $v_T$. Thus, one may neglect the shift it induces in formula (2.4) defining the local equilibrium distribution function. Indeed, an order of magnitude estimate can be obtained from (3.21) in the local regime:

$$\mathbf{j}_e = \frac{32e^2 n_e Z}{3\pi m_e (Z+5\phi)\nu_{ei}^T}\left[\mathbf{E} + \frac{m_e v_T^2}{e}\left(\frac{\boldsymbol{\nabla} n_e}{n_e} + \frac{5}{2}\frac{\boldsymbol{\nabla} T_e}{T_e}\right)\right]$$

Substituting $\mathbf{E}_{\mathrm{SH}}$ (2.18) in this formula leads to:

$$\frac{|\mathbf{u}_e|}{v_T} = \frac{120[5/2 - \xi(Z)]}{1 + 5\phi(Z)/Z}\mathrm{Kn}$$

For any $Z$ the ratio $|\mathbf{u}_e|/v_T$ is three times smaller than Kn, and so is negligible compared to 1. This statement holds if, in place of $\phi$ (3.23), the new correction,

$$\frac{Z}{7}\left[\zeta(Z)\left(\frac{7}{2} - \xi(Z)\right) - 1\right],$$

required to recover the SH's heat flux density in the local regime is used. By using $\mathbf{E}_{\mathrm{SH}}$ together with this new correction, JASMINE provides the heat flux density plotted with the red dashed curve (a) in Fig. 3.2.5.

It may be observed that the electric field changes sign. The two terms in (2.18) describe the space charge induced by the gradients of density and temperature. For a constant pressure, which implies $\boldsymbol{\nabla} n_e/n_e = -\boldsymbol{\nabla} T_e/T_e$, the electric field can be either expressed through the gradient of density or temperature only, and thus keeps the same sign. As density and temperature inhomogeneities relax on different timescales, the pressure is not constant in the case shown in Fig. 3.2.6, and its gradient is responsible for the negative part of the electric field. It accelerates electrons in the direction opposite to the temperature gradient, thus enhancing the deformation of the distribution function in the cold region.

#### 3.2.3.2 Comparison of distribution functions

Integrands of the heat flux density, $q_{1z} = (2\pi m_e/3)v^5 f_{1z}$, are shown in Figs. 3.2.7, 3.2.8 and 3.2.9. These three figures correspond to the three positions at which the temperature profile is marked in Fig. 3.2.5. Although the overall shapes are similar at a given position, there are shifts induced by the different treatments of collisions between electrons.

In the local regime, the shape of $q_{1z}$ (3.28) remains qualitatively the same everywhere in the temperature profile. Its position on the velocity axis, together with its amplitude, are defined by the local values of temperature and density gradients because the local Maxwellian distribution function (2.4) is entirely specified by these two hydrodynamic quantities. This is not the case in the nonlocal regime. As shown in Figs. 3.2.8 and 3.2.9, the shape of $q_{1z}$ is qualitatively different within and beyond the region of maximum temperature gradient. The transition between the two shapes occurs in a small region near the foot of the temperature profile, illustrated in Fig. 3.2.10.

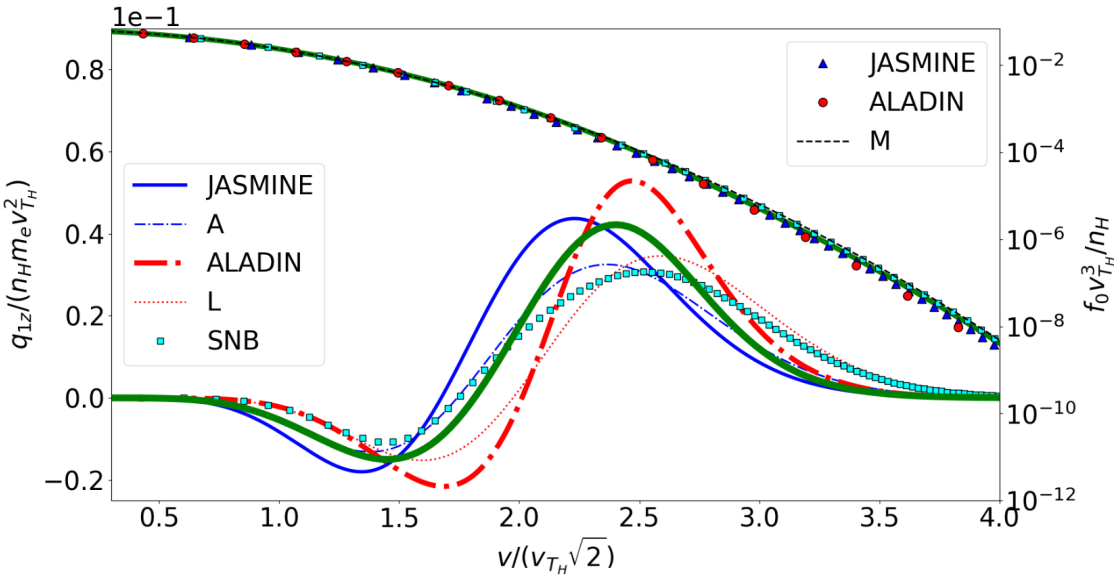


Figure 3.2.7: Comparison of the distribution functions $f_0$ (right axis) and $q_{1z} = (2\pi m_e/3)v^5 f_{1z}$ (left axis) calculated with JASMINE, ALADIN, OSHUN and SNB codes at the point of hot region marked by a star in Fig. 3.2.5 ($z/\lambda_{ei}^{T_H} \simeq 11$). Black dashed line (right axis) shows the Maxwellian (M) distribution function. Fine lines show the heat flux densities integrand $q_{1z}$ associated to the analytic solution $f_{1,\mathrm{A}}$ (3.19) in dashed-dot blue and $f_{1,\mathrm{L}}$ (3.26) in dotted red. Other parameters and notations are the same as in Fig. 3.2.5.

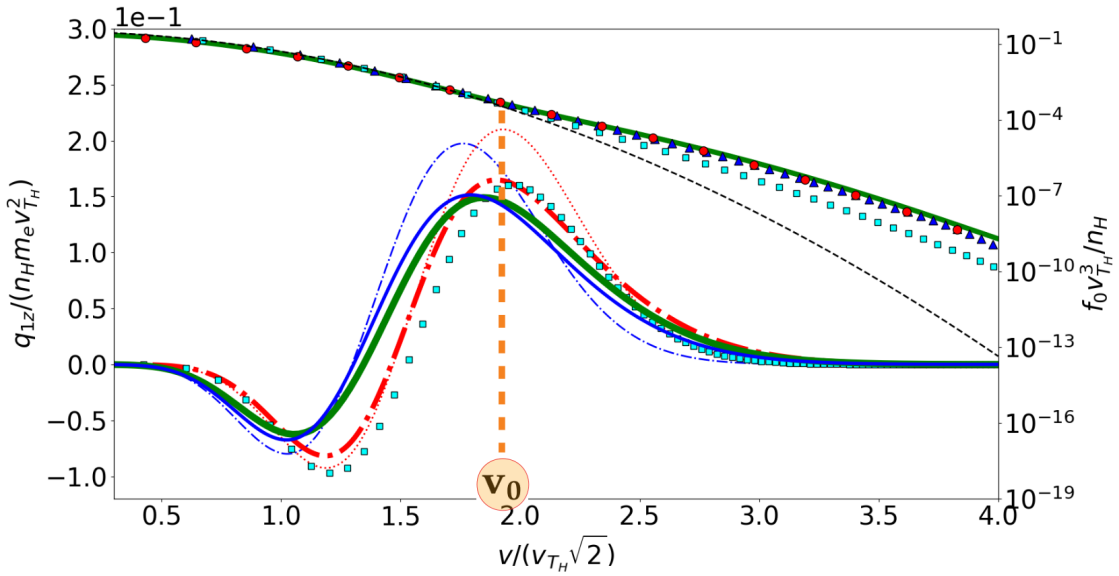


Figure 3.2.8: Same as in Fig. 3.2.7 for the point at the middle of the temperature gradient marked by a circle in Fig. 3.2.5 ($z/\lambda_{ei}^{T_H} \simeq 16.5$).

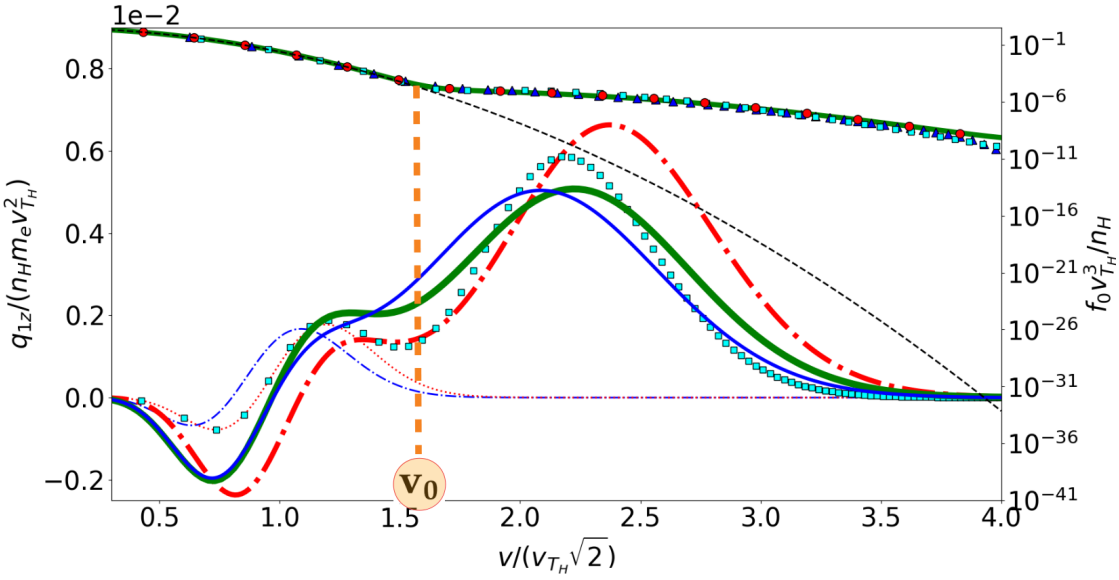


Figure 3.2.9: Same as in Fig. 3.2.7 for the point at the foot of the temperature gradient marked by a triangle in Fig. 3.2.5 ($z/\lambda_{ei}^{T_H} \simeq 18.5$).

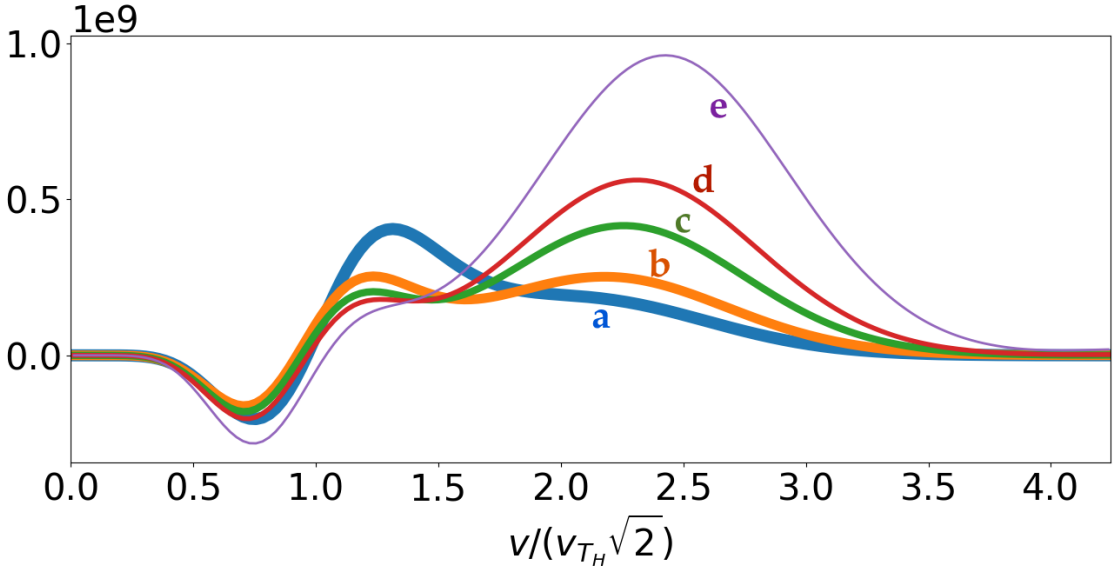


Figure 3.2.10: Graph of $q_{1z} = (2\pi m_e/3)v^5 f_{1z}$ as computed by OSHUN at the points $z/\lambda_{ei}^T \simeq 17.8$ (a), 18.2 (b) 18.5 (c), 18.8 (d), and 19.9 (e). In order to obtain comparable magnitudes at all these points, $q_{1z}$ is divided by the position-dependent term $(n_e/n_H)(|\boldsymbol{\nabla} T_e|/\max|\boldsymbol{\nabla} T_e|)/(T_e/T_H)^{1/2}$.

There, the temperature gradient is smoother and so the diffusive part of the heat flux density is strongly decreased. More precisely, from Eq. (3.19) we can estimate that its overall magnitude behaves like $n_e|\boldsymbol{\nabla} T_e|/T_e^{1/2}$. Such a tendency is confirmed by the Fig. 3.2.10 given the adopted normalizing factor. Because the temperature itself decreases, this diffusive contribution to forward heat current shifts to low velocities. On the contrary, the relative contribution of the convective part of the flux carried by fast electrons [66] is enhanced, and the position of its maximum is shifted toward higher velocities. This phenomenon has a kinematic origin: to access the cold region an electron must have the appropriate velocity. The further from the region of maximum temperature gradient a region is, the faster the electrons it contains.

The point in velocity space, $v_0$, separating these two contributions corresponds to an abrupt variation of the slope of $f_0$. Such a kinetic discontinuity has been carefully studied by Gurevich and Istomin [66], whose work is discussed in depth in the Complementary Note 6.2. Within the region of maximum temperature gradient, the magnitude of $q_{1z}$ is weaker than the prediction of any formulae related to the local regime. Everything appears as if the missing, convective part is delocalized in regions with lower temperatures. Beyond the region of maximum temperature gradient, the isotropic part of the distribution function is close to the local Maxwellian distribution function for velocities $v$ smaller than $v_0$, whereas for higher velocities, $v \geq v_0$, it is a convolution of the isotropic functions of hotter regions. As visible in Fig. 3.2.9, for $v \leq v_0$ the heat flux density integrand $q_{1z}$ provided by the local theory is not recovered. This is because the local thermodynamic conditions are modified by the presence of the delocalized electrons. More precisely, in the expression (3.19),

$$\mathbf{f}_1 = -\int_v^\infty \left(\frac{w}{v}\right)^\alpha \left[\frac{\boldsymbol{\nabla} f_0}{\nu_{ee}^*} - \frac{e\mathbf{E}}{m_e w \nu_{ee}^*}\partial_w f_0\right] dw,$$

the integration is performed from $v$ to $\infty$. So, for a given velocity $v$, the value of $\mathbf{f}_1$ is only determined by $f_0$ for velocities greater than $v$. The convective component ($v \geq v_0$) of $q_{1z}$ is thus independent from the local Maxwellian part of the electron distribution, whereas the component of $q_{1z}$ related to the diffusive part ($v \leq v_0$) is affected by the deformation of $f_0$ for $v \geq v_0$. As we move away from the temperature gradient, there only remains the convective part, together with the return current of cold electrons created by the local electric field.

On the contrary, the heat flux density integrand $q_{1z}$ provided by the SNB's model is equal to $q_{1,\mathrm{L}}$ for low velocities. This is because the source term in Eq. (2.45) is negligible for $v \ll v_T$. Indeed, the characteristic time for diffusion of the perturbation $\delta f_0$ on a macroscopic length $L$ is $3L^2\nu_{ei}^E/v^2$, behaving as $1/v^5$, whereas its dissipation occurs on a time, $1/(r\nu_{ee})$, roughly proportional to $v^3$. For $v = v_T$, the latter value is of the same order of magnitude than the time required to reach the quasi-stationary kinetic state described by Eq. (2.45). For high velocities, the diffusion occurs in a duration much smaller than dissipation, thus leading to significant values of the perturbations. Such a high velocity diffusion corresponds to macroscopic displacements toward cold region within the plasma. They are inhibited by the electric field, which is implicitly accounted for in the diffusion coefficient. For low velocities, the dissipation dominates and the perturbation is

only determined by the source term. Therefore, $\delta f_0 \ll f_M$ and $||\delta \mathbf{f}_1|| \ll ||\mathbf{f}_{1,\mathrm{L}}||$ in the low velocity domain. Such a drawback could be corrected by considering

$$-v\boldsymbol{\nabla} \cdot \left( \frac{v^2}{2v_T^2} - 4 \right) \frac{v f_M}{3\zeta(Z)\nu_{ei}} \frac{\boldsymbol{\nabla} T_e}{T_e}$$

as a source term in Eq. (2.45).

## 3.3 Conclusion

The model consisting of a P1 system within which appears the electron-electron operator introduced by Albritton *et al.* [82] has been analysed and improved. After having exhibited and examined as meticulously as possible the hypotheses leading to the operator itself, we revealed the necessity of renormalizing the electron-electron collision frequency by a corrective factor $\phi(Z)$. For this we especially made the link between the friction force experienced by the electrons and the amplitude of the forward and return currents.

The semi-analytical expression (3.2.1) of $\phi(Z)$ has been derived, as well as that, given by Eq. (3.29), of the correction $r(Z)$ necessary in the case where the electron-electron collision operator of Bhatnagar *et al.* is used instead of that of Albritton *et al.* Each of these formulae is in agreement with the numerical observations made by several authors. Their derivations were possible because we had the explicit value of the electric field appearing in the expression of the heat flux density (3.20) in the local regime. In both cases this value is the Lorentz's one, as we have shown that for none of these operators was fulfilled the condition (3.22) for self-consistently recovering the effect of the ionisation number on the electric field. Thanks to this, a definitive formula (3.25) for the anisotropic component of the distribution function could also be written in the local regime. It well tends towards the Lorentz's value (3.26) in the limit of high $Z$, but gradually shifts towards low velocities for increasingly low values of $Z$. This trend is in line with the kinetic simulations. The differential nature of the electron-electron operator is the key ingredient for capturing this effect, which persists in the nonlocal regime.

There, the heat flux calculated with the model in conditions relevant to ICF agrees with a maximum difference of 10% with the full kinetic computation, while requiring a much smaller computation time. This precision is reduced by iterating with the Spitzer-Härm's electric field or by approximating $\boldsymbol{\mathcal{C}}_{ee}^{1}$ via a renormalization of the electron-ion collision frequency (3.27), as it is done in many codes to gain numerical efficiency. The behaviors of the components of the distribution function present all the expected characteristics with an acceptable deviation from the reference code. The appearance of the kinetic discontinuity on $f_0$ has been put in parallel with the shape of $\mathbf{f}_1$, which changes qualitatively at the vicinity of the foot of the temperature gradient. This has been qualitatively interpreted in light of the pioneering work, deepened in the Complementary Note 6.2, identifying the diffusive and convective components involved in electron heat transport.

This page is unintentionally left not blank.

# Chapter 4

# A deterministic numerical scheme for the kinetic model

One of the adopted strategies [137] to simulate the plasma over macroscopic scales is to manage its evolution through hydrodynamic equations [33], but with kinetic computations of heat flux density, stress viscosity and self-consistent electromagnetic fields. This means that between two macroscopic time steps, the microscopic solver must provide the quasi-stationary kinetic state reached for the given hydrodynamic constraints. In this thesis, we consider as a candidate the reduced kinetic model studied in the previous chapter, a version of which has already been implemented by Holec *et al.* [128] and Del Sorbo *et al.*. In the course of their studies, however, they encountered numerical difficulties revealing the inadequacy of their schemes for dealing with the nonlocal regime. Despite the very different numerical methods they employed, the authors were in fact faced with the same decisive problem. It is at the heart of this chapter, whose purpose is to expose the solution we developed.

Let us remember that, because the spherical Laplacian in the phase space is a common part of all collision operators, the distribution function is expanded on some of its eigenfunctions, the Maxwell's multipoles. The physical quantities of interest in electron heat transport depend explicitly on a few number of them. For this reason, the study is restricted by an appropriate procedure to a closed system of partial differential equations on the concerned components of the distribution function. It is derived in an original way within App. 4.A. This P1 system is of first order due to the fact that the collision operator contains a first order derivative in electron energy. Such decisive feature allows to implement the model with the Godunov's method, which is reviewed in App. 4.B. The Sec. 4.1 is devoted to the numerical implementation of the model by providing its discrete formulation. The convergence in mesh is examined in Sec. 4.2 for local and nonlocal regimes. The accuracy of the numerical results is determined by comparison with analytical formulae and existing codes within which more complete kinetic descriptions are used. Finally, the interplay between the macroscopic evolution governed by hydrodynamic equations and the kinetic calculations is highlighted in Sec. 4.3.

## 4.1 Discrete formulation

The framework within which our numerical method is developed was introduced by Del Sorbo *et al* [132]. Unlike their work, however, a slightly different change of variable is used, the convenience of which is demonstrated in Sec. 4.1.1 presenting the matrix formulation of the P1 system considered in this thesis. In addition, the time variable is retained despite the stationary nature of the model. This is justified in Sec. 4.1.2 devoted to the numerical scheme. There, the major problem encountered by Del Sorbo *et al* and Holec *et al* is clearly highlighted for the first time, with emphasis on how our approach solves it.

### 4.1.1 Matrix equation of conservation with a source term

At any time $t$, the electrons in position $\mathbf{r}$ will be described by the distribution function in energy defined by:

$$\Psi(t,\mathbf{r},\epsilon(v),\mathbf{\Omega}) = v^\beta f_e(t,\mathbf{r},v,\mathbf{\Omega}), \tag{4.1}$$

where $\epsilon(v) = m_e v^2/2$ is the electron kinetic energy, and $\beta > 0$, whose value will be fixed hereafter. Such a change of variable has no other motivation than an easier comparison with the work of Del Sorbo *et al.* [57]. Since in zero, $v \mapsto f_e(t,\mathbf{r},v,\mathbf{\Omega})$ is bounded, $v \mapsto \Psi(t,\mathbf{r},\epsilon(v),\mathbf{\Omega})$ vanishes; in $+\infty$, both functions vanish. The value of $\beta$ thus determines the rate of convergence toward 0 in those two limits. From the chain rule,

$$\partial_\epsilon = (2m_e\epsilon)^{1/2}\partial_v,$$

we deduce from Eq. (4.1) that the function $\Psi$ obeys the following kinetic equation:

$$\left(\frac{m_e}{2\epsilon}\right)^{1/2}\partial_t\Psi + \mathbf{\Omega}\cdot\boldsymbol{\nabla}\Psi - \frac{e\mathbf{E}}{\epsilon}\cdot\left[\mathbf{\Omega}\left(\epsilon\partial_\epsilon\Psi - \frac{\beta}{2}\Psi\right) + \frac{1}{2}(\mathsf{I}-\mathbf{\Omega}\otimes\mathbf{\Omega})\cdot\partial_{\mathbf{\Omega}}\Psi\right] = \left(\frac{2\epsilon}{m_e}\right)^{(\beta-1)/2}[\mathcal{C}_{\rm ei}(\Psi)+\mathcal{C}_{\rm ee}(\Psi,\Psi_M)], \tag{4.2}$$

where

$$\left(\frac{2\epsilon}{m_e}\right)^{(\beta-1)/2}\mathcal{C}_{\rm ei}(\Psi) = \frac{S_\epsilon Z}{4\epsilon\phi(Z)}(-\mathsf{L}^2)(\Psi), \tag{4.3}$$

$$\left(\frac{2\epsilon}{m_e}\right)^{(\beta-1)/2}\mathcal{C}_{\rm ee}(\Psi,\Psi_M) = \frac{S_\epsilon}{\epsilon}\left[\frac{1}{4}(-\mathsf{L}^2)(\Psi) + \epsilon^{1+\beta/2}\partial_\epsilon\epsilon^{-\beta/2}(\Psi-\Psi_M)\right]. \tag{4.4}$$

The friction force in the high velocity limit is denoted by

$$S_\epsilon = \nu_{\rm ee}\sqrt{2m_e\epsilon} = \frac{\phi(Z)n_e Y_{ee}}{\epsilon},$$

and the Maxwellian equilibrium distribution function is transformed as:

$$\Psi_M(\mathbf{r},\epsilon) = \left(\frac{2\epsilon}{m_e}\right)^{(\beta-2)/2}\frac{N_e(\mathbf{r})}{(2\pi)^{3/2}}\left(\frac{m_e}{\epsilon_T(\mathbf{r})}\right)^{1/2}\frac{2\epsilon}{\epsilon_T(\mathbf{r})}\exp\left(-\frac{\epsilon}{\epsilon_T(\mathbf{r})}\right), \tag{4.5}$$

where $\epsilon_T(\mathbf{r}) = k_B T(\mathbf{r})$ is the thermal energy. Then, by projecting Eq. (4.2) on Maxwell's multipoles of zero and first order, we obtain

$$\begin{aligned}
&\left(\frac{m_e}{2\epsilon}\right)^{1/2} \partial_t \Psi_0 + \frac{1}{3}\boldsymbol{\nabla}\cdot\boldsymbol{\Psi}_1 - \partial_\epsilon S_T \Psi_0 \\
&= -\partial_\epsilon S_\epsilon \Psi_M + \frac{1-\beta/2}{\epsilon}\left(S_T\Psi_0 - S_\epsilon \Psi_M\right), \qquad (4.6)\\
&\left(\frac{m_e}{2\epsilon}\right)^{1/2} \partial_t \boldsymbol{\Psi}_1 + \boldsymbol{\nabla}\Psi_0 - \partial_\epsilon S_T \boldsymbol{\Psi}_1 - \partial_\epsilon\left[e\mathbf{E}\cdot\left(1 - \frac{\boldsymbol{\Psi}_1\otimes\boldsymbol{\Psi}_1}{3\Psi_0^2}\right)\Psi_0\right] \\
&= -\frac{S_\epsilon}{2\epsilon}\left(\beta - 1 + \frac{Z}{\phi(Z)}\right)\boldsymbol{\Psi}_1 - \frac{\beta}{2}\frac{e\mathbf{E}}{\epsilon}\Psi_0, \qquad (4.7)
\end{aligned}$$

where, following Ref. [57], we have introduced the quantity $S_T$ designated as the total stopping force:

$$S_T = S_\epsilon + \frac{e\mathbf{E}}{3}\cdot\frac{\boldsymbol{\Psi}_1}{\Psi_0}. \qquad (4.8)$$

The system of Eqs. (4.6)-(4.7) is derived in the App. 4.A. An alternative approach would have been to use an angular decomposition on Heaviside's distributions. It corresponds to the discrete ordinates method [92], which is used to provide an estimate of integral terms as discrete sum in kinetic equations. This advantage is, however, irrelevant here because Eq. (4.2) does not contain such terms. In addition, the spherical Laplacian, which is elliptic on $\mathbb{S}^2$, is here transformed as an algebraic operator as being restricted to its eigenspaces. As a result, it will be shown hereafter that Eqs. (4.6)-(4.7) form an hyperbolic system. These equations were written in Ref. [57] for $\beta = 3$. However, the choice $\beta = 2$ appears more appropriate as it cancels the term $(1-\beta/2)\left(S_T\Psi_0 - S_\epsilon\Psi_M\right)/\epsilon$ in equation (4.6). Both choices are in principle equivalent for smooth solutions, but they may correspond to different path toward convergence. In practical usage of the kinetic module within an hydrodynamic simulation, it may have consequences on the control of the committed error for a given mesh. In what follows we use

$$\beta = 2.$$

The system (4.6)-(4.7) is now written in the form of a matrix conservation equation:

$$\left(\frac{m_e}{2\epsilon}\right)^{1/2}\partial_t\boldsymbol{\Phi} + \partial_z(\mathsf{H}_z\cdot\boldsymbol{\Phi}) + \partial_\epsilon(\mathsf{H}_\epsilon\cdot\boldsymbol{\Phi}) = \mathsf{L}\cdot\boldsymbol{\Phi} + \mathbf{M}, \qquad (4.9)$$

where $\boldsymbol{\Phi} = (\Psi_0, \Psi_{1z})^T$, $\mathbf{M} = (-\partial_\epsilon S_\epsilon \Psi_M, 0)^T$,

$$\mathsf{H}_z = \begin{pmatrix} 0 & \frac{1}{3} \\ 1 & 0 \end{pmatrix}, \quad \mathsf{H}_\epsilon = \begin{pmatrix} -S_T & 0 \\ -\left[1 - \frac{\Psi_{1z}^2}{3\Psi_0^2}\right] eE_z & -S_T \end{pmatrix}, \qquad (4.10)$$

and

$$\mathsf{L} = \begin{pmatrix} 0 & 0 \\ -\frac{eE_z}{\epsilon} & -\left[1 + \frac{Z}{\phi(Z)}\right]\frac{S_\epsilon}{2\epsilon} \end{pmatrix}. \qquad (4.11)$$

The Jacobian matrix $\mathsf{J}_z$ of the space flux $\mathbf{F}_z(\mathbf{\Phi}) = \mathsf{H}_z \cdot \mathbf{\Phi}$ is $\mathsf{H}_z$ by linearity. Its spectrum is:

$$\mathrm{Sp}(\mathsf{J}_z) = \left\{ -\frac{1}{\sqrt{3}}, +\frac{1}{\sqrt{3}} \right\} \tag{4.12}$$

The Jacobian matrix of the energy flux $\mathbf{F}_\epsilon(\mathbf{\Phi}) = \mathsf{H}_\epsilon \cdot \mathbf{\Phi}$ is $\mathsf{J}_\epsilon = \mathsf{H}_\epsilon + \mathbf{\Phi} \cdot \partial_{\mathbf{\Phi}} \mathsf{H}_\epsilon$, whose components are:

$$\begin{aligned}
(\mathsf{J}_\epsilon)_{00} &= (\mathsf{H}_\epsilon)_{00} + \Psi_0 \frac{\partial (\mathsf{H}_\epsilon)_{00}}{\partial \Psi_0} + \Psi_{1z} \frac{\partial (\mathsf{H}_\epsilon)_{01}}{\partial \Psi_0} \\
&= -S_T + \Psi_0 \frac{eE_z}{3} \frac{\Psi_{1z}}{\Psi_0^2} = -S_\epsilon,
\end{aligned}$$

$$\begin{aligned}
(\mathsf{J}_\epsilon)_{10} &= (\mathsf{H}_\epsilon)_{10} + \Psi_0 \frac{\partial (\mathsf{H}_\epsilon)_{10}}{\partial \Psi_0} + \Psi_{1z} \frac{\partial (\mathsf{H}_\epsilon)_{11}}{\partial \Psi_0} \\
&= -\left[ 1 - \frac{\Psi_{1z}^2}{3\Psi_0^2} \right] eE_z - \Psi_0 \frac{eE_z}{3} \frac{2\Psi_{1z}^2}{\Psi_0^3} + \Psi_{1z} \frac{eE_z}{3} \frac{\Psi_{1z}}{\Psi_0^2} = -eE_z,
\end{aligned}$$

$$\begin{aligned}
(\mathsf{J}_\epsilon)_{01} &= (\mathsf{H}_\epsilon)_{01} + \Psi_0 \frac{\partial (\mathsf{H}_\epsilon)_{00}}{\partial \Psi_{1z}} + \Psi_{1z} \frac{\partial (\mathsf{H}_\epsilon)_{01}}{\partial \Psi_{1z}} \\
&= - \Psi_0 \frac{eE_z}{3\Psi_0} = -\frac{eE_z}{3},
\end{aligned}$$

and:

$$\begin{aligned}
(\mathsf{J}_\epsilon)_{11} &= (\mathsf{H}_\epsilon)_{11} + \Psi_0 \frac{\partial (\mathsf{H}_\epsilon)_{10}}{\partial \Psi_{1z}} + \Psi_{1z} \frac{\partial (\mathsf{H}_\epsilon)_{11}}{\partial \Psi_{1z}} \\
&= -S_T + \Psi_0 \frac{eE_z}{3} \frac{2\Psi_{1z}}{\Psi_0^2} - \Psi_{1z} \frac{eE_z}{3\Psi_0} = -S_\epsilon.
\end{aligned}$$

It is worth mentioning that the derivative of the electric field $E_z$ with respect to $\mathbf{\Phi}$ does not appear, in spite of the zero electric current condition yielding to:

$$E_z = -\frac{1}{e} \frac{\phi(Z) n_e Y_{ee} \left[ \epsilon \Psi_{1z} \right]_0^{+\infty} - \int_0^{+\infty} \epsilon^2 \left[ \left( \frac{m_e}{2\epsilon} \right)^{1/2} \partial_t \Psi_{1z} + \partial_z \Psi_0 \right] d\epsilon}{\left[ \epsilon^2 \Psi_0 \right]_0^{+\infty} - 3 \int_0^{+\infty} \epsilon \Psi_0 d\epsilon}. \tag{4.13}$$

Indeed, $E_z$ is a function of $(t, z)$ and has the status of a parameter when solving the system of Eqs. (4.6)-(4.7) with unknowns $\Psi_0$ and $\mathbf{\Psi}_1$. The space of solutions is restricted by the condition of zero electric current density. It leads to Eq. (4.13), which provides the value of $E_z$ required to fulfill the condition. The spectrum of

$$\mathsf{J}_\epsilon = \begin{pmatrix} -S_\epsilon & -\frac{eE_z}{3} \\ -eE_z & -S_\epsilon \end{pmatrix}, \tag{4.14}$$

is thus:

$$\mathrm{Sp}(\mathsf{J}_\epsilon) = \left\{ -S_\epsilon - \frac{e|E_z|}{\sqrt{3}}, -S_\epsilon + \frac{e|E_z|}{\sqrt{3}} \right\} \tag{4.15}$$

Since the eigenvalues of the Jacobian matrices are real, the conservation equation (4.9) is hyperbolic in both space and energy, which allows us to use a Godunov's method. It is reviewed in App. 4.B. By definition, the $z$ and $\epsilon$ axes are orthogonal, and so the homogeneous advection problem along one of them can be treated independently from the other: $-\partial_\epsilon \mathbf{F}_\epsilon(\mathbf{\Phi})$ is a source term for advection along the $z$-axis and *vice versa*.

### 4.1.2 Scheme

The spatial domain contains $I$ cells of constant size $\Delta z$ indexed by $i \in \{0, ...I-1\}$, and the energy domain contains $G$ cells of constant size $\Delta\epsilon$ indexed by $g$. Time steps, of size $\Delta t$, are indexed by $n$. Integrating Eq. (4.9) on the control volume $[t^n, t^{n+1}] \times [z_{i-1/2}, z_{i+1/2}] \times [\epsilon_{g-1/2}, \epsilon_{g+1/2}]$ leads to the following discretization:

$$\left(\frac{m_e}{2\epsilon_g}\right)^{1/2} \frac{\mathbf{\Phi}_{i,g}^{n+1} - \mathbf{\Phi}_{i,g}^{n}}{\Delta t} + [\partial_z \mathbf{F}_z]_{i,g}^n + [\partial_\epsilon \mathbf{F}_\epsilon]_{i,g}^n = \mathsf{L}_{i,g}^{n+1} \cdot \mathbf{\Phi}_{i,g}^{n+1} + \mathbf{M}_{i,g}^n, \tag{4.16}$$

where

$$[\partial_z \mathbf{F}_z]_{i,g}^n = \frac{(\mathbf{F}_z)_{i+1/2,g}^n - (\mathbf{F}_z)_{i-1/2,g}^n}{\Delta z}, \quad [\partial_\epsilon \mathbf{F}_\epsilon]_{i,g}^n = \frac{(\mathbf{F}_\epsilon)_{i,g+1/2}^n - (\mathbf{F}_\epsilon)_{i,g-1/2}^n}{\Delta \epsilon}.$$

This yields the following set of equations:

$$\left[\left(\frac{m_e}{2\epsilon_g}\right)^{1/2} \frac{\mathsf{I}}{\Delta t} - \mathsf{L}_{i,g}^{n+1}\right] \mathbf{\Phi}_{i,g}^{n+1} = \left(\frac{m_e}{2\epsilon_g}\right)^{1/2} \frac{\mathbf{\Phi}_{i,g}^{n}}{\Delta t} - [\partial_z \mathbf{F}_z]_{i,g}^n - [\partial_\epsilon \mathbf{F}_\epsilon]_{i,g}^n + \mathbf{M}_{i,g}^n. \tag{4.17}$$

In $\mathsf{L}_{i,g}^{n+1}$ there appears $E_i^{n+1}$, which is not computed yet. For that reason the estimation $E_i^n$ is used instead, without any effect on the convergence in time. We thus have to solve a system whose determinant:

$$\left(\frac{m_e}{2\epsilon^g}\right)^{1/2} \left[\left(\frac{m_e}{2\epsilon^g}\right)^{1/2} + \left(1 + \frac{Z}{\phi(Z)}\right) \frac{(S_\epsilon)_g}{2\epsilon_g}\right],$$

never vanishes. Because the system is of dimension two, Cramer's formulas are directly used, without any extra computational cost compared to approximate inversion algorithms. The implicit estimation of the linear term $\mathsf{L}_{i,g}^{n+1} \cdot \mathbf{\Phi}_{i,g}^{n+1}$ is done in order to avoid an instability due to low energy groups $g$ and large values of $Z$. The source term could also have been treated by splitting in time the resolution of the homogeneous advection equation and the ordinary differential equation along characteristics. As detailed in Ref. [138], this fractional steps method is however not suited for time-marching scheme toward quasi-steady state. This is because $(m_e/2\epsilon)^{1/2}\partial_t \mathbf{\Phi}$ is small compared to the flux terms and the source terms which should exactly balance at convergence. The delicate occurrence of this quasi-steady state strongly depends on the respective accuracy of the numerical methods used to solve the homogeneous advection equation and the ordinary differential equation, leading each on their side to large variations of $\mathbf{\Phi}$.

#### 4.1.2.1 Fluxes

The eigenvalues of $\mathsf{J}_z$, the Jacobian matrix of the flux in space, are the constants $(S_R)^n_{i+1/2} = 1/\sqrt{3} = -(S_L)^n_{i+1/2}$. Thus, Eq. (4.55) within App. 4.B leads to:

$$(\mathbf{F}_z)^n_{i+1/2,g} = \frac{(\mathbf{F}_z)^n_{i+1,g} + (\mathbf{F}_z)^n_{i,g}}{2} - \frac{1}{\sqrt{3}} \frac{\mathbf{\Phi}^n_{i+1,g} - \mathbf{\Phi}^n_{i,g}}{2}. \tag{4.18}$$

This inter-cell flux is equal to $\mathsf{H}_z \cdot (\mathbf{\Phi}^*)^{n+1}_{i+1/2,g}$, which can be directly obtained from expression (4.47) because $\mathsf{H}_z$ is constant.

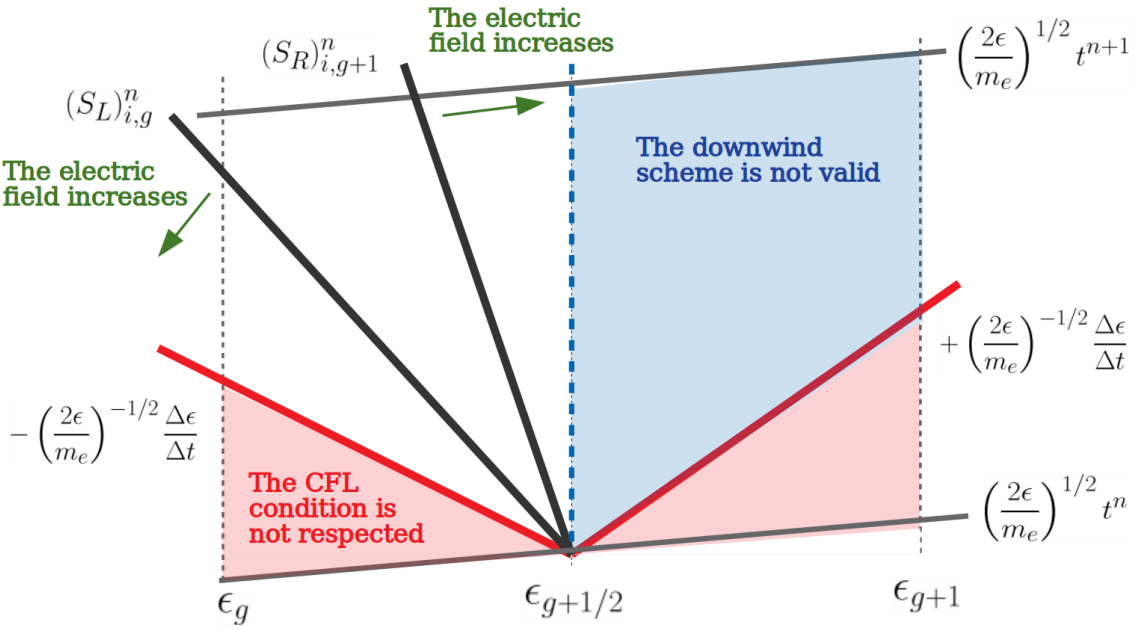


Figure 4.1.1: Geometry of local Riemann's problems along the energy axis. The time-like axis is inclined with respect to the horizontal to account for the growth of $(2\epsilon/m_e)^{1/2}t$ with $\epsilon$. If the characteristic associated to $(S_R)^n_{i,g+1}$ crosses the blue dashed vertical line, the downwind scheme cannot be employed. If the characteristic associated to $(S_L)^n_{i,g}$ crosses the red inclined line, the CFL's condition is not respected. These situations occur for too high electric fields.

The estimation of inter-cell fluxes along the energy axis relies on the signs of the eigenvalues of $\mathsf{J}_\epsilon$, which depend on the energy through $S_\epsilon$. The velocities of the fastest waves emerging from $\epsilon_{g+1/2}$ are considered as being the two extreme eigenvalues of $\mathrm{Sp}(\mathsf{J}_\epsilon)^n_{i,g} \cup \mathrm{Sp}(\mathsf{J}_\epsilon)^n_{i,g+1}$, denoted by:

$$(S_L)^n_{i,g} = -(S_\epsilon)_g - \frac{e|(E_z)^n_i|}{\sqrt{3}}, \quad (S_R)^n_{i,g+1} = -(S_\epsilon)_{g+1} + \frac{e|(E_z)^n_i|}{\sqrt{3}}. \tag{4.19}$$

The corresponding characteristics are drawn in Fig. 4.1.1. Because $(S_L)^n_{i,g} < 0$ always holds, the inter-cell fluxes are uniquely determined by the sign of $(S_R)^n_{i,g+1}$. If $(S_R)^n_{i,g+1} \leq 0$,

$$(\mathbf{F}_\epsilon)^n_{i,g+1/2} = \mathbf{F}_\epsilon(\mathbf{\Phi}^n_{i,g+1}) = (\mathsf{H}_\epsilon)^n_{i,g+1} \cdot \mathbf{\Phi}^n_{i,g+1},$$

and if $(S_L)_{i,g} < 0 < (S_R)_{i,g+1}$, then:

$$(\mathbf{F}_\epsilon)^n_{i,g+1/2} = \frac{(S_R)^n_{i,g+1}\mathbf{F}_\epsilon(\mathbf{\Phi}^n_{i,g}) - (S_L)^n_{i,g}\mathbf{F}_\epsilon(\mathbf{\Phi}^n_{i,g+1}) + (S_L)^n_{i,g}(S_R)^n_{i,g+1}\left(\mathbf{\Phi}^n_{i,g+1} - \mathbf{\Phi}^n_{i,g}\right)}{(S_R)^n_{i,g+1} - (S_L)^n_{i,g}}.$$

When $(S_R)^n_{i,g+1} \leq 0$, a finite difference estimation of the divergence of fluxes is recovered:

$$[\partial_\epsilon \mathbf{F}_\epsilon]^n_{i,g} = \frac{(\mathbf{F}_\epsilon)^n_{i,g+1/2} - (\mathbf{F}_\epsilon)^n_{i,g-1/2}}{\Delta\epsilon} = \frac{(\mathsf{H}_\epsilon)^n_{i,g+1} \cdot \mathbf{\Phi}^n_{i,g+1} - (\mathsf{H}_\epsilon)^n_{i,g} \cdot \mathbf{\Phi}^n_{i,g}}{\Delta\epsilon}. \tag{4.20}$$

As shown in Fig. 4.1.1, for an electric field smaller than $S_\epsilon\sqrt{3}/e$, the two extreme waves emerging from local Riemann's problems propagate from high to low energies. This allows to use a *downwind scheme* in energy as done in Refs. [57, 128]. In this case, the time variable $t$ is no longer necessary and the stationary kinetic equations can be directly solved. It means considering $\partial_t \mathbf{\Phi} = \mathbf{0}$ in equation (4.9) and $\epsilon$ as a time-like variable of iteration with the above finite difference estimation (4.20) of $[\partial_\epsilon \mathbf{F}_\epsilon]^n_{i,g}$. The integration is then performed from high to low energy.

As we just have seen, this procedure is justified for $(S_R)^n_{i,g+1} \leq 0$. The condition $S_T \leq 0$ given in Ref. [57] is therefore wrong. It would be the correct requirement if the Jacobian matrix (4.14) of the energy flux were reduced to $\mathsf{H}_\epsilon$, whose degenerate eigenvalue is $-S_T$. For too steep temperature gradients such an approach is not valid because the electric field exceeds the critical value $S_\epsilon\sqrt{3}/e$. It turns out that problems of interest in ICF often correspond to such high values of spatial gradients, and therefore, justify the alternative method proposed here.

#### 4.1.2.2 Algorithm. The local time step strategy.

The algorithm implemented in our code JASMINE is the following. Firstly, $\mathbf{\Phi}^0_{i,g}$ and $(E_z)^0_i$ are initialized. Then, for $n \geq 0$, and until convergence:

*Step 1*: for $g = 0$ to $G-1$, for $i = 0$ to $I-1$,

A *local time step* is computed. As being only interested by the stationary solution of Eq. (4.9), we improved the rate of convergence by setting its value through the number of Courant, Friedrichs and Lewy (CFL) [139]: $\Delta t = (\Delta t)^n_{i,g}$, where

$$(\Delta t)^n_{i,g} = \left(\frac{m_e}{2\epsilon_g}\right)^{1/2} \left[\frac{|(S_L)_{i,g}|}{\Delta\epsilon} + \frac{1/\sqrt{3}}{\Delta z}\right]^{-1}. \tag{4.21}$$

Then, $\mathbf{\Phi}^{n+1}_{i,g}$ is computed by solving Eq. (4.17).

*Step 2*: $(E_z)^{n+1}_i$ is computed with expression (4.13) by setting $\partial_t \mathbf{\Psi}_1 = \mathbf{0}$. Accounting for this term would require to store all the values $\mathbf{\Phi}^n_{i,g}$, which are erased during the first step of the algorithm. This has no consequence since the state reached at convergence is stationary.

The gain in performance obtained by using a local time step (4.21) is examined in Sec. 4.2. In all the considered cases the convergence was reached. This success can be understood by analogy with the method of domain decomposition [140].

Using $(\Delta t)_{i,g}^n$ is indeed equivalent to performing a different number of iterations on each cells with a constant time step. The consequence is to modify the heights of the jumps between values of the piece-wise distribution function in adjacent cells. The local time step strategy we propose offers an alternative to the often preferred implicit method to find steady-state solution [141], but avoids a large matrix inversion. These aspects deserve a deeper analysis and a mathematical proof of the convergence of the scheme may be addressed in a future work.

#### 4.1.2.3 Conditions at the edges

The initial conditions are as follows. The hydrodynamic variables are the electron density, mean velocity and temperature. At a given time, they are completely encoded through the data of local Maxwellian function $\Psi_M(\mathbf{r}, \epsilon)$ (4.5) at each point of the plasma. This is why the latter is chosen to initialise $\Psi_0$ in the considered physical problem. Despite the isotropy of $\Psi_M$, it leads to non-zero first order components $\mathbf{\Psi}_1$. They can thus be initialised to zero, even if appropriate values can be chosen to improve convergence. Due to the P1 closure, our numerical scheme leaves stable the subspace generated by $P_0$ and $\mathbf{P}_1$. This means that with the aforementioned initialization, higher order components $\Psi_{\ell,i_1\dots i_\ell}$ with $\ell \geq 3$ remain null and the solution of the kinetic equation (4.2) is searched in the form $\Psi_0 + \mathbf{\Omega} \cdot \mathbf{\Psi}_1$. For the physical problem of interest, this therefore justifies the assumption made in Ref. [57] to derive Eqs. (4.6)-(4.7).

As soon as initial conditions are given, boundary conditions cannot be prescribed arbitrarily. The resulting initial-boundary values problem may be ill-posed at the edges if solutions along characteristic provided by initial and boundary conditions are not compatible. The way to approach this issue, reviewed in Ref. [142], is to examine whether characteristics are coming into or leaving from the space-energy domain. In the latter case, boundary conditions are no longer necessary because initial conditions already determine the solution at the edges. In JASMINE, the choice is made to replace boundary conditions by initial conditions for ghost cells. No matter the configuration of characteristic at the edges, values at each time step must be prescribed in these cells. By doing so, the way inter-cell fluxes are computed does not need to be changed at the edges. Conditions in space are fixed by the physical problem. The spatial domain is chosen such that the temperature gradient is zero at the edges. The gradient of $\Psi_0$ is also zero at the edges because $T_e = 1/(3N_e k_B)\,(2/m_e)^{1/2} \int_0^{+\infty} \epsilon^{1/2} \Psi_0 d\epsilon$. For a smooth temperature gradient, $\mathbf{\Psi}_1$ is proportional to it. Thus, the boundary conditions - *i.e* values in ghost cells - in space are:

$$(\Psi_0)_{-1,g}^n = (\Psi_0)_{0,g}^n, \quad (\Psi_0)_{I-1,g}^n = (\Psi_0)_{I,g}^n, \tag{4.22}$$

$$(\Psi_{1z})_{-1,g}^n = 0, \quad (\Psi_{1z})_{I,g}^n = 0. \tag{4.23}$$

The conditions in energy are not uniquely determined by the physical context. Several choices lead to the same result beyond the few cells at the edges. The most natural choice is an extrapolation based on the derivative of the distribution function at the edges. As it can lead to negative values of the distribution function, which are due to numerical errors, it appeared judicious to impose that $\Psi_0$ has the

same local derivative as $\Psi_M$ (4.5): $\partial_\epsilon \Psi_M = [1 - \epsilon/(\epsilon_T)]\,\Psi_M/\epsilon$. At $\epsilon_0 \ll 2\epsilon_T$, we write

$$\frac{(\Psi_0)^n_{i,0} - (\Psi_0)^n_{i,-1}}{\Delta\epsilon} = \frac{(\Psi_0)^n_{i,-1}}{\epsilon_0},$$

such that $(\Psi_0)^n_{i,-1} = [1 - \Delta\epsilon/\epsilon_0]\,(\Psi_0)^n_{i,0} \simeq \exp(-\Delta\epsilon/\epsilon_0)\,(\Psi_0)^n_{i,0}$, the last approximation ensuring positiveness. In the same way, at $\epsilon_{G-1} \gg 2\epsilon_T$, we write

$$\frac{(\Psi_0)^n_{i,G} - (\Psi_0)^n_{i,G-1}}{\Delta\epsilon} = -\frac{\epsilon_{G-1}}{2\epsilon_T}\frac{(\Psi_0)^n_{i,G-1}}{\epsilon_{G-1}},$$

which leads to $(\Psi_0)^n_{i,G} = [1 - \Delta\epsilon/(2\epsilon_T)]\,(\Psi_0)^n_{i,G-1} \simeq \exp(-\Delta\epsilon/(2\epsilon_T))^n_{i,G-1}$.

A more appropriate value can be prescribed at $\epsilon_0$, as $\Psi_0$ is always extremely close to $\Psi_M$. In the neighborhood of $\epsilon_{G-1}$, however, it is not. As it will be observed hereafter, the difference $|\Psi_0 - \Psi_M|$ is an increasing function of the energy and of the Knudsen number. At the edges, $\Psi_{1z}$ can be put to zero or to the values obtained with the same procedure as for $\Psi_0$. In the cells close to the edges, the difference between the aforementioned choices are below the precision of the model as soon as $\epsilon_{G-1}$ is sufficiently large compared to $\epsilon_T$.

## 4.2 Convergence in mesh

The convergence toward the kinetic solution in local and nonlocal regimes are analysed within Secs. 4.2.1 and 4.2.2 respectively. The initial electron temperature is given by Eq. (1.3),

$$T_e(z) = T_H - \frac{(T_H - T_C)}{2}\Big(1 + \tanh[s(z - z_0)]\Big).$$

The electron density is $n_e = 5 \times 10^8 \mu\text{m}^{-3}$, the Coulomb's logarithm is $\ln\Lambda = 7.09$, its value at $z_0 = L/2$. In the following figures, $\epsilon_{T_H}$, $\lambda_{ei}^{T_H}$ and $(S_\epsilon)_H = 2\phi(Z)n_e Y_{ee}/\epsilon_{T_H}$ denote respectively the thermal energy, the average thermal mean free path and the thermal stopping force in the hot region of the considered case.

The energy grid extends from $\epsilon_0 = \epsilon_{G-1}/10^5$ to $\epsilon_{G-1} = 18\epsilon_{T_H}$. Zero cannot be chosen for $\epsilon_0$ because the stopping force diverge at that point. The value of $\epsilon_{G-1}$ is constrained by the following considerations. At any point $z$ and for any energy $\epsilon$, the stopping force $S_\epsilon$ equals $(S_\epsilon)_H$ multiplied by $\epsilon_{T_H}/(2\epsilon)$, and so the eigenvalue (4.19) can be expressed as

$$S_R = -S_\epsilon\left[1 - \frac{|E_z|}{(S_\epsilon)_H\sqrt{3}/e}\frac{2\epsilon}{\epsilon_{T_H}}\right].$$

Thus, the downwind scheme discussed in Sec. 4.1, and used in Refs. [57, 128], can be applied if:

$$\frac{|E_z|}{(S_\epsilon)_H\sqrt{3}/e} < \frac{\epsilon_{T_H}}{2\epsilon_{G-1}}. \tag{4.24}$$

The right hand side is equal to 1/36 for the chosen energy grid. In order to use the downwind scheme, it may appear sufficient, for a given temperature profile, to set $\epsilon_{G-1}$ as small as required to fulfill the condition (4.24). However, attention must be paid to the resulting length of the energy axis, which must be large enough to describe electrons with the highest energies.

Without any other explicit mention, the numbers of cells in space and energy coordinates used in JASMINE are $I = G = 11200$. In what follows, all the values we will consider are positive or negative powers of two multiplied by 700 to make the mesh refinement process convenient. 11200 is the highest of them. The reason for the particular choice of 700, although being somewhat arbitrary, will appear natural to the reader in the following. It is the chosen one within the reference codes of Sec. 4.2.2.

### 4.2.1 Local regime

In this case, the temperature profile does not evolve during the establishment of the heat flux density and electric field. For that reason, the comparisons made with analytical formulae are done for the initial temperature profile. The parameters are: $Z = 79$, $k_B T_H = 120$ eV, $k_B T_C = 80$ eV, $s = 9 \times 10^{-3}$ $\mu$m$^{-1}$, and $L = 700$ $\mu$m. The Knudsen's number at $z_0$ is $\mathrm{Kn} = 9.4 \times 10^{-6}$.

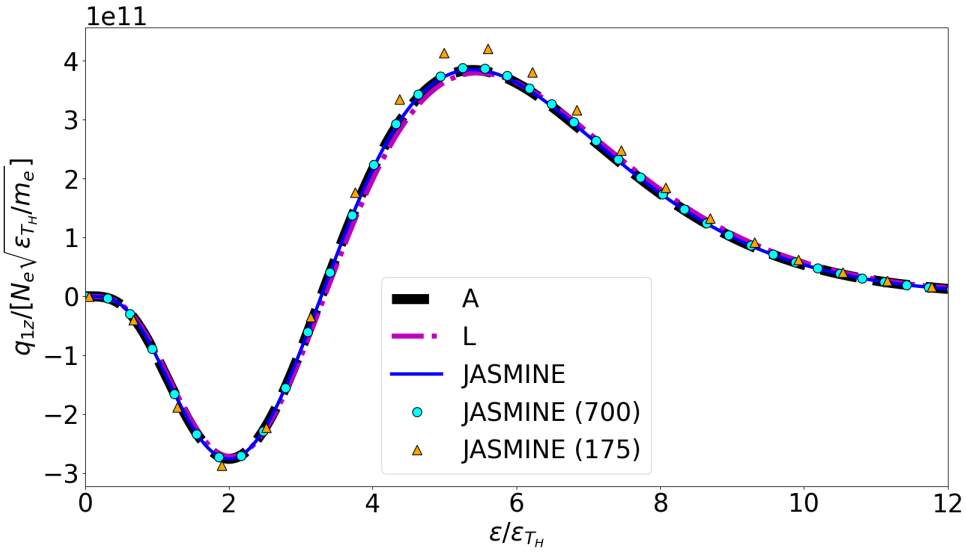


Figure 4.2.1: Local case. Comparison between the distribution functions $q_{1z} = \epsilon\Psi_{1z}/m_e$ in $z_0$ calculated by JASMINE (solid, blue) and by Albritton *et al* (A) (dashed, black) and Lorentz (L) (dashed-dot, violet) formulas. The cyan circles and orange triangles represent calculations by JASMINE for $I = G = 700$ and $I = G = 175$ respectively.

The distribution function $q_{1z} = \epsilon\Psi_{1z}/m_e$ is plotted in 4.2.1. It is the integrand of the heat flux density when expressed as an integral over the energy axis, and therefore differs by a factor $\epsilon^{1/2}$ from the definition used in Chap. 3 for convenience. As expected, the curve obtained with JASMINE (solid, blue) overlaps with those given by our Albritton *et al*' formula (3.24) (A) (dashed, black), as well as by

the Lorentz' (L) one (3.26) (dashed-dot, violet). The cyan circles and orange triangles represent the calculations made by JASMINE for $I = G = 700$ and $I = G = 175$ respectively. Whereas in the first case the limit curve can be considered to be reached, in the second one a clear deviation appears for energies around the maximum of $q_{1z}$. Although it may seem small, it is responsible for a significant error on the heat flux density $q_{ez}$.

It is itself plotted in Fig. 4.2.2. Except for $I = G = 175$, the heat flux density calculated by JASMINE (solid, blue) agrees without surprise to that given by the Spitzer-Harm's (SH) formula (2.19) (dashed, black). The electric field, plotted in 4.2.3, is less sensitive to the number of cells. Even for the smallest one JASMINE provides the expected Lorentz' value (dashed, black) with acceptable accuracy. As we guessed, since the maximum of $E/[(S_\epsilon)_H\sqrt{3}/e]$ is about $6 \times 10^{-4} < 1/36$, the inequality (4.24) is fulfilled such that the downwind scheme can be here employed.

The relative errors of the distribution functions, heat flux density and electric field are plotted in Fig. 4.2.4 for several meshes. For $q_{ez}$ and $E_z$, both norms $||.||_\infty$ and $||.||_2$ are plotted whereas for the distribution functions only the latter is shown. Recall that, given a vector, $||.||_\infty$ is the maximum of the absolute values of its coordinates, while $||.||_2$ is the root of the sum of their squares. Obviously here, the underlying spaces are of finite dimensions, which implies the equivalence of these norms despite they provide different information. Having used zero order estimations of inter-cells fluxes in Sec. 4.1, the resulting scheme is expected to be of first order in both space and energy. This is confirmed in Figs. 4.2.4a and 4.2.4b, where the graphs of the relative errors are straight lines with a slope $-1$ in the logarithmic scale. Varying $I$ and $G$ separately gives the same results. Indeed, if $N$ denotes either $I$ or $G$, and $\Delta$ is the corresponding cell's size, then the product $N\Delta$ is a constant equal to the length of the domain. Hence, independently from the norm the error behaves as

$$\Delta^o \propto N^{-o},$$

with $o$ the order of the scheme. The specific choice of a norm only determines the value of the constant of proportionality between the error and $N^{-o}$. This explains why the lines associated with $||.||_\infty$ and $||.||_2$ are parallel.

Finally, in Fig. 4.2.4a, $||\Psi_{1,\mathrm{L}\ z} - \Psi_{1z}||_2$ tends toward a non-zero value of about 5% of $||\Psi_{1,\mathrm{L}z}||_2$. This quantifies the error which is committed when electron-electron collisions are not explicitly accounted for in Eq. (4.7) for the case $Z = 79$. Given the high value of the ionization number here, such a small error could have been expected.

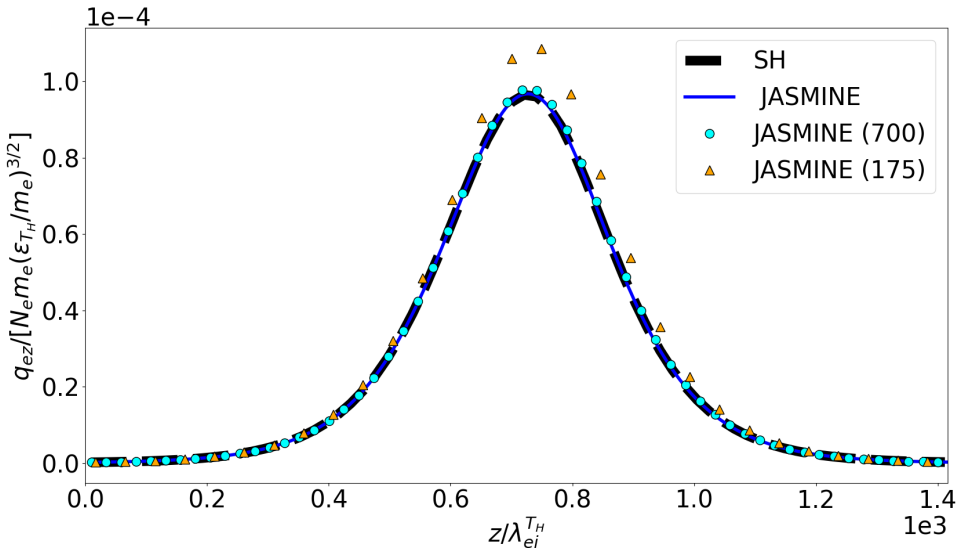


Figure 4.2.2: Local case. Comparison between the heat flux densities calculated by JASMINE (solid, blue) and by Spitzer-Harm's (SH) formula (dashed, black). Other notations are the same as in Fig.4.2.1.

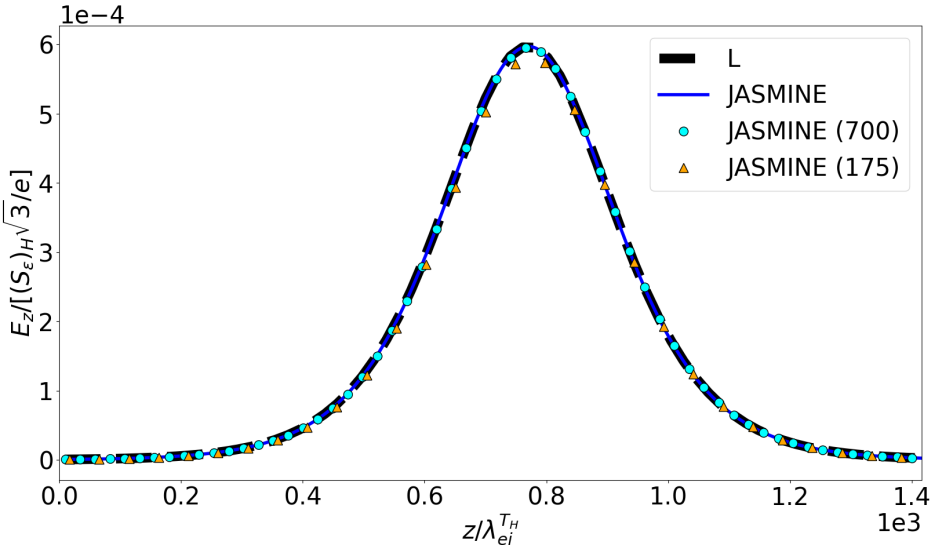


Figure 4.2.3: Local case. Comparison between the electric fields calculated by JASMINE (solid, blue) and by Lorentz (L) formula (dashed, black). Other notations are the same as in Fig. 4.2.1.

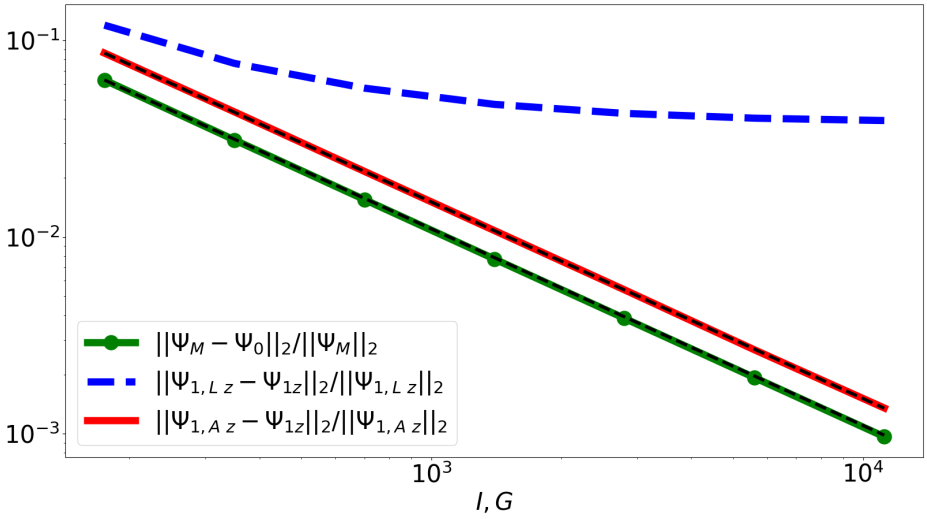


(a)

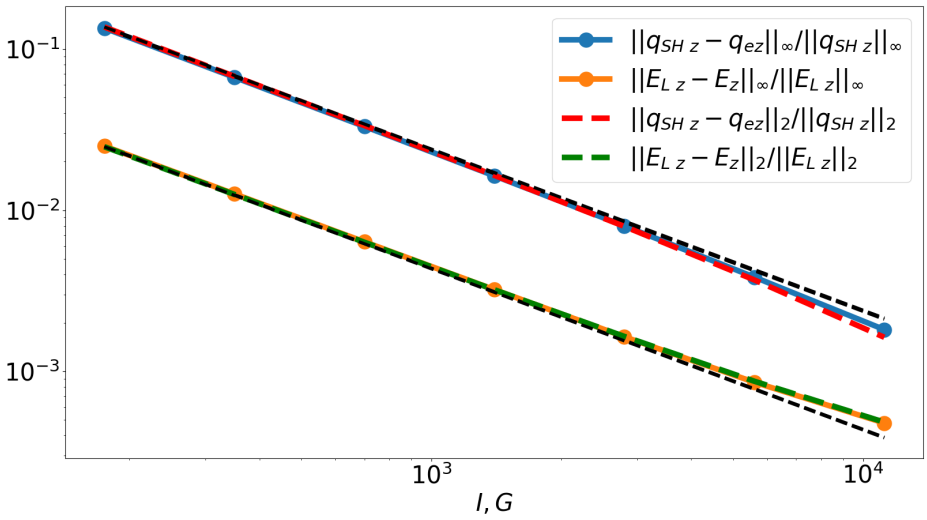


(b)

Figure 4.2.4: Local case. Relative errors in function of the number of cells in space $I$ and energy $G$ for: (a) the distributions functions, and for (b) the heat flux densities and electric field. The fine dashed black lines correspond to the exact first order behaviour of the error.

### 4.2.2 Nonlocal regime

The initial plasma parameters are $Z = 1$, $k_B T_H = 1000$ eV, $k_B T_C = 150$ eV, $s = 2 \times 10^{-2}$ $\mu$m$^{-1}$, and $L = 850$ $\mu$m.

Here, the comparisons are made after a duration of 20 ps $= 6.4$ $(\nu_{ei}^{T_H})^{-1}$, where $\nu_{ei}^{T_H} = (\epsilon_{T_H}/m_e)^{1/2}/\lambda_{ei}^{T_H}$ [42] is the average thermal collision frequency in the hot region. During this period, the heat flux densities and electric fields establish in OSHUN, CALDER and ALADIN. In CALDER [143, 144], the particle-in-cell method is used with appropriate Markov's chains for electron-electron and electron-ion collisions. At the time of comparison, the Knudsen's number at $z_0$ is $\mathrm{Kn} = 6.7 \times 10^{-2}$.

The distribution function $\Psi_0$ is plotted in Fig. 4.2.5. Just as in the nonlocal case considered in Ch. 3, the expected deviation from the Maxwell-Boltzmann's distribution function (2.4) (M) (dotted, black) beyond a certain energy is correctly reproduced by JASMINE (solid, blue), even for a number of cells equals to $I = G = 700$ and $I = G = 175$. The corresponding curves remain close to those given by OSHUN (solid, green), ALADIN (dashed-dot, red) and CALDER (solid, violet). The oscillations in the solution provided by the latter are the manifestation of the noise induced by the finite number of quasi-particles for each group. Their amplitude increases for higher and higher energies due to the lower and lower number of electrons. Such a feature is also visible in Fig. 4.2.6 where $q_{1z} = \epsilon \Psi_{1z}/m_e$ is plotted. Here, ALADIN gives a result which differs significantly from the others. As explained in Ch. 3, this comes from the particular treatment (3.27) of electron-electron collisions made within the underlying P1 system. Except for $I = G = 175$, the curve provided by JASMINE (dotted, blue) appears to be, in spite of the noise, closer to that coming from CALDER than is that coming from OSHUN.

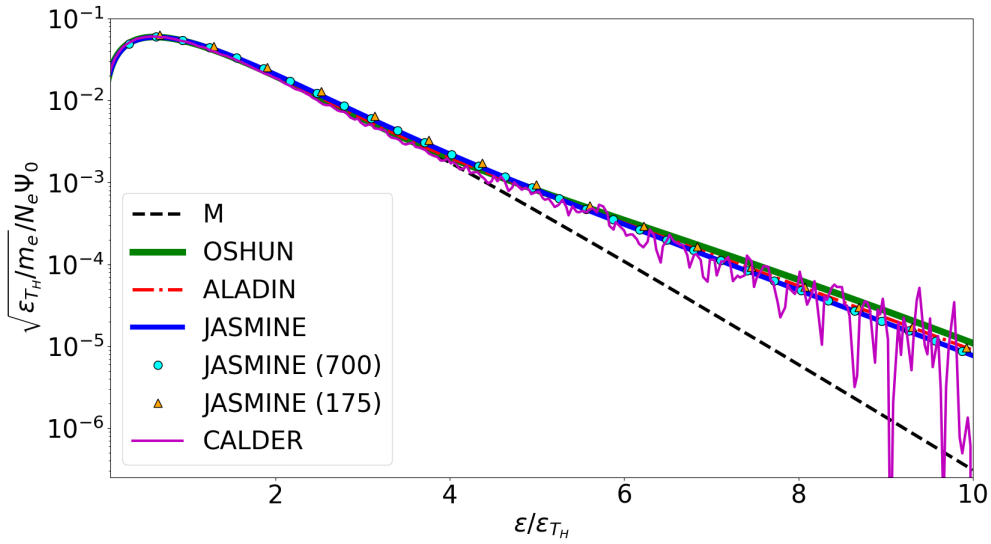


Figure 4.2.5: Nonlocal case. Comparison between the distribution functions $\Psi_0$ in $z_0$ calculated by JASMINE (solid, blue), OSHUN (solid, green), ALADIN (dashed-dot, red), CALDER (solid, violet) and by Maxwell (M) formula (dotted, black). Other notations are the same as in Fig. 4.2.1.

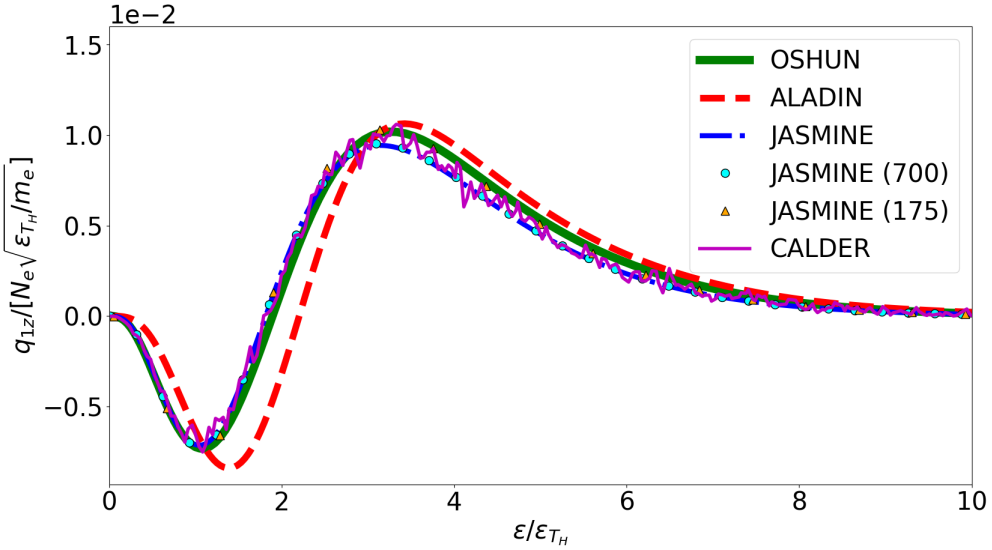


Figure 4.2.6: Nonlocal case. Comparison between the distribution functions $q_{1z} = \epsilon\Psi_{1z}/m_e$ in $z_0$ calculated by JASMINE (dashed-dot, blue), OSHUN (solid, green), ALADIN (dashed, red) and CALDER (solid, violet). Other notations are the same as in Fig. 4.2.1.

Such a fact does not hold for the heat flux density plotted in Fig. 4.2.7. Here, OSHUN and CALDER are in agreement while JASMINE deviates from these references around the peak. Compared to their overall difference from the Spitzer-Harm's (SH) heat flux density (2.19) (dotted, black), the deviation between curves provided by these codes remains small. It is of the same order of magnitude as the convergence error which is committed when JASMINE is used with $I = G = 175$. This gives an indication of the requirement to be had during its practical use. The disparities between electric fields plotted in Fig. 4.2.8 are more marked. The one calculated by JASMINE (solid, blue), together with that coming from ALADIN (dashed, red), are close to the curve obtained through the Lorentz' limit (L) (dashed-dot, red) rather than with the Spitzer-Harm's formula (2.18) (dashed, black). The origin of this defect has already been explained in Ch. 3. The ratio $E_z/[(S_\epsilon)_H\sqrt{3}/e]$ in Fig. 4.2.8 reaches values around $14/100 > 1/36$ in the region $z/\lambda_{ei}^{T_H} \simeq 13.3$. We conclude that there exists a neighborhood of that point within which the inequality (4.24) does not hold. This is confirmed by looking directly to $S_R$ at some positions. Therefore the downwind scheme is here inapplicable and the considered situation justifies the use our scheme.

Finally, since $E_z$ has a magnitude comparable to $E_L$, the condition (4.24) can be expressed in an approximate form involving the Knudsen's number:

$$\mathrm{Kn} \lesssim \frac{3(3\pi/2)^{1/2}\phi(Z)}{5Z}\frac{\epsilon_{T_C}}{\epsilon_{G-1}}. \tag{4.25}$$

In the local case of the previous subsection, the right hand side is equal to $3.3\times10^{-4}$, and to $4.9\times10^{-3}$ for the present, nonlocal case. If compared to Knudsen's numbers in both cases, these values are consistent with our previous conclusions about the applicability of the downwind scheme.

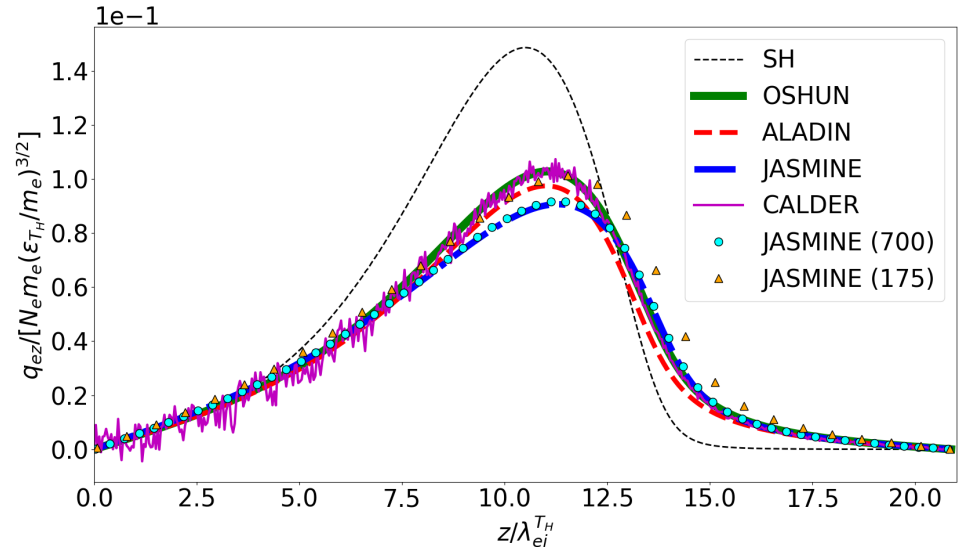


Figure 4.2.7: Nonlocal case. Comparison between the heat flux densities calculated by JASMINE (dashed-dot, blue), OSHUN (solid, green), CALDER (solid, violet), ALADIN (dashed, red) and by Spitzer-Harm (SH) formula (dotted, black). Other notations are the same as in Fig. 4.2.1.

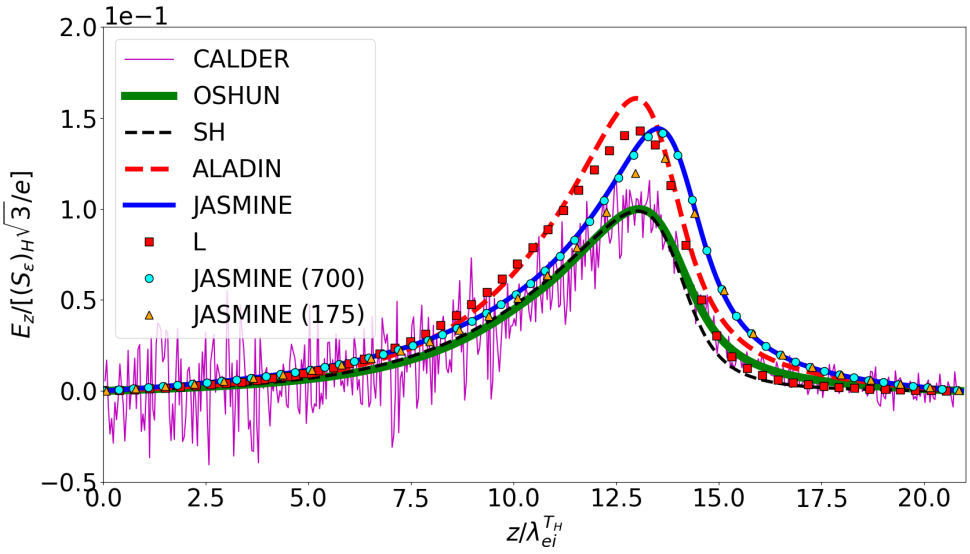


Figure 4.2.8: Nonlocal case. Comparison between the electric fields calculated by JASMINE (solid, blue), OSHUN (solid, green), CALDER (solid, violet), ALADIN (dashed, red) and by Spitzer-Harm (SH) (dashed, black) and Lorentz (L) (dashed-dot, violet) formulas. Other notations are the same as in Fig. 4.2.1.

The relative errors of the distribution functions, heat flux density and electric field are plotted in Fig. 4.2.9 for several meshes. For $q_{ez}$ and $E_z$, both norms $||.||_\infty$ and $||.||_2$ are plotted, whereas for distribution functions only the latter is shown. Having no analytical formulas, we used reference solutions $(r)$ provided by JASMINE for $I, G = 11200$. Consequently, in Fig. 4.2.9 the observed acceleration of convergence is not proper to our scheme but is artificial.

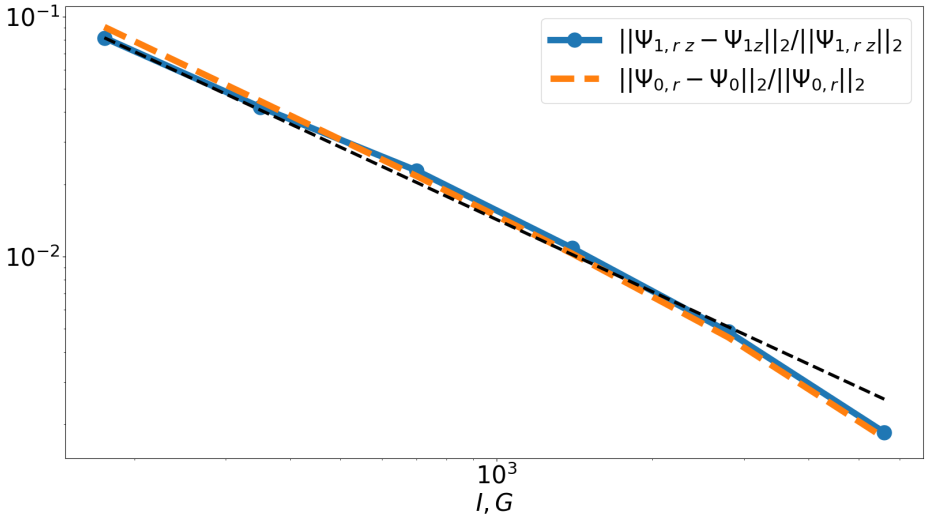


(a)

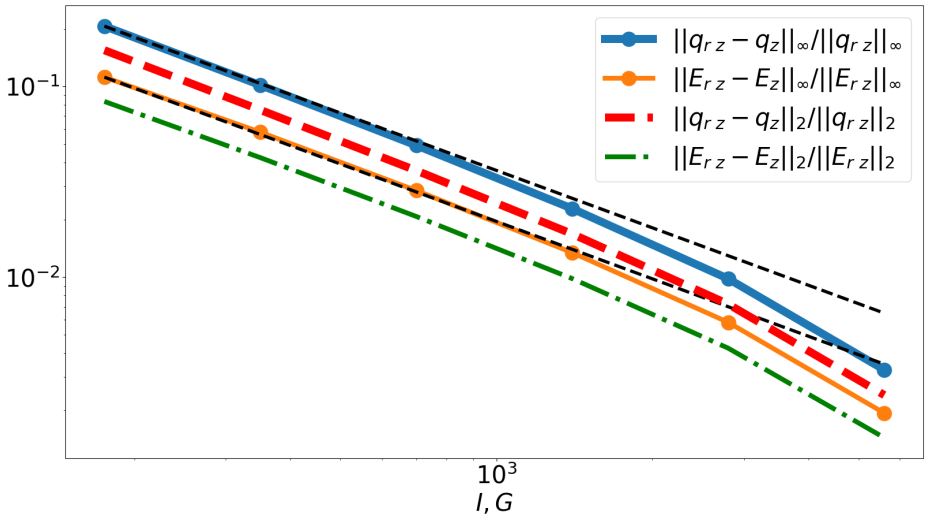


(b)

Figure 4.2.9: Nonlocal case. Relative errors in function of the number of cells in space $I$ and energy $G$. The subscript $r$ denotes the results provided by JASMINE for $I, G = 11200$. Other notations are the same as in Fig. 4.2.4.

## 4.3 Coupling to macroscopic evolution

In order to fulfill the mission for which it was designed, the kinetic module must provide the asymptotic solutions with sufficient efficiency. In view of this, the usage of a local time step within the scheme was proposed. In Sec. 4.3.1, the resulting gains in performance are quantified by examining the convergence in time. Estimates are especially made regarding the computation times when the coupling to a macroscopic solver is done. Here, the conservation properties of the model can be decisive in maintaining accuracy. This issue is addressed in the Sec. 4.3.2.

### 4.3.1 Dependence on initial conditions. Performances.

The evolution of electrons is governed by hydrodynamic equations, which are projections on $P_0$, $(2m_e\epsilon)^{1/2}\mathbf{P}_1$ and $\epsilon P_0$ of the Vlasov-Landau's kinetic equation, integrated over energies. At a given time, the heat flux density, stress viscosity and - in case of high $Z$ - electric field are computed from the kinetic model. Depending on the precision requirement, these values may be used for several time steps of the macroscopic evolution before being computed again. As a consequence, each kinetic computation may start from the values obtained in one of the previous hydrodynamic time steps. This has been done for the nonlocal case considered in Sec. 4.2.

A first temperature profile $T_1$ is used in JASMINE for $2 \times 10^4$ iterations. Starting from solutions obtained with $T_1$, JASMINE then performs $2 \times 10^4$ additional iterations with another temperature profile $T_2$. Between $T_1$ and $T_2$, the temperature evolved during one average collision time in the hot region, $(\nu_{ei}^{T_H})^{-1}$, corresponding to a variation of about 5% of the heat flux density in OSHUN, CALDER or ALADIN. As shown in Figs. 4.3.1 and 4.3.2, this naturally leads to a faster convergence toward the kinetic solution associated to $T_2$. In any phase, the *local* time step (4.21) (solid blue and dashed orange curves) leads to a significant improvement of the convergence compared to the conventional, *global*, time step (solid green and dashed red).

| Number of groups | Computation time [s] | |
|---|---|---|
| | SNB | JASMINE |
| 300 | 4 | 13 |
| 1000 | 13 | 40 |

Table 4.3.1: Computation times required by SNB and JASMINE, without parallelization, for 300 and 1000 velocity groups in the nonlocal case of the Sec. 3.2.3 considered in the previous chapter. The number of cells in space is 2000.

The price for improving the accuracy of the distribution functions is, however, a greater computation time compared to the multigroup method of Schurtz *et al* [91] (SNB). Without parallelization and for 2000 cells in space, the computation times for the nonlocal case treated in the previous chapter are given in Tab. 4.3.1.

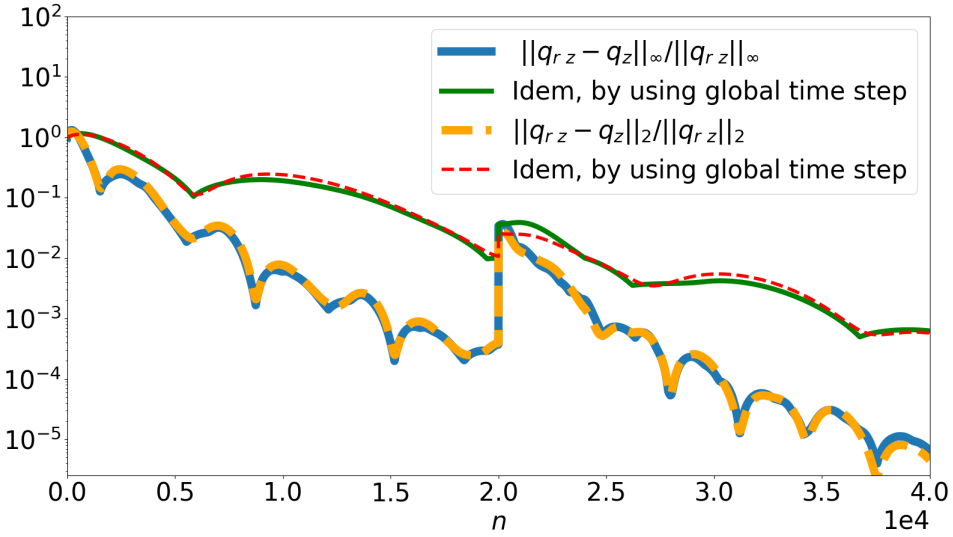


Figure 4.3.1: Nonlocal case. Relative errors on $q_z$ in function of the number of iteration $n$ with norms $||.||_\infty$ (solid, blue) and $||.||_2$ (dashed, orange). The finer curves (solid, green) and (dashed, red) represent error for the former and latter norm respectively, but by using the global time step determined by the more restrictive CFL condition. At $n = 2 \times 10^4$, the temperature profile is slightly changed to mimic its hydrodynamic evolution.

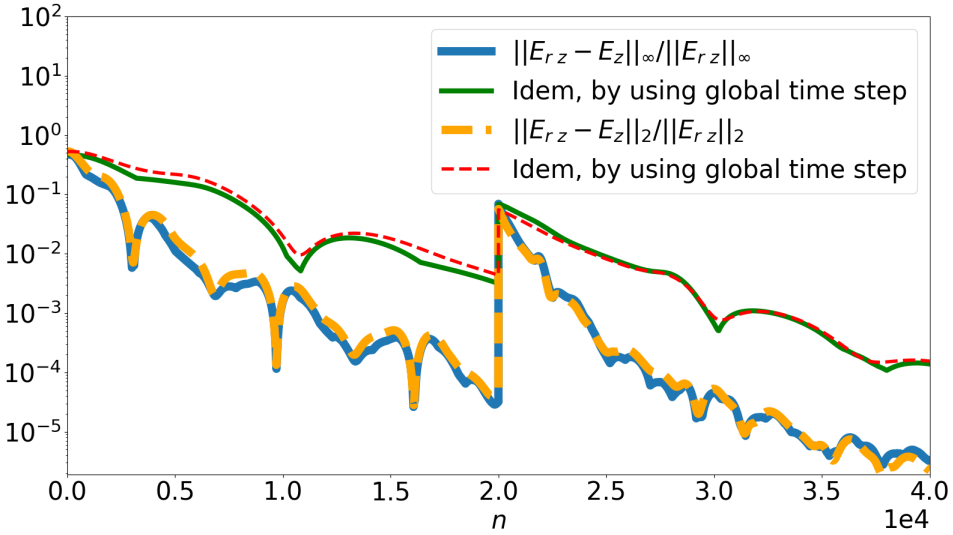


Figure 4.3.2: Same as in Fig.4.3.1 but for the electric field $E_z$.

Results shown in Sec. 3.2.3 correspond to 1000 groups in velocity. With JASMINE, this number can be reduced to 300 by having a tolerance of about 5% on the maximum error committed on the heat flux density. With SNB, the number of groups in velocity required to obtain a converged heat flux density is lower than for reaching convergence of the distribution function: a few dozen are sufficient and the computation time is a fraction of a second.

JASMINE, and SNB, provides a stationary kinetic solution for fixed hydrodynamic profiles, whereas ALADIN and OSHUN solve non-stationary kinetic equations. Thus, a rigorous comparison between the computational performances of these codes deserves a special attention, and we only give here an estimate on the order of magnitude with our current implementation: in a macroscopic scale simulation, JASMINE would reduce, at least, the computational time by a factor three with respect to ALADIN, and by a factor thirty with respect to OSHUN.

### 4.3.2 Conservation properties

As a consequence of the local conservation laws of electrons, linear momentum and energy, the functions 1, $(2m_e\epsilon)^{1/2}\mathbf{\Omega}$ and $\epsilon$ must be collisional invariants [33]. This means that all integrals of the set

$$\{\mathcal{S}_N, \mathcal{S}_\mathbf{P}, \mathcal{S}_\mathcal{E}\} = \int_{\mathbb{S}^2\times\mathbb{R}_+} \{P_0, (2m_e\epsilon)^{1/2}\mathbf{P}_1, \epsilon P_0\} \left(\frac{2\epsilon}{m_e}\right)^{1/2} \mathcal{C}_{\rm ee}(\Psi, \Psi_M) m_e^{-1} d\epsilon d^2\Omega, \tag{4.26}$$

must be equal to zero. By using the expansion $\Psi = \Psi_{\ell,i_1\ldots i_\ell} P_{\ell,i_1\ldots i_\ell}$, the contributions of the spherical Laplacian in the collision operator (4.4) are the opposite of

$$\frac{\ell(\ell+1)}{4} n_e \phi(Z) Y_{ee} \int_0^{+\infty} \epsilon^{-2} \Psi_{\ell,i_1\ldots i_\ell} \left( \int_{\mathbb{S}^2} \{P_0, (2m_e\epsilon)^{1/2}\mathbf{P}_1, \epsilon P_0\} P_{\ell,i_1\ldots i_\ell} m_e^{-1} d^2\Omega \right) d\epsilon.$$

By orthogonality, the spherical Laplacian therefore preserves the number of electrons and the energy as expected. It is, however, responsible for an algebraic creation of linear momentum per unit time and volume equals to

$$-\frac{4\pi}{3}\phi(Z) n_e Y_{ee} \int_0^{+\infty} \frac{\mathbf{\Psi}_1}{(2m_e\epsilon)^{1/2}} \frac{d\epsilon}{\epsilon}.$$

The contributions of the remaining part of operator (4.4) are:

$$\phi(Z) n_e Y_{ee} \int_{\mathbb{S}^2\times\mathbb{R}_+} \{P_0, (2m_e\epsilon)^{1/2}\mathbf{P}_1, \epsilon P_0\} \partial_\epsilon \epsilon^{-1} (\Psi - \Psi_M) m_e^{-1} d\epsilon d^2\Omega.$$

Thus, the total algebraic creation per unit time and volume of electrons $\mathcal{S}_n$, linear momentum $\mathcal{S}_\mathbf{p}$, and energy $\mathcal{S}_\mathcal{E}$, are:

$$\mathcal{S}_n = \frac{3}{2}\frac{\phi(Z)}{Z}(2\pi\epsilon_{T_H})^{3/2}\nu_{ei}^{T_H} \left[\frac{\Psi_0 - \Psi_M}{\epsilon}\right]_0^\infty, \tag{4.27}$$

$$\mathcal{S}_\mathbf{p} = \frac{\phi(Z)}{Z}(2\pi\epsilon_{T_H})^{3/2} m_e^{1/2}\nu_{ei}^{T_H} \left( \left[\frac{\mathbf{\Psi}_1}{\sqrt{2m_e\epsilon}}\right]_0^\infty - \int_0^\infty \frac{\mathbf{\Psi}_1}{\sqrt{2m_e\epsilon}} \frac{d\epsilon}{\epsilon} \right), \tag{4.28}$$

$$\mathcal{S}_\mathcal{E} = \frac{3}{2}\frac{\phi(Z)}{Z}(2\pi\epsilon_{T_H})^{3/2}\nu_{ei}^{T_H} \left( [\Psi_0 - \Psi_M]_0^\infty - \int_0^\infty \frac{\Psi_0 - \Psi_M}{\epsilon} d\epsilon \right). \tag{4.29}$$

We used $n_e Y_{ee} = (3/2) m_e^{1/2} \epsilon_{T_H}^{3/2} \nu_{ei}^{T_H} / Z$. The numerical values of these creation terms will be given in the nonlocal case presented in Sec. 4.2.2. On a duration $(\nu_{ei}^{T_H})^{-1}$, the algebraic number of electrons created, $\mathcal{S}_n (\nu_{ei}^{T_H})^{-1}$, is on average about 14% of the electron density $n_e$. Likewise, $\mathcal{S}_\mathcal{E} (\nu_{ei}^{T_H})^{-1} / [3/2 n_e \epsilon_{T_H}]$ is, on average, about 1%. The algebraic creation of linear momentum per unit time and volume, $\mathcal{S}_\mathbf{p}$, is, on that duration, negligible. Indeed, in the used reference frame the electron mean velocity is zero, as visible in the formula (4.5) defining $\Psi_M$. The ions are at rest in this reference frame because it is associated to the ion hydrodynamic flow of velocity $u_i$ in the laboratory frame. The ion population carries a linear momentum per unit volume of about $n_i m_i u_i$ in the laboratory frame, whereas that one carried by the electron population is about $\mathcal{S}_\mathbf{P} (\nu_{ei}^{T_H})^{-1} + n_e m_e u_i$. These two terms have comparable magnitudes. We noted $n_i = n_e / Z$ the ion density and $m_i \gtrsim 1800\ m_e$ the ion mass. Thus, the relative importance of $\mathcal{S}_\mathbf{p}$ is measured by the ratio $[\mathcal{S}_\mathbf{p} (\nu_{ei}^{T_H})^{-1} + n_e m_e u_i] / (n_i m_i u_i) \simeq m_e / m_i \lesssim 0.1\%$ for typical values of $u_i$ in ICF plasmas [3].

The duration of the implosion process described in the introduction of this thesis is about three thousands $(\nu_{ei}^{T_H})^{-1}$. Hence these creation terms may become very large. This is unimportant, because the kinetic model is only involved to provide the instantaneous values of the heat flux density, stress viscosity tensor and electric field which are used in the hydrodynamic equations managing the plasma evolution. Latter equations are not those derived from the reduced model, but those obtained from the Vlasov-Landau's kinetic equation, whose collision operators fulfill the conservation laws [33]. Problems may arise if, in order to keep details about the behaviour of the distribution function on a certain duration and spatial domain, the plasma evolution is divided between the resolutions of Eqs. (4.6)-(4.7) and the hydrodynamic equations.

In that case, even if $\mathcal{S}_n$, $\mathcal{S}_\mathbf{p}$ and $\mathcal{S}_\mathcal{E}$ can be minimized by choosing appropriate boundary conditions in energy, they cannot be set to zero simultaneously. An alternative approach would be to add the opposite of these algebraic creations per unit time and volume as source terms in the corresponding hydrodynamic equations. This is not an artificial way of compensating these creation terms, since such a procedure can be justified by analysing the physical framework of the operator $\mathcal{C}_{ee}$ (4.4). We shall precise this point. As we emphasized in Ref. [42], the expression of $\mathcal{C}_{ee}$ is derived by focusing on collisions between - highly energetic - suprathermal electrons (S) with - low energetic - thermal electrons at equilibrium (M). This implicitly means separating the electron population in two open subsystems of populations (S) and (M) that exchange particles, linear momentum and energy. Because density, mean velocity and temperature are low order moments of the distribution function, they mainly depend on the behaviour of the population (M), whereas high order moments such as heat flux density are sensitive to the dynamic of the population (S). The electron-electron operator (4.4) may thus be noted $\mathcal{C}_{\mathrm{SM}}$ and the conservation laws are fulfilled when all integrals of the following set are equal to zero:

$$\int_{\mathbb{S}^2 \times \mathbb{R}_+} \{P_0, (2 m_e \epsilon)^{1/2} \mathbf{P}_1, \epsilon P_0\} \left( \frac{2\epsilon}{m_e} \right)^{1/2} [\mathcal{C}_{\mathrm{SM}} + \mathcal{C}_{\mathrm{MS}}]\, m_e^{-1} d\epsilon d^2\Omega.$$

If so, the contributions of the electron-electron collisions do not appear when considering the projections of the kinetic equation (4.2) on $P_0$, $(2m_e\epsilon)^{1/2}\mathbf{P}_1$ and $\epsilon P_0$. As the kinetic model only accounts for $\mathcal{C}_{\mathrm{SM}}$, the number of electrons, linear momentum and energy would be conserved if integrals $\{-\mathcal{S}_n, -\mathcal{S}_{\mathbf{p}}, -\mathcal{S}_{\mathcal{E}}\}$ are added as source terms in the corresponding hydrodynamic equations.

## 4.4 Conclusion

A deterministic numerical scheme for the reduced kinetic model improved in the previous chapter has been developed. Compared to the work of Del Sorbo *et al* [57], a different variable change was adopted to reduce the complexity of the resulting P1 system. The underlying equations have been derived, in App. 4.A, with a less restrictive assumption on the distribution function.

Thanks to a detailed analysis of local Riemann's problems, the condition for applicability of the schemes proposed by Del Sorbo *et al* and Holec *et al* in Refs. [57, 128] was determined for the first time. It is linked to one of the eigenvalues of the Jacobian of the energy flux, the sign of which can change when the electric field becomes too large. This situation is encountered when the electron temperature profile is sufficiently steep. An explicit threshold (4.25) on the Knudsen's number has been derived, exploiting the fact that the electric field given by the model remains very close to that given by the Lorentz's formula, even in the nonlocal regime.

Such limitation has been overcame by considering a stationary solution of the *non-stationary* kinetic equations. The advantage of introducing the time variable is justified by an appropriate treatment of fluxes in energy. The convergence of the resulting scheme has been improved by introducing a *local* time step, the value of which is set by the local CFL's condition. Nevertheless, it remains to perform a mathematical analysis to determine the range of applicability of this original approach. Finally, we pointed out the non conservative properties of the model by deriving the terms of electron, momentum and energy creation. Although this is not an obstacle to the use of the model, we have proposed, if necessary, a solution based on physical arguments to couple it to an hydrodynamic code.

This page is unintentionally left not blank.

# Appendix

## 4.A Derivation of the hyperbolic system

In Ref. [57], the author used the expansion on $\ell$-degree monomials $\Omega_{i_1}\Omega_{i_2}...\Omega_{i_\ell}$, whereas most of them are neither pairwise orthogonal nor eigenfunctions of the spherical Laplacian $(-\mathsf{L}^2)$. As a results the form $\Psi = \Psi_0 + \mathbf{\Psi_1}\cdot\mathbf{\Omega}$ was supposed to handle calculations. As shown hereafter, a decomposition through Maxwell's multipoles allows to free ourselves from this assumption, and higher order components $\Psi_{\ell,i_1...i_\ell}$ with $\ell \geq 3$ may be non-zero, having their own evolution.

### 4.A.1 Projection on $P_0$

After a division by $4\pi$, Eq. (4.2) projected on $P_0 = 1$ reads:

$$\left(\frac{m_e}{2\epsilon}\right)\partial_t\Psi_0 + \frac{\boldsymbol{\nabla}\cdot\mathbf{\Psi}_1}{3} - \frac{e\mathbf{E}}{\epsilon}\cdot\left(\frac{\epsilon\partial_\epsilon\mathbf{\Psi_1} - \beta/2\mathbf{\Psi}_1}{3} + \frac{1}{8\pi}\int_{\mathbb{S}^2}(\mathsf{I}-\mathbf{\Omega}\otimes\mathbf{\Omega})\cdot\partial_{\mathbf{\Omega}}\Psi d^2\Omega\right)$$
$$= \frac{S_\epsilon}{16\pi\epsilon}\left(1+\frac{Z}{\phi(Z)}\right)\int_{\mathbb{S}^2}(-\mathsf{L}^2)(\Psi)d^2\Omega + \frac{S_\epsilon}{\epsilon}\epsilon^{1+\beta/2}\partial_\epsilon\epsilon^{-\beta/2}(\Psi_0-\Psi_M). \quad (4.30)$$

By using the expansion $\Psi = \Psi_{\ell,i_1...i_\ell}P_{\ell,i_1...i_\ell}$ and orthogonality relation (2.11), the integral containing the spherical Laplacian vanishes because the eigenvalue associated to $P_0$ is zero:

$$\int_{\mathbb{S}^2}(-\mathsf{L}^2)(\Psi)d^2\Omega = -\ell(\ell+1)\Psi_{\ell,i_1...i_\ell}\int_{\mathbb{S}^2}P_0P_{l,i_1...i_\ell}d^2\Omega = 0.$$

We note

$$I_x(\Psi) = \int_{\mathbb{S}^2}(\delta_{xj}-\Omega_x\Omega_j)\frac{\partial}{\partial\Omega_j}\Psi d^2\Omega, \quad (4.31)$$

the $x$-component of the integral in which the gradient of $\Psi$ along $\mathbf{\Omega}$ is involved. This integral cannot be computed through a by parts integration, because $\mathbb{S}^2$ has no boundary. We give two options to compute $I_x(\Psi)$. According to Stokes' theorem, the flux through $\mathbb{S}^2$ of the curl of any smooth vector field $\mathbf{V}$ vanishes:

$$\int_{\mathbb{S}^2}\partial_{\mathbf{\Omega}}\times\mathbf{V}\cdot\mathbf{\Omega}\ d^2\Omega = 0, \quad (4.32)$$

because $\mathbb{S}^2$ leans on a contour reduced to a point. We consider a vector field of the form $\mathbf{V} = \Psi\mathbf{W}$ such that $\partial_{\mathbf{\Omega}}\times\mathbf{V}\cdot\mathbf{\Omega} = \Psi\partial_{\mathbf{\Omega}}\times\mathbf{W}\cdot\mathbf{\Omega} + \partial_{\mathbf{\Omega}}\Psi\times\mathbf{W}\cdot\mathbf{\Omega}$.

Here, we employed the notation $\Psi$ for a function of $\mathbb{R}^3$ whose restriction to $\mathbb{S}^2$ is the distribution function introduced in Sec. The integral of the first term, $\Psi\partial_{\mathbf{\Omega}}\times\mathbf{W}\cdot\mathbf{\Omega}$, will be easily expressed in terms of the components of $\Psi$ on Maxwell's multipoles. We look for a vector field $\mathbf{W}$ such that the integral of the second term, $\partial_{\mathbf{\Omega}}\Psi\times\mathbf{W}\cdot\mathbf{\Omega}$, is equal to the researched integral $I_x(\Psi)$. A sufficient condition is:

$$(\delta_{xj}-\Omega_x\Omega_j)K_j=\epsilon_{jab}K_aW_b\Omega_j, \tag{4.33}$$

where $\epsilon_{jab}$ is the Levi-Civita's symbol and $\mathbf{K}=\partial_{\mathbf{\Omega}}\Psi$. By looking to the left hand side, we conclude that $W_b$ must depend on the components of $\mathbf{e}_x=(1,0,0)^T$ and $\mathbf{\Omega}$. Moreover, $(\delta_{xj}-\Omega_x\Omega_j)$ is symmetric with respect to permutations of indices, whereas $\epsilon_{jab}\Omega_j$ is anti-symmetric. Therefore $W_b$ must have an anti-symmetric expression. The simplest choice for $W_b$ is $\epsilon_{bcd}\Omega_c(\mathbf{e}_x)_d$. Substituting this expression in the right hand side of Eq. (4.33) leads to:

$$\begin{aligned}\epsilon_{jab}\epsilon_{bcd}\Omega_c(\mathbf{e}_x)_dK_a\Omega_j&=(\delta_{jc}\delta_{ad}-\delta_{jd}\delta_{ac})\Omega_c\Omega_j(\mathbf{e}_x)_dK_a\\&=(\mathbf{e}_x)_aK_a-(\mathbf{e}_x)_j\Omega_j\Omega_aK_a=(\delta_{xa}-\Omega_x\Omega_a)K_a,\end{aligned}$$

which is exactly the left hand side of Eq. (4.33). Thus, $\mathbf{W}=\mathbf{\Omega}\times\mathbf{e}_x$. Otherwise, we can explicitly write Eq. (4.33) on $\mathbb{S}^2$:

$$(\Omega_y^2+\Omega_z)^2K_x-\Omega_x\Omega_yK_y-\Omega_x\Omega_zK_z \tag{4.34}$$
$$=(K_yW_z-K_zW_y)\Omega_x+(K_zW_x-K_xW_z)\Omega_y$$
$$+(K_xW_y-K_yW_x)\Omega_z. \tag{4.35}$$

The first term in left hand side (4.34) is recovered in the right hand side (4.35) by imposing $W_y=\Omega_z$ and $W_z=-\Omega_y$. By doing so the remaining terms in (4.34) automatically appear in (4.35) and we may set $W_x=0$. So $\partial_{\mathbf{\Omega}}\times\mathbf{W}\cdot\mathbf{\Omega}=-2\Omega_x$ and Eq. (4.32) reads:

$$I_x(\Psi)-2\int_{\mathbb{S}^2}\Omega_x\Psi d^2\Omega=0, \tag{4.36}$$

leading to $I_x(\Psi)=8\pi/3\Psi_{1,x}$. The integrals $I_y(\Psi)$ and $I_z(\Psi)$ are computed in the same way.

An alternative derivation of this result is as follows. We use the expansion $\Psi=\Psi_{\ell,i_1\ldots i_\ell}P_{\ell,i_1\ldots i_\ell}$ to write

$$I_x(\Psi)=\Psi_{\ell,i_1\ldots i_\ell}\int_{\mathbb{S}^2}(\delta_{xj}-\Omega_x\Omega_j)\frac{\partial}{\partial\Omega_j}P_{\ell,i_1\ldots i_\ell}d^2\Omega, \tag{4.37}$$

together with the following equality, written in Ref. [52]:

$$\int_{\mathbb{S}^2}P_{\ell,i_1\ldots i_\ell}\ \Omega_{j_1}\Omega_{j_2}\ldots\Omega_{j_{\ell'}}d^2\Omega=0\text{ if }\ell'<\ell. \tag{4.38}$$

For a given $\ell$, $\partial P_{\ell,i_1\ldots i_\ell}/\partial\Omega_j$ is of order $\ell-1$ and so can be expanded on the Maxwell's multipoles of order $\ell-1$. Because of the relation (4.38), the integral of its product with $\delta_{xj}-\Omega_x\Omega_j$ vanishes if $2<\ell-1$. Thus, in the sum (4.37) there

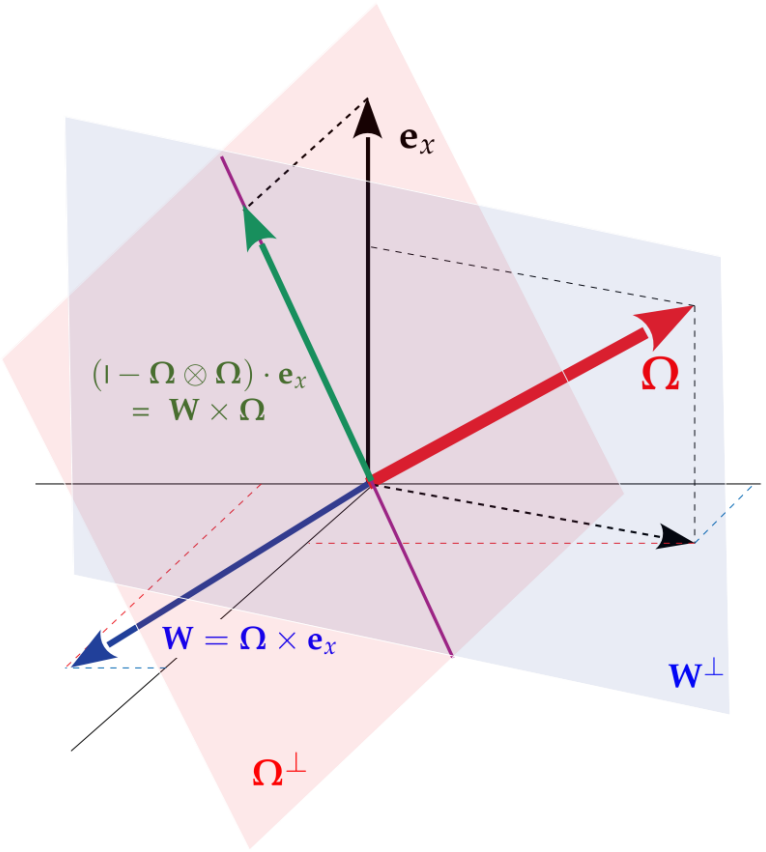


Figure 4.A.1: Illustration of Eq. (4.33).

only remains the terms corresponding to $\ell = 1, 2, 3$. As $\delta_{xj} - \Omega_x\Omega_j$ is an even function, the terms for which $\ell - 1 = 1$ vanish. Thus,

$$I_x(\Psi) = \int_{\mathbb{S}^2} (\delta_{xj} - \Omega_x\Omega_j) \left[ \Psi_{1,i} \frac{\partial P_{1,i}}{\partial \Omega_j} + \Psi_{3,k\ell m} \frac{\partial P_{3,k\ell m}}{\partial \Omega_j} \right] d^2\Omega,$$

where the Maxwell's multipoles of order $\ell = 3$ are

$$P_{3,klm} = \Omega_k\Omega_l\Omega_m - \frac{3}{5}(\Omega_k\delta_{\ell m} + \Omega_l\delta_{mk} + \Omega_m\delta_{kl}).$$

Since

$$\begin{aligned} \frac{\partial P_{3,klm}}{\partial \Omega_j} &= \delta_{jk}\Omega_l\Omega_m + \Omega_k\delta_{jl}\Omega_m + \Omega_k\Omega_l\delta_{jm} \\ &\quad - \frac{3}{5}\big[\delta_{jk}\delta_{lm} + \delta_{jl}\delta_{km} + \delta_{jm}\delta_{kl}\big], \end{aligned}$$

we have,

$$\begin{aligned} \int_{\mathbb{S}^2} (\delta_{xj} - \Omega_x\Omega_j) \frac{\partial P_{3,klm}}{\partial \Omega_j} d^2\Omega &= (\delta_{xk}\delta_{lm} + \delta_{xl}\delta_{km}) \frac{4\pi}{3} - 3 \int_{\mathbb{S}^2} \Omega_x\Omega_k\Omega_l\Omega_m d^2\Omega \\ &\quad - \frac{3}{5}\big[\delta_{xk}\delta_{lm} + \delta_{xl}\delta_{km} + \delta_{xm}\delta_{kl}\big] \left(4\pi - \frac{4\pi}{3}\right) \\ &= 0, \end{aligned}$$

because the integral of $\Omega_x\Omega_k\Omega_l\Omega_m$ over $\mathbb{S}^2$ is equal to $(4\pi/5)(\delta_{xk}\delta_{lm}+\delta_{xl}\delta_{km}+\delta_{xm}\delta_{kl})$. Thus, in the sum (4.37) there only remain the one order terms $\ell=1$:

$$I_x(\Psi)=\Psi_{1,i}\int_{\mathbb{S}^2}(\delta_{xj}-\Omega_x\Omega_j)\delta_{ij}d^2\Omega=\frac{8\pi}{3}\Psi_{1,x}.$$

Finally, we introduce $S_T$ (4.8) in (4.30). To that purpose, we remark that $S_\epsilon\propto 1/\epsilon$, and so for any function $X$ of $\epsilon$:

$$S_\epsilon\partial_\epsilon X=\partial_\epsilon S_\epsilon X+\frac{S_\epsilon}{\epsilon}X. \tag{4.39}$$

This relation (4.39) with $X=\Psi_0-\Psi_M$ allows to write:

$$\begin{aligned}\frac{S_\epsilon}{\epsilon}\epsilon^{1+\beta/2}\partial_\epsilon\epsilon^{-\beta/2}\left(\Psi_0-\Psi_M\right)&=\frac{S_\epsilon}{\epsilon}\left[-\frac{\beta}{2}(\Psi_0-\Psi_M)+\epsilon\partial_\epsilon(\Psi_0-\Psi_M)\right]\\&=\partial_\epsilon S_\epsilon(\Psi_0-\Psi_M)+\frac{1-\beta/2}{\epsilon}S_\epsilon(\Psi_0-\Psi_M).\end{aligned}$$

Thus the Eq. (4.6) is recovered.

### 4.A.2 Projection on $\mathbf{P}_1$

After a division by $4\pi/3$, Eq. (4.2) projected on $\mathbf{P}_1=\mathbf{\Omega}$ reads:

$$\begin{aligned}&\left(\frac{m_e}{2\epsilon}\right)\partial_t\mathbf{\Psi}_1+\boldsymbol{\nabla}\cdot\frac{3}{4\pi}\int_{\mathbb{S}^2}\mathbf{\Omega}\otimes\mathbf{\Omega}\Psi d^2\Omega-\frac{e\mathbf{E}}{\epsilon}\cdot\Big(\epsilon\partial_\epsilon\frac{3}{4\pi}\int_{\mathbb{S}^2}\mathbf{\Omega}\otimes\mathbf{\Omega}\Psi d^2\Omega\\&-\frac{\beta}{2}\frac{3}{4\pi}\int_{\mathbb{S}^2}\mathbf{\Omega}\otimes\mathbf{\Omega}\Psi d^2\Omega+\frac{3}{8\pi}\int_{\mathbb{S}^2}\mathbf{\Omega}[\mathsf{I}-\mathbf{\Omega}\otimes\mathbf{\Omega}]\cdot\partial_{\mathbf{\Omega}}\Psi d^2\Omega\Big)\\&=\frac{3S_\epsilon}{16\pi\epsilon}\left(1+\frac{Z}{\phi(Z)}\right)\int_{\mathbb{S}^2}\mathbf{\Omega}(-\mathsf{L}^2)(\Psi)d^2\Omega+\frac{S_\epsilon}{\epsilon}\epsilon^{1+\beta/2}\partial_\epsilon\epsilon^{-\beta/2}\mathbf{\Psi}_1.\end{aligned}\tag{4.40}$$

By using the expansion $\Psi=\Psi_{\ell,i_1\dots i_\ell}P_{\ell,i_1\dots i_\ell}$ and orthogonality relation (2.11), the $k$-component of the integral containing the spherical Laplacian reads:

$$\int_{\mathbb{S}^2}\Omega_k(-\mathsf{L}^2)(\Psi)d^2\Omega=-\ell(\ell+1)\Psi_{\ell,i_1\dots i_\ell}\int_{\mathbb{S}^2}P_{1,k}P_{\ell,i_1\dots i_\ell}d^2\Omega=-2\frac{4\pi}{3}\Psi_{1,k},$$

and

$$\int_{\mathbb{S}^2}\Omega_i\Omega_j\Psi d^2\Omega=\int_{\mathbb{S}^2}\left(\frac{\delta_{ij}}{3}P_0+P_{2,ij}\right)\Psi d^2\Omega=\frac{4\pi}{3}\delta_{ij}\Psi_0+\frac{2}{3}||P_{2,ij}||^2\Psi_{2,ij}.$$

We note

$$J_{kx}(\Psi)=\int_{\mathbb{S}^2}\Omega_k(\delta_{xj}-\Omega_x\Omega_j)\frac{\partial}{\partial\Omega_j}\Psi d^2\Omega. \tag{4.41}$$

The relation (4.36) is valid for any smooth function $\Psi$. We apply it for $\Omega_k\Psi$, which yields:

$$\begin{aligned}2\int_{\mathbb{S}^2}\Omega_x\Omega_k\Psi d^2\Omega&=\int_{\mathbb{S}^2}(\delta_{xj}-\Omega_x\Omega_j)\left(\delta_{jk}\Psi+\Omega_k\frac{\partial\Psi}{\partial\Omega_j}\right)d^2\Omega\\&=\int_{\mathbb{S}^2}(\delta_{xk}-\Omega_x\Omega_k)\Psi d^2\Omega+J_{kx}(\Psi).\end{aligned}\tag{4.42}$$

So,

$$J_{kx}(\Psi) = \int_{\mathbb{S}^2} (3\Omega_k\Omega_x - \delta_{kx})\Psi d^2\Omega = 3||P_{2,kx}||^2\Psi_{2,kx}.$$

In order to have a closed system on $\Psi_0$ and $\mathbf{\Psi}_1$, we must express the components $\Psi_{2,ij}$ as a combination of $\Psi_0$, $\Psi_{1,i}$ and $\Psi_{1,j}$. The simplest choice, called the P1 closure, is $\Psi_{2,ij} = 0$, for which Eq. (4.40) is:

$$\begin{aligned}&\left(\frac{m_e}{2\epsilon}\right)\partial_t\mathbf{\Psi}_1 + \boldsymbol{\nabla}\Psi_0 - \frac{e\mathbf{E}}{\epsilon}\cdot\left(\epsilon\partial_\epsilon\Psi_0 - \frac{\beta}{2}\Psi_0\right)\\ &= -\frac{S_\epsilon}{2\epsilon}\left(1 + \frac{Z}{\phi(Z)}\right)\mathbf{\Psi}_1 + \frac{S_\epsilon}{\epsilon}\epsilon^{1+\beta/2}\partial_\epsilon\left(\epsilon^{-\beta/2}\mathbf{\Psi}_1\right).\end{aligned} \tag{4.43}$$

We then use the relation (4.39) with $X = \mathbf{\Psi}_1$ in order to express the right hand side of the above equation (4.43) as

$$-\frac{S_\epsilon}{2\epsilon}\left(\beta - 1 + \frac{Z}{\phi(Z)}\right)\mathbf{\Psi}_1 + \partial_\epsilon S_\epsilon\mathbf{\Psi}_1.$$

Finally, we introduce $S_T$ (4.8) explicitly by adding and subtracting the following term:

$$-\partial_\epsilon\left(e\frac{\mathbf{E}}{3}\cdot\frac{\mathbf{\Psi_1}}{\Psi_0}\right),$$

in the left hand side of Eq. (4.43) and Eq. (4.7) is recovered.

This page is unintentionally left not blank.

# 4.B Godounov's method. The approximate Riemann's solver of Harten, Lax and van Leer.

## 4.B.1 Idea

We consider the homogeneous advection equation:

$$\partial_\tau \mathbf{\Phi} + \partial_X \mathbf{F}(\mathbf{\Phi}) = \mathbf{0}, \tag{4.44}$$

where $X = z$ or $\epsilon$, and $\tau$ is a time variable. The link between $\tau$ and $t$ will be specified later. Here, we employ $\mathbf{\Phi}$ to denote one of the partial applications $(\tau, z) \mapsto \mathbf{\Phi}(t(\tau), z, \epsilon)$ and $(\tau, \epsilon) \mapsto \mathbf{\Phi}(t(\tau), z, \epsilon)$. The spatial domain contains $I$ cells of size $\Delta X$ indexed by $i \in \{0, ...I-1\}$. Time steps, of size $\Delta\tau$, are indexed by $n$. Integrating Eq. (4.44) on the control volume $[\tau^n, \tau^{n+1}] \times [X_{i-1/2}, X_{i+1/2}]$ leads to

$$\begin{aligned}\int_{X_{i-1/2}}^{X_{i+1/2}} \mathbf{\Phi}(\tau^{n+1}, X)dX = &\int_{X_{i-1/2}}^{X_{i+1/2}} \mathbf{\Phi}(\tau^n, X)dX \\ &- \int_{\tau^n}^{\tau^{n+1}} \left(\mathbf{F}[\mathbf{\Phi}(\tau, X_{i+1/2})] - \mathbf{F}[\mathbf{\Phi}(\tau, X_{i-1/2})]\right) d\tau. \end{aligned} \tag{4.45}$$

A cell, $[X_{i-1/2}, X_{i+1/2}]$, encloses by definition the smallest volume under which the variations of $\mathbf{\Phi}$ are not taken into account. Therefore, a discretized version of $\mathbf{\Phi}$ consists, at each time $\tau^n$, of a piecewise constant function whose value, $\mathbf{\Phi}_i^n$, jumps across the boundary of adjacent cells. The point is to precise the link between this piecewise function and the continuous function solution of Eq. (4.44). As suggested by the above integral relation, the finite-volume approach define these constants $\mathbf{\Phi}_i^n$ as the mean value of the exact function over the corresponding cells:

$$\mathbf{\Phi}_i^n = \frac{1}{X_{i+1/2} - X_{i-1/2}} \int_{X_{i-1/2}}^{X_{i+1/2}} \mathbf{\Phi}(\tau^n, X)dX \tag{4.46}$$

By developing the integrand around the middle of the cell $X_i$, we see that $\mathbf{\Phi}_i^n$ approaches $\mathbf{\Phi}(\tau^n, X_i)$ with an accuracy $\mathcal{O}(\Delta X^2)$. With this definition of $\mathbf{\Phi}_i^n$, the evolution of the piecewise function is provided by Eq. (4.45):

$$\mathbf{\Phi}_i^{n+1} = \mathbf{\Phi}_i^n - \frac{\tau^{n+1} - \tau^n}{X_{i+1/2} - X_{i-1/2}} [\mathbf{F}_{i+1/2}^n - \mathbf{F}_{i-1/2}^n],$$

where:

$$\mathbf{F}_{i+1/2}^n = \frac{1}{\tau^{n+1} - \tau^n} \int_{\tau^n}^{\tau^{n+1}} \mathbf{F}[\mathbf{\Phi}(\tau, X_{i+1/2})]d\tau. \tag{4.47}$$

As it is, this expression is not usable and must be approximated as a combination of the values of the piecewise function. We shall look for an estimation of $\mathbf{F}_{i+1/2}$ in terms of $\mathbf{\Phi}_i^n$ and $\mathbf{\Phi}_{i+1}^n$. By doing this, we are implicitly choosing the numerical domain of dependence of the point $(X_{i+1/2}, \tau^{n+1})$, *i.e.* the past cone of the event spotted by $(X_{i+1/2}, \tau^{n+1})$. Because the piecewise function has the same value $\mathbf{\Phi}_i^{n+1}$ in all the points $(X, \tau^{n+1})$ within the cell, the past cones of all the corresponding

events have the same vertex angle. These numerical domains of dependence are delimited by the purple, dotted lines with slopes $\pm\Delta X/\Delta\tau$ within the space-time diagram $(X,\tau)$ in Fig. 4.B.1. The ratio $\Delta X/\Delta\tau$ cannot be chosen arbitrarily. As shown by Courant, Friedrichs and Lewy (CFL) in Ref. [139], it must be chosen such that the numerical domain of dependence contains the exact domain of dependence associated to the partial differential equation (4.44). If the spectrum of the Jacobian $\partial\mathbf{F}/\partial\mathbf{\Phi}$ is real, Eq. (4.44) is hyperbolic and its domain of dependence is bounded by its two extreme characteristics, whose slopes are the lowest and the highest eigenvalues. In Fig. 4.B.1, these characteristics are the symmetric, green solid lines, corresponding to the case of constant eigenvalues $-S$ and $S$.

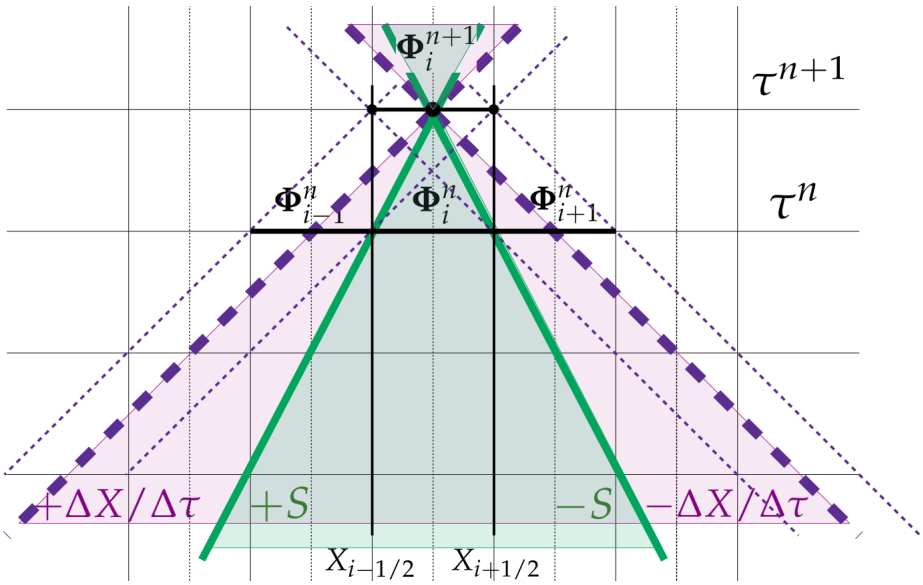


Figure 4.B.1: Space-time diagram with the domains of dependence of $(X_i,\tau^{n+1})$, associated to Eq. (4.44) (green) and to its numerical approximation (violet). The green cone is delimited by the green, solid characteristics with slopes $\pm S$. The violet cone is delimited by the violet, dashed lines with slopes $\pm\Delta X/\Delta\tau$. The fine dashed violet lines delimit the numerical domains of dependence of the extreme points $(X_{i-1/2},\tau^{n+1})$ and $(X_{i+1/2},\tau^{n+1})$ of the cell. If an expression of $\mathbf{F}_{i+1/2}$ would have been searched in terms of $\mathbf{\Phi}_{i-1}^n$, $\mathbf{\Phi}_i^n$, $\mathbf{\Phi}_{i+1}^n$ and $\mathbf{\Phi}_{i+1}^n$, the slopes delimiting the numerical domain of dependence would have been $\pm 2\Delta X/\Delta\tau$.

The inter cells flux $\mathbf{F}_{i+1/2}^n$ must account for the combined influence of $\mathbf{\Phi}_i^n$ and $\mathbf{\Phi}_{i+1}^n$ on the value $\mathbf{\Phi}_i^{n+1}$. As proposed by Godounov [145], this can be done by solving the local Riemann's problem centered in $X_{i+1/2}$, with initial states $\mathbf{\Phi}_i^n$ at left, and $\mathbf{\Phi}_{i+1}^n$ at right.

## 4.B.2 Approximate Riemann's solver

We consider the following Riemann's problem: a solution of the homogeneous advection equation (4.44) is researched on the domain $[X_i, X_{i+1}]$, with the following initial condition:

$$\mathbf{\Phi}(\tau^n, X) = \begin{cases} \mathbf{\Phi}_i^n & \text{if } X < X_{i+1/2} \\ \mathbf{\Phi}_{i+1}^n & \text{if } X > X_{i+1/2} \end{cases} \tag{4.48}$$

The lowest and the highest eigenvalues of $\partial\mathbf{F}/\partial\mathbf{\Phi}$, supposed constant within the volume $[\tau^n, \tau^{n+1}] \times [X_i, X_{i+1}]$, are noted $(S_L)^n_{i+1/2}$ and $(S_R)^n_{i+1/2}$ respectively. The CFL's condition is fulfilled for $X_i < X_{i+1/2} + (\tau^{n+1} - \tau^n)(S_L)^n_{i+1/2}$ and $X_{i+1} > X_{i+1/2} + (\tau^{n+1} - \tau^n)(S_R)^n_{i+1/2}$. Therefore, the values of $\mathbf{\Phi}$ at the edges of the cells are not disturbed on the interval $[\tau^n, \tau^{n+1}]$:

$$\mathbf{\Phi}(\tau, X_i) = \mathbf{\Phi}^n_i, \quad \mathbf{\Phi}(\tau, X_{i+1}) = \mathbf{\Phi}^n_{i+1}. \tag{4.49}$$

In the region delimited by the two extreme characteristics, called the star region, the solution of the Riemann problem results from the combination of all waves with intermediates velocities. Harten, Lax and van Leer [146] proposed to approximate the solution in all the points of the star region by the mean state:

$$\mathbf{\Phi^*}_{i+1/2}(\tau) = \frac{1}{(\tau^{n+1} - \tau)[(S_R)^n_{i+1/2} - (S_L)^n_{i+1/2}]} \int_{X_{i+1/2}+(\tau^{n+1}-\tau)(S_L)^n_{i+1/2}}^{X_{i+1/2}+(\tau^{n+1}-\tau)(S_R)^n_{i+1/2}} \mathbf{\Phi}(\tau, X) dX \tag{4.50}$$

In the two-dimensional case, as considered here, the Jacobian matrix of the flux has only two eigenvalues and $\mathbf{\Phi^*}_{i+1/2}$ is the exact solution in the star region. For the purpose of expressing the inter-cell flux $\mathbf{F}_{i+1/2}$ in Sec. , we need to express $\mathbf{\Phi^*}^{n+1}_{i+1/2} = \mathbf{\Phi^*}_{i+1/2}(\tau^{n+1})$ in terms of $\mathbf{\Phi}^n_i$ and $\mathbf{\Phi}^{n+1}_i$. This will be done by expressing the integral of $\mathbf{\Phi}(\tau^{n+1}, X)$ on $[X_i, X_{i+1}]$ in two ways. The first manner relies on the Chasles' rule:

$$\begin{aligned}\int_{X_i}^{X_{i+1}} \mathbf{\Phi}(\tau^{n+1}, X) dX = &\int_{X_i}^{X_{i+1/2}+(\tau^{n+1}-\tau^n)(S_L)^n_{i+1/2}} \mathbf{\Phi}(\tau^{n+1}, X) dX \\ &+ \int_{X_{i+1/2}+(\tau^{n+1}-\tau^n)(S_L)^n_{i+1/2}}^{X_{i+1/2}+(\tau^{n+1}-\tau^n)(S_R)^n_{i+1/2}} \mathbf{\Phi}(\tau^{n+1}, X) dX \\ &+ \int_{X_{i+1/2}+(\tau^{n+1}-\tau^n)(S_R)^n_{i+1/2}}^{X_{i+1}} \mathbf{\Phi}(\tau^{n+1}, X) dX \end{aligned} \tag{4.51}$$

The first integral in the right hand side is equal to $[X_{i+1/2} + (\tau^{n+1} - \tau^n)(S_L)^n_{i+1/2} - X_i]\mathbf{\Phi}^n_i$, and the third one is equal to $[X_{i+1} - X_{i+1/2} - (\tau^{n+1} - \tau^n)(S_R)^n_{i+1/2}]\mathbf{\Phi}^n_{i+1}$. The second integral is the researched one. Now, we integrate Eq. (4.44) on $[\tau^n, \tau^{n+1}] \times [X_i, X_{i+1}]$. This leads to:

$$\begin{aligned}\int_{X_i}^{X_{i+1}} \mathbf{\Phi}(\tau^{n+1}, X) dX = &\int_{X_i}^{X_{i+1}} \mathbf{\Phi}(\tau^n, X) dX \\ &- \int_{\tau^n}^{\tau^{n+1}} \Big(\mathbf{F}[\mathbf{\Phi}(\tau, X_{i+1})] - \mathbf{F}[\mathbf{\Phi}(\tau, X_i)]\Big) d\tau \end{aligned} \tag{4.52}$$

By using the Chasles' rule and Eq. (4.48), the first integral of the right hand side is:

$$\begin{aligned}\int_{X_i}^{X_{i+1}} \mathbf{\Phi}(\tau^n, X) dX &= \int_{X_i}^{X_{i+1/2}} \mathbf{\Phi}(\tau^n, X) dX + \int_{X_{i+1/2}}^{X_{i+1}} \mathbf{\Phi}(\tau^n, X) dX \\ &= (X_{i+1/2} - X_i)\mathbf{\Phi}^n_i + (X_{i+1} - X_{i+1/2})\mathbf{\Phi}^n_{i+1}. \end{aligned}$$

Using Eq. (4.49), the second integral of Eq. (4.52) is equal to $(\tau^{n+1}-\tau^n)[\mathbf{F}(\mathbf{\Phi}^n_{i+1})-\mathbf{F}(\mathbf{\Phi}^n_i)]$. Then, we compare the expressions (4.51) and (4.52), and we deduce that

$$\int_{X_{i+1/2}+(\tau^{n+1}-\tau^n)(S_L)^n_{i+1/2}}^{X_{i+1/2}+(\tau^{n+1}-\tau^n)(S_R)^n_{i+1/2}} \mathbf{\Phi}(\tau^{n+1},X)dX$$
$$= (\tau^{n+1}-\tau^n)\Big[(S_R)^n_{i+1/2}\mathbf{\Phi}^n_{i+1} - (S_L)^n_{i+1/2}\mathbf{\Phi}^n_i - \mathbf{F}(\mathbf{\Phi}^n_{i+1}) + \mathbf{F}(\mathbf{\Phi}^n_i)\Big].$$

Thus, the mean state (4.50) within the star region is, at $\tau = \tau^{n+1}$:

$$(\mathbf{\Phi}^*)^{n+1}_{i+1/2} = \frac{(S_R)^n_{i+1/2}\mathbf{\Phi}^n_{i+1} - (S_L)^n_{i+1/2}\mathbf{\Phi}^n_i - \mathbf{F}(\mathbf{\Phi}^n_{i+1}) + \mathbf{F}(\mathbf{\Phi}^n_i)}{(S_R)^n_{i+1/2} - (S_L)^n_{i+1/2}} \tag{4.53}$$

### 4.B.3 Expressions of the inter-cell fluxes

Integrating Eq. (4.44) on $[\tau^{n+1},\tau^n]\times[X_{i+1/2}+(\tau^{n+1}-\tau^n)(S_L)^n_i, X_{i+1/2}]$ leads to:

$$\int_{X_{i+1/2}+(\tau^{n+1}-\tau^n)(S_L)^n_{i+1/2}}^{X_{i+1/2}} \mathbf{\Phi}(\tau^{n+1},X)dX$$
$$= -(\tau^{n+1}-\tau^n)\Big[(S_L)^n_{i+1/2}\mathbf{\Phi}^n_i + \mathbf{F}_{i+1/2} + \mathbf{F}(\mathbf{\Phi}^n_i)\Big]$$

Thus,

$$\mathbf{F}^n_{i+1/2} = \mathbf{F}(\mathbf{\Phi}^n_i) - (S_L)^n_{i+1/2}\mathbf{\Phi}^n_i - \frac{1}{\tau^{n+1}-\tau^n}\int_{X_{i+1/2}+(\tau^{n+1}-\tau^n)(S_L)^n_{i+1/2}}^{X_{i+1/2}} \mathbf{\Phi}(\tau^{n+1},X)dX \tag{4.54}$$

Obviously, integrating Eq. (4.44) on $[\tau^{n+1},\tau^n]\times[X_{i+1/2}, X_{i+1/2}+(\tau^{n+1}-\tau^n)(S_R)^n_i,]$ would have lead to another expression of the inter-cell flux, but this expression is the same as in Eq. (4.54) in virtue of Eq. (4.52). Then, in order to express the integral in Eq. (4.54), we must distinguish two cases.

**Case of eigenvalues with different signs:**

This is the configuration represented in Fig. 4.B.2: $(S_L)^n_{i+1/2} \le 0 \le (S_R)^n_{i+1/2}$. Thus, in Eq. (4.54) the integration line entirely lies in the star region, on which $\mathbf{\Phi}(\tau^{n+1},X) = (\mathbf{\Phi}^*)^{n+1}_i$:

$$-\frac{1}{\tau^{n+1}-\tau^n}\int_{X_{i+1/2}+(\tau^{n+1}-\tau^n)(S_L)^n_{i+1/2}}^{X_{i+1/2}} \mathbf{\Phi}(\tau^{n+1},X)dX = (S_L)^n_{i+1/2}(\mathbf{\Phi}^*)^{n+1}_i,$$

and the inter-cell flux (4.54) takes the form:

$$\mathbf{F}^n_{i+1/2} = \frac{(S_R)^n_{i+1/2}\mathbf{F}(\mathbf{\Phi}^n_i) - (S_L)^n_{i+1/2}\mathbf{F}(\mathbf{\Phi}^n_{i+1}) + (S_R)^n_{i+1/2}(S_L)^n_{i+1/2}(\mathbf{\Phi}^n_{i+1} - \mathbf{\Phi}^n_i)}{(S_R)^n_{i+1/2} - (S_L)^n_{i+1/2}} \tag{4.55}$$

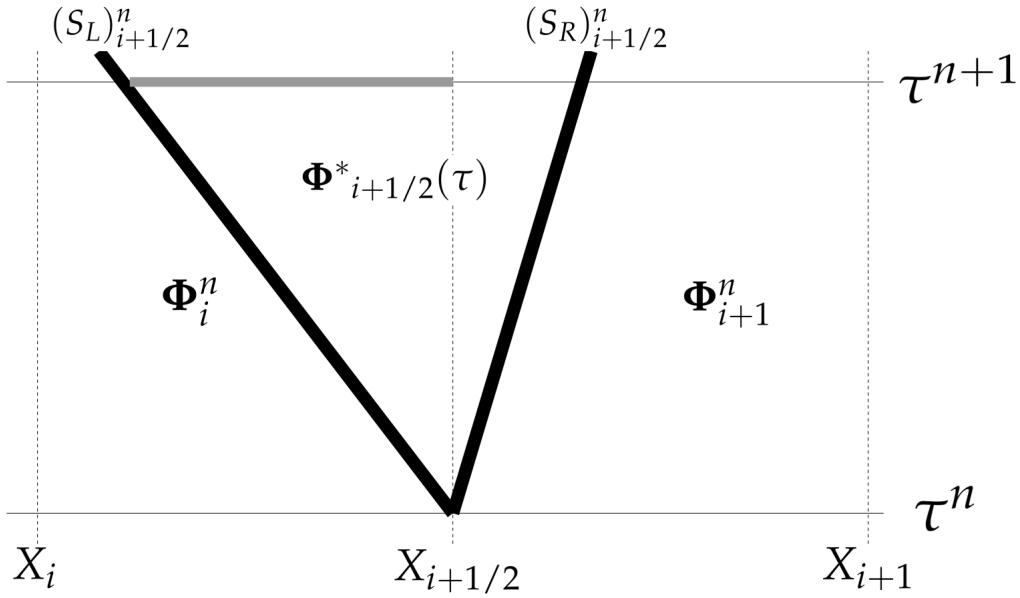


Figure 4.B.2: Geometry of the local Riemann's problem in the case $(S_L)^n_{i+1/2} \leq 0 \leq (S_R)^n_{i+1/2}$. The solid, grey segment represents the line along which the integration of $X \mapsto \mathbf{\Phi}(\tau^{n+1}, X)$ is performed in Eq. (4.54).

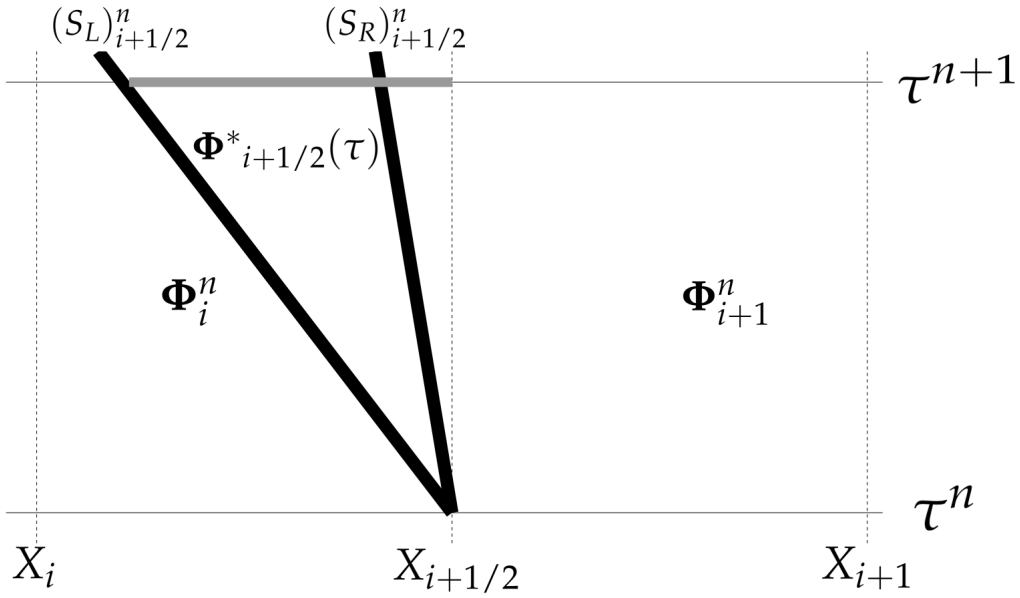


Figure 4.B.3: Geometry of the local Riemann's problem in the case$(S_L)^n_{i+1/2} \leq 0$ and $(S_R)^n_{i+1/2} \leq 0$ with $(S_L)^n_{i+1/2} \leq (S_R)^n_{i+1/2}$. The solid, grey segment represents the line along which the integration of $X \mapsto \mathbf{\Phi}(\tau^{n+1}, X)$ is performed in Eq. (4.54).

**Case of eigenvalues with the same sign:**

Without lost of generality, we assume $(S_L)^n_{i+1/2} \leq 0$ and $(S_R)^n_{i+1/2} \leq 0$ with $(S_L)^n_{i+1/2} \leq (S_R)^n_{i+1/2}$. This configuration is represented in Fig. 4.B.3. The case $0 \geq (S_L)^n_{i+1/2} \geq (S_R)^n_{i+1/2}$ is obtained by exchanging the roles played by $(S_L)^n_{i+1/2}$ and $(S_R)^n_{i+1/2}$ in all formulae. Within Eq. (4.54), the line of integration crosses the characteristic with slope $(S_R)^n_{i+1/2}$, requiring to split the integral as:

$$\int_{X_{i+1/2}+(\tau^{n+1}-\tau^n)(S_L)^n_{i+1/2}}^{X_{i+1/2}} \mathbf{\Phi}(\tau^{n+1},X)dX = \int_{X_{i+1/2}+(\tau^{n+1}-\tau^n)(S_L)^n_{i+1/2}}^{X_{i+1/2}+(\tau^{n+1}-\tau^n)(S_R)^n_{i+1/2}} \mathbf{\Phi}(\tau^{n+1},X)dX + \int_{X_{i+1/2}+(\tau^{n+1}-\tau^n)(S_R)^n_{i+1/2}}^{X_{i+1/2}} \mathbf{\Phi}(\tau^{n+1},X)dX$$

The first integral of the right hand side is $(\tau^{n+1}-\tau^n)[(S_R)^n_{i+1/2}-(S_L)^n_{i+1/2}](\mathbf{\Phi}^*)^{n+1}_i$, and the second one is equal to $-(\tau^{n+1}-\tau^n)(S_R)^n_{i+1/2}\mathbf{\Phi}^n_{i+1}$. Substituting these expressions in Eq. (4.54), we find:

$$\mathbf{F}_{i+1/2} = \mathbf{F}(\mathbf{\Phi}^n_{i+1}). \tag{4.56}$$

By symmetry, the configuration corresponding to positive values of both $(S_L)^n_{i+1/2}$ and $(S_R)^n_{i+1/2}$ leads to $\mathbf{F}_{i+1/2} = \mathbf{F}(\mathbf{\Phi}^n_i)$.

This page is unintentionally left not blank.

This page is unintentionally left not blank.

# Chapter 5

# Conclusion

Inertial fusion by lasers has entered a new era since ignition has been achieved. The development of a commercial reactor requires to transform one successful shot per year into several ones in a second. This means significantly improving the robustness of the implosion control. To do so the dialogue between experimental progresses and theoretical understanding must be strengthened through the creation of accurate simulation tools. In such a perspective, this thesis addressed the problem of modeling electron heat transfer within the conduction region of the ablative flow. Theoretical and numerical aspects inherent to quasi-static nonlocal electron heat transport within an isolated, one-dimensional and unmagnetized plasma have been investigated. In what follows the motivations are restated, our results summarized, as well as some perspectives given.

## 5.1 Motivations

Our work was motivated by the need to provide a closure to the hydrodynamic equations describing the ablative flow. An accurate modeling of its structure is of paramount importance to understand how to optimize the implosion process in order to enhance the efficiency of the resulting thermonuclear burn. Given the variety of phenomena at play, it appeared that to refine the macroscopic description the approach of exactly solving reduced kinetic equations with an efficient numerical method is promising since its flexibility constitutes the most fertile ground for progressive extensions.

Nevertheless, designing a reduced kinetic model is not a straightforward task, even when its purpose is restricted to treating the problem, which should be seen as a first step, considered in this manuscript. This is due to the subtle relationship between the computational efficiency and the mathematical formulation, whose level of complexity is correlated to the desired accuracy itself difficult to set. Over the decades, numerous works have been devoted to the heat flux density induced by a steep temperature gradient. Despite the hindsight these studies give us, a clear enough vision about the main mathematical ingredients necessary to grasp certain physical behaviours is lacking. This is because most of the time a set of equations only serves as a starting point to derive a practical formula for the heat flux density without being solved directly. This is done to avoid the computational

cost associated with an insufficiently fast algorithm, but has for consequence the use of many approximations whose effects are intertwined.

In view of this, our ambition was twofold. While deepening the understanding and improving a reduced kinetic model in Ch. 3, we developed an efficient numerical scheme in Ch. 4 to make it usable. The prototype consists of a set of two coupled partial differential equations obtained after projecting the stationary kinetic equation on the Maxwell's multipoles of zero and first orders. No term is neglected in our P1 system. It mainly owes its lightness to the desired fact that the Lorentz's operator describing electron-ion encounters reduces to terms proportional to the components of the electron distribution function. Having access to the first order of them is mathematically sufficient to compute the heat flux density.

## 5.2 Results

### 5.2.1 Physical analysis of the model

The heart of the model is the operator chosen to describe collisions among electrons. The procedure leading to its expression is dictated by the nature of the disequilibrium that must be described. Here, it is a distortion of the electron distribution function localized in the high velocity domain. Within this region of the phase space the collision operator must properly set the amount of the out-of-equilibrium population. Because of their scarcity the few collisions occurring among such fast electrons generate negligible modulations of their distribution compared to encounters between them and the equilibrium background within which they evolve. This situation echoes Chandrasekhar's paradigm and legitimates the linearization of the Landau's integral. Since the vast majority of Maxwellian electrons have a velocity which, at most, only slightly exceeds the thermal speed, only the first term of the high velocity expansion of the operator is retained.

As we have shown in Sec. 3.1.1, this last approximation implies an overestimation of the friction force experienced by slow electrons. This effect is beneficial because, in the local regime, this makes the anisotropic part of the electron distribution function roughly homothetic to that given by the Spitzer-Härm's expression. The ratio between their amplitudes has been set to one thanks to a correction factor of the electron-electron collision frequency that we determined analytically as a function of the ionization number in Sec. 3.2.2.1.

Taking it into account allowed us in Sec. 3.2.3.1 to recover the heat flux density with a maximum difference of around 10 % from the reference kinetic code in the nonlocal regime. This is not the case for the electric field. As we proved in Sec. 3.2.2.1, the expected effect of the ionization number cannot be recovered self-consistently with a P1 system within which the operator of Albritton *et al* [82] or Bhatnagar *et al* [73] are used. The condition to be verified by the projection of the operator on the first order Maxwell's multipoles is not fulfilled. This, obviously, also applies to all the codes in which this term is omitted in favour of a renormalization of the electron-ion collision frequency. On this basis, in Sec. 3.2.3.1 we explored the behaviour of the model without calculating the field at each iteration but by using the correct value of Spitzer-Härm together with the

adequate correction of the electron-electron collision frequency resulting from this choice. The accuracy turned out to be a little worse but not prohibitive, without perceptible gain in computation time.

This striking flaw about the field is not visible at the kinetic level shown in Sec. 3.2.3.2. The break in slope of the isotropic part of the electron distribution function is correctly reproduced. It reflects the discontinuity of the local effective temperature whose emergence is analogous to the breaking of a simple Riemann's wave in hydrodynamics. In the Gurevich-Istomin's terminology, the velocity at which it occurs separates the diffusive and convective contributions to transport. Near the foot of the temperature gradient, the first disappears in favor of the second which manifests itself, as we have shown, by a transition in shape of the anisotropic part in the nonlocal regime. In the local one, we provided a definitive formula for this component in Sec. 3.2.2.2. This allowed us to explain its expected shift towards low velocities, accompanying the drop in the amplitudes of the forward and return currents, for increasingly lower values of the ionization number. Such effect cannot be caught with the algebraic operator of Bhatnagar *et al* but relies on the differential character of Albritton *et al*'s.

### 5.2.2 Numerical implementation of the model

The degree of the latter determined the class to which our numerical method belongs. After being linearized and expanded to the lowest order in the high velocity limit the Landau's collision operator has a radial part, in spherical coordinates, containing a second order differential term. It is only by substituting it with its equilibrium value that the Albritton *et al*'s form is recovered. This procedure was examined in Sec. 3.1.2. Its consequence is to make hyperbolic our P1 system which we have formulated as a matrix equation of conservation with a source term in Sec. 4.1.1. On this occasion we proposed a new derivation in App. 4.A which involves Stokes' theorem and does not require to assume the development of the electron distribution function on the Maxwell's multipoles as being limited to order one. Our final set of coupled equations was, by the way, lighter than that written by Del Sorbo *et al* [132, 57] thanks to an alternative change of variable.

The Godounov's method we employed follows the choice of these authors, although our scheme significantly differs from theirs. The latter, just like that proposed by Holec *et al* [128], uses energy as a time-like variable to integrate. As we explained in Sec. 4.1.2 by rigorously analysing local Riemann's problems along the energy axis, their downwind method can only be applied for electric fields below a threshold value that we have determined. It is inevitably exceeded in case of an electron temperature gradient relevant to inertial fusion. Such a statement comes from looking the condition we derived in Sec. 4.2.2 on the Knudsen's number reflecting this limitation.

As we have detailed, the problem arises because the most energetic electrons experience an electric Lorentz' force whose magnitude is greater than that of friction. This makes positive one of the Jacobian's eigenvalues of the flux in energy, meaning the existence of waves propagating in the direction of increasing energies. In order to simultaneously describe these and the counter-propagating ones we proposed to reintroduce the time variable. This additional degree of freedom makes the

model non-stationary but allowed to properly estimate fluxes in energy according to the well-known approximation of Harten, Lax and van Leer. The desired, stationary solution was obtained thanks to a time-marching strategy whose efficiency has been significantly improved by the use of a local time step introduced in Sec. 4.1.2.2. The latter was both non-uniform and non-stationary by being determined by the local Courant–Friedrichs–Lewy's condition at each iteration. Although we proposed it without any attempt at formal analysis, our code converged correctly in all the situations we considered in Sec. 4.2, with the expected behaviour of the numerical error.

As we shown in Sec. 4.3.1 the algorithm turned out to be only three times slower than that of Schurtz *et al* [91], whose performance remains today the best on the problem we studied here. This makes it possible to couple our kinetic module to a hydrodynamic code. Depending on how this is done, the non-conservative nature of the model we pointed out in Sec. 4.3.2 may be problematic. If so, the underlying creation rates per unit volume have been calculated and their opposite can potentially be added as source terms in the macroscopic equations.

## 5.3 Perspectives

Our work can be continued along several complementary axes. Other mechanisms leading to distortion of the electron distribution function can be taken into account by adding appropriate operators along with the collision ones. Like the latter they will behave as source terms for the evolution on the characteristics of the Vlasov's equation. Laser heating flattens the peak of the electron distribution function, while the incoming flow of energetic electrons produced by parametric instabilities can cause a tail to appear at more than seven times the value of the thermal velocity at the critical density. Although these phenomena seem to concern different domain of the phase space they are coupled by the collisions. Taking into account their interplay with the diffusion induced by the strong temperature gradient does not seem to have been much explored until now.

Furthermore, within the conduction region any deviation from the situation of parallel gradients of electron density and temperature generates a magnetic field which may enhance the asymmetry from which it originates. Its growth rate is the opposite of the curl of the electric field induced by the heat transfer, itself altered by the magnetic field causing its rotation and reduction. If strong enough, it can magnetize the electrons whose outward flow carries its field lines with it, further complicating its topology. The importance of a combined analysis of magnetic field generation and heat flux density behavior has been highlighted for a long time, giving rise to a considerable number of works. Unfortunately, all the attempts to include such a coupling have proved to be far too cumbersome numerically, regardless of their ability to reproduce or not the key phenomena. It is unlikely to be any different for a naive generalisation of our scheme. The question of whether a paradigm shift is needed is an open one, and although the author has several ideas in mind, they seem too immature to know whether they will still be relevant by the time these lines are read. Thus we will not say any more by stopping our discussion here.

This page is unintentionally left not blank.

This page is unintentionally left not blank.

# Bibliography


[1] Statistical Review of World Energy. *71st edition* (2022).

[2] R. Allan, P. Arias, S. Berger, J. Canadell, C. Cassou, D. Chen, A. Cherchi, S. Connors, E. Coppola, A. Cruz, et al. Intergovernmental Panel on Climate Change (IPCC). Summary for Policymakers. Cambridge University Press, (2023).

[3] S. Atzeni and J. Meyer-ter-Vehn. *The physics of inertial fusion: beam plasma interaction, hydrodynamics, hot dense matter*. Vol. 125. OUP Oxford, (2004).

[4] N. Bohr and J. Wheeler. The mechanism of nuclear fission. *Physical Review* 56.5 (1939).

[5] World Nuclear Association. *Supply of Uranium*. https://world-nuclear.org. (2023).

[6] World Nuclear Association. *Generation IV Nuclear Reactors*. https://world-nuclear.org. (2020).

[7] World Nuclear Association. *Fast Neutron Reactors*. https://world-nuclear.org. (2020).

[8] G. Gamow. Zur quantentheorie des atomkernes. *Zeitschrift für Physik* 51.3 (1928).

[9] J.-M. Rax. *Physique des Tokamaks*. Ed. de l'Ecole Polytechnique, (2011).

[10] S. Wurzel and S. Hsu. Progress toward fusion energy breakeven and gain as measured against the Lawson criterion. *Phys. Plasmas* 29.6 (2022).

[11] H. Abu-Shawareb, R. Acree, P. Adams, J. Adams, B. Addis, R. Aden, P. Adrian, B. Afeyan, M. Aggleton, L. Aghaian, et al. Lawson criterion for ignition exceeded in an inertial fusion experiment. *Phys. Rev. Lett.* 129.7 (2022).

[12] D. Clery. Explosion marks laser fusion breakthrough. *Science* 378 (2022).

[13] World Nuclear Association. *Heat Values of Various Fuels*. https://world-nuclear.org.

[14] J. Knaster, A. Moeslang, and T. Muroga. Materials research for fusion. *Nature Physics* 12.5 (2016).

[15] T. Rider. Fundamental limitations on plasma fusion systems not in thermodynamic equilibrium. PhD thesis. MIT, (1995).

[16] M. Sikora and H. Weller. A new evaluation of the 11 B (p, $\alpha$) $\alpha$ $\alpha$ reaction rates. *Journal of Fusion Energy* 35.3 (2016).

[17] S. Meschini, F. Laviano, F. Ledda, D. Pettinari, R. Testoni, D. Torsello, and B. Panella. Review of commercial nuclear fusion projects. *Frontiers in Energy Research* 11 (2023).

[18] Fusion Industry Association. https://www.fusionindustryassociation.org/.

[19] D. Whyte, C. Paz-Soldan, and B. Wirth. The academic research ecosystem required to support the development of fusion energy. *Phys. Plasmas* 30.9 (2023).

[20] V. Tikhonchuk and G. Schurtz. *Principles of laser fusion.* Université de Bordeaux. (2013).

[21] R. Betti and O. Hurricane. Inertial-confinement fusion with lasers. *Nature Physics* 12.5 (2016).

[22] J. Nuckolls, L. Wood, A. Thiessen, and G. Zimmerman. Laser compression of matter to super-high densities: Thermonuclear (CTR) applications. *Nature* 239.5368 (1972).

[23] V. Goncharov, T. Sangster, T. Boehly, S. Hu, I. Igumenshchev, F. Marshall, R. McCrory, D. Meyerhofer, P. Radha, W. Seka, et al. Demonstration of the highest deuterium-tritium areal density using multiple-picket cryogenic designs on OMEGA. *Phys. Rev. Lett.* 104.16 (2010).

[24] R. Betti, C. Zhou, K. Anderson, L. Perkins, W. Theobald, and A. Solodov. Shock ignition of thermonuclear fuel with high areal density. *Phys. Rev. Lett.* 98.15 (2007).

[25] A. Tentori. Experimental and theoretical study of hot electrons in the context of the shock ignition approach to inertial confinement fusion. PhD thesis. Université de Bordeaux, (2022).

[26] V. Shcherbakov. Ignition of a laser-fusion target by a focusing shock wave. *Sov. Plas. Phys.* 9.2 (1983).

[27] K. Anderson, T. Arber, S. Atzeni, D. Barlow, D. Batani, J. Bates, S. Baton, F. Beg, R. Betti, B. Canaud, et al. Shock Ignition: High Gain Target Performance for Inertial Fusion Energy. Workshop at the Laboratory for Laser Energetics. (2022).

[28] F. Daninos. Des expériences de fusion par laser pour simuler les armes nucléaires. *Sciences et Avenir* 913 (2023).

[29] D. Batani, A. Colaïtis, F. Consoli, C. Danson, L. Gizzi, J. Honrubia, T. Kühl, S. Le Pape, J.-L. Miquel, J. Perlado, et al. Future for Inertial Fusion Energy in Europe: A roadmap. *High Power Laser Science and Engineering* (2023).

[30] W. Manheimer, D. Colombant, and J. Gardner. Steady-state planar ablative flow. *Phys. Fluids* 25.9 (1982).

[31] R. Fabbro, C. Max, and E. Fabre. Planar laser-driven ablation: Effect of inhibited electron thermal conduction. *Phys. Fluids* 28.5 (1985).

[32] G. Varillon, J.-M. Clarisse, and A. Couairon. Non-modal linear stability analysis of ablation flows relative to inertial confinement fusion. *IUTAM Laminar-Turbulent Transition: 9th IUTAM Symposium, London, UK, September 2–6, 2019*. Springer. (2022).

[33] S. Braginskii. Transport Processes in a Plasma. *Rev. Plasma Phys.* 1,205 (1965).

[34] V. Bychenkov, J.-P. Matte, and T. Johnston. Nonlocal electron transport in spherical plasmas. *Phys. Plasmas* 3.4 (1996).

[35] R. Malone, R. McCrory, and R. Morse. Indications of strongly flux-limited electron thermal conduction in laser-target experiments. *Phys. Rev. Lett.* 34.12 (1975).

[36] V. Tikhonchuk. Progress and opportunities for inertial fusion energy in Europe. *Phil. Trans. R. Soc. A* 378.2184 (2020).

[37] A. Brantov and V. Bychenkov. Nonlocal transport in hot plasma. Part I. *Plasma Phys. Rep.* 39.9 (2013).

[38] A. Brantov and V. Bychenkov. Nonlocal transport in hot plasma. Part II. *Plasma Phys. Rep.* 40.7 (2014).

[39] R. Balescu and A. Kuszell. Kinetic equation for an inhomogeneous plasma far from equilibrium. *Journal of Mathematical Physics* 5.8 (1964).

[40] V. Senecha, A. Brantov, V. Bychenkov, and V. Tikhonchuk. Temperature relaxation in hot spots in a laser-produced plasma. *Physical Review E* 57.1 (1998).

[41] A. Chrisment, P. Loiseau, J.-L. Feugeas, P.-E. Masson-Laborde, J. Mathiaud, V. Tikhonchuk, and Ph. Nicolaï. Erratum:"Analysis of a kinetic model for electron heat transport in inertial confinement fusion plasmas"[Phys. Plasmas 29, 062301 (2022)]. *Physics of Plasmas* 29.7 (2022).

[42] A. Chrisment, P. Loiseau, J.-L. Feugeas, P.-E. Masson-Laborde, J. Mathiaud, V. Tikhonchuk, and Ph. Nicolaï. Analysis of a kinetic model for electron heat transport in inertial confinement fusion plasmas. *Physics of Plasmas* 29.6 (2022).

[43] A. Chrisment, A. Debayle, J.-L. Feugeas, P. Loiseau, P.-E. Masson-Laborde, J. Mathiaud, Ph. Nicolaï, and V. Tikhonchuk. A deterministic numerical scheme for an electron heat transport model. *Mathematics and Computers in Simulation* 205 (2023).

[44] J.-F. Luciani and P. Mora. Resummation methods of the Chapman-Enskog expansion for a strongly inhomogeneous plasma. *Journal of statistical physics* 43 (1986).

[45] J. Brodrick, D. Del Sorbo, and C. Ridgers. An alternative justification for the stationary assumption made by many reduced models for nonlocal electron heat flow in plasmas. *Phys. Plasmas* 30.5 (2023).

[46] L. Landau. Die kinetische Gleiehung fur den Fall Coulombscher Wecgselwirkung. *Phys. Z. Sowjet. 10, 154. See also"Collected papers of L. D. Landau, ed. by D. Ter Haar, Pergamon Press, Oxford, 1965, p. 163* (1936).

[47] V. Krainov, V. Rantsev-Kartinov, and E. Trofimovich. Theory of Thermoelectric Field in LTE Plasmas. *Strongly Coupled Coulomb Systems*. Springer, (2002).

[48] L. Landau and E. Lifshitz. *Statistical Physics, part 1*. Butterworth-Heinemann, Elsevier Ltd, (1981).

[49] M. Rosenbluth, W. MacDonald, and D. Judd. Fokker-Planck equation for an inverse-square force. *Physical Review* 107.1 (1957).

[50] V. Arnold. *Lectures on Partial Differential Equations*. Springer, (2004).

[51] T. Johnston. Cartesian tensor scalar product and spherical harmonic expansions in Boltzmann's equation. *Physical Review* 120.4 (1960).

[52] M. Houtput and J. Tempere. Revisiting the Maxwell multipoles for vectorized angular functions. *arXiv preprint arXiv:2110.06732* (2021).

[53] A. Decoster, P. Markowich, and B. Perthame. *Modeling of Collisions*. Vol. 2. Elsevier Masson, (1998).

[54] V. Bouchard. *Group Theory in Physics*. https://sites.ualberta.ca/~vbouchar/MAPH464/front.html.

[55] K. Thorne. Multipole expansions of gravitational radiation. *Reviews of Modern Physics* 52.2 (1980).

[56] V. Arnold. Topological content of the Maxwell theorem on multipole representation of spherical functions. *Topol. Methods Nonlinear Anal* 7.2 (1996).

[57] D. Del Sorbo. An entropic approach to magnetized nonlocal transport and other kinetic phenomena in high-energy-density plasmas. PhD thesis. Bordeaux, (2015).

[58] L. Spitzer Jr. and R. Härm. Transport phenomena in a completely ionized gas. *Phys. Rev.* 89.5 (1953).

[59] V. Krainov, V. Rantsev-Kartinov, and E. Trofimovich. Theory of Thermoelectric Field in LTE Plasmas. *Strongly Coupled Coulomb Systems* (1998).

[60] E. Epperlein. Effect of electron collisions on ion-acoustic waves and heat flow. *Phys. Plasmas* 1.1 (1994).

[61] R. Balescu. *Transport Processes in Plasmas*. Vol. I. Elsevier, (1988).

[62] J. Krommes. Projection-operator methods for classical transport in magnetized plasmas. Part 1. Linear response, the Braginskii equations and fluctuating hydrodynamics. *Journal of Plasma Physics* 84.4 (2018).

[63] J. Krommes. Projection-operator methods for classical transport in magnetized plasmas. Part 2. Nonlinear response and the Burnett equations. *Journal of Plasma Physics* 84.6 (2018).

[64] Y. Kishimoto and K. Mima. An extension of Spitzer-Härm theory on thermal transport to steep temperature gradient case. I. General formulation. *Journal of the Physical Society of Japan* 52.10 (1983).

[65] Y. Kishimoto, K. Mima, and M. Haines. An extension of Spitzer-Härm theory on thermal transport to steep temperature gradient case. II. Integral representation. *Journal of the Physical Society of Japan* 57.6 (1988).

[66] A. Gurevich and Ya. Istomin. Thermal runaway and convective heat transport by fast electrons in a plasma. *Sov. Phys.-JETP* 50.3 (1979).

[67] M. Abramowitz, I. A Stegun, and R. Romer. *Handbook of mathematical functions with formulas, graphs, and mathematical tables*. (1988).

[68] S. Schot. Aberrancy: Geometry of the third derivative. *Mathematics Magazine* 51.5 (1978).

[69] A. Bell, R. Evans, and D. Nicholas. Elecron energy transport in steep temperature gradients in laser-produced plasmas. *Physical Review Letters* 46.4 (1981).

[70] N. Ljepojevic and P. MacNeice. Heat flux in a non-Maxwellian plasma. *Physical Review A* 40.2 (1989).

[71] W. Manheimer, D. Colombant, and V. Goncharov. The development of a Krook model for nonlocal transport in laser produced plasmas. I. Basic theory. *Physics of Plasmas* 15.8 (2008).

[72] H. Grad. Asymptotic theory of the Boltzmann equation. *The Physics of Fluids* 6.2 (1963).

[73] P. Bhatnagar, E. Gross, and M. Krook. A model for collision processes in gases. I. Small amplitude processes in charged and neutral one-component systems. *Phys. Rev.* 94.3 (1954).

[74] F. Tricomi. *Differential equations*. Blackie & Son Limited, (1953).

[75] J.-F. Luciani, P. Mora, and J. Virmont. Nonlocal heat transport due to steep temperature gradients. *Phys. Rev. Lett.* 51.18 (1983).

[76] P. Mora and J.-F. Luciani. Nonlocal electron transport in laser created plasmas. *Laser Part. Beams* 12.3 (1994).

[77] S. Krasheninnikov. On nonlocal electron heat conduction. *Phys. Fluids B* 5.1 (1993).

[78] J.-Y. Ji and E. Held. Electron parallel closures for arbitrary collisionality. *Phys. Plasmas* 21.12 (2014).

[79] C. Lu, V. Tikhonchuk, and S. Weber. Analytic solutions for delocalized heat transport. *Plasma Phys. Control. Fusion* 63.7 (2021).

[80] A. Dimits, I. Joseph, and M. Umansky. A fast non-Fourier method for Landau-fluid operators. *Phys. Plasmas* 21.5 (2014).

[81] J.-F. Luciani, P. Mora, and A. Bendib. Magnetic field and nonlocal transport in laser-created plasmas. *Phys. Rev. Lett.* 55.22 (1985).

[82] J. Albritton, E. Williams, I. Bernstein, and K. Swartz. Nonlocal electron heat transport by not quite Maxwell-Boltzmann distributions. *Phys. Rev. Lett.* 57.15 (1986).

[83] P. Holstein and A. Decoster. Comparison between two models of nonlocal heat flux in laser-generated plasma. *Journal of applied physics* 62.9 (1987).

[84] V. Silin. Theory of nonlocal transport in laser produced plasmas. *Phys. Scripta* T63 (1996).

[85] E. Epperlein and R. Short. A practical nonlocal model for electron heat transport in laser plasmas. *Phys. Fluids B* 3.11 (1991).

[86] O. Batishchev, V. Bychenkov, F. Detering, W. Rozmus, R. Sydora, C. Capjack, and V. Novikov. Heat transport and electron distribution function in laser produced plasmas with hot spots. *Physics of Plasmas* 9.5 (2002).

[87] J. Albritton. Laser absorption and heat transport by non-Maxwell-Boltzmann electron distributions. *Phys. Rev. Lett.* 50.26 (1983).

[88] A. Bendib, J.-F. Luciani, and J.-P. Matte. An improvement of the nonlocal heat flux formula. *Phys. Fluids* 31.4 (1988).

[89] M. Prasad and D. Kershaw. Nonviability of some nonlocal electron heat transport modeling. *Phys. Fluids B: Plasma Phys.* 1.12 (1989).

[90] J. Sanmartín, J. Ramirez, R. Fernández-Feria, and F. Minotti. Self-consistent, nonlocal electron heat flux at arbitrary ion charge number. *Phys. Fluids B: Plasma Phys.* 4.11 (1992).

[91] G. Schurtz, Ph. Nicolaï, and M. Busquet. A nonlocal electron conduction model for multidimensional radiation hydrodynamics codes. *Phys. Plasmas* 7.10 (2000).

[92] S. Chandrasekhar. *Radiative transfer*. Courier Corporation, (1950).

[93] J. Brodrick, R. J Kingham, et al. Testing nonlocal models of electron thermal conduction for magnetic and inertial confinement fusion applications. *Phys. Plasmas* 24.9 (2017).

[94] M. Sherlock, J. Brodrick, and C. Ridgers. A comparison of non-local electron transport models for laser-plasmas relevant to inertial confinement fusion. *Phys. Plasmas* 24.8 (2017).

[95] J. Breil and P.-H. Maire. A cell-centered diffusion scheme on two-dimensional unstructured meshes. *Journal of Computational Physics* 224.2 (2007).

[96] D. Cao, G. Moses, and J. Delettrez. Improved non-local electron thermal transport model for two-dimensional radiation hydrodynamics simulations. *Phys. Plasmas* 22.8 (2015).

[97] M. Rosen. The physics issues that determine inertial confinement fusion target gain and driver requirements: A tutorial. *Phys. Plasmas* 6.5 (1999).

[98] A. Marocchino, M. Tzoufras, S. Atzeni, Ph. Schiavi A.and Nicolaï, J. Mallet, V. Tikhonchuk, and J.-L. Feugeas. Comparison for non-local hydrodynamic thermal conduction models. *Phys. Plasmas* 20.2 (2013).

[99] R. Henchen, M. Sherlock, W. Rozmus, J. Katz, D. Cao, J. Palastro, and D. Froula. Observation of nonlocal heat flux using Thomson scattering. *Phys. Rev. Lett.* 121.12 (2018).

[100] R. Henchen, M. Sherlock, W. Rozmus, J. Katz, P.-E. Masson-Laborde, D. Cao, J. Palastro, and D. Froula. Measuring heat flux from collective Thomson scattering with non-Maxwellian distribution functions. *Phys. Plasmas* 26.3 (2019).

[101] W. Manheimer, D. Colombant, and A. Schmitt. Calculations of nonlocal electron energy transport in laser produced plasmas in one and two dimensions using the velocity dependent Krook model. *Phys. Plasmas* 19.5 (2012).

[102] Ph. Nicolaï, J.-L. Feugeas, and G. Schurtz. A practical nonlocal model for heat transport in magnetized laser plasmas. *Phys. Plasmas* 13.3 (2006).

[103] S. Chandrasekhar. *Principles of Stellar Dynamics*. Courier Corporation, (2005).

[104] S. Ichimaru. *Statistical plasma physics, volume I: basic principles*. CRC Press, (2018).

[105] N. Rostoker. Superposition of dressed test particles. *The Physics of Fluids* 7.4 (1964).

[106] J. Krommes. Two new proofs of the test particle superposition principle of plasma kinetic theory. *The Physics of Fluids* 19.5 (1976).

[107] R. Balescu. *Statistical mechanics of charged particles*. Vol. 4. Interscience Publishers, (1963).

[108] N. Bogoliubov. *Problems of Dynamic Theory in Statistical Physics*. Technical Information Service, United States Atomic Energy Commission., (1960).

[109] A. Vlasov. The vibrational properties of an electron gas. *Phys. Z. Sowjet. 8, 291* (1938).

[110] S. Chandrasekhar. *Plasma Physics*. The University of Chicago Press, (1960).

[111] M. Rosenbluth and N. Rostoker. Theoretical structure of plasma equations. *The Physics of Fluids* 2.1 (1959).

[112] L. Landau. On the vibrations of the electronic plasma. *Phys. Z. Sowjet. 16, 574. See also "Collected papers of L. D. Landau, ed. by D. Ter Haar, Pergamon Press, Oxford, 1965, p. 445* (1946).

[113] C. Mouhot and C. Villani. On landau damping. *Acta Math.* (2011).

[114] L. Landau and E. Lifshitz. *Electrodynamics of continuous media.* Vol. 8. Butterworth-Heinemann, Elsevier Ltd, (2013).

[115] H. Nyquist. Regeneration theory. *Bell System Tech. J.* 11.1 (1932).

[116] O. Penrose. Electrostatic instabilities of a uniform non-Maxwellian plasma. *Phys. of Fluids* 3.2 (1960).

[117] N. van Kampen. On the theory of stationary waves in plasmas. *Physica* 21.6-10 (1955).

[118] G. Backus. Linearized plasma oscillations in arbitrary electron velocity distributions. *Journal of Mathematical Physics* 1.3 (1960).

[119] J. Malmberg, C. Wharton, R. Gould, and T. O'neil. Plasma wave echo experiment. *Physical Review Letters* 20.3 (1968).

[120] R. Gould, T. O'neil, and J. Malmberg. Plasma wave echo. *Physical Review Letters* 19.5 (1967).

[121] R. Guernsey. The kinetic theory of fully ionized gases. *Off. Nav. Res. Contract No. Nonr* 15 (1960).

[122] A. Lenard. On Bogoliubov's kinetic equation for a spatially homogeneous plasma. *Annals of Physics* 10.3 (1960).

[123] R. Balescu. Irreversible processes in ionized gases. *The Physics of Fluids* 3.1 (1960).

[124] N. Rostoker and M. Rosenbluth. Test particles in a completely ionized plasma. *The physics of fluids* 3.1 (1960).

[125] J. Krommes. An introduction to the physics of the Coulomb logarithm, with emphasis on quantum-mechanical effects. *Journal of Plasma Physics* 85.1 (2019).

[126] P. Mora. Coulomb logarithm accuracy in a Yukawa potential. *Phys. Rev. E* 102.3 (2020).

[127] S. Chandrasekhar. Stochastic problems in physics and astronomy. *Reviews of modern physics* 15.1 (1943).

[128] M. Holec, P. Loiseau, A. Debayle, J. Brodrick, D. Del Sorbo, C. Ridgers, V. Tikhonchuk, J.-L. Feugeas, Ph. Nicolai, B. Dubroca, et al. AWBS kinetic modeling of electrons with nonlocal Ohms law in plasmas relevant to inertial confinement fusion. *arXiv preprint arXiv:1901.11378* (2018).

[129] W. Rozmus, T. Chapman, A. Brantov, B. Winjum, R. Berger, S. Brunner, V. Bychenkov, A. Tableman, M. Tzoufras, and S. Glenzer. Resonance between heat-carrying electrons and Langmuir waves in inertial confinement fusion plasmas. *Phys. Plasmas* 23.1 (2016).

[130] C. Karney. Fokker-Planck and quasilinear codes. *Computer Physics Reports* 4.3-4 (1986).

[131] S. Krasheninnikov and O. Bakunin. Electron heat conduction and suprathermal particles. *Contributions to Plasma Physics* 32.3-4 (1992).

[132] D. Del Sorbo, J.-L. Feugeas, Ph. Nicolaï, M. Olazabal-Loumé, B. Dubroca, S. Guisset, M. Touati, and V. Tikhonchuk. Reduced entropic model for studies of multidimensional nonlocal transport in high-energy-density plasmas. *Phys. Plasmas* 22.8 (2015).

[133] J. Nikl, I. Göthel, M. Kuchařík, S. Weber, and M. Bussmann. Implicit reduced Vlasov–Fokker–Planck–Maxwell model based on high-order mixed elements. *J. Comp. Phys.* 434 (2021).

[134] private communication: Aladin is a Vlasov-Fokker-Planck code developed at CEA by D. Deck and K.-C. Le Thanh based on [147] ().

[135] M. Tzoufras, A. Tableman, F. Tsung, W. Mori, and A. Bell. A multi-dimensional Vlasov-Fokker-Planck code for arbitrarily anisotropic high-energy-density plasmas. *Physics of Plasmas* 20.5 (2013).

[136] A. Joglekar, B. Winjum, A. Tableman, H. Wen, M. Tzoufras, and W. Mori. Validation of OSHUN against collisionless and collisional plasma physics. *Plasma Phys. Control. Fusion* 60.6 (2018).

[137] E. Weinan. *Principles of multiscale modeling*. Cambridge University Press, (2011).

[138] R. LeVeque. Balancing source terms and flux gradients in high-resolution Godunov methods: the quasi-steady wave-propagation algorithm. *Journal of computational physics* 146.1 (1998).

[139] R. Courant, K. Friedrichs, and H. Lewy. Über die partiellen Differenzengleichungen der mathematischen Physik. *Mathematische annalen* 100.1 (1928).

[140] H. Tang, R. Haynes, and G. Houzeaux. A review of domain decomposition methods for simulation of fluid flows: Concepts, algorithms, and applications. *Archives of Computational Methods in Engineering* 28.3 (2021).

[141] S. Clerc. A domain decomposition method for nonlinear steady-state flow computations. *Nuclear science and engineering* 123.3 (1996).

[142] R. Higdon. Initial-boundary value problems for linear hyperbolic system. *SIAM review* 28.2 (1986).

[143] E. Lefebvre, N. Cochet, S. Fritzler, V. Malka, M.-M. Aléonard, J.-F. Chemin, S. Darbon, L. Disdier, J. Faure, A. Fedotoff, et al. Electron and photon production from relativistic laser–plasma interactions. *Nuclear Fusion* 43.7 (2003).

[144] F. Pérez, L. Gremillet, A. Decoster, M. Drouin, and E. Lefebvre. Improved modeling of relativistic collisions and collisional ionization in particle-in-cell codes. *Phys. Plasmas* 19.8 (2012).

[145] S. Godunov. Finite difference method for numerical computation of discontinuous solutions of the equations of fluid dynamics. *Matematičeskij sbornik* 47.3 (1959).

[146] A. Harten, P. Lax, and B. van Leer. On upstream differencing and Godunov-type schemes for hyperbolic conservation laws. *SIAM review* 25.1 (1983).

[147] R. Kingham and A. Bell. An implicit Vlasov-Fokker-Planck code to model non-local electron transport in 2D with magnetic fields. *Journal of Computational Physics* 194.1 (2004).

[148] Ph. Morrison. The Maxwell-Vlasov equations as a continuous Hamiltonian system. *Phys. Lett. A* 80.5-6 (1980).

[149] J. Marsden and A. Weinstein. The Hamiltonian structure of the Maxwell-Vlasov equations. *Physica D* 4.3 (1982).

[150] Ph. Morrison. Structure and structure-preserving algorithms for plasma physics. *Phys. of Plasmas* 24.5 (2017).

[151] A. Kaufman. Dissipative Hamiltonian systems: A unifying principle. *Phys. Lett. A* 100.8 (1984).

[152] Ph. Morrison. Bracket formulation for irreversible classical fields. *Phys. Lett. A* 100.8 (1984).

[153] Ph. Morrison. A paradigm for joined Hamiltonian and dissipative systems. *Physica D: Nonlinear Phenomena* 18.1-3 (1986).

[154] Ph. Morrison and M. Updike. An inclusive curvature-like framework for describing dissipation: metriplectic 4-bracket dynamics. *arXiv preprint* (2023).

[155] E. Hirvijoki. Structure-preserving marker-particle discretizations of Coulomb collisions for particle-in-cell codes. *Plasma Physics and Controlled Fusion* 63.4 (2021).

[156] M. Born and L. Infeld. On the quantization of the new field theory II. *Proc. Royal Society.* 150.869 (1935).

[157] M. Kraus and E. Hirvijoki. Metriplectic integrators for the Landau collision operator. *Phys. Plasmas* 24.10 (2017).

[158] P. Gritsyk and B. Somov. An Analytical Model for the Propagation of Thermal Runaway Electrons in Solar Flares. *Astronomy Letters* 45.4 (2019).

[159] S. Chapman and T. Cowling. *The mathematical theory of non-uniform gases: an account of the kinetic theory of viscosity, thermal conduction and diffusion in gases*. Cambridge university press, (1990).

[160] B. Dubroca, J.-L. Feugeas, and M. Frank. Angular moment model for the Fokker-Planck equation. *Europ. Phys. J. D* 60 (2010).

[161] R. Balescu. *Equilibrium and nonequilibrium statistical mechanics*. John Wiley & Sons, (1975).

[162] G. Laval, R. Pellat, and M. Vuillemin. Calcul de l'entropie statistique d'un plasma hors équilibre. *Journal de Physique* 28.8-9 (1967).

[163] L. Landau and E. Lifshitz. *Fluid Mechanics*. Vol. 6. Butterworth-Heinemann, Elsevier Ltd, (2013).

[164] B. Kadomtsev. *Collective phenomena in plasma*. (1988).

[165] L. Schwartz. *Théorie des distributions*. Hermann, (1966).

[166] C. Curtiss and J. Hirschfelder. Integration of stiff equations. *Proceedings of the National Academy of Sciences* 38.3 (1952).

[167] https://docs.scipy.org/doc/scipy/reference/generated/scipy.integrate.solve_ivp.html.

This page is unintentionally left not blank.

# Chapter 6

# Complementary notes

## 6.1 Few words on the metriplectic formulation

The success of a numerical method often reflects the judicious choice of a specific mathematical formulation of the model. This appendix concerns the schemes which aim to control the correctness of the solution to very high accuracy. Within the system constituted by the Vlasov-Landau and Maxwell's equations, there is only one, clearly identified term responsible for dissipation: the Landau's collision integral. This split suggests not abandoning the Hamiltonian formulation of the Vlasov-Maxwell's system [148, 149], well adapted for structure-preserving schemes [150], by incorporating the effect of the collision operator in an appropriate way. Such an endeavour may be achieved through the metric formulation of the collision operator, as it has been proposed by Kaufman [151] and Morrison [152, 153]. The resulting system combining these conservative and dissipative parts takes the qualifier of metriplectic.

The Vlasov-Maxwell' part is described by an Hamiltonian, $\mathsf{H}$, in association with some non-canonical Poisson's brackets, $\{\cdot,\cdot\}$. This bracket is anti-symmetrical, $\{\mathcal{O}_1,\mathcal{O}_2\} = -\{\mathcal{O}_2,\mathcal{O}_1\}$, and verifies the Jacobi's identity:

$$\{\mathcal{O}_1,\{\mathcal{O}_2,\mathcal{O}_3\}\} + \{\mathcal{O}_2,\{\mathcal{O}_3,\mathcal{O}_1\}\} + \{\mathcal{O}_3,\{\mathcal{O}_1,\mathcal{O}_2\}\} = 0,$$

with $\mathcal{O}_1$, $\mathcal{O}_2$, $\mathcal{O}_3$ any three observables. The temporal rate of change of any observable $\mathcal{O}$ is $\{\mathcal{O},\mathsf{H}\}$. Some of them, called Casimir's invariants, are such that their Poisson's brackets with any other obervable is zero. In particular, they do not evolve and trajectories of the system are confined to lie in surfaces defined by the constancy of the Casimir's invariants. These are actually symplectic manifolds embedded in the entire phase space. Among Casimir's invariants, the generalized entropy, $\mathsf{S}$, plays a central role. It determines the rate of dissipation due to collision, $(f_e, -T_e\mathsf{S})$, with $(\cdot,\cdot)$ some symmetrical metric brackets leaving invariant the Hamiltonian and the Vlasov's mean fields. Here, their constancy defines Riemannian manifolds in the phase space. We will not give further details, referring to Morrison's article [153]. To conclude, for any observable $\mathcal{O}$ belonging to the metriplectic system,

$$\partial_t\mathcal{O} = \{\mathcal{O},\mathsf{F}\} + (\mathcal{O},\mathsf{F}),$$

where $\mathsf{F} = \mathsf{H} - T_e\mathsf{S}$ is the generalized free energy. In the following sections, we provide a little more detail on each parts of the system. Since the pioneering work of Kaufman and Morrison, the metriplectic formalism has continued to develop [154], accompanied by several works on related numerical schemes. Among them we will cite Ref. [155].

### 6.1.1 Hamiltonian formulation of the Vlasov-Maxwell's system

The system that combines the Vlasov's equation and the Maxwell's equations can be viewed as the dynamical equations of a continuous infinite dimensional Hamiltonian system. The observables are the scalar field $f_e$ and the two vector fields $\mathbf{E}$ and $\mathbf{B}$. For convenience these vector fields will often be viewed as 3-dimensional scalar fields. The generalized energy, or Hamiltonian, is the functional defined as

$$\mathsf{H}[f_e, \mathbf{E}, \mathbf{B}] = \int \frac{m_e v^2}{2} f_e \; d^6\mathbf{X} + \int \left( \frac{\epsilon_0 \mathbf{E}^2}{2} + \frac{\mathbf{B}^2}{2\mu_0} \right) \; d^3\mathbf{r}, \tag{6.1}$$

where $d^6\mathbf{X} = d^3\mathbf{r}d^3\mathbf{v}$. The evolution of any of the seven scalar observables, $\mathcal{O}$, is given by

$$\partial_t \mathcal{O} = \{\mathcal{O}, \mathsf{H}\} = \sum_{\ell=1}^{4} \mathcal{T}_{\mathcal{O}}^{(\ell)},$$

where we have decomposed the underlying, noncanonical Poisson's brackets, $\{\cdot,\cdot\}$, of $\mathcal{O}$ and $\mathsf{H}$ in four terms for convenience. By noting $\boldsymbol{\nabla}$ and $\boldsymbol{\partial}$, the gradient operators within position and velocity spaces respectively, they are:

$$\mathcal{T}_{\mathcal{O}}^{(1)} = \int \frac{f_e}{m_e} \left( \boldsymbol{\nabla} \frac{\delta \mathcal{O}}{\delta f_e} \cdot \boldsymbol{\partial} \frac{\delta \mathsf{H}}{\delta f_e} - \boldsymbol{\nabla} \frac{\delta \mathsf{H}}{\delta f_e} \cdot \boldsymbol{\partial} \frac{\delta \mathcal{O}}{\delta f_e} \right) \; d^6\mathbf{X}',$$

$$\mathcal{T}_{\mathcal{O}}^{(2)} = \frac{1}{\epsilon_0} \int \left( \frac{\delta \mathcal{O}}{\delta \mathbf{E}} \cdot \boldsymbol{\nabla} \times \frac{\delta \mathsf{H}}{\delta \mathbf{B}} - \frac{\delta \mathsf{H}}{\delta \mathbf{E}} \cdot \boldsymbol{\nabla} \times \frac{\delta \mathcal{O}}{\delta \mathbf{B}} \right) \; d^3\mathbf{r}',$$

$$\mathcal{T}_{\mathcal{O}}^{(3)} = \frac{e}{\epsilon_0 m_e} \int f_e \left( \frac{\delta \mathcal{O}}{\delta \mathbf{E}} \cdot \boldsymbol{\partial} \frac{\delta \mathsf{H}}{\delta f_e} - \frac{\delta \mathsf{H}}{\delta \mathbf{E}} \cdot \boldsymbol{\partial} \frac{\delta \mathcal{O}}{\delta f_e} \right) \; d^6\mathbf{X}',$$

and

$$\mathcal{T}_{\mathcal{O}}^{(4)} = -\frac{e}{m_e^2} \int f_e \mathbf{B} \cdot \left( \boldsymbol{\partial} \frac{\delta \mathcal{O}}{\delta f_e} \times \boldsymbol{\partial} \frac{\delta \mathsf{H}}{\delta f_e} \right) \; d^6\mathbf{X}'.$$

The functional derivatives of $\mathcal{O}$ must be understood as those of the associated, trivial field of functionals defined at the same points as $\mathcal{O}$. More precisely, the functional at a given point associates to the function $\mathcal{O}$ the value of this function at the considered point. The definition of the Frechet's functional derivative is recalled in the Complementary Note 6.2. By omitting the time variable, $f_e(\mathbf{r}, \mathbf{v}) = \int \delta(\mathbf{r}' - \mathbf{r})\delta(\mathbf{v}' - \mathbf{v}) \; f_e(\mathbf{r}', \mathbf{v}') \; d^6\mathbf{X}$, such that we will allow ourself to write

$$\frac{\delta f_e(\mathbf{r}, \mathbf{v})}{\delta f_e(\mathbf{r}', \mathbf{v}')} = \delta(\mathbf{r}' - \mathbf{r})\delta(\mathbf{v}' - \mathbf{v}). \tag{6.2}$$

The same is for the electric and magnetic fields' components. For any of them, for instance any of the electric field,

$$\frac{\delta E_i(\mathbf{r})}{\delta E_j(\mathbf{r}')} = \delta_{ij}\delta(\mathbf{r}' - \mathbf{r}). \tag{6.3}$$

These abuses of notations are quite commons in field theories. It clearly appears that the electric and magnetic fields are not considered as functionals of $f_e$ in spite of the Maxwell-Gauss and Maxwell-Ampère's equations which link them to charge and current densities. In fact, such a coupling between the evolutions of the electron distribution function and the electric and magnetic fields is ensured by $\mathcal{T}_{\mathcal{O}}^{(3)}$ and $\mathcal{T}_{\mathcal{O}}^{(4)}$. Together with Eq. (6.1), $\mathcal{T}_{\mathcal{O}}^{(2)}$ allows to recover the Maxwell's equations in vacuum, and $\mathcal{T}_{\mathcal{O}}^{(1)}$ the Vlasov's equation. Although $\mathcal{T}_{\mathcal{O}}^{(3)}$ was already written by Born and Infield in Ref. [156], the other terms, together with the idea of formulating the Vlasov-Maxwell's equations as an Hamiltonian system belongs to Morrison [148]. In his original work, however, he proposed empirically an expression for $\mathcal{T}_{\mathcal{O}}^{(4)}$ that differs from the one written above, derived by Marsden and Weinstein [149]. Although both verify the Jacobi's identity and lead to the correct dynamical equations, the latter is preferable for reasons, detailed in Ref. [149], which we will not dwell on here.

For the sake of transparency, let us recover the Vlasov and Maxwell's equations. From Eq. (6.1), it is straightforward to write

$$\frac{\delta \mathsf{H}}{\delta f_e} = \frac{m_e v^2}{2}; \quad \frac{\delta \mathsf{H}}{\delta \mathbf{E}} = \epsilon_0 \mathbf{E}; \quad \frac{\delta \mathsf{H}}{\delta \mathbf{B}} = \frac{\mathbf{B}}{\mu_0}.$$

Then, the second term of $\mathcal{T}_{f_e}^{(1)}$ is zero because $\boldsymbol{\nabla}(\delta\mathsf{H}/\delta f_e) = \mathbf{0}$. In the remaining one there appears $\boldsymbol{\partial}(\delta\mathsf{H}/\delta f_e) = m_e\mathbf{v}$, such that

$$\mathcal{T}_{f_e}^{(1)} = \int f_e \delta(\mathbf{v}' - \mathbf{v})\boldsymbol{\nabla}\delta(\mathbf{r}' - \mathbf{r}) \cdot \mathbf{v}' \; d^6\mathbf{X}' = -\mathbf{v} \cdot \boldsymbol{\nabla} f_e,$$

where we used Eq. (6.2) to write the first equality, and integrated by parts to write the second. It is obvious that $\mathcal{T}_{f_e}^{(2)} = 0$. Concerning $\mathcal{T}_{f_e}^{(3)}$, the first term is zero and the other is

$$\mathcal{T}_{f_e}^{(3)} = -\frac{e}{m_e}\int f_e \mathbf{E}\delta(\mathbf{r}' - \mathbf{r}) \cdot \boldsymbol{\partial}\delta(\mathbf{v}' - \mathbf{v}) \; d^6\mathbf{X}' = \frac{e}{m_e}\mathbf{E} \cdot \boldsymbol{\partial} f_e.$$

Here again, we used Eq. (6.2) and then integrated by parts. In the same way,

$$\begin{aligned}\mathcal{T}_{f_e}^{(4)} &= -\frac{e}{m_e}\int f_e \mathbf{B} \cdot \delta(\mathbf{r}' - \mathbf{r})\boldsymbol{\partial}\delta(\mathbf{v}' - \mathbf{v}) \times \mathbf{v}' \; d^6\mathbf{X}' \\ &= \frac{e}{m_e}\mathbf{B} \cdot \boldsymbol{\partial} f_e \times \mathbf{v} = \frac{e}{m_e}\mathbf{v} \times \mathbf{B} \cdot \boldsymbol{\partial} f_e.\end{aligned}$$

Hence, $\partial_t f_e = \mathcal{T}_{f_e}^{(1)} + \mathcal{T}_{f_e}^{(3)} + \mathcal{T}_{f_e}^{(4)}$ is well the Vlasov's equation. We consider now the evolution of the $i$-th component of the electric field. Obviously, $\mathcal{T}_{E_i}^{(1)} = 0$. In $\mathcal{T}_{E_i}^{(2)}$, the second term is zero. By using Eq. (6.3), the second one is

$$\mathcal{T}_{E_i}^{(2)} = \frac{1}{\epsilon_0\mu_0}\int \delta_{ij}\delta(\mathbf{r}' - \mathbf{r})\epsilon_{jkl}\nabla_k B_l \; d^3\mathbf{r}' = c^2(\boldsymbol{\nabla} \times \mathbf{B})_i.$$

Likewise, the second term of $\mathcal{T}^{(3)}_{E_i}$ is zero, whereas the first one is

$$\mathcal{T}^{(3)}_{E_i} = \frac{e}{\epsilon_0}\int f_e \delta_{ij}\delta(\mathbf{r}'-\mathbf{r})v'_j \; d^6\mathbf{X}' = -j_{e\ i}/\epsilon_0,$$

the $i$-th component of the electric current density divided by $-\epsilon_0$. Finally, $\mathcal{T}^{(4)}_{E_i} = 0$. Thus, the Maxwell-Ampère's equation, $\partial_t E_i = \mathcal{T}^{(2)}_{E_i} + \mathcal{T}^{(3)}_{E_i}$, is recovered. It is now the turn of the Maxwell-Faraday's equation. Here again, $\mathcal{T}^{(1)}_{B_i} = \mathcal{T}^{(4)}_{B_i} = 0$. It is also clear that $\mathcal{T}^{(3)}_{B_i} = 0$. There only remains the second term of $\mathcal{T}^{(2)}_{B_i}$, equals to

$$\mathcal{T}^{(2)}_{B_i} = -\int E_j \epsilon_{jkl}\nabla_k \delta_{il}\delta(\mathbf{r}'-\mathbf{r})\; d^3\mathbf{r}' = \epsilon_{jki}\int \delta(\mathbf{r}'-\mathbf{r})\nabla_k E_j \; d^3\mathbf{r}' = -(\boldsymbol{\nabla}\times\mathbf{E})_i$$

The second equality is obtained through a by parts integration, whereas the last one relies on the anti-symmetry of the Levi-Civita's symbol: $\epsilon_{jki} = -\epsilon_{ikj}$. The remaining two Maxwell's equations are viewed as initial conditions. Indeed they express the divergences of the fields, which actually are Casimir's invariants. In order to show this result we need in particular

$$\frac{\delta}{\delta\mathbf{E}(\mathbf{r}')}[\boldsymbol{\nabla}\cdot\mathbf{E}](\mathbf{r}) = -\boldsymbol{\nabla}\delta(\mathbf{r}'-\mathbf{r}). \tag{6.4}$$

This equality is obtained, as usual, by writing $[\boldsymbol{\nabla}\cdot\mathbf{E}](\mathbf{r}) = \int \delta(\mathbf{r}'-\mathbf{r})[\boldsymbol{\nabla}\cdot\mathbf{E}](\mathbf{r}')\; d^3\mathbf{r}'$. For any test field $\eta\boldsymbol{\phi}$ with $\eta$ an arbitrarily small parameter,

$$\begin{aligned}[\boldsymbol{\nabla}\cdot(\mathbf{E}+\eta\boldsymbol{\phi})](\mathbf{r}) - [\boldsymbol{\nabla}\cdot\mathbf{E}](\mathbf{r}) &= \int \delta(\mathbf{r}'-\mathbf{r})\boldsymbol{\nabla}\cdot\eta\boldsymbol{\phi}\; d^3\mathbf{r}' \\ &= -\int \eta\boldsymbol{\phi}\cdot\boldsymbol{\nabla}\delta(\mathbf{r}'-\mathbf{r})\; d^3\mathbf{r}',\end{aligned}$$

after having integrated by parts. The last equality allows us to identify the functional derivative written above. Then we define

$$\mathcal{C}_{\mathbf{E}} = \boldsymbol{\nabla}\cdot\mathbf{E} - \rho/\epsilon_0; \quad \mathcal{C}_{\mathbf{B}} = \boldsymbol{\nabla}\cdot\mathbf{B}. \tag{6.5}$$

The charge density is viewed as a functional of $f_e$,

$$\rho[f_e] = e\left(Zn_i - \int f_e \; d^3\mathbf{v}'\right),$$

such that $\delta\rho(\mathbf{r})/\delta f_e(\mathbf{r}') = -e\delta(\mathbf{r}'-\mathbf{r})$. Consider any observable $\mathcal{O}$. The Poisson's bracket $\{\mathcal{O},\mathcal{C}_{\mathbf{E}}\}$ is the sum of the four terms $\mathcal{T}^{(\ell)}_{\mathcal{O}}$ in which $\mathsf{H}$ is substituted by $\mathcal{C}_{\mathbf{E}}$. The functional derivative of $\mathcal{C}_{\mathbf{E}}$ with respect to the magnetic field is zero, so is the last term of the Poisson's bracket. By taking into account $\delta\mathcal{C}_{\mathbf{E}}(\mathbf{r})/\delta\mathbf{E}(\mathbf{r}') = -\boldsymbol{\nabla}\delta(\mathbf{r}'-\mathbf{r})$ and $\delta\mathcal{C}_{\mathbf{E}}(\mathbf{r})/\delta f_e(\mathbf{r}') = e\delta(\mathbf{r}'-\mathbf{r})/\epsilon_0$, the sum of the three other terms is

$$\begin{aligned}\{\mathcal{O},\mathcal{C}_{\mathbf{E}}\} = &-\int \frac{f_e}{m_e}\frac{e}{\epsilon_0}\boldsymbol{\nabla}\delta(\mathbf{r}'-\mathbf{r})\cdot\boldsymbol{\partial}\frac{\delta\mathcal{O}}{\delta f_e}\; d^6\mathbf{X}' + \frac{1}{\epsilon_0}\int \boldsymbol{\nabla}\delta(\mathbf{r}'-\mathbf{r})\cdot\boldsymbol{\nabla}\times\frac{\delta\mathcal{O}}{\delta\mathbf{B}}\; d^3\mathbf{r}' \\ &+ \frac{e}{\epsilon_0 m_e}\int f_e\boldsymbol{\nabla}\delta(\mathbf{r}'-\mathbf{r})\cdot\boldsymbol{\partial}\frac{\delta\mathcal{O}}{\delta f_e}\; d^6\mathbf{X}' = 0.\end{aligned}$$

Indeed, the first and last integrals cancel, and the second one is zero. Hence $\mathcal{C}_{\mathbf{E}}$ is well a Casimir's invariant. The same is for $\mathcal{C}_{\mathbf{B}}$. In particular, they are constant in time. This means that if both the Maxwell-Gauss and Maxwell-Thomson's equations are verified at the origin of time, they remain so for ever as expected.

### 6.1.2 Metric structure of the Landau's integral

The rate of change of the electron distribution function due to electron-electron collisions is given by

$$\mathcal{C}_{ee}[f_e, f_e] = -\frac{Y_{ee}}{m_e}\frac{\partial}{\partial v_k}\int U_{kl}(\mathbf{v}-\mathbf{v}')V_{ee\ l}(\mathbf{v},\mathbf{v}')\ d^3\mathbf{v}',$$

with

$$V_{ee\ l}(\mathbf{v},\mathbf{v}') = \frac{f_e(\mathbf{v})}{m_e}\frac{\partial f_e}{\partial v_l'}(\mathbf{v}') - \frac{f_e(\mathbf{v}')}{m_e}\frac{\partial f_e}{\partial v_l}(\mathbf{v}), \tag{6.6}$$

where we omitted the spatial and temporal variables for clarity. $\mathcal{C}_{ee}[f_e, f_e]$ will be expressed as the symmetric bracket $(f_e, -T_e\mathsf{S})$, with the generalized entropy functional defined as

$$\mathsf{S}[f_e] = -k_B\int f_e \ln \widetilde{f}_e\ d^3\mathbf{v}.$$

The normalization of the distribution function in argument of the logarithm is the same as in App. 6.2.1.2: $\widetilde{f}_e = h^3 f_e/m_e^3$. It remains to precise the bracket, $(\cdot,\cdot)$. For this purpose, we recall that $\delta\mathsf{S}/\delta f_e = -k_B(1+\ln\widetilde{f}_e)$. Therefore $\partial(\delta\mathsf{S}/\delta f_e)/\partial v_l = -(k_B/f_e)\partial f_e/\partial v_l$, such that Eq. (6.6) can be expressed as

$$\frac{f_e(\mathbf{v})f_e(\mathbf{v}')}{m_e k_B T_e}\left(\frac{\partial}{\partial v_l'}\frac{\delta[-T_e\mathsf{S}]}{\delta f_e(\mathbf{v}')} - \frac{\partial}{\partial v_l}\frac{\delta[-T_e\mathsf{S}]}{\delta f_e(\mathbf{v})}\right).$$

Here, the electron temperature is not considered as a functional of $f_e$, but as a scalar field in space. Then, we introduce a dummy velocity variable, $\mathbf{v}''$, to write $\mathcal{C}_{ee}[f_e, f_e]$ as $-Y_{ee}/m_e$ multiplied by

$$\begin{aligned}\int \delta(\mathbf{v}''-\mathbf{v})\left(\frac{\partial}{\partial v_k''}\int U_{kl}(\mathbf{v}''-\mathbf{v}')V_{ee\ l}(\mathbf{v}'',\mathbf{v}')\ d^3\mathbf{v}'\right)\ d^3\mathbf{v}''&\\ = -\int \frac{\partial}{\partial v_k''}\frac{\delta f_e(\mathbf{v})}{\delta f_e(\mathbf{v}'')}U_{kl}(\mathbf{v}''-\mathbf{v}')V_{ee\ l}(\mathbf{v}'',\mathbf{v}')\ d^3\mathbf{v}'d^3\mathbf{v}'',&\end{aligned}$$

where we integrated by parts, and expressed the delta by means of Eq. (6.2). The integrand expression is anti-symmetrical with respect to an exchange of the variables of integration. As a result, the electron-electron collision operator is the following half-sum:

$$-\frac{Y_{ee}}{2m_e}\int\left(\frac{\partial}{\partial v_k'}\frac{\delta f_e(\mathbf{v})}{\delta f_e(\mathbf{v}')} - \frac{\partial}{\partial v_k''}\frac{\delta f_e(\mathbf{v})}{\delta f_e(\mathbf{v}'')}\right)U_{kl}(\mathbf{v}''-\mathbf{v}')V_{ee\ l}(\mathbf{v}'',\mathbf{v}')\ d^3\mathbf{v}'\ d^3\mathbf{v}''$$

Thus, we shown that $\mathcal{C}_{ee}[f_e, f_e] = (f_e, -T_e\mathsf{S})$, with, for any observable $\mathcal{O}$:

$$\begin{aligned}(\mathcal{O}, -T_e\mathsf{S}) = \frac{Y_{ee}}{2k_BT_e}\int\left(\frac{1}{m_e}\frac{\partial}{\partial v_k'}\frac{\delta\mathcal{O}}{\delta f_e(\mathbf{v}')} - \frac{1}{m_e}\frac{\partial}{\partial v_k''}\frac{\delta\mathcal{O}}{\delta f_e(\mathbf{v}'')}\right)U_{kl}(\mathbf{v}''-\mathbf{v}')&\\ f_e(\mathbf{v}')f_e(\mathbf{v}'')\left(\frac{1}{m_e}\frac{\partial}{\partial v_l'}\frac{\delta[-T_e\mathsf{S}]}{\delta f_e(\mathbf{v}')} - \frac{1}{m_e}\frac{\partial}{\partial v_l''}\frac{\delta[-T_e\mathsf{S}]}{\delta f_e(\mathbf{v}'')}\right)d^3\mathbf{v}'d^3\mathbf{v}''&\end{aligned} \tag{6.7}$$

An extension of this formula to multi-species collisions can be found in Ref. [157]. The electric and magnetic fields, together with the Hamiltonian (6.1), are left invariant by this bracket. Indeed, the functional derivatives of the fields with respect to $f_e$ are zero. That of the Hamiltonian is $\delta\mathsf{H}/\delta f_e(\mathbf{v}) = m_e v^2/2$, such that within the integrand of $(\mathcal{O}, \mathsf{H})$ there appears

$$U_{kl}(\mathbf{v}'' - \mathbf{v}') \left( \frac{1}{m_e} \frac{\partial}{\partial v_l'} \frac{\delta \mathsf{H}}{\delta f_e(\mathbf{v}')} - \frac{1}{m_e} \frac{\partial}{\partial v_l''} \frac{\delta \mathsf{H}}{\delta f_e(\mathbf{v}'')} \right) = U_{kl}(\mathbf{v}'' - \mathbf{v}')(v_l' - v_l'') = 0.$$

Indeed, the Landau's kernel tensor, $U_{kl}(\mathbf{v}'' - \mathbf{v}')$ is the projector on $(\mathbf{v}'' - \mathbf{v}')^\perp$ divided by $|\mathbf{v}'' - \mathbf{v}'|$.

This page is unintentionally left not blank.

This page is unintentionally left not blank.

## 6.2 Discussion around the kinetic discontinuity

In this complementary note, we discuss and deepen most of the results obtained by Gurevich and Istomin in Ref. [66]. Their work provides a rather complete treatment of the problem of the one dimensional quasi-static nonlocal electron transport induced by a steep temperature gradient. The major flat is the neglect of the electric field, bypassing the problem of its self-consistent determination through the distribution function. Apart from this point, the work of Gurevich and Istomin is pioneering in many respects as it will be shown hereafter.

The considered situation, one-dimensional, is described at the beginning of the Ch. 2. As usual, the electron-ion collisions are modelled through the Lorentz's operator,

$$\frac{\nu_{ei}}{2}\frac{\partial}{\partial\cos\theta}\sin^2\theta\frac{\partial f_e}{\partial\cos\theta},$$

and electron-electron collisions through the lowest order of the high velocity limit of $\mathcal{C}_{ee}[f_e, f_M]$, derived in App. 2.B:

$$\frac{\nu_{ee}}{2}\frac{\partial}{\partial\cos\theta}\sin^2\theta\frac{\partial f_e}{\partial\cos\theta}+\nu_{ee}v\partial_v\left(f_e+\frac{v_T^2}{v}\partial_v f_e\right).$$

As a consequence of their assumptions Gurevich and Istomin obtained a linear problem. Obviously, this property should not be considered sufficient to judge the relevance of their study, since the mathematical convenience is never an argument by itself. However, in Ch. 3 it is shown that the electric field stays close to the Spitzer-Harm's value. In a first approximation, it may, therefore, be seen as a *parameter* fixed by the local hydrodynamic variables rather than the distribution function itself. The essential role it plays to properly describe the phenomenon, emphasized in Ch. 2, pushes us to consider it, at least in a first time, in the kinetic equation,

$$\begin{aligned}v\cos\theta\nabla_z f_e-\frac{eE_z}{m_e}\left(\frac{\sin^2\theta}{v}\frac{\partial f}{\partial\cos\theta}+\cos\theta\partial_v f\right)\\ =\nu_{ee}v\partial_v\left(f_e+\frac{v_T^2}{v}\partial_v f_e\right)+k\nu_{ee}\frac{\partial}{\partial\cos\theta}\sin^2\theta\frac{\partial f_e}{\partial\cos\theta},\end{aligned}\tag{6.8}$$

while preserving the linearity of the problem. Following Gurevich and Istomin, we noted $k=(1+Z)/2$, considering that $\nu_{ei}=Z\nu_{ee}$, at usual.

### 6.2.1 Reduced system of equations

The mathematical framework proposed by Gurevich and Istomin begins with a judicious choice of variables presented in Sec. 6.2.1.1. An extended version of the resulting equation is derived, with an explicit account for the the electric field. In Sec. 6.2.1.2, the unknown is developed in a manner similar to that of Chapman-Enskog. This makes the overall approach close to the so-called M1 closure, about which we briefly digress. Then, the system of equations coupling the successive terms of the expansion is derived, still with the electric field term. When neglecting the latter take the form of those written by Gurevich and Istomin.

#### 6.2.1.1 The set of variables

In place of $f_e$, we consider the function $g_e$ defined by

$$f_e(z, v, \theta) = g_e\Big(\tau(z), \beta(v), \mu(\theta)\Big), \tag{6.9}$$

where $\mu = \cos\theta$, and

$$\tau(z) = \frac{|\nabla_z T_e|_M}{T_H n_H} \int_0^z n_e(z')dz', \tag{6.10}$$

with $|\nabla_z T_e|_M = \max|\nabla_z T_e|$ the maximum of the absolute value of the temperature gradient. $T_H$ and $n_H$ are, respectively, the electron temperature and density in the hot region of the plasma. By following again Gurevich and Istomin, we note

$$\gamma = \frac{\lambda_H}{T_H}|\nabla_z T_e|_M, \tag{6.11}$$

where $\lambda_H = \lambda_{ee}(v_{T_H}) = Z\lambda_{ei}(v_{T_H}) = Z\lambda_{ei}^{T_H}/[3(\pi/2)^{1/2}]$ is the thermal electron-electron mean free path in the hot region. Then, $\tau$ appears as being analogous to an optical depth normalized to $\gamma/\lambda_H$. Finally, $\beta$, which is noted $z$ by Gurevich and Istomin, is a normalized energy

$$\beta = \gamma^{1/2}\frac{m_e v^2}{k_B T_H}. \tag{6.12}$$

The factor $\gamma^{1/2}$ is here so that $\beta \geq 1$ means $\lambda_{ee} \geq T_H/|\nabla_z T_e|_M = \lambda_H/\gamma$. The last variable we wish to introduce is the normalized temperature

$$t = T_e/T_H. \tag{6.13}$$

As a result, the left hand side of Eq. (6.8) is

$$v\mu\frac{|\nabla_z T_e|_M}{T_H}\frac{n_e}{n_H}\partial_\tau g_e - \frac{eE_z}{m_e}\left(\frac{1-\mu^2}{v}\partial_\mu g_e + \frac{2\mu\beta}{v}\partial_\beta g_e\right),$$

whereas the right hand side is the sum of the angular Laplacian, $\partial_\mu(1-\mu^2)\partial_\mu$, multiplied by $k\nu_{ee}$, and of the radial part,

$$\nu_{ee} v\partial_v\left(f + \frac{v_T^2}{v}\partial_v f\right) = \nu_{ee} 2\beta\partial_\beta\left(g + 2\gamma^{1/2}t\partial_\beta g\right).$$

We used $(v_T/v)^2 = k_B T_H/(m_e v^2)t = \gamma^{1/2}t/\beta$. By dividing the resulting kinetic equation by $\nu_{ee}$, we obtain

$$\mu\beta^2\partial_\tau g_e - r\Big[(1-\mu^2)\partial_\mu g_e + 2\mu\beta\partial_\beta g_e\Big] = k\partial_\mu(1-\mu^2)\partial_\mu g_e + 2\beta\partial_\beta\left(g_e + 2\gamma^{1/2}t\partial_\beta g_e\right), \tag{6.14}$$

where we have introduced the ratio between the electric force and the stopping force in the high velocity limit:

$$r = \frac{eE_z}{m_e v\nu_{ee}} = \frac{\beta}{\gamma^{1/2}}\frac{eE_z}{m_e v_{T_H}\nu_H} := \frac{\beta}{\gamma^{1/2}}r_H. \tag{6.15}$$

In Eq. (6.14), the coefficient in front of $\partial_\tau g_e$ comes from

$$\mu\frac{|\nabla_z T_e|_M}{T_H}\frac{n}{n_H}\frac{v}{\nu_{ee}} = \mu\frac{\gamma}{\lambda_H}\frac{n}{n_H}\lambda_{ee} = \mu\gamma\frac{v^4}{v_{T_H}^4} = \mu\beta^2.$$

Finally, following Gurevich and Istomin, we introduce the function $\varphi$ defined through

$$g_e = e^{-\varphi}. \tag{6.16}$$

Such a variable change does not require any assumption because $g_e$ is, by definition, strictly positive. For any $X = \tau, \beta, \mu$, $\partial_X g_e = -g_e \partial_X \varphi$ and

$$\partial_X^2 g_e = g_e\left[(\partial_X\varphi)^2 - \partial_X^2\varphi\right]$$

Therefore, the left hand side of Eq. (6.14) is

$$-g_e\left(\mu\beta^2\partial_\tau\varphi - r\left[(1-\mu^2)\partial_\mu\varphi + 2\mu\beta\partial_\beta\varphi\right]\right).$$

In the right hand side, we develop the Laplacian, such that

$$k\left[-2\mu\partial_\mu g_e + (1-\mu^2)\partial_\mu^2 g_e\right] = g_e k\left[2\mu\partial_\mu\varphi + (1-\mu^2)(\partial_\mu\varphi)^2 - (1-\mu^2)\partial_\mu^2\varphi\right],$$

whereas the radial term is transformed as,

$$2\beta\partial_\beta\left(g_e + 2\gamma^{1/2}t\partial_\beta g_e\right) = -g_e\left(2\beta\left[1 - 2\gamma^{1/2}t\partial_\beta\varphi\right]\partial_\beta\varphi + 4\gamma^{1/2}t\beta\partial_\beta^2\varphi\right).$$

We distributed $2\beta\partial_\beta$, and regrouped the terms in $\partial_\beta\varphi$. Dividing each side of the kinetic equation by $g_e$ leads to

$$\begin{aligned}\mu\beta^2\partial_\tau\varphi - r\Big[&(1-\mu^2)\partial_\mu\varphi + 2\mu\beta\partial_\beta\varphi\Big]\\ &- 2\beta\Big[1 - 2\gamma^{1/2}t\partial_\beta\varphi\Big]\partial_\beta\varphi - 4\gamma^{1/2}t\beta\partial_\beta^2\varphi\\ &+ k\Big[2\mu\partial_\mu\varphi + (1-\mu^2)(\partial_\mu\varphi)^2 - (1-\mu^2)\partial_\mu^2\varphi\Big] = 0.\end{aligned} \tag{6.17}$$

By taking $r = 0$, this Eq. (6.17) is the same as Eq. (11) written by Gurevich and Istomin in Ref. [66]. In Ref. [158], Gritsyk and Somov applied the formalism of Gurevich and Istomin to study the nonlocal electron transport in solar flares. They pretend that Eq. (6.17) with $r = 0$ is only valid for $\gamma \ll 1$. As we just have seen, this condition is not required and we disagree with their claim.

#### 6.2.1.2 Expansion in the small parameter $\gamma$. Digression on the similarity with the M1 closure.

Whether in the case of a plasma or a neutral gas, for increasing values of $\gamma$ the transport regime gradually takes a nonlocal character. However, a significant deviation from the local regime predictions occurs for lower values of $\gamma$ in a plasma, due to the strong velocity dependence of the electron mean free path. Values of $\gamma$ just above, or even equal to, few percent already correspond to situations in which the nonlocal character of the transport must be taken into account. The values of $\gamma$ we wish to consider hardly exceed the tens of percent. Therefore, we see the

possibility of describing strongly out-of-equilibrium regimes while considering $\gamma$ as a small parameter. This, obviously, is not possible in case of a neutral gas.

Considering now the smallness of $\gamma$, we look for a solution of the form

$$\varphi = \gamma^{-1/2}\varphi_0 + \gamma^{-1/4}\varphi_1 + \varphi_2 + \gamma^{1/4}\varphi_3 + ... = \sum \gamma^{p/4-1/2}\varphi_p. \tag{6.18}$$

The sum is performed from $p = 0$ to, at least, $p = 2$. Such a development is analogous to a Chapman-Enskog's expansion, about which information can be found in *e.g* Ref. [159], within the Ch. 7, around the Par. 15. The choice of expansion (6.18) can be understood if we notice that the equilibrium distribution function can be written as $\exp(-\varphi_M)$ with

$$\varphi_M = \frac{\beta}{2t\gamma^{1/2}} + \ln\left(\frac{(2\pi t)^{3/2}v_{T_H}^3}{n_e}\right) \tag{6.19}$$

Hence, in the limit of very low gamma values, $\varphi_0 = \beta/(2t)$, $\varphi_1 = 0$, $\varphi_2 = \ln[(2\pi t)^{3/2}v_{T_H}^3/n_e]$ and $\varphi_p = 0$ for $p \geq 3$.

The form in which the solutions of Eq. (6.17) are sought is quite similar to the *M1 closure* [160], which deserves a brief digression. Although it corresponds to a variable change, it can be introduced from the extremization of the functional

$$H_{\mathbf{r},v}[f_e] = -\int_{\mathbb{S}^2}\left[\ln\left(\frac{h^3}{m_e^3}f_e\right) - 1\right] f_e \; d^2\Omega,$$

under the constraints that $f_0$ and $\mathbf{f}_1$ are the first order components of the distribution function. The appearance of $h$, the Planck's constant, together with $-f_e$ in the integrand will be understood later. Introducing the Lagrange's multipliers $g_0$ and $\mathbf{g}_1$, we therefore look for extremizing $L_{\mathbf{r},v}[f_e] = H_{\mathbf{r},v}[f_e] + K_{\mathbf{r},v}[f_e]$, where

$$K_{\mathbf{r},v}[f_e] = -4\pi g_0\left(f_0 - \frac{1}{4\pi}\int_{\mathbb{S}^2} f_e \; d^2\Omega\right) - 4\pi \boldsymbol{g}_1/3 \cdot \left(\mathbf{f}_1 - \frac{3}{4\pi}\int_{\mathbb{S}^2} \boldsymbol{\Omega} f_e \; d^2\Omega\right).$$

The functional derivative, $\delta H_v/\delta f_e$, of $H_v$ is the linear form defined, for any test function $\phi$ of $\mathbb{S}^2$, by

$$\int_{\mathbb{S}^2} \phi \frac{\delta H_{\mathbf{r},v}}{\delta f_e} \; d^2\Omega' = \lim_{\varepsilon\to 0} \frac{H_{\mathbf{r},v}[f_e + \varepsilon\phi] - H_{\mathbf{r},v}[f_e]}{\varepsilon},$$

Since $H_{\mathbf{r},v}$ is a functional defined through an integral, we shall allow ourselves to consider the Dirac's distribution centered at $\boldsymbol{\Omega}$ as a test function, and will note the corresponding functional derivative as $\delta H_{\mathbf{r},v}[f_e]/\delta f_e(\boldsymbol{\Omega})$. This abuse is quite common. For the sake of convenience, we momentarily note $\widetilde{f}_e = h^3 f_e/m_e^3$. Omitting to write the space variable in arguments,

$$\begin{aligned} H_{\mathbf{r},v}[f_e + \varepsilon\delta] &= -\int_{\mathbb{S}^2}\Big[\ln\Big(\widetilde{f}_e(\boldsymbol{\Omega}') + \varepsilon\widetilde{\delta}(\boldsymbol{\Omega} - \boldsymbol{\Omega}')\Big) - 1\Big]\Big[f_e(\boldsymbol{\Omega}') + \varepsilon\delta(\boldsymbol{\Omega} - \boldsymbol{\Omega}')\Big] d^2\Omega' \\ &\simeq -\int_{\mathbb{S}^2}\Big[\ln\widetilde{f}_e(\boldsymbol{\Omega}') - 1 + \varepsilon\frac{\delta(\boldsymbol{\Omega} - \boldsymbol{\Omega}')}{f_e(\boldsymbol{\Omega}')}\Big]\Big[f_e(\boldsymbol{\Omega}') + \varepsilon\delta(\boldsymbol{\Omega} - \boldsymbol{\Omega}')\Big] d^2\Omega', \end{aligned}$$

where we used the first order expansion of the logarithm. Therefore, to first order in $\varepsilon$, $H_{\mathbf{r},v}[f_e + \varepsilon\delta]$ is equal to the sum of $H_{\mathbf{r},v}[f_e]$ and

$$-\varepsilon \int_{\mathbb{S}^2} \Big( \ln \widetilde{f}_e(\mathbf{\Omega}') - 1\Big)\delta(\mathbf{\Omega} - \mathbf{\Omega}')d^2\Omega' - \int_{\mathbb{S}^2} \varepsilon \frac{\delta(\mathbf{\Omega} - \mathbf{\Omega}')}{f_e(\mathbf{\Omega}')}\Big[f_e(\mathbf{\Omega}') + \varepsilon\delta(\mathbf{\Omega} - \mathbf{\Omega}')\Big]d^2\Omega'$$
$$\simeq -\varepsilon \int_{\mathbb{S}^2} \ln \widetilde{f}_e(\mathbf{\Omega}')\delta(\mathbf{\Omega} - \mathbf{\Omega}')d^2\Omega' = -\varepsilon \ln \widetilde{f}_e(\mathbf{\Omega}).$$

Therefore,

$$\frac{\delta H_{\mathbf{r},v}[f_e]}{\delta f_e(\mathbf{\Omega})} = -\ln \widetilde{f}_e(\mathbf{\Omega}).$$

In the same manner, $K_{\mathbf{r},v}[f_e + \varepsilon\delta]$ is equal to $K_{\mathbf{r},v}[f_e]$ plus,

$$g_0 \int_{\mathbb{S}^2} \varepsilon\delta(\mathbf{\Omega} - \mathbf{\Omega}')d^2\Omega' + \mathbf{g}_1 \cdot \int_{\mathbb{S}^2} \mathbf{\Omega}'\varepsilon\delta(\mathbf{\Omega} - \mathbf{\Omega}')d^2\Omega' = \varepsilon\big(g_0 + \mathbf{g}_1 \cdot \mathbf{\Omega}\big).$$

Therefore, $\delta K_{\mathbf{r},v}[f_e]/\delta f_e(\mathbf{\Omega}) = g_0 + \mathbf{g}_1 \cdot \mathbf{\Omega}$. Thus, $\delta L_{\mathbf{r},v}[f_e]/\delta f_e(\mathbf{\Omega}) = 0$ leads to $\widetilde{f}_e = \exp(g_0 + \mathbf{g}_1 \cdot \mathbf{\Omega})$. This form almost corresponds to the variable change (6.16), with a P1 expansion of the function in argument of the exponential. As researched, it provides an expression of $\int_{\mathbb{S}^2} \mathbf{\Omega} \otimes \mathbf{\Omega} f_e d^2\Omega$ in function of $f_0$ and $\mathbf{f}_1$. From a numerical perspective, the fact such a form may be obtained by minimizing a functional may certainly be exploited. However, calling it an entropic closure [57] calls for certain precautions. As is well-known, the Boltzmann's function,

$$H = -k_B \int f_e \ln\left(\frac{h^3}{e^1 m_e^3} f_e\right) v^2 dv d^2\Omega d^3\mathbf{r} = -k_B \int H_{\mathbf{r},v}[f_e] v^2 dv d^3\mathbf{r},$$

where the spatial integration is performed on the entire volume $V = \int d^3\mathbf{r}$ of the plasma supposed isolated, is an increasing function of time as soon as the electron distribution function obeys a kinetic equation with either the Landau or BGL's collision operator [161]. We noted $e^1 = \exp(1)$ the Euler's number. Such an increase is only ensured by collisions. Indeed, when using the kinetic equation to compute the time derivative of $H$, there appears integrals over the entire phase space of the divergence of vector fields, that can be transformed though Stokes' theorem into integrals of fluxes on the edges. The integral over the surface of the plasma is zero because, by definition, no electrons nor ions enter or leave from the volume occupied by the plasma. Similarly, the integral in velocity is zero as being performed on a infinitely distant surface from that delimiting the support of the distribution function. The limit of $H$ is

$$H(\infty) = -k_B \int F_M \ln\left(\frac{h^3}{e^1 m_e^3} F_M\right) v^2 dv d^2\Omega d^3\mathbf{r}$$
$$= -k_B n_e V \left[\ln\left(n_e \left[\frac{h}{(2\pi)^{1/2} m_e v_T}\right]^3\right) - \frac{5}{2}\right],$$

where $F_M = n_e/[(2\pi)^{3/2} v_T^3] \exp(-v^2/[2v_T^2])$ is the global equilibrium distribution function of the entire plasma, with uniform electron density, $n_e$, and temperature, $T_e$. The last expression of $H(\infty)$, in which appears the product of the electron

density by the cube of the thermal de Broglie's length, $h/[(2\pi)^{1/2}m_e v_T]$, is nothing else than the Sackur-Tetrode's formula, giving the entropy of a monoatomic ideal gas. In order to obtain it, we used the relation

$$\int_0^\infty v^{2p} e^{-v^2/(2v_T^2)} dv = \frac{(2p)!}{2^{2p}p!}\frac{\pi^{1/2}}{2}\left(v_T\sqrt{2}\right)^{2p+1},$$

with $p = 1$ and 2. Therefore we may be tempted to identify $H(\infty)$ as the thermodynamic entropy of the plasma. Going even further, when the plasma is in a weakly out-of-equilibrium macroscopic state, it would still appear possible to associate a thermodynamic entropy to each local mesoscopic volume at equilibrium. These mesoscopic volumes are not isolated, and for time increments much larger than the duration needed for the local equilibrium distribution to be established, the following integral,

$$-k_B \int_0^\infty f_e \ln\left(\frac{h^3}{e^1 m_e^3} f_e\right) v^2 dv d^2\Omega = -k_B \int_0^\infty H_{\mathbf{r},v}[f_e] v^2 dv,$$

may be identified as the entropy density. Out of any equilibrium, it would be reasonable to call $H$ the kinetic entropy, as we do in the case of the temperature. These conclusions are, obviously, questionable. Like for any system, the entropy of the plasma is defined as

$$S = k_B \ln W,$$

where $W$ is the statistical weight of the considered macroscopic state. It corresponds to the number of microscopic states, or configurations within the phase space, that lead to the aforementioned macroscopic state. As Landau and Lifchitz detail in Par. 40 of Ref. [48], this formula only coincides with $H$ in the case of an ideal gas, for which the correlations associated to the interactions between its constituents do not exist. This results, indeed, into considerable simplifications when enumerating the microscopic states, and to the possibility of expressing $S$ with the single particle distribution function $f_e$ only. The question is therefore to know in what extent $H$ is a good approximation of $S$. This problem is addressed by Laval *et al.* in Ref. [162]. They shown that $S \leq H$, reflecting the higher degree of order induced by the interactions, and computed the lowest order correction induced by binary correlations within the plasma out-of-equilibrium. The retention of such an order is consistent with the closure of the Bogoliubov-Born-Green-Kirkwood-Yvon's hierarchy that leads to the kinetic equation, since the collision operator results from the consideration of the second order correlation function in the cluster expansion of the Liouville's distribution. Thus, while $H$ is obtained by neglecting any interactions, its increase is ensured by them.

In global equilibrium, the correction found by Laval *et al.* is in agreement with that given by Balescu in Ref. [107]:

$$S(\infty) \simeq H(\infty) - \frac{k_B n_e V}{24\pi n_e \lambda_{De}^3},$$

with $\lambda_{De} = (\epsilon_0 k_B T_e/[n_e e^2])^{1/2}$ the electron Debye's length. As it could be expected, the additional term is proportional to $N_{De}^{-1} = (4\pi n_e \lambda_{De}^3/3)^{-1}$, the inverse of the

number of electrons a Debye's sphere contains. It is equal to $3(4\pi)^{1/2}\Gamma_{ee}^{3/2}$, where $\Gamma_{ee}$ is the electron-electron coupling parameter. The lower this coupling parameter, the more the electron plasma behaves like an ideal gas. Out of equilibrium, Laval *et al.* showed that $H$ is no longer an increasing function of time if the plasma is unstable. Only the sum of $H$ and the corrective term has such a property, which they interpret as follows. The plasma can be considered as being constituted by two interacting sub-systems: a gas of weakly coupled charges which trend toward equilibrium is measured by the increase of $H$, and a set of incoherent electrostatic waves emitted and absorbed by these charges. As none of these systems is isolated, there is no reason to expect from each of them to evolve at each time toward equilibrium. As a conclusion to this digression, we hope that the reader will agree that the physical interpretation underlying the maximization of $H_{\mathbf{r},v}$, which is not even $H$, is fragile. It seems better to present the M1 closure as a change of variable, which is, by the way, a fully justified procedure.

We shall now substitute the expansion (6.18) up to order three in the kinetic equation (6.17). For clarity, this substitution is explicitly written:

$$
\begin{aligned}
0 =& \mu\beta^2\partial_\tau\left[\frac{\varphi_0}{\gamma^{1/2}}+\frac{\varphi_1}{\gamma^{1/4}}+\varphi_2+\gamma^{1/4}\varphi_3\right]\\
&+k\Bigg[2\mu\partial_\mu\left(\frac{\varphi_0}{\gamma^{1/2}}+\frac{\varphi_1}{\gamma^{1/4}}+\varphi_2+\gamma^{1/4}\varphi_3\right)\\
&+(1-\mu^2)\left(\partial_\mu\left[\frac{\varphi_0}{\gamma^{1/2}}+\frac{\varphi_1}{\gamma^{1/4}}+\varphi_2+\gamma^{1/4}\varphi_3\right]\right)^2\\
&-(1-\mu^2)\partial_\mu^2\left(\frac{\varphi_0}{\gamma^{1/2}}+\frac{\varphi_1}{\gamma^{1/4}}+\varphi_2+\gamma^{1/4}\varphi_3\right)\Bigg]\\
&-r_H\beta\Bigg[(1-\mu^2)\partial_\mu\left(\frac{\varphi_0}{\gamma}+\frac{\varphi_1}{\gamma^{3/4}}+\frac{\varphi_2}{\gamma^{1/2}}+\frac{\varphi_3}{\gamma^{1/4}}\right)\\
&+2\mu\beta\partial_\beta\left(\frac{\varphi_0}{\gamma}+\frac{\varphi_1}{\gamma^{3/4}}+\frac{\varphi_2}{\gamma^{1/2}}+\frac{\varphi_3}{\gamma^{1/4}}\right)\Bigg]\\
&-2\beta\Big[1-2t\partial_\beta\left(\varphi_0+\gamma^{1/4}\varphi_1+\gamma^{1/2}\varphi_2+\gamma^{3/4}\varphi_3\right)\Big]\\
&\times\partial_\beta\left(\frac{\varphi_0}{\gamma^{1/2}}+\frac{\varphi_1}{\gamma^{1/4}}+\varphi_2+\gamma^{1/4}\varphi_3\right)\\
&-4t\beta\partial_\beta^2\left(\varphi_0+\gamma^{1/4}\varphi_1+\gamma^{1/2}\varphi_2+\gamma^{3/4}\varphi_3\right)
\end{aligned}
\tag{6.20}
$$

The effect of the factor $r = r_H\beta/\gamma^{1/2}$ is to decrease the degree by 1/2. As we shall look to terms up to order $-1/4$, the expansion must be pushed up to the order $p$ such that $p/4-1=-1/4$. This is the reason why we accounted for $\gamma^{1/4}\varphi_3$ despite this term does not appear in the analysis of Gurevich and Istomin. We then equate terms with the same power of $\gamma$ in Eq. (6.20):

1. Terms in $1/\gamma$:

$$0 = (1-\mu^2)[\partial_\mu\varphi_0]^2 - r_H\beta\left[(1-\mu^2)\partial_\mu\varphi_0 + 2\mu\beta\partial_\beta\varphi_0\right] \tag{6.21}$$

   It must be noticed that if the electric field is neglected, $r_H = 0$, $\varphi_0$ is spherically symmetric, $\partial_\mu\varphi_0 = 0$.

2. Terms in $1/\gamma^{3/4}$:

$$0 = 2k(1-\mu^2)(\partial_\mu\varphi_0)(\partial_\mu\varphi_1) - r_H\beta\left[(1-\mu^2)\partial_\mu\varphi_1 + 2\mu\beta\partial_\beta\varphi_1\right] \tag{6.22}$$

   The equation corresponding to this power of $\gamma$ does not appear in Ref. [66]. This is because, for $r_H = 0$, it is automatically verified by taking into account (6.21). Supposing that $\partial_\mu\varphi_1$ has no singularity in $\mu = 1$, above equation implies that $\partial_\beta\varphi_1 = 0$ in that direction.

3. Terms in $1/\gamma^{1/2}$:

$$\begin{aligned} 0 =& \mu\beta^2\partial_\tau\varphi_0 - 2\beta\left[1 - 2t\partial_\beta\varphi_0\right]\partial_\beta\varphi_0 \\ &+ k\Big[2\mu\partial_\mu\varphi_0 - (1-\mu^2)\partial_\mu^2\varphi_0 + 2(1-\mu^2)(\partial_\mu\varphi_0)(\partial_\mu\varphi_2) + (1-\mu^2)[\partial_\mu\varphi_1]^2\Big] \\ &- r_H\beta\left[(1-\mu^2)\partial_\mu\varphi_2 + 2\mu\beta\partial_\beta\varphi_2\right] \end{aligned} \tag{6.23}$$

   It can be observed that the electric field is responsible for terms proportional to $\varphi_2$ but also for terms containing $\partial_\mu\varphi_0$. The later are, however, vanishing for $r_H = 0$ according to equation (6.21).

4. Terms in $1/\gamma^{1/4}$:

$$\begin{aligned} 0 = \mu\beta^2\partial_\tau\varphi_1 - 2\beta\left[1 - 4t\partial_\beta\varphi_0\right]\partial_\beta\varphi_1 + k\Big[&2\mu\partial_\mu\varphi_1 + 2(1-\mu^2)(\partial_\mu\varphi_1)(\partial_\mu\varphi_2) \\ &+ 2(1-\mu^2)(\partial_\mu\varphi_0)(\partial_\mu\varphi_3) - (1-\mu^2)\partial_\mu^2\varphi_1\Big] \end{aligned} \tag{6.24}$$

   In the right hand side of Eq. (6.20), the terms proportional to $\partial_\beta\varphi_1$ were $-2\beta\left[1 - 2t\partial_\beta\varphi_0\right]\partial_\beta\varphi_1 - 2\beta\partial_\beta\varphi_0(-)2t\partial_\beta\varphi_1$.

For $r_H = 0$, Eqs. (6.21), (6.23) and (6.24) exactly are Eqs. (13), (14) and (15) of Ref. [66], respectively.

### 6.2.2 Case of neglect of the electric field effect

From here $r_H = 0$, bringing us back to the case considered by Gurevich and Istomin. The Sec. 6.2.2.1 is dedicated to the isotropic component of $\varphi$. Its behaviour is examined within and far beyond the region of temperature transition. Except one, clearly mentioned, all our results agree with those of Ref. [66]. Some of them are accompanied by a more in-depth analysis than that done by Gurevich and Istomin. The same is for the Sec. 6.2.2.2 which concerns the anisotropic part of $\varphi$. Finally, the calculation of the heat flux density is scratched in Sec. 6.2.2.3.

#### 6.2.2.1 Study of $\varphi_0$. Properties of the kinetic discontinuity.

As already mentioned, we deduce from Eq. (6.21) that $\varphi_0$ is isotropic. In the absence of any electron source, the derivative $\partial_\mu \varphi_1$ has, in velocity space, no singularity at $\mu = 1$. At that point, Eq. (6.23) is

$$\beta \partial_\tau \varphi_0 - 2\Big[1 - 2t\partial_\beta \varphi_0\Big]\partial_\beta \varphi_0 = 0, \tag{6.25}$$

after having simplified by $\beta$. Therefore there is no guarantee that the solution at $\beta = 0$ is correct. Fortunately, at that point the above equation leads to $\partial_\beta \varphi_0|_{\beta=0} = 1/2t$, which is the expected solution. Following Gurevich and Istomin, we shall note

$$y = 2\partial_\beta \varphi_0. \tag{6.26}$$

Multiplying Eq. (6.25) by 2, dividing by $\beta$ and then deriving with respect to $\beta$ leads to Eq. (19) of Ref. [66],

$$\partial_\tau y - \partial_\beta \Big[2y(1 - ty)/\beta\Big] = 0. \tag{6.27}$$

To obtain this equation we supposed that $2\partial^2_{\beta\tau}\varphi_0 = 2\partial^2_{\tau\beta}\varphi_0 = \partial_\tau y$. According to Schwarz's theorem, a sufficient condition for exchanging the order in the derivatives is that $\varphi_0$ is of class $C^2$. It is fortunate that this condition is not necessary because $y$ is expected to be discontinuous. Indeed, let us give an interpretation of this quantity. To the lowest order in the small parameter $\gamma$, $y = 2\partial_\beta \gamma^{1/2}\varphi$. Since $\varphi = -\ln g_e$ and $\beta = \gamma^{1/2} m_e v^2/(k_B T_H)$, we have,

$$y = 2\gamma^{1/2}\frac{v}{2\beta}\partial_v(-\ln f_e) = -\frac{k_B T_H}{m_e v}\partial_v \ln f_e = \frac{T_H}{T_e^*},$$

where we used $\partial v/\partial\beta = v/(2\beta)$. The local effective temperature, $T_e^*$, has been defined as

$$k_B T_e^* = -\frac{m_e v}{\partial_v \ln f_e} = -\left[\frac{d\ln f_e}{d(m_e v^2/2)}\right]^{-1}.$$

This definition is quite natural. In case of the Maxwell distribution function, $\ln f_M$ is equal to $-v^2/(2v_T^2) = -m_e v^2/(2k_B T_e)$ plus a velocity-independent term, such that $d\ln f_M/d(m_e v^2/2) = -1/(k_B T_e)$.

To summarize, since $y$ is the derivative of $\varphi_0$ with respect to $\beta$, its discontinuities are breaks in the slope of $\varphi_0$. From a physical point of view, such breaks correspond to discontinuities of the local effective temperature. As suggested by Gurevich and Istomin, Eq. (6.27) mathematically contains the onset of a kinetic discontinuity. To reach this conclusion, they put forward the analogy with equations describing finite amplitude waves [163, 164], often referred as *simple* waves. According to the fundamental equations of hydrodynamics, a finite amplitude wave cannot propagate without being deformed, even if such a wave is plane. Due to the non-linearity of the aforementioned equations, there no longer exists a unique wave velocity but a different one for every point of the perturbation profile, leading to a change in shape over time. This deformation is obviously not observed when these equations are linearized to describe the propagation of small amplitude, sound waves.

We shall solve Eq. (6.27) in the cold region, far enough from the temperature transition to neglect its thickness and approximate it as a step function:

$$t(\tau) = \Theta(-\tau+\tau_0) + \frac{T_C}{T_H}\Theta(\tau-\tau_0) = \begin{cases} 1 & \text{for } \tau < \tau_0 \\ T_C/T_H & \text{for } \tau \geq \tau_0 \end{cases}, \tag{6.28}$$

with $\tau_0 > 0$ and $\Theta$ the Heaviside function. Eqs. (6.27)-(6.28) do not contain any characteristic scales with respect to $\tau$ and $\beta$. Therefore, $y$ must be self-similar, depending only on the ratio of $\tau$ and $\beta$. Following Gurevich and Istomin, we choose to introduce the variable $p = \beta/\tau^\alpha$, where $\alpha$ will be chosen hereafter. We continue to note $y$ the new function of $p$. The chain rules leads to

$$\partial_\tau = (\partial_\tau p)\partial_p = \beta\frac{(-)\alpha}{\tau^{\alpha+1}}\partial_p = -\frac{\alpha p}{\tau}\partial_p; \quad \partial_\beta = \tau^{-\alpha}\partial_p = \frac{p}{\beta}\partial_p.$$

Then, Eq. (6.27) becomes

$$\begin{aligned}\frac{\alpha p}{\tau}\partial_p y &= -\frac{p}{\beta}\partial_p\left[\frac{2}{\beta}y(1-ty)\right] \\ &= -\frac{2p}{\beta}\left[-\frac{1}{\beta^2}\tau^\alpha y(1-ty) + \frac{1}{\beta}\partial_p y(1-ty)\right],\end{aligned}$$

after having multiplied by $-1$ on both sides. Then, we develop $\partial_p y(1-ty) = (1-2ty)\partial_p y$, factorize by $-1/(\beta p)$, use $\tau^\alpha = \beta/p$ and $1/\beta^2 = 1/(p^2\tau^{2\alpha})$ in order to write the right hand side of the above equation as

$$\frac{2}{p^2\tau^{2\alpha}}\Big[y(1-ty) - p(1-2ty)\partial_p y\Big].$$

By regrouping terms in $\partial_p y$, Eq. (6.27) takes the form

$$\Big[1-2ty+\frac{\alpha}{2}p^2\tau^{2\alpha-1}\Big]p\partial_p y = y(1-ty).$$

Therefore we choose $\alpha = 1/2$, and note $y'$ the derivative of $y$ instead of $\partial_p y$. Hence, we finally obtain the Eq. (26) of Ref. [66],

$$\Big[1-2ty+\frac{p^2}{4}\Big]py' = y(1-ty). \tag{6.29}$$

This is a non autonomous first order nonlinear equation with boundary conditions

$$y(0) = T_H/T_C; \quad y(\infty) = 1. \tag{6.30}$$

Such a condition comes from the hypothesis that $\varphi$ is equal to $\varphi_M$ in the neighborhood of zero, *i.e* for small velocities, which leads to $\varphi_0 = \beta/(2t)$ and then to $y = 1/t$ in this region. The expression $1-2ty+p^2/4$ vanishes for $y = [1+p^2/4]/(2t)$, which is not a solution of Eq. (6.29). Disregarding this function and excluding the line $p = 0$, latter equation can therefore be put in the form $y' = F(p,y)$ with $F(p,y) = y(1-ty)/[(1-2ty+p^2/4)p]$. This equation means that, in the $(p,y)$-plane,

integral curves are tangent at any point to the vector field $\Big(1, F(p,y)\Big)$. According to the Picard-Lindelöf-Lipschitz-Cauchy's theorem [74], the existence and uniqueness of these integral curves are guaranteed at each point $(p,y)$ at which $F$ is continuous and satisfies the Lipschitz's condition in $y$ in the neighbourhood of the considered point: there exists a constant $L_y$ such that for any points $(p,y_1)$ and $(p,y_2)$ that belong to the neighbourhood of $(p,y)$, $|F(p,y_2)-F(p,y_1)| \leq L_y|y_2-y_1|$.

As already mentioned, $F$ is singular along the algebraic curves $2ty+p^2/4=1$ and $p=0$. Apart from these curves, $y \mapsto F(p,y)$ is Lipschitzian as being a rational function of $y$ with the degree of the numerator inferior, or equal to, that of the denominator. This last result can be easily demonstrated by deriving the function and observing that the derivative is bounded. Therefore, the integral curves may not pass through these curves of singularity, or may intersect at some of their points. We shall see that it is the latter possibility that is realised. It appears of little interest to push forward the qualitative study by means of examining the vector field $\Big((1-2ty+p^2/4)p, y(1-ty)\Big)$. In Ref. [74], Tricomi details the analysis in the case where $F(p,y)$ is a homographic function of $y$, while pointing out considerable difficulties for rational function with higher degrees. We will not venture into these considerations here.

Like in the case of finite amplitude waves, we shall now obtain implicit solutions of Eq. (6.27). The functions $y=0$ and $y=1/t$ are solutions. Disregarding them we write Eq. (6.27) as

$$\frac{1}{p}\frac{dp}{dy} = \frac{1-2ty+p^2/4}{y(1-ty)}. \tag{6.31}$$

It would be convenient to obtain an equation with separated variables. For this purpose we look for a solution of the form $p(y) = y(1-ty)p_1(y)$. On the one hand we have, by deriving this expression,

$$\frac{1}{p}\frac{dp}{dy} = \frac{1}{y(1-ty)p_1}\Big[(1-2ty)p_1 + y(1-ty)\frac{dp_1}{dy}\Big] = \frac{1-2ty}{y(1-ty)} + \frac{1}{p_1}\frac{dp_1}{dy}.$$

On the other hand, by substituting the expression of $p(y)$ in the right hand side of Eq. (6.31), we obtain

$$\frac{1}{p}\frac{dp}{dy} = \frac{1-2ty}{y(1-ty)} + \frac{y^2(1-ty)^2p_1^2}{4y(1-ty)}.$$

Equating these two expressions of $p^{-1}dp/dy$ gives $dp_1/p_1^3 = y(1-ty)/4dy$, which by direct integration leads to

$$-\frac{1}{2p_1^2} = \frac{1}{4}\left(\frac{y^2}{2} - t\frac{y^3}{3} + \frac{C}{2}\right) = \frac{1}{8}\Big[y^2 - \frac{2}{3}ty^3 - C\Big],$$

where $C$ is a constant to be determined later. Hence $p_1(y) = 2/[-y^2+2ty^3/3+C]^{1/2}$, and so

$$p(y) = \frac{2y(1-ty)}{\big[C-y^2+\frac{2}{3}ty^3\big]^{1/2}}. \tag{6.32}$$

There is no continuous solution of this form that simultaneously satisfies both boundary conditions (6.30). There is only one solution satisfying $y = 1$ for $p = \infty$. Substituting $y = 1$ in Eq. (6.32) gives $p = 2(1-t)/\big[C - 1 + 2t/3\big]^{1/2}$, and so, for $t \neq 1$, the condition $p = \infty$ leads to $C = 1 - 2t/3$. Latter value corresponds to the solution

$$p(y) = \frac{2y(1-ty)}{\Big[1 - y^2 + \frac{2}{3}t(y^3 - 1)\Big]^{1/2}}. \tag{6.33}$$

Then, for $y = 1/t$ the condition $p = 0$ is automatically fulfilled unless the denominator in Eq. (6.32) vanishes. Latter case corresponds to $0 = C - 1/t^2 + 2/(3t^2)$, *i.e* $C = 1/(3t^2)$. The associated solution is

$$p(y) = \frac{2y(1-ty)}{\Big[\frac{1}{3t^2} - y^2 + \frac{2}{3}ty^3\Big]^{1/2}} = \frac{2\sqrt{3}ty(1-ty)}{\Big[1 - 3(ty)^2 + 2(ty)^3\Big]^{1/2}} = \frac{2\sqrt{3}ty}{\Big[1 + 2ty\Big]^{1/2}} \tag{6.34}$$

The last equality is obtained by factorizing the polynomial under the square root as $1 - 3(ty)^2 + 2(ty)^3 = (1-ty)\big[1 + ty - 2(ty)^2\big] = (1-ty)^2\big[1 + 2ty\big]$.

The solution, which we recall is obtained far from the transition region, $\tau \gg \tau_0$, is plotted in Figs. 6.2.1-6.2.2 for two values of the parameter $t = T_C/T_H$. As it cannot be triple-valuated, discontinuities are formed that correspond to jumps among the three branches. Due to the first condition (6.30), in the neighbourhood of $p = 0$, $y$ must approaches 1 for increasingly small values of the temperature jump, or, equivalently, when the ratio $T_H/T_C = y(0)$ tends toward 1. This behaviour is only fulfilled by the solution $y = 1/t$ associated to the branch (a), which, obviously, also fulfill the second condition (6.30) in the limit $T_H/T_C = 1$. For values of this ratio below 1, latter condition is only fulfilled by the solution associated to the branch (c). Therefore, for increasing values of $p$, there exists only one jump from branch (a) to (c) at a certain abscissa $p_0$.

Like their previous results, the authors are short on details concerning the study of this discontinuity. They employ, without any explanation, the notation $[X]_{w_0}$ for a function $X$ of $w$ with a single discontinuity at $w_0$. By examining their Eq. (30) in Ref. [66], we guess that this is the singular part of the derivative of $X$ with respect to $w$,

$$[X]_{w_0} = \Delta X \delta(w - w_0), \text{ where } \Delta X = X(w_0^+) - X(w_0^-).$$

The function itself being expressed as

$$X(w) = \Delta X \Theta(w - w_0) + \mathcal{X}(w),$$

with $\mathcal{X}$ the regular, continuously differentiable part of $X$. For $w \leq w_0$, the graph of $X$ is that of the regular part $\mathcal{X}$, whereas for $w > w_0$ it is that of $\mathcal{X}$ vertically translated by the quantity $\Delta X$. The decomposition $X'(w) = [X]_{w_0} + \mathcal{X}'(w)$ must, obviously, be considered with a certain detachment from mathematical rigour. Since $\Theta$ is locally integrable, it can be confused with its associated distribution, defined, for any test function with compact support, by the integral over the real axis of the product of $\Theta$ by this test function. Indeed, by virtue of the

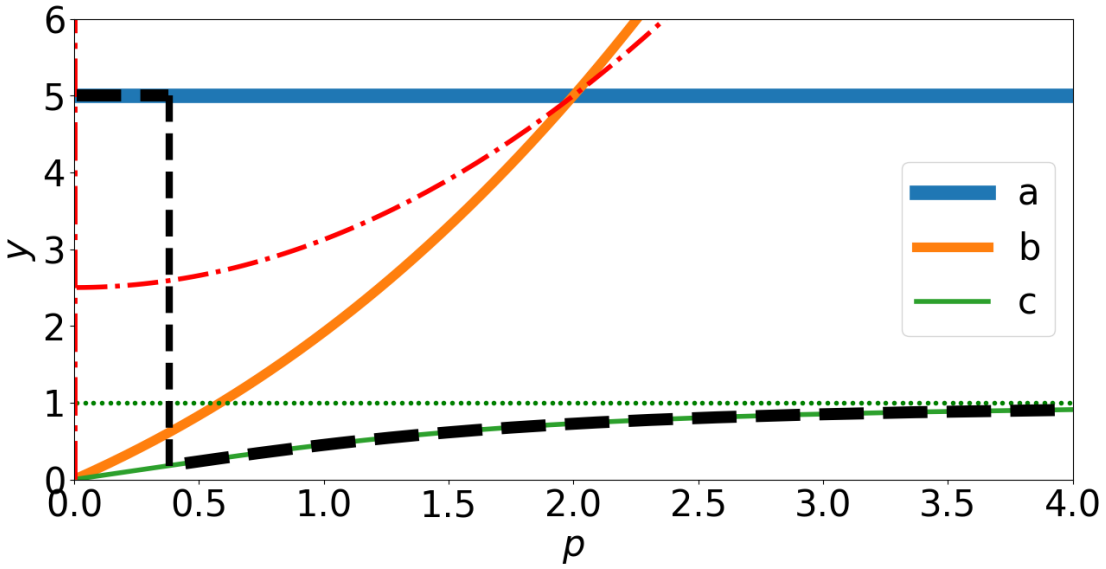


Figure 6.2.1: Case $t = 0.2$. Graph of the solution $y$ (dashed-black) far from the temperature transition ($\tau \gg \tau_0$). The horizontal branch (a) in (solid, blue) represents the solution $y = 1/t$ satisfying the first condition (6.30). The second condition is full-filled by the solutions implicitly given by Eqs. (6.34)-(6.33), represented by the branches (b) in (solid, orange) and (c) in (solid, green), respectively. The red, dot-dashed lines, $p = 0$ and $1 - 2ty + p^2/4 = 0$, are curves of singularity along which integral curves of Eq. (6.29) are susceptible to cross.

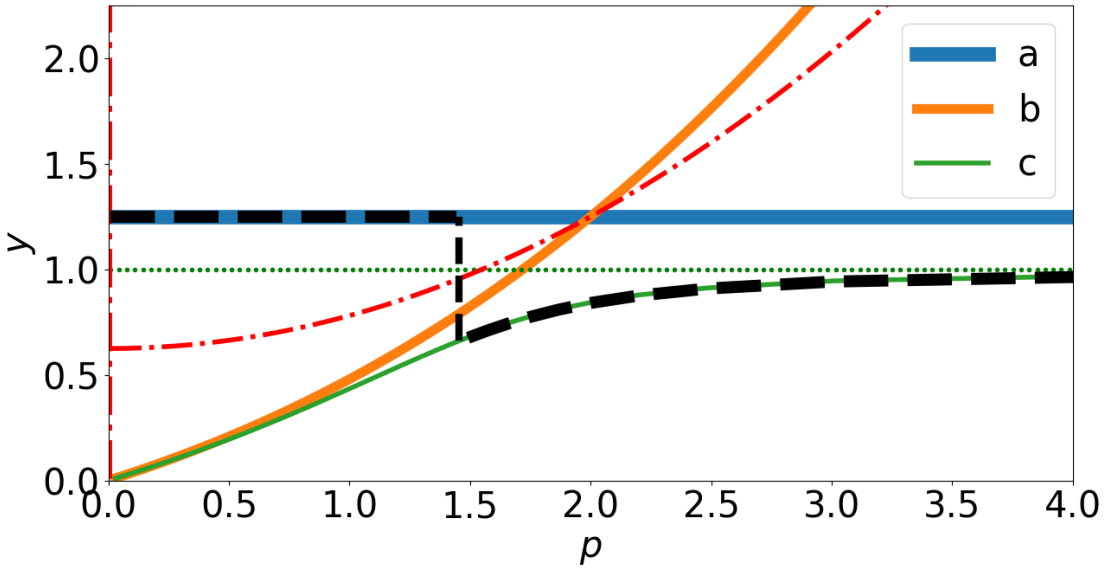


Figure 6.2.2: Case $t = 0.8$. Notations are the same as in Fig. 6.2.1.

Riesz–Markov–Kakutani's representation theorem, the application that associates the distribution with a function as above is bijective. However, the Dirac distribution, $\delta$, which is the distributional derivative of $\Theta$, is not associated to any locally integrable function. Its misuse as a infinitely quilted function at a point is very common, and, if required, the conscientious reader is referred to the treatise of Schwartz [165] to find a formulation that meets its mathematical expectations.

By integrating Eq. (6.27) on a rectangle of measure zero centered at $(\tau, \beta)$, the contribution of the continuous part of the derivative is zero, and we obtain the Eq. (30) of Ref. [66],

$$[y]_\tau - \left[\frac{2}{\beta} y(1-ty)\right]_\beta = 0 \tag{6.35}$$

For any positive reals $\tau_0$ and $\beta_0$ such that $\beta_0/\tau_0^{1/2} = p_0$,

$$\delta(\beta-\beta_0) = \delta(p-p_0)\frac{dp}{d\beta} = \delta(p-p_0)\frac{p}{\beta}, \quad \text{and } \delta(\tau-\tau_0) = -\delta(p-p_0)\frac{p}{2\tau}.$$

Thus, Eq. (6.35) is transformed as $[-p/(2\tau)\ y - 2p/\beta^2\ y(1-ty)]_{p_0}$, that is

$$\left[\frac{p}{4}y + \frac{y}{p}(1-ty)\right]_{p_0} = 0, \tag{6.36}$$

because $p/\beta^2 = 1/(\tau p)$. This is Eq. (31) of Ref. [66]. It can also be obtained directly from Eq. (6.29). The Eq. (6.36) means that the quantity between brackets is conserved when crossing the discontinuity at $p = p_0$. Just before, at $p = p_0^-$, the solution belongs to the branch (a) corresponding to $y = 1/t$. Hence, on that branch at $p = p_0^-$, $p/4y + y/p(1-ty) = p_0/(4t)$. Just after the discontinuity, at $p = p_0^+$, the solution belongs to the branch (c) corresponding to Eq. (6.33). Thus, by noting $y_0 = y(p_0^+)$, Eq. (6.36) takes the following form:

$$0 = \frac{p_0}{4}y_0 + \frac{y_0}{p_0}\big(1-ty_0\big) - \frac{p_0}{4t} = \big(1-ty_0\big)\left(\frac{y_0}{p_0} - \frac{p_0}{4t}\right).$$

So $y_0 = p_0^2/(4t)$. Therefore, the square of Eq. (6.33) evaluated at $p = p_0^+$ is

$$4ty_0 = \frac{4y_0^2(1-ty_0)^2}{1-y_0^2-\frac{2}{3}t(1-y_0^3)},$$

which can be put in the form of an algebraic equation,

$$0 = t\left(1-\frac{2}{3}t\right) - y_0 + ty_0^2 - \frac{t^2}{3}y_0^3.$$

This equation possesses only one real solution, whose expression is $ty_0 = 1-(1-t)^{2/3}(2t+1)^{1/3}$. Hence, the abscissa of the discontinuity is

$$p_0 = 2\Big[1-(1-t)^{2/3}(2t+1)^{1/3}\Big]^{1/2}, \tag{6.37}$$

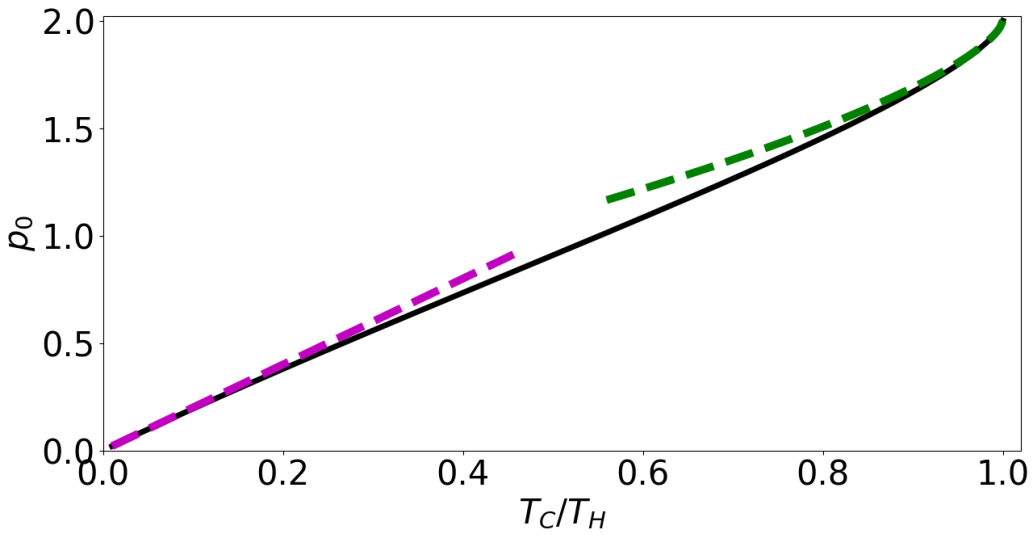


Figure 6.2.3: Abscissa $p_0 = \beta_0 \tau^{1/2}$ (solid, black) given by Eq. (6.37), at which the kinetic discontinuity occurs in the region far from the temperature transition ($\tau \gg \tau_0$). The violet and green dashed lines represent its low values, $2t$, and high values, $2 - 3^{1/3}(1-t)^{2/3}$ approximations, respectively.

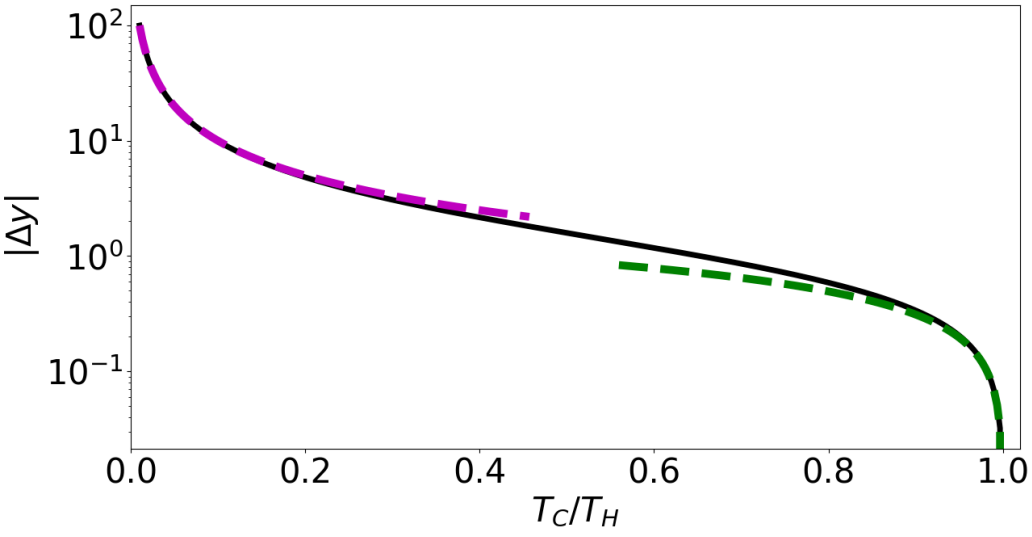


Figure 6.2.4: Absolute value of the jump $|\Delta y|$ given by Eq. (6.38) in the region far from the temperature transition ($\tau \gg \tau_0$). The violet and green dashed lines represent its low values, $-1/t$, and high values, $-3^{1/3}(1-t)^{2/3}$ approximations, respectively.

and the magnitude of the jump is

$$\begin{aligned}\Delta y = y(p_0^+) - y(p_0^-) &= y_0 - 1/t \\ &= -t^{-1}(1-t)^{2/3}(2t+1)^{1/3}. \end{aligned} \tag{6.38}$$

These functions are plotted in Figs. 6.2.3-6.2.4. For small values of $t = T_C/T_H$, they can be approximated as $p_0 \simeq 2t$ and $\Delta y \simeq -1/t$, whereas for $t \simeq 1$, we find $p_0 \simeq 2 - 3^{1/3}(1-t)^{2/3}$ and $\Delta y \simeq -3^{1/3}(1-t)^{2/3}$.

In the self-similar variable, Eq. (6.26) takes the form $y = 2\tau^{-1/2}\varphi_0'$, where, as for $y$, we have again noted $\varphi_0$ the function of $p$. Near $p = 0$, $\varphi_0 = p\tau^{1/2}/(2t)$, implying that $\varphi_0(0) = 0$. Therefore,

$$\varphi_0 = \frac{\tau^{1/2}}{2}\int_0^p y\ d\tilde{p}.$$

For $p < p_0$, $y = 1/t$, and so $\varphi_0 = p\tau^{1/2}/(2t)$. For $p \geq p_0$, $\varphi_0 = p_0\tau^{1/2}/(2t) + \tau^{1/2}/2\int_{p_0}^p y\ d\tilde{p}$, with $y$ implicitly given by Eq. (6.33). Integrating by parts, the last integral can be expressed as,

$$\begin{aligned}\int_{p_0}^p y\ d\tilde{p} &= \left[y\tilde{p}\right]_{p_0}^p - \int_{y_0}^y p\ d\tilde{y} \\ &= yp - y_0p_0 - \int_{y_0}^y \frac{2\tilde{y}(1-t\tilde{y})}{\left[1-\tilde{y}^2-\frac{2}{3}t(1-\tilde{y}^3)\right]^{1/2}}\ d\tilde{y},\end{aligned}$$

In order to follow Gurevich and Istomin, we have left the integral in this form, despite the fact that it can be expressed as

$$\int_{y_0}^y \frac{2\tilde{y}(1-t\tilde{y})}{\left[1-\tilde{y}^2-\frac{2}{3}t(1-\tilde{y}^3)\right]^{1/2}}\ d\tilde{y} = -2\left[\left(1-\tilde{y}^2-\frac{2}{3}t(1-\tilde{y}^3)\right)^{1/2}\right]_{y_0}^y = \left[\frac{4y(1-ty)}{p(y)}\right]_y^{y_0},$$

by using Eq. (6.33). Back in the $(\tau, \beta)$ variables, the solution for $\tau \gg \tau_0$ is therefore

$$\begin{aligned}\varphi_0 =& \left[1-\Theta(\beta-\beta_0)\right]\frac{\beta}{2t} \\ &+ \Theta(\beta-\beta_0)\left[\frac{\beta_0}{2t} + \frac{y\beta - y_0\beta_0}{2} - \tau^{1/2}\int_{y_0}^y \frac{\tilde{y}(1-t\tilde{y})}{\left[1-\tilde{y}^2-\frac{2}{3}t(1-\tilde{y}^3)\right]^{1/2}}\ d\tilde{y}\right],\end{aligned} \tag{6.39}$$

with $\beta_0 = p_0\tau^{1/2}$. Such a solution is plotted in Fig. 6.2.5. As expected, the distributions function far from the transition region is, in rough approximation, doubly Maxwellian. At low energies, $\varphi_0$ is equal to $\beta/(2t)$, which corresponds to the local Maxwellian of the cold region at temperature $T_C$. In the limit $\beta \gg \beta_0$, $y = 1$, so that the following compensation occurs in Eq. (6.39):

$$\frac{\beta_0}{2t} - \frac{y_0\beta_0}{2} - \tau^{1/2}\int_{y_0}^1 \frac{\tilde{y}(1-t\tilde{y})}{\left[1-\tilde{y}^2-\frac{2}{3}t(1-\tilde{y}^3)\right]^{1/2}}\ d\tilde{y} = 0.$$

Indeed, $\beta_0/(2t) - y_0\beta_0/2 = -\tau^{1/2}p_0\Delta y/2$, which is exactly the opposite of the integral term, obtained by using our aforementioned explicit expression together

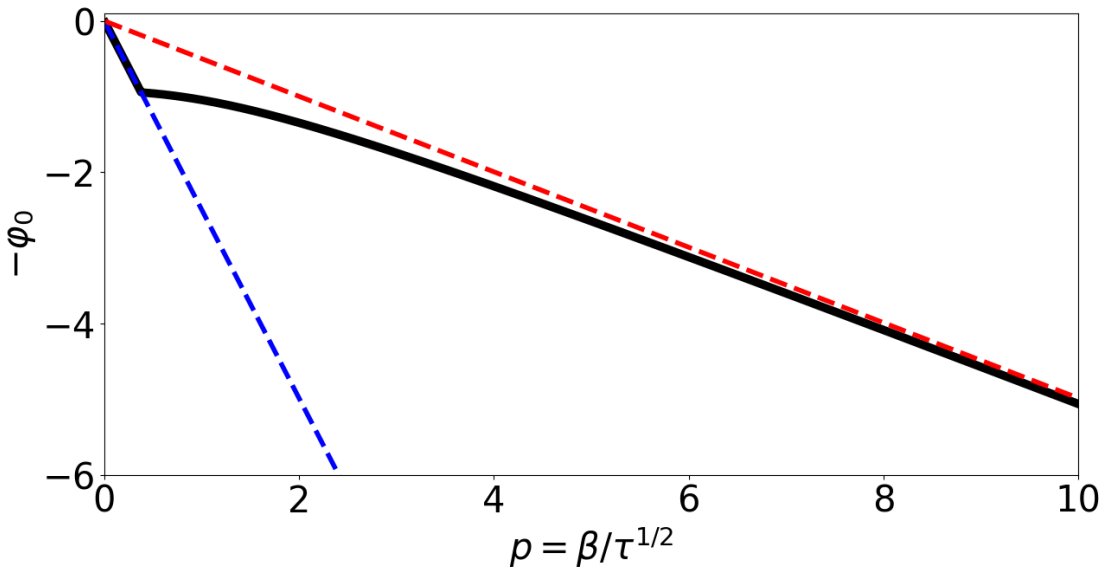


Figure 6.2.5: Case $t = 0.2$ and $\tau = 1$. Graphs of $-\varphi_0$ (6.39) (solid, black) far from the temperature transition ($\tau \gg \tau_0$), $-\beta/(2t)$ (dashed, violet), and $-\beta/2$ (dashed, red).

with the relation $4ty_0 = p_0^2$. Hence, $\varphi_0$ is equal to $\beta/2$ in the limit $\beta \gg \beta_0$, corresponding to the local Maxwellian of the hot region with temperature $T_H$.

Within the region of the temperature transition, $\tau \simeq \tau_0$, the solution $y$ almost behaves like that of the self-similar situation previously treated. Gurevich and Istomin shown numerically that, for increasing values of $\tau$, *i.e* passing from the hot to the cold part of the plasma, the solution $\beta \mapsto y(\tau, \beta)$ gradually changes. The steepness of its profile around the inflexion point increases up to infinity, meaning the appearance of a kinetic discontinuity. The solution can be obtained analytically in the region of constant gradient of temperature. Here again, $y$ is a triply-valuated function of $\beta$. The solution satisfying the second boundary condition (6.30), say $y(\tau, \infty) = 1$, is implicitly given by

$$\beta = \frac{\sqrt{3}y(1-ty)}{[1-y^3]^{1/2}}, \tag{6.40}$$

whereas that satisfying the second condition (6.30), $y(\tau, 0) = 1/t$, are obtained by solving the following ordinary differential equation,

$$\eta\Big[\eta - 4(1-2h)\Big]h' = -h\Big[\eta + 2(1-h)\Big], \tag{6.41}$$

directly obtained from Eq. (6.27) where $\eta = \beta^2/t(\tau)$ and $h\Big(\eta(\tau,\beta)\Big) = t(\tau)y(\tau,\beta)$. This equation is singular on the lines of equations $\eta = 0$ and $h = (1-\eta/4)/2$. Here again, outside these lines of singularity the following function,

$$H(\eta, h) = -\frac{h[\eta + 2(1-h)]}{\eta[\eta - 4(1-2h)]},$$

is continuous and locally Lipschitzian in the variable $h$. The equation $h' = H(\eta, h)$ is numerically integrated by mean of an implicit multi-step variable-order method,

proposed by Curtis and Hirschfelder [166], based on a backward differentiation formula for the derivative approximation [167]. The solution, plotted in Figs. 6.2.6-6.2.7, is doubly valuated. Starting from the point $h = 1$ and $\eta = 0$, it decreases faster and faster until a turning point, at an abscissa $\eta \simeq 0.788$, at which the derivative is infinite. Then, the solution decreases in the descending direction of the $\eta$-axis until the origin. These two branches, (a) and (b), cannot be obtained in one go by means of the aforementioned numerical solver. It is necessary to decompose the resolution from $(1, 0)$ to the turning point, and then start just below latter point to solve up to the origin.

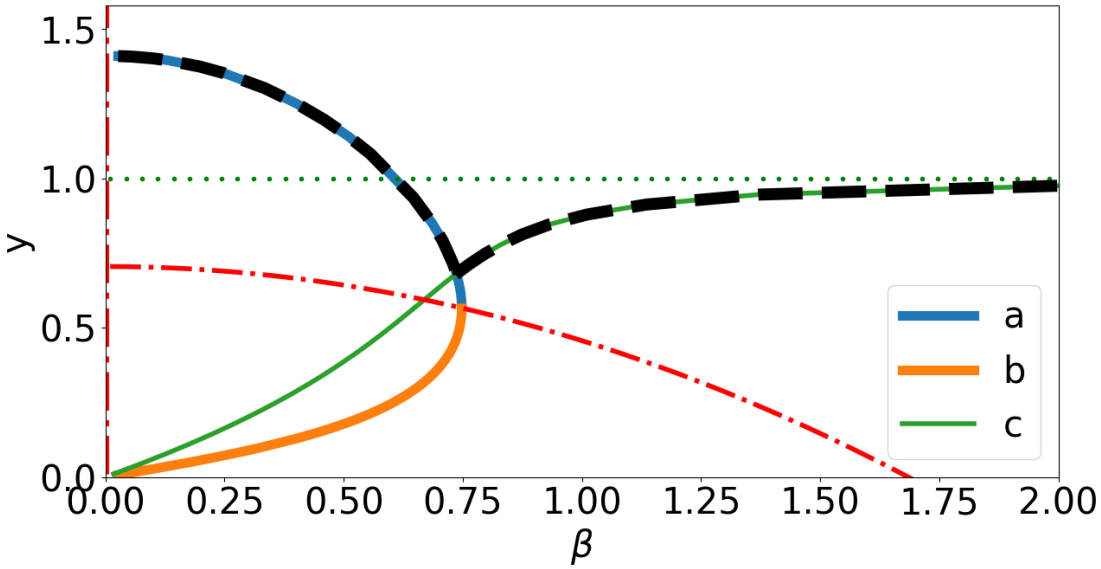


Figure 6.2.6: Limit case, $t = t_c \simeq 0.709$, with no kinetic discontinuity. Graph of the solution $y$ (dashed-black) inside the temperature transition ($\tau \simeq \tau_0$). The part constituted by the branches (a) in (solid, blue) and (b) in (solid, orange) corresponds to the solution of (6.41), verifying $y(\tau, \beta = 0) = 1/t$. The branch (c) is associated to the solution verifying $y(\tau, \beta = \infty) = 1$, implicitly given by Eq. (6.40). The red, dot-dashed lines, $\beta = 0$ and $ty = [1 - \beta^2/(4t)]/2$, are curves of singularity along which integral curves of Eq. (6.41) are susceptible to cross.

From Figs. 6.2.6-6.2.7 it may be observed that, depending on the value of $t$, there may be no kinetic discontinuity. While moving down to lower temperatures, $t = T/T_H$ is decreasing. For $t \geq t_c$, the solution $y$ continuously passes from one branch to an other experiencing a discontinuity of its derivative only. The critical value of the temperature ratio, $t_c \simeq 0.709$, corresponds to the situation in which the branch (c), associated to Eq. (6.40), is passing just above the turning point. For $t \leq t_c$, a kinetic discontinuity appears at a certain abscissa $\beta_0$. It is found through Eq. (6.35), which turns out to express, in the considered case, the conservation of $h(1-h)$ to the crossing of the kinetic discontinuity. For different values of $t$ below $t_c$, we numerically computed $\beta_0$. Its dependence to the temperature is found to be rather cubic:

$$\beta_0 \simeq t(1.32t^2 + 0.24t + 0.20). \tag{6.42}$$

This result, plotted in Fig. 6.2.8, qualitatively differs from that of Gurevich and Istomin, who found a linear dependence. Unfortunately, they give no indication on how they get their result.

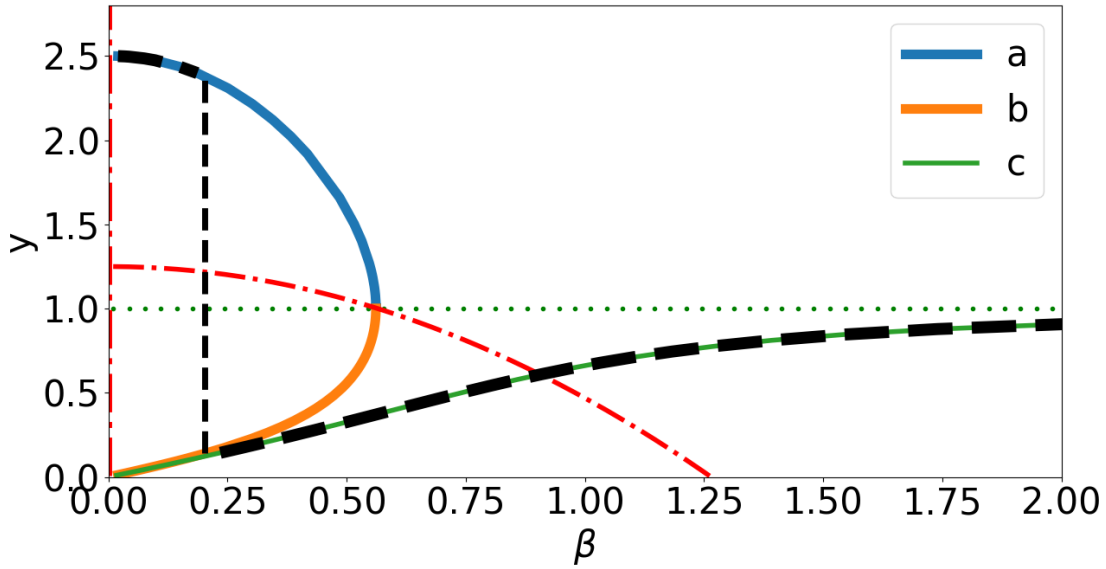


Figure 6.2.7: Case $t = 0.4$, for which a kinetic discontinuity takes place at an energy given by Eq. (6.42). Other notations are the same as in Fig. 6.2.6.

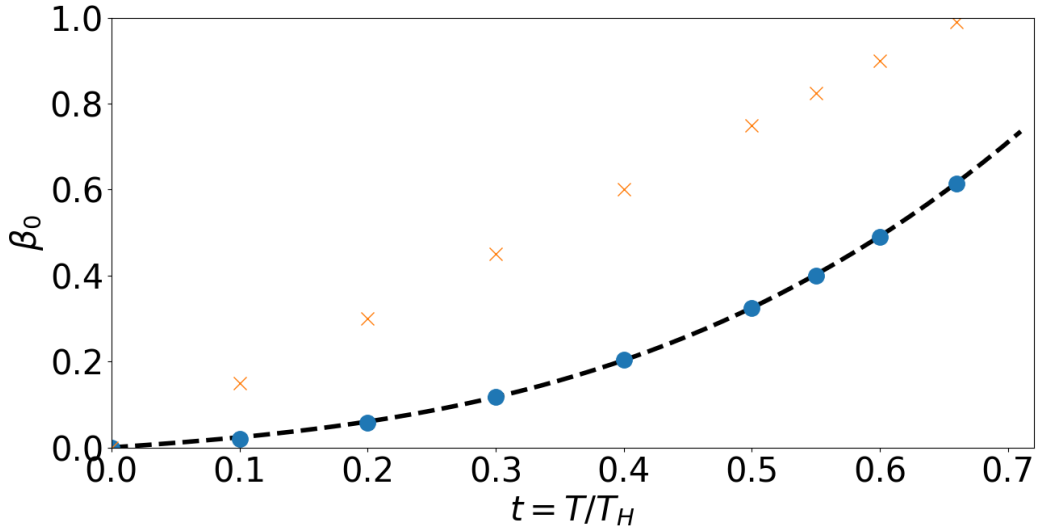


Figure 6.2.8: Graph of the abscissa, $\beta_0$, at which the kinetic discontinuity occurs, according to us (disk, blue) and to Gurevich and Istomin (cross, orange). The dashed black lines represents the formula (6.42).

Then, from Eq. (6.26), which takes the form $y = 4(\eta/t)^{1/2}\partial_\eta\varphi_0$, the solution may be expressed as

$$\varphi_0 = \frac{t^{1/2}}{4}\int_0^\eta \tilde\eta^{-1/2} y(\tilde\eta)\ d\tilde\eta.$$

For $\beta \le \beta_0$, it is equal to $1/(4t^{1/2})\int_0^\eta \tilde\eta^{-1/2}h(\tilde\eta)\ d\tilde\eta$, whereas for $\beta \ge \beta_0$, it is equal to the latter integral with upper bound $\eta = \eta_0$, plus the following term,

$$\begin{aligned}\frac{t^{1/2}}{4}\int_{\eta_0}^\eta \tilde\eta^{-1/2} y(\tilde\eta)\ d\tilde\eta &= \frac{1}{2}\int_{\beta_0}^\beta y(\tilde\beta)\ d\tilde\beta \\ &= \frac{1}{2}\Big[y\beta - y_0\beta_0 - \int_{y_0}^y \frac{\sqrt{3}\tilde y(1-t\tilde y)}{[1-\tilde y^3]^{1/2}}\ d\tilde y\Big],\end{aligned}$$

where we integrated by parts and used Eq. (6.40). Hence, the solution within the region of temperature transition, $\tau \simeq \tau_0$, may be expressed as

$$\begin{aligned}\varphi_0 = &\Big[1-\Theta(\beta-\beta_0)\Big]\frac{1}{4t^{1/2}}\int_0^{\beta^2/t}\tilde\eta^{-1/2}h(\tilde\eta)\ d\tilde\eta \\ &+\Theta(\beta-\beta_0)\left[\frac{1}{4t^{1/2}}\int_0^{\beta_0^2/t}\tilde\eta^{-1/2}h(\tilde\eta)\ d\tilde\eta + \frac{y\beta - y_0\beta_0}{2} - \frac{\sqrt{3}}{2}\int_{y_0}^y \frac{\tilde y(1-t\tilde y)}{[1-\tilde y^3]^{1/2}}d\tilde y\right].\end{aligned} \tag{6.43}$$

This solution is plotted in Figs. 6.2.9-6.2.10 for two different values of $t$. Unlike the self-similar case, the integral term cannot be expressed as a combination of usual functions. To give an alternative form, we separate the integrand as $-t\tilde y^2/[1-\tilde y^3] + \tilde y/[1-\tilde y^3]$. The first term has an obvious primitive,

$$-\int^y \frac{t\tilde y^2}{[1-\tilde y^3]^{1/2}}d\tilde y = \frac{2}{3}t[1-y^3]^{1/2},$$

while that of the second involves the Gauss's hypergeometric function, a compact expression of which is given by the Euler's integral representation formula [67],

$${}_2F_1(a,b;c;x) = \frac{\Gamma(c)}{\Gamma(b)\Gamma(c-b)}\int_0^1 \frac{w^{b-1}(1-w)^{c-b-1}}{(1-wx)^a}dw,$$

where all arguments are real numbers. Disregarding a rather tedious algebra of little interest that involves the properties of ${}_2F_1$, the result is as follows

$$\int_{y_0}^y \frac{\tilde y(1-t\tilde y)}{[1-\tilde y^3]^{1/2}}d\tilde y = \left[\frac{2}{3}t[1-\tilde y^3]^{1/2} + \frac{1}{2}\tilde y^2\ {}_2F_1\Big(\frac{1}{2},\frac{2}{3};\frac{5}{3};\tilde y^3\Big)\right]_{y_0}^y.$$

As it may have been guessed from Eqs. (6.39)-(6.43), $\varphi_0$ behaves somewhat differently within ($\tau \simeq \tau_0$) and far beyond ($\tau \gg \tau_0$) the temperature jump.

As already mentioned, a difference is the absence of any kinetic discontinuity near the hot region, for $t \ge t_c$. Here, for increasing values of the energy, $\varphi_0$ passes from the local Maxwellian at temperature $T$, $\beta/(2t)$, to that of the hot region,

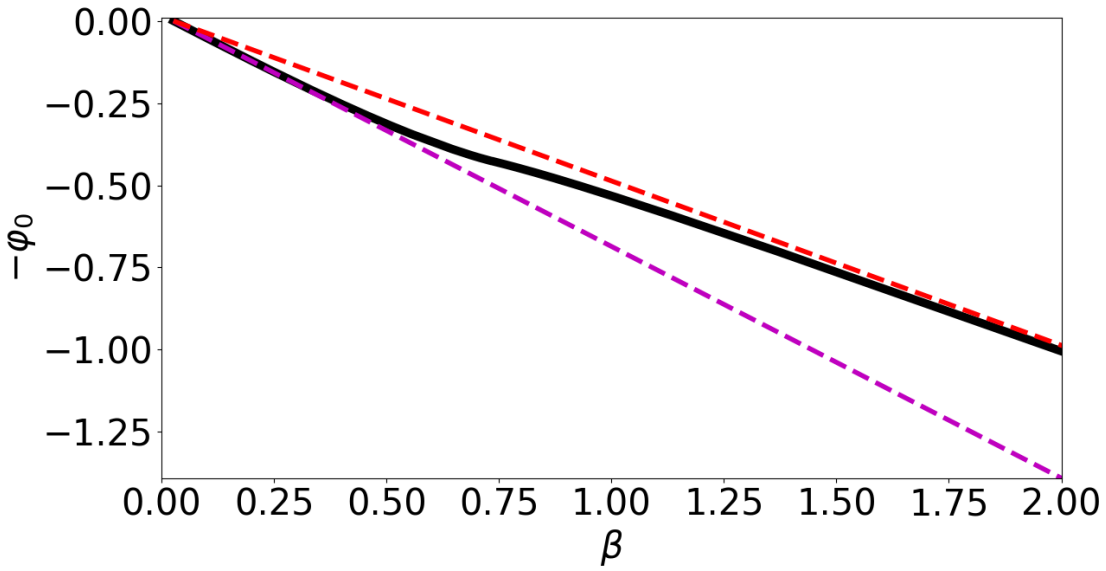


Figure 6.2.9: Limit case, $t = t_c \simeq 0.709$, with no kinetic discontinuity. Graphs of $-\varphi_0$ (6.43) (solid, black) inside the temperature transition ($\tau \simeq \tau_0$), $-\beta/(2t)$ (dashed, violet), and $-\beta/2$ (dashed, red).

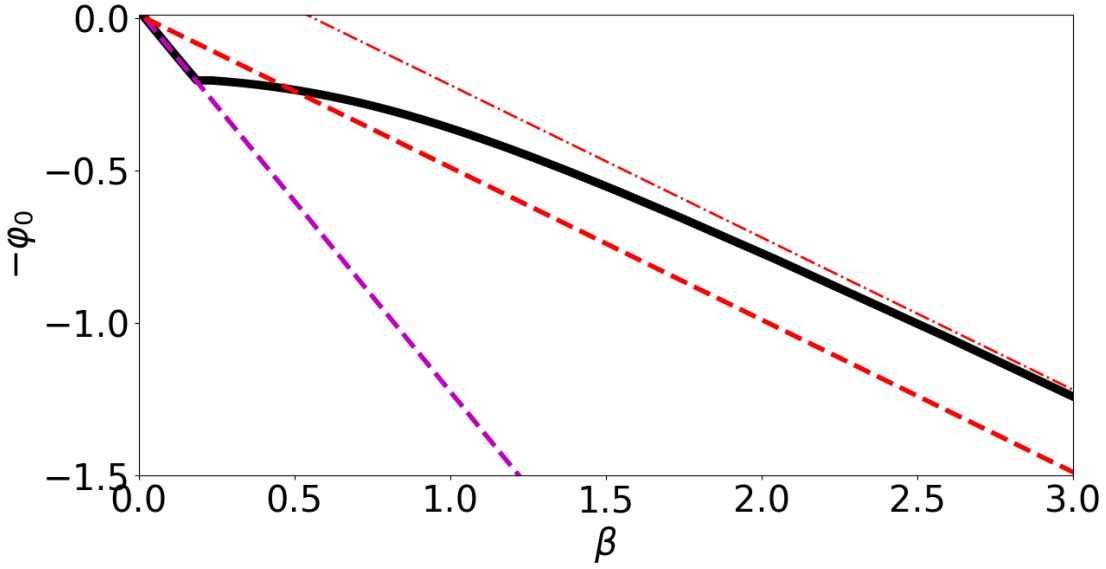


Figure 6.2.10: Case $t = 0.4$, for which a kinetic discontinuity takes place at an energy given by Eq. (6.42). The red, thin, dot-dashed line represents $-\beta/2 + \mathcal{M}$, with $\mathcal{M} \simeq t_c - t$. Other notations are the same as in Fig. 6.2.9.

$\beta/2$, with no break in the slope. For $t < t_c$, the kinetic discontinuity occurs at an abscissa, $\beta_0$, that behaves as a polynomial of order three of $\tau$, if it supposed that the electron density is constant. If the electron density evolves linearly with the position $z$, $\beta_0$ becomes a three-order polynomial of $\tau^{1/2}$. This differs from that far from the transition region, within which $\beta_0$ is proportional to $\tau^{1/2}$. An other difference between these regions lies in the asymptotic behaviour of $\varphi_0$. While for small energy it is equal to $\beta/(2t)$ with an high degree of accuracy, it tends toward $\beta/2 - \mathcal{M}$ at high energies, with

$$\mathcal{M} = -\frac{1}{4t^{1/2}} \int_0^{\beta_0^2/t} \tilde{\eta}^{-1/2} h(\tilde{\eta})\ d\tilde{\eta} + \frac{y_0\beta_0}{2} + \frac{\sqrt{3}}{2} \int_{y_0}^1 \frac{\tilde{y}(1-t\tilde{y})}{[1-\tilde{y}^3]^{1/2}} d\tilde{y}.$$

This additional term is numerically found to be a positive, decreasing function of $t$ that behaves as $\mathcal{M} \simeq t_c - t$, and to be independent from $\beta$ to a high degree of accuracy. For $t \leq t_c$, the distribution function at high energies is therefore equal to the Maxwellian distribution function of the hot region with, however, an effective electron density equal to $n_H$ multiplied by

$$e^{\mathcal{M}/\gamma} \simeq e^{(t_c-t)/\gamma}.$$

As expected, for increasingly high values of $\gamma$, which corresponds to steeper temperature gradients, this term tends toward 1 and the effective electron density is that of the hot region. Indeed, in this limit the thickness of the transition region decreases until it can be considered null, bringing us back to the self-similar situation. With finite $\gamma$, the effective electron density of energetic electron, $n_H\ e^{\mathcal{M}/\gamma}$, increases as one moves down the temperature gradient. This accumulation of energetic electrons occurs because, in contrast to the case of a Heaviside's temperature profile, they have to pass through regions of lower - but still high - temperatures in which their coupling with the plasma remains strong. As a result the different terms in the expression of $\mathcal{M}$ do not compensate. Given their respective signs after having explicitly expressed the integral with bounds $y_0$ and 1, it appears that

$$\frac{y_0\beta_0}{2} + \frac{(3\pi)^{1/2}}{4} \frac{\Gamma(5/3)}{\Gamma(7/6)}$$

may be interpreted as being related to the local *source* of energetic electrons, whereas,

$$-\frac{\beta_0}{2t} - \frac{t}{\sqrt{3}}(1-y_0^3)^{1/2} - \frac{\sqrt{3}}{4} y_0^2\ {}_2F_1\left(\frac{1}{2}, \frac{2}{3}; \frac{5}{3}; y_0^3\right)$$

may quantify their *escape* fraction toward neighbouring regions. In last expression we approximated $1/(4t^{1/2}) \int_0^{\beta_0^2/t} \tilde{\eta}^{-1/2} h(\tilde{\eta})\ d\tilde{\eta}$ by $\beta_0/(2t)$. The transition between the behaviour at the core of the temperature transition and well beyond will not be treated in the framework proposed by Gurevich and Istomin. It is studied numerically in the Ch. 3.

Until then, we found that the kinetic discontinuity occurred at a precise abscissa. To account for the finite width of this region of strong variation, Gurevich and Istomin considered an additional term in the left hand side of Eq. (6.25), which

was previously neglected as being smaller by a factor $\gamma^{1/2}$ compared to other terms. Such a term, $-4\gamma^{1/2}t\partial_\beta^2\varphi$, is appearing by considering Eq. (6.17) with $r=0$, $\mu=1$, and $\partial_\mu\varphi=0$. Latter identity is consistent with the approximation that, in the dominant order in the small parameter $\gamma$, $\varphi$ is spherically symmetric near the kinetic discontinuity. The additional term is responsible for the smearing of the discontinuity region. Within it, the solution found by Gurevich and Istomin is

$$y=\frac{y^+ + y^-}{2}-\frac{\Delta y}{2}\tanh\left(\frac{\Delta y}{4\gamma^{1/2}}[\beta-\beta_0]\right), \tag{6.44}$$

where $\Delta y = y^+ - y^-$ with $y^\pm = y(\tau,\beta_0^\pm)$. Thus, the strong variation of the derivative of $\varphi_0$ occurs on an interval in energy of size $\gamma^{1/2}/\Delta y$ centered at $\beta_0$. The magnitude of this variation , *i.e* the length of the interval in $y$ centered at the mean value $(y^+ + y^-)/2$, is $\Delta y$ as expected.

#### 6.2.2.2 Study of $\varphi_1$. Properties of the directional component.

The function $\varphi_1$ can be determined from Eq. (6.23). Since, in the absence of any electric field, $r_H=0$ and $\partial_\mu\varphi_0=0$, this equation is

$$\begin{aligned}0&=\mu\beta^2\partial_\tau\varphi_0-2\beta\big[1-2t\partial_\beta\varphi_0\big]\varphi_0+k(1-\mu^2)(\partial_\mu\varphi_1)^2\\&=(\mu-1)\beta^2\partial_\tau\varphi_0+k(1-\mu)(1+\mu)(\partial_\mu\varphi_1)^2,\end{aligned}$$

where we used Eq. (6.25). For $\mu\neq 1$, we divide the above equation by $(1-\mu)$ and obtain the following solution,

$$\varphi_1-\varphi_{10}(\tau,\beta)=\pm\beta\left[\frac{\partial_\tau\varphi_0}{k}\right]^{1/2}\int_{-1}^{\mu}\frac{d\tilde{\mu}}{(1+\tilde{\mu})^{1/2}}=\pm 2\beta\left[\frac{\partial_\tau\varphi_0}{k}\right]^{1/2}(1+\mu)^{1/2}.$$

We shall focus on the negative determination of the square root, and note

$$\varphi_{11}=-2\beta\left[\frac{\partial_\tau\varphi_0}{k}\right]^{1/2}=-2\left[\frac{\beta y(1-ty)}{k}\right]^{1/2}, \tag{6.45}$$

the corresponding function of $(\tau,\beta)$ plotted in Fig. 6.2.11; we used the Eqs. (6.25)-(6.26) for the second equality.

Except at the kinetic discontinuity, the solution, $\varphi_1=(1+\mu)^{1/2}\varphi_{11}+\varphi_{10}$, is continuously differentiable and therefore solution for $\mu=1$. Thus, the chosen sign is such that the function $g_e=\exp(-\varphi)$ reaches its maximum within that plan, as it should be given the physical situation under consideration. Since $\varphi_{11}$ is completely determined by $\varphi_0$, it remains to find $\varphi_{10}$. This is done by considering the Eq. (6.24) for $\mu=1$. After having divided by $\beta$, it reads

$$\beta\partial_\tau\big[2^{1/2}\varphi_{11}+\varphi_{10}\big]-2\big(1-4t\partial_\beta\varphi_0\big)\partial_\beta\big[2^{1/2}\varphi_{11}+\varphi_{10}\big]=-\frac{k}{\beta\sqrt{2}}\varphi_{11}. \tag{6.46}$$

For $\tau\gg\tau_0$, we obtained the formula (6.39) for $\varphi_0$ in the limit of infinitely thin region of temperature variation. We shall solve Eq. (6.46) within this framework. For $\beta<\beta_0$, we found $\varphi_0=\beta/(2t)$, leading to $\varphi_{11}=0$ and therefore to

$$\beta\partial_\tau\varphi_{10}+2\partial_\beta\varphi_{10}=0.$$

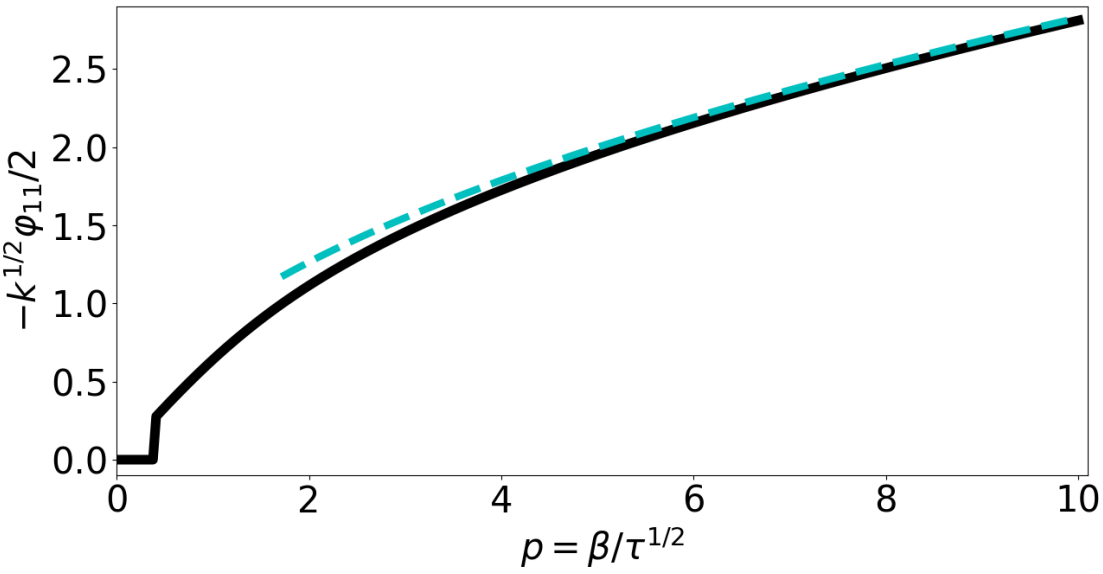


Figure 6.2.11: Case $t = 0.2$, $\tau = 1$, far from the transition region ($\tau \gg \tau_0$). Graph of $-k^{1/2}\varphi_{11}/2$ (solid, black) given by Eq. (6.45). The cyan dashed line represents the high energy limit, $\big[\beta(1-t)\big]^{1/2}$. The graph corresponding to the case $t = 0.4$, within the transition region ($\tau \simeq \tau_0$), is rather the same except near the kinetic discontinuity where that of $-k^{1/2}\varphi_{11}/2$ is less pronounced.

This equation means that, in the $(\tau, \beta)$-plane, the vector field $(\beta, 2)$ is normal to the gradient, $(\partial_\tau, \partial_\beta)$, of $\varphi_{10}$, and so is tangent to the integral curves. By noting $(d\tau, d\beta)$ an infinitesimal displacement along one of these curves, we thus have,

$$0 = \begin{vmatrix} d\tau & \beta \\ d\beta & 2 \end{vmatrix} = d\big[2\tau - \beta^2/2\big],$$

which means the conservation of $2\tau - \beta^2/2$. Hence, the solution is $\varphi_{10}(\tau, \beta) = \overline{\varphi}_{10}(2\tau - \beta^2/2)$, with $\overline{\varphi}_{10}$ an arbitrary differentiable function of one variable. At the point of intersection of any integral curve of equation $2\tau - \beta^2/2 = \omega$, with the line $\beta = 0$, $\overline{\varphi}_{10}(\omega) = 0$ because it is supposed that $\varphi = \varphi_M$ (6.19) in the neighbourhood of $\beta = 0$. Hence, $\varphi_{10} = 0$ everywhere.

Without mentioning it explicitly, Gurevich and Istomin assumed that this identity is still valid for $\beta \geq \beta_0$. They even extended it to the solution within the transition region ($\tau \simeq \tau_0$). In both cases, this can only be possible if $\varphi_{11}$ satisfies Eq. (6.46) with $\varphi_{10} = 0$, *i.e* if $\varphi_0$ satisfies

$$\begin{aligned} k\partial_\tau\varphi_0 &= -\beta^2\partial_\tau^2\varphi_0 + 4\big(1 - 4t\partial_\beta\varphi_0\big)\left[\partial_\tau\varphi_0 + \frac{\beta}{2}\partial^2_{\beta\tau}\varphi_0\right] \\ &= 4\big(1 - 4t\partial_\beta\varphi_0\big)\partial_\tau\varphi_0, \end{aligned}$$

where, to write the second equality, we used the derivative of Eq. (6.25) with respect to $\tau$:

$$0 = \beta\partial_\tau^2\varphi_0 - 2\partial_{\tau\beta}\varphi_0 + 8t(\partial_\beta\varphi_0)(\partial^2_{\tau\beta}\varphi_0).$$

The former equation is verified by none of the solutions (6.39)-(6.43) for an obvious reason: they are independent from $k$. The required relation, $\partial_\beta \varphi_0 = (4-k)/(4t) = (7-Z)/(8t)$, cannot be full-filled, which means that $\varphi_{10}$ can only be considered zero up to a certain error.

Actually, to the order at which we stopped the development (6.18), $f_{1z}$ is equal to a spherically symmetrical term multiplied by $\int_{-1}^{+1} \mu \exp(-\varphi_1/\gamma^{1/4})\ d\mu$. The absence of any return current of electrons implies that there exists an energy below which this integral vanishes. By symmetry of the integrand, this means $0 = \varphi_1 = (1+\mu)^{1/2}\varphi_{11} + \varphi_{10}$ below that energy. This equality is true for any value of $\mu$, in particular for $\mu = -1$ that leads to $\varphi_{10} = 0$ and then to $\varphi_{11} = 0$. As just being seen, these equalities only hold far from the transition region ($\tau \gg \tau_0$) below $\beta_0$. This indicates that higher order terms of the expansion (6.18) must be included to compensate $-\varphi_1/\gamma^{1/4}$ in the argument of the exponential below a certain energy.

#### 6.2.2.3 Heat flux density: diffusive and convective parts

By taking into account the azimuthal symmetry around the $z$-axis in velocity space, the heat flux density is

$$q_{ez} = \pi m_e \int v^3 \cos\theta f_e\ v^2 dv d(\cos\theta) = \frac{\pi m_e}{2} \frac{v_{T_H}^6}{\gamma^{3/2}} \int g_e \mu \beta^2\ d\mu d\beta.$$

Following Gurevich and Istomin, we limited the study to the first two terms of the expansion (6.18). The third one, unaltered, is fixed by the constraint $\varphi = \varphi_M$ near $\beta = 0$. Substituting the resulting distribution function,

$$g_e = \frac{n_e}{(2\pi t)^{3/2} v_{T_H}^3} e^{-\left(\varphi_0/\gamma^{1/2} + \varphi_1/\gamma^{1/4}\right)},$$

into the above expression of the heat flux density leads to

$$q_{ez} = \frac{1}{4(\gamma t)^{3/2}} \frac{n_e m_e v_{T_H}^3}{(2\pi)^{1/2}} \int_0^\infty \left( \beta^2 e^{-\varphi_0/\gamma^{1/2}} \int_{-1}^{+1} \mu e^{-\varphi_1/\gamma^{1/4}}\ d\mu \right) d\beta.$$

The integral over $\mu$ can be expressed as

$$e^{-\varphi_{10}/\gamma^{1/4}} \int_{-1}^{+1} \mu e^{-(1+\mu)^{1/2}\varphi_{11}/\gamma^{1/4}}\ d\mu = e^{-\varphi_{10}/\gamma^{1/4}} \mathcal{B}\left(\frac{\varphi_{11}}{\gamma^{1/4}}\right),$$

with $\mathcal{B}$ the function defined as

$$\begin{aligned} \mathcal{B}(x) &= 2\int_0^{\sqrt{2}} w(w^2-1)e^{-xw}\ dw \\ &= \frac{2}{x^4}\Big[6 - x^2 - e^{-x\sqrt{2}}\big(x^3\sqrt{2} + 5x^2 + 6[1 + x\sqrt{2}]\big)\Big]. \end{aligned} \tag{6.47}$$

The second expression is obtained, supposing $x \neq 0$, by performing three successive by parts integrations. At the origin this function vanishes, $\mathcal{B}(0) = 0$. Finally we

split the integral in energy as

$$q_{ez} = \frac{1}{4(\gamma t)^{3/2}} \frac{n_e m_e v_{T_H}^3}{(2\pi)^{1/2}} \Big( \int_0^{\beta_0} \beta^2 e^{-(\varphi_0/\gamma^{1/2} + \varphi_{10}/\gamma^{1/4})} \mathcal{B}\left(\frac{\varphi_{11}}{\gamma^{1/4}}\right) d\beta + \int_{\beta_0}^{\infty} \beta^2 e^{-(\varphi_0/\gamma^{1/2} + \varphi_{10}/\gamma^{1/4})} \mathcal{B}\left(\frac{\varphi_{11}}{\gamma^{1/4}}\right) d\beta \Big) = q_{eD\ z} + q_{eC\ z}, \tag{6.48}$$

where $q_{eD\ z}$, corresponding to the contribution of electrons with energies comprised between 0 and $\beta_0$, will be designated as the *diffusive* part of the heat flux density, and $q_{eC\ z}$ its *convective* one. Gurevich and Istomin provided these contributions explicitly. Circumstances have not yet allowed us to push our calculations far enough to compare them with their formulae. As frustrating as it may seem, we will stop our work here.

### 6.2.3 Conclusion, and possible extensions of this study

The onset of the discontinuity in the slope of the isotropic part of the distribution function has been finely studied. Despite its obviousness from a physical perspective, the mathematical mechanism of its appearance is interesting. It is analogous to the breaking of Riemann's waves in hydrodynamics. Such a kinetic discontinuity corresponds to a jump of the local effective temperature but also, because of the absence of the electric field, to the transformation of the distribution function from spherically symmetrical to sharply directional. The success of the analysis is partly based on the choice of a judicious change of variable proposed by Gurevich and Istomin, which, as we have seen, is a precursor to the so-called M1 closure. The only difference lies in the way the argument of the exponential is expanded. In the former case it is a P1 expansion, whereas Gurevich and Istomin proposed a development similar to Chapman-Enskog's one. By retaining the first three terms of this expansion they handled the calculation of the heat flux density, recoved the Spitzer-Harm's result for the diffusive part, and obtained intelligible, local, formulae for the convective one, both within and far beyond the temperature transition. However, these last results, not recovered here, would require further work before they could be compared with complete kinetic simulations.

One improvement would be to account for the electric field effect. An approach may consist of a perturbation method with small parameter $r_H$ (6.15). By examining Eq. (6.21), it can be seen that the correction breaks the spherical symmetry of $\varphi_0$. This seems to lead to a considerable higher degree of complexity, and therefore, to intractable calculations. The inclusion of the effect of a constant magnetic field is mentioned by Gurevich and Istomin. Nevertheless, it seems quite obvious that taking into account a self-generated field coupled to the electric one would lead to an even higher degree of complexity. However, the author has not ventured into these areas and refrains himself from making a definitive judgement on such extensions.

In conclusion, it may be desirable to see how the results are sensitive to a different choice of electron-electron collision operator. Of particular interest are those of Albritton *et al.* [82], $-\nu_{ee}\partial_v(f - f_M)$, and of Bhatnagar *et al.* [73], $-\nu_{ee}(f - f_M)$.

Choosing them means substituting in Eq. (6.17) the term

$$-2\beta\big[1-2\gamma^{1/2}t\partial_\beta\varphi\big]\partial_\beta\varphi-4\gamma^{1/2}t\beta\partial_\beta^2\varphi$$

by, respectively,

$$-2\beta\partial_\beta\varphi+\frac{e^{\varphi-\varphi_M}}{2\gamma^{1/2}t},\qquad e^{\varphi-\varphi_M}-1.$$

The treatment of these cases would require an additional attention during the perturbation method when equating equal power of the parameter $\gamma$, because of the exponential term,

$$e^{\varphi-\varphi_M}=e^{-\varphi_M}\sum_{\ell=0}^{\infty}\sum_{s=0}^{\ell}\frac{(-1)^s}{s!\;(\ell-s)!\;\varphi_M^s}\sum_{p=0}^{P}\gamma^{p/4-1/2}\varphi_p.$$

Above, $\varphi$ have been expended according to Eq. (6.18) with $P\geq 2$.

This page is unintentionally left not blank.

This page is unintentionally left not blank.

This page is unintentionally left not blank.

# Étude théorique du transport électronique non local dans les plasmas de fusion par confinement inertiel


## Résumé:

La fusion inertielle par laser est entrée dans une nouvelle ère depuis que l'allumage a été réalisée. Le développement d'un réacteur commercial nécessite de transformer un tir réussi par an en plusieurs tirs en une seconde. Cela implique d'améliorer significativement la robustesse du contrôle de l'implosion. Pour ce faire, le dialogue entre les progrès expérimentaux et la compréhension théorique doit être renforcé par la création d'outils de simulation précis. Cette thèse aborde le problème de la modélisation du transfert électronique de chaleur dans la région de conduction de l'écoulement ablatif. Compte tenu de la variété des phénomènes à l'origine de la déformation de la fonction de distribution des électrons, il est apparu que pour fermer les équations macroscopiques, l'approche consistant à résoudre exactement des équations cinétiques réduites à l'aide d'une méthode numérique efficace est prometteuse car sa flexibilité constitue le terrain le plus fertile pour des extensions progressives. Dans ce manuscrit, nous approfondissons la compréhension, améliorons et implémentons efficacement un modèle cinétique réduit dont l'objectif est limité au traitement du problème du transport non local quasi-statique dans un plasma isolé, unidimensionnel et non magnétisé.



## Mots-clés:

Fusion par confinement inertiel; Théorie cinétique; Transport nonlocal

# Theoretical Study of Nonlocal Electron Transport in Plasmas Relevant to Inertial Confinement Fusion


## Abstract:

Inertial fusion by lasers has entered a new era since ignition has been achieved. The development of a commercial reactor requires to transform one successful shot per year into several ones in a second. This means significantly improving the robustness of the implosion control. To do so the dialogue between experimental progresses and theoretical understanding must be strengthened through the creation of accurate simulation tools. This thesis addresses the problem of modeling electron heat transfer within the conduction region of the ablative flow. Given the variety of phenomena causing the distortion of the electron distribution function, it appeared that to close the macroscopic equations the approach of exactly solving reduced kinetic equations with an efficient numerical method is promising since its flexibility constitutes the most fertile ground for progressive extensions. In this manuscript, we deepen the understanding, improve and efficiently implement a reduced kinetic model whose purpose is restricted to treating the problem of quasi-static nonlocal transport within an isolated, one-dimensional and unmagnetized plasma.



## Keywords:

Inertial Confinement Fusion; Kinetic Theory; Nonlocal Transport